UNIVERSITÉ LAVAL

Development of design tools for convection mitigation techniques to preserve permafrost under northern transportation infrastructure

Thèse

Xiangbing Kong

Doctorat en génie civil
Philosophiæ doctor (Ph. D.)

Québec, Canada

UNIVERSITÉ LAVAL

Development of design tools for convection mitigation techniques to preserve permafrost under northern transportation infrastructure

Thèse

Xiangbing Kong

Sous la direction de :

Guy Doré, directeur de recherche
Fabrice Calmels, codirecteur de recherche

RÉSUMÉ

Les infrastructures de transport jouent un rôle majeur dans le développement socio-économique des régions nordiques. La construction de remblais combinés aux changements climatiques engendrent des impacts négatifs sur le pergélisol sous-jacent, causant la dégradation des infrastructures. Des techniques de mitigation ont été proposées et testées pour limiter la dégradation du pergélisol. Toutefois, il y a peu d'informations disponibles sur les procédures de conception ou sur des lignes directrices. Le but de cette recherche est de développer des outils d'ingénierie améliorés pour les techniques de stabilisation convectives, se concentrant sur le remblai à convection d'air (ACE) et le drain thermique. Plus spécifiquement, l'approche du bilan thermique est proposée pour déterminer la condition thermique de remblais conventionnels et pour permettre la sélection de la technique de mitigation la plus appropriée pour extraire la chaleur en excès transmise au sol, si le système est actuellement instable, ou pour donner un facteur de sécurité considérant une instabilité future estimée. Quatre modèles thermiques ont été développés et calibrés à partir de données mesurées sur des sites expérimentaux. Un abaque de bilan thermique pour les remblais conventionnels ainsi que plusieurs abaques de capacité d'extraction de chaleur pour l'ACE et le drain thermique ont été développés et validés utilisant, respectivement, des simulations numériques et les données de sites d'essais du Yukon et du Nord du Québec, Canada. Ces abaques permettent aux concepteurs et ingénieurs de concevoir des remblais à convection d'air et des drains thermiques optimisés pour limiter, ou même éviter, le dégel du pergélisol à des sites spécifiques.

Mots clés: Dégradation du pergélisol; Infrastructure de transport; Outils de conception; Remblais à convection d'air (ACE); Drain thermique

ABSTRACT

Transportation infrastructure plays a vital role in the social and economic development of northern regions. The construction of embankments and climate change can lead to negative impacts on the underlying permafrost, causing degradation of the infrastructure. Mitigation techniques have been proposed and tested to limit permafrost degradation. However, there is limited information on the design procedures or guidelines. The purpose of this research is to develop improved engineering tools for convective stabilization techniques, focussing on air convection embankment (ACE) and heat drain. More specifically, the heat balance approach is proposed to determine the thermal condition of conventional embankments and to allow the selection of suitable mitigation techniques to extract the amount of extra heat flowing into the foundation, if the system is currently unstable, or give a safety factor considering estimated future instability. Four thermal models have been built and calibrated with field data from experimental sites. One heat balance chart for conventional embankments and, several heat extraction capacity charts for ACE and heat drain have been developed using numerical simulations and have been validated using data from test sites in Yukon and Northern Quebec, Canada. These charts allow designers and engineers to design optimized ACE and heat drain to limit or even avoid the thawing of permafrost at specific sites.

Keywords: Permafrost degradation; Transportation infrastructure; Design tools; Air convection embankment (ACE); Heat drain

TABLE OF CONTENTS

LIST OF TABLES

LIST OF FIGURES

ACKNOWLEDGEMENTS

First of all, I would like to thank my supervisor Prof. Guy Doré for the research project opportunity and also for being patient and supportive in the research progress. Thank you very much for giving me all this time to proceed and for the valuable research discussion and guidance through my project. I really appreciate the chance I had to work with Prof. Guy Doré, and this is one of the best decisions in my life.

I also want to thank my co-supervisor Dr. Fabrice Calmels (Yukon College) for the research meeting, discussion and enthusiastic comments that contributed to improving the research project. The research discussions with you are an invaluable part of this project and they are inspirational. Thank you for your time and your excellent knowledge of permafrost.

I also thank Mrs. Chantal Lemieux for her research advice, technical support and document review. During the study, she gives tremendous help. I also thank Mr. Jean-Pascal Bilodeau for his passions on research, which is really encouraging. Talking with them created favourable conditions during the whole Ph.D. study.

I warmly thank every ARQULUK fellow student. The discussions and help from them are tremendous to me. Special thanks to Dr. Heather Brooks for the kindly research skills sharing and personal talking on many related topics in the process of research project. Also thanks to ARQULUK partners for supporting the research program.

I extend my sincere thanks to my parents, brothers and grandma for the family support. Without their encouragements, it would have been hard for me to finish my Ph.D. project.

FOREWORD

This thesis is in a paper-based format and it includes 8 chapters. Chapter 1 presents the state of knowledge related to this project. Chapter 2 identifies the knowledge gaps and states the objective of this project. Chapter 3 to 7 include five peer-reviewed papers. Chapter 8 and Conclusion present the discussion and conclusion obtained from this project. The papers included in this thesis are:

Chapter 3

- Kong, X., Doré, G., Calmels, F. (2019). Thermal modeling of heat balance through embankments in permafrost regions. *Cold Regions Science and Technology*, 158, 117-127.

Chapter 4

- Kong, X., Doré, G., Calmels, F., Lemieux C. Modeling the thermal response of air convection embankment in permafrost regions. *Cold Regions Science and Technology*. (under review, should be accepted with minor modifications required from the editor).

Chapter 5

- Kong, X., Doré, G., Calmels, F., Lemieux C. Field and numerical studies on the thermal performance of air convection embankment to protect side slopes in permafrost environments. *Cold Regions Science and Technology*. (under review).

Chapter 6

- Kong, X., Doré, G., Calmels, F., Lemieux C. Investigation on the heat extraction capacity of the heat drain for thermal stabilization of embankments on thaw sensitive permafrost. *Cold Regions Science and Technology*. (under review).

Chapter 7

- Kong, X., Doré, G. Thermal stabilization of embankments built on thaw sensitive permafrost. *Journal of Cold Regions Engineering*. (under review).

The author of this thesis is the principal author of the papers mentioned above. The contribution of the first author in these papers mainly consisted of field data analysis, thermal modeling and writing. The co-authors of

these papers mainly oversaw the work, reviewed the contexts and improved the research methodology and results analysis and presentation.

General introduction

Context

This project is part of the ARQULUK northern engineering research program, chaired by Prof. Guy Doré at the Department of Civil and Water Engineering of Université Laval. The program focused on the development of innovative tools to support designing and managing transportation infrastructure built on permafrost, considering climate change. The research program's objectives were to develop a better understanding of factors contributing to permafrost degradation, improve investigation techniques for thaw-sensitive permafrost to locate and characterize problem areas, and develop cost-effective protection techniques.

This project is part of the last objective and has developed design tools for convection mitigation techniques to limit permafrost degradation and thus preserving northern infrastructure.

Problem description

Permafrost underlies about 24% of the northern hemisphere's land surface (Brown, 1997) and permafrost is important to be considered when designing transportation infrastructure. Permafrost is often ice-rich and sensitive to changes in its thermal regime. The construction of infrastructure embankments and climate change disturb the thermal equilibrium, leading to a larger amount of heat flowing into the foundation. Permafrost degradation is problematic for infrastructure stability, mostly due to the risk of excessive thaw settlements. The two main types of engineering problems related to permafrost degradation are the differential settlements and the lateral spreading. Those can affect the comfort and safety of road users, as well as increase maintenance cost.

Linear infrastructure built on permafrost is commonly affected by the deformations resulting from the thawing of underlying frozen soils in permafrost regions (Kondratiev, 2010). Ground thermal regime equilibrium requires approximately 3 years in the case of the summer construction, or up to 5 years for the winter construction conditions (Lingnau, 1985). In order to prevent dramatic thawing of permafrost, road construction strategies must be adapted to northern environments (M-Lepage et al., 2012). Global warming is happening at a fast rate in Arctic areas with air temperature increasing at least 1.5 to 2 times larger than in the rest of the word (Kaplan and New, 2006). However, the effect of global warming was seldom considered in the design of civil infrastructure (Doré et al., 2016). Under such conditions, much of the northern civil infrastructure is located in the high hazard region (Nelson et al., 2001). As a result, maintenance and design practices will be impacted by climate change (Warren et al., 2004).

New knowledge and better understanding of permafrost degradation and mitigation techniques to limit or even avoid permafrost degradation are required to secure the stability of civil infrastructure in northern regions, in response to climate change.

Thesis organization

This thesis is in the paper-based format, and it includes 8 chapters. Each peer-reviewed paper has a research background and the state of knowledge in Chapter 1 may have some repetitions in peer-reviewed papers. The content of each chapter is presented in the following paragraphs:

Chapter 1 presents the state of knowledge related to this project, including permafrost, permafrost degradation and its associated effect on transportation infrastructure, heat transfer principles, mitigation techniques, method application considerations and available design tools for methods based on natural convection.

Chapter 2 identifies the knowledge gaps and states the objective of this project.

Chapters 3 to 7 include the five peer-reviewed papers. Chapter 3 was published in the journal “Cold Regions Science and Technology”. Chapters 4, 5 and 6 have been submitted to the journal “Cold Regions Science and Technology”, and they are at different states of the review process. Chapter 7 has been submitted to Journal of Cold Regions Engineering. In each paper (Chapters 3 to 6), data measured on field sites are first analyzed to determine the ground thermal regime. Then, one model is developed and described in detail, including material types and properties, meshing and boundary conditions. The models have been calibrated to the measured data and validated using additional data from other field sites. The methodology used assured the reliability of heat balance charts and heat extraction capacity charts developed as part of the project.

Chapter 8 presents the discussion including a research critical review, a description of practical engineering application, and recommendations for future research.

Finally, the main conclusions of this project are given.

Chapter 1 Literature review

1.1 Permafrost

Frozen ground is generally classified into two categories: seasonally frozen ground with freezing and thawing on an annual base, and perennially frozen ground. Permafrost refers to soil, rock, ice and organic material, with temperatures at or below 0 °C for at least two consecutive years. This definition is applied without regard to material composition, phase of water, or cementation. The presence of permafrost is determined by local factors, such as, but not limited to, the type of vegetation, climate conditions, and soil types. Climate cannot provide a reliable indication of the existence of permafrost. For example, permafrost can exist at the locations with the mean annual air temperature above 0 °C (Goodrich, 1982), due to the difference between air temperature and surface temperature, but mainly due to the differences in the thermal conductivity of soils in frozen and unfrozen states (Klene et al., 2001).

Permafrost covers about 24% of the exposed land area in the northern hemisphere (Davis, 2001) and about half the Canadian landmass is underlain by permafrost (Smith, 2011).

1.2 Permafrost degradation and its effect on transportation infrastructure

Permafrost is sensitive to the change of thermal disturbance, especially when ice-rich, in warm regions (-1 °C ~ 0 °C) (Goering and Kumar, 1999). Permafrost generally supports the load of embankments and traffics sufficiently. Mechanical changes in the foundation directly affect the normal operations of roads.

The main physical causes of permafrost degradation around a transportation embankment are: (1) changing ground surface properties; (2) the modification of surface topography and drainage patterns; and (3) climate change (expected increase of air temperature and precipitation) (Doré et al., 2016).

The construction of transportation infrastructure changes the ground surface, tending to warmer conditions (Goering and Kumar, 1999). In addition to that, embankment slope, surface and orientation influence the amount of solar energy absorbed by the ground. The embankment surface covered by mineral soils or asphaltic materials has low albedo and absorbs more solar heat, compared to the pre-exiting vegetation cover, such as trees or shrubs (Dumais and Doré, 2016). The presence of embankments can be considered as an insulation layer with low thermal conductivity and the underlying permafrost is generally better protected along the centerline. Under the slopes of the embankment, the embankment fill thickness is less and the geometry can accentuate the snow accumulation where cross-side winds are dominant (Ficheur, 2011). Due to the embankment geometry and wintertime wind, snow accumulates on the side slopes. In summer, water flows

into the ground due to the melting of snow and precipitations and also tends to accumulate at the toe of the embankment slope. Snow highly insulates the side slope surfaces, which reduce heat extraction during winter and leads to engineering problems that usually occur first along the toe of embankments. The insulation capacity of the snow cover is a direct function of thickness and is inversely related to snow density. Linear transportation infrastructure, such as roads, railways and airstrips, are likely cross surface and subsurface water flow paths and water is therefore often concentrated along the embankment. As a result, more water flow along the ditch or along embankments (Doré, et al., 2016). It is often difficult to predict the adverse impact of water flow on the thermal stability of the underlying permafrost in field sites (Calmels et al., 2016). Figure 1.1 shows these concepts, descripted above.

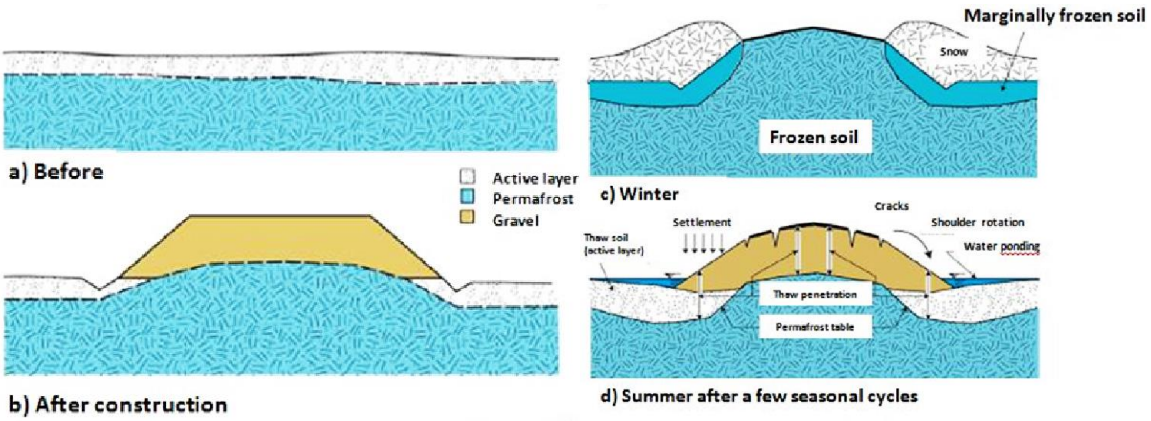

Figure 1. 1: Concepts of permafrost degradation due to the construction of transportation infrastructure.

Climate change, associated with changes in the air temperature, precipitation conditions, wind patterns and extreme weather events, plays an important role in permafrost degradation. In Alaska, the mean annual air temperature rose from -3.6 °C to -2.2 °C with an increase of 1.4 °C in the last century (Wendler and Shulski, 2009). With the associated global warming record since the second half of 20th century, permafrost degradation has significantly affected transportation infrastructure in permafrost regions (Doré, et al., 2016). The MAAT (mean annual air temperature) warming trend observed in Alaska, Canada and Russia, is shown in Figure 1.2. Global warming trend was also observed on Qinghai-Tibet plateau, China. The mean increase per year of active layer thickness inferred from ground temperature data (1995 to 2000) is about 4.0～8.4 cm, 0.8～6.5 cm and 3～5 cm for high-mountain, high-plain and mid-lower mountain areas, respectively (Wu et al., 2010). Global warming trend will continue and more severe changes are expected in Arctic regions than the rest of the world (Figure 1.3) (Assessment, A. C. I., 2004). Global warming is often not considered in the design of transportation infrastructure (Doré et al., 2016). Therefore, much of infrastructure will be at high risk, in response to global warming (Figure 1.4, Nelson et al., 2001).

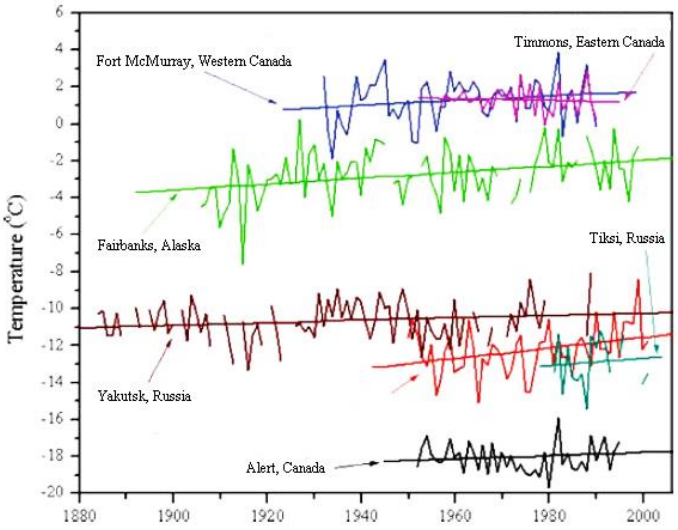

Figure 1. 2: Increase of mean annual air temperature in Alaska, Canada and Russia (modified from Hinzman et al., 2005).

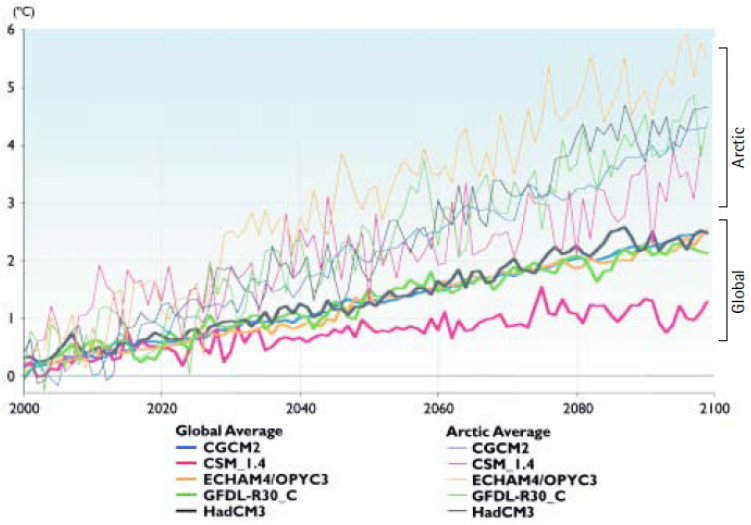

Figure 1. 3: Predicted surface air temperature change (Assessment, A. C. I., 2004).

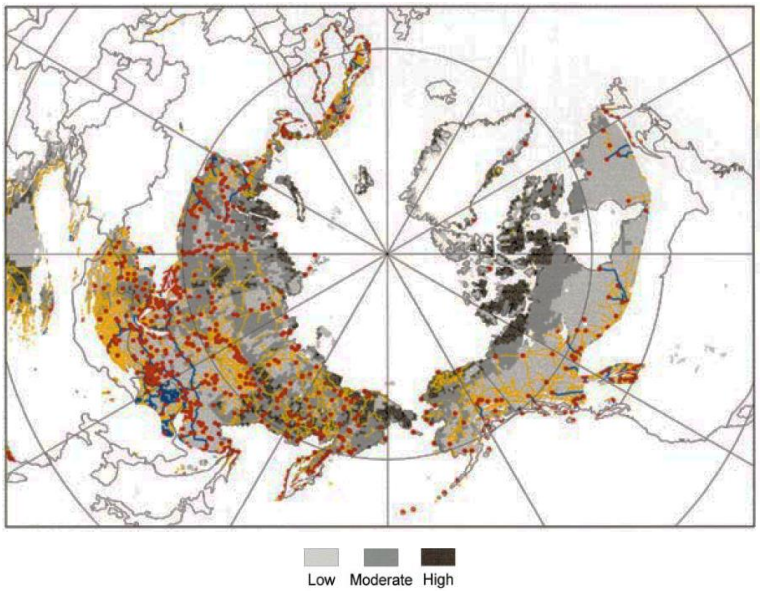

Figure 1. 4: Permafrost hazard potential in the northern hemisphere (yellow: undifferentiated roads and trails; blue: railroads; red: airfields) (Nelson et al., 2001).

Engineering problems such as longitudinal cracking, differential settlement, sinkholes and guardrail settlements, are commonly observed in the northern area (Figure 1.5 and Figure 1.6). Due to the environmental restrictions in Arctic areas, it is important to regulate construction activities to minimize the impacts of construction on the permafrost.

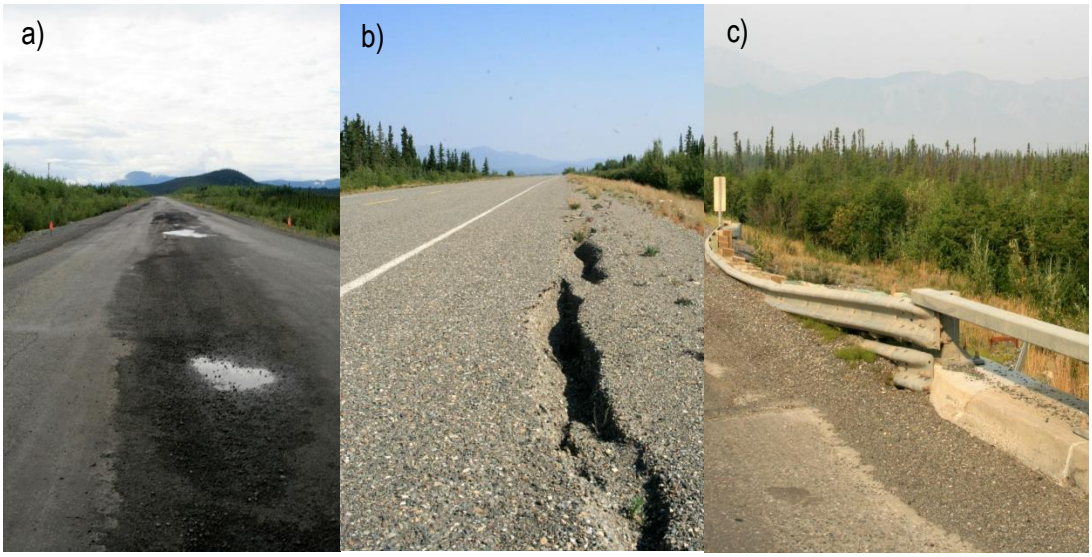

Figure 1. 5: Engineering problems: a) sinkhole; b) longitudinal cracking; c) guardrail sinking.

Figure 1. 6: Differential settlement.

1.3 Heat transfer principles

Porous medium is defined as a material consisting of a solid matrix with interconnected voids (Nield and Bejan, 2006). Heat transfer modes in the porous medium, are classified into three types: heat conduction, convection and radiation. The soil texture and degree of saturation have a significant influence on the heat transfer mode (Figure 1.7). In the theoretical study of heat transfer in soils, homogeneous and uniform heat transfer were generally assumed and soils were considered as “unit cell” to simplify the heat transfer (De Vries, 1958).

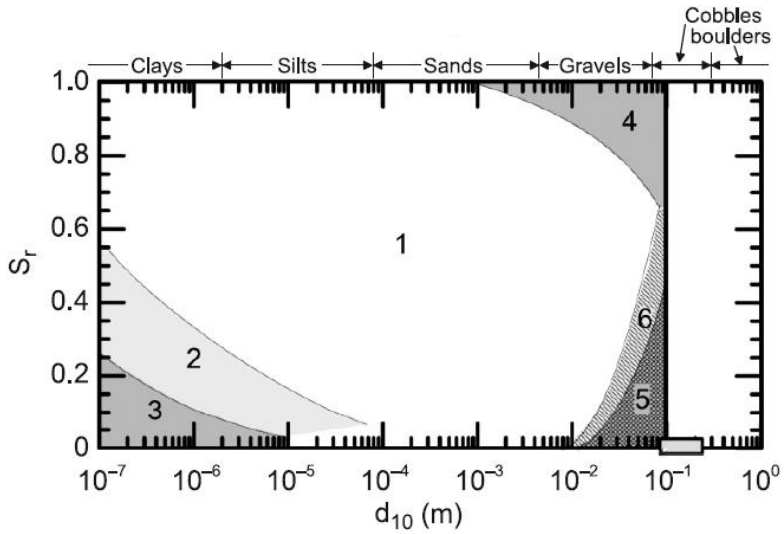

Figure 1. 7: Heat transfer modes in a porous medium with a relation to particle size and degree of water saturation (Côté et al., 2011, cited from Johansen, 1975). 1- conduction, 2- redistribution of moisture, 3- vapour distribution due to the moisture gradient, 4- free (natural) convection in water, 5- free (natural) air convection, 6-heat radiation.

where S_r is the degree of saturation and d_{10} is the particle diameter (10% of the whole material mass has particles smaller than 10%). For coarse gravel with a low degree of saturation, such as ACE with the rock diameter range from 150–300 mm, natural convection and heat radiation heat transfers become significant.

1.3.1 Heat conduction

In the soil medium, conduction can be complex because of co-existence of multiple phases and the arrangement between those (Pham, 2013). Heat conduction is defined as the transfer of heat occurring through one material without bulk motion, with heat passing from warmer to colder regions. It occurs in all the soils constituents, such as soil solid, water and air in the pores, and it is the main mode of heat transfer in soils, as convection and radiation have small or negligible effects, due to the low porosity. In general, heat transfer through the solid grains in contact accounts the main part of conduction.

Higher soil dry density and degree of saturation lead to a bigger amount of heat transferred by conduction (Farouki, 1981). Heat flux due to conduction can be calculated using the Fourier's conduction law, expressed as:

$$q = -k\frac{dT}{dz} \tag{1.1}$$

where $q =$ heat flux; $k =$ thermal conductivity of soils; $_{dT} =$ temperature difference; $_{dz} =$ depth difference.

1.3.2 Heat convection

It is the mode of energy transfer between a solid surface and an adjacent liquid or gas that is in motion, and it includes the combined effect of conduction and fluid motion. Convection only occurs in the fluid, such as air and water. Based on the difference of driving forces, convection can be classified into forced convection and natural convection. Natural convection occurring in fluids is due to the change of density with temperature. At a lower temperature, the density of fluids is larger, resulting in downward displacement and the lighter warm fluid will tend to move upward. A dimensionless parameter, the Rayleigh number Ra , can be used to quantify the strength of natural convection, and it is expressed as (Goering, 2002):

$$Ra = \frac{C\beta gKH\Delta T}{\nu k} \tag{1.2}$$

where $_{C,\beta}$, and ν are the heat capacity, thermal expansion, and kinematic viscosity of the fluid, respectively. g is the gravitational acceleration. K and k are the intrinsic permeability and thermal conductivity of the material, respectively. ΔT is the temperature difference between top and bottom boundaries. Natural convection draws much attention in the engineering application, such as roadways and rock-fill dams. The stability analysis for a horizontal layer with impermeable boundaries of uniform temperature at the base and upper surface, indicate that: 1) Ra <40, convection is negligible and conduction is the predominant heat transfer process; 2) 40≤ Ra < 280 to 400, stationary convection can be reached; 3) Ra ≥ 400, air convection

is disordered and unstable (Straus, 1974). For the same temperature difference ΔT, a larger layer thickness H could provide a larger value of Ra, resulting in stronger natural convection. This leads to the practical design theory that increasing embankment thickness was considered to be a good solution to provide enough natural convection in air convection embankment (ACE), with high permeability to extract heat from the ground in winter (Esch, 1983; McHattie and Goering, 2009). The effects of natural convection in ACE were experimentally determined by Johansen (1975) and Goering (1998). More information about ACE can be found in Chapter 2.4.1. The effect of air convection in a rock-fill dam was also largely studied (e.g., Mukhetdinov, 1971; Lebeau and Konrad, 2009).

Another important parameter is Nusselt number, which represents the ratio of the heat transferred by convection to that to that due to thermal conduction alone, and it is defined as:

$$Nu = \frac{q\Delta z}{k\Delta T} = \begin{cases} 1 \\ \dfrac{Ra}{40} \end{cases} \tag{1.3}$$

where q = actual upward heat transfer through the layer, Δz = layer height, ΔT = temperature difference, and Ra = Rayleigh number. In summer, heat transfer occurs by conduction with Nu = 1. In winter, Nu > 1, if natural convection happens.

Forced convection occurs when currents of fluids are forced to move through the porous medium due to the external forces acting on fluids, such as wind and subsurface water flow. Forced convection has a high potential to transfer heat transfer in the porous medium. Johansen (1975) indicated that even a small wind speed (2.0 m/s) could induce a huge heat transfer in the 50 cm thick ACE, with the effective thermal conductivity increasing by approximately two times in winter (from 0.45 W/m-K to 1.46 W/m-K). Convection can be expressed as a function of the convection coefficient and the temperature difference between surface temperature and moving air close to the surface. The relationship (Newton's law) can be expressed as:

$$q = h(T_s - T_a) \tag{1.4}$$

where q, h are heat flux and convection coefficient, respectively. T_s, T_a are surface temperature of pipe and air temperature, respectively. Convection coefficient h increases with wind speed v, and for the smooth embankment surface, it can be simplify determined using empirical function (McAdams, 1954):

$$h = 5.678 + 1.05v \tag{1.5}$$

where h is a function of the surface drag coefficient, air density, specific heat of air, air Prandtl number and winder speed, and it is difficult to assess h for water flow in a porous medium (Doré and Zubeck, 2009).

1.3.3 Heat radiation

Thermal radiation is a mode of heat transfer by the emission of electromagnetic waves without support, compared to conduction and convection. All materials can emit energy that is moving randomly and can be absorbed, reflected or transmitted when reaching one surface. The net radiation q from hotter materials to colder materials can be assessed using Stefan-Boltzmann law using the following equation:

$$q = \sigma(\varepsilon_1 T_1^4 - \varepsilon_2 T_2^4) \tag{1.6}$$

where σ is the constant Stean-Boltzmann coefficient equals to 5.7E-8 W/m^2-K^4. ε_1 and ε_2 are the emission coefficient of hot and cold solid materials, respectively, and T_1, T_2 are respectively temperatures for the cold and hot solid materials. For different materials, the emission coefficient can change a lot. For example, the typical values for soils and sandstones are 0.90～0.95, 0.59, respectively. Within a pore medium, like fine-grained soils, the heat transfer by conduction and convection is much higher than by radiation, and as a result, radiation is often neglected (Lunardini, 1981). However, within the medium with large particle size, such as crushed rocks, increasing the particle size will increase the effect of radiation, which cannot be neglected (Côté et al., 2011). Considering the overall heat transfer, the effect of radiation in sand, accounts for less than 1% (Farouki, 1981), however, it rises to 10% in the gravel-size material with a particle size of 20 mm (Wakao and Kato, 1969). The proportion of radiation in heat transfer increase with the pore area and temperature (Farouki, 1981).

1.4 Mitigation techniques

Recent studies describe mitigation techniques used to stabilize embankments built over thaw-sensitive permafrost. They are generally classified into four categories: (1) Methods based on wintertime heat extraction from the ground, such as air ducts, air convection embankment (ACE), thermosyphons and heat drain; (2) Methods based on reducing heat intake to permafrost in the summer, such as high-albedo surface, sun shed and insulation; (3) Methods based on embankment reinforcement, such as geogrids and geotextiles; (4) other methods, such as pre-thawing, excavation and replacement, built and maintain, and snow removal.

The mechanical properties of permafrost, such as shear strength, stiffness and compression strength, are sensitive to its thermal state and long-term stability of embankments heavily relies on favorable ground thermal conditions. Some typical results of strength vs. temperature for different types of soils are shown in Figure 1.8.

The successful design of linear transportation infrastructure primarily relies on the long-term thermal stability of the underlying permafrost in permafrost environments (Doré and Zubeck, 2009).

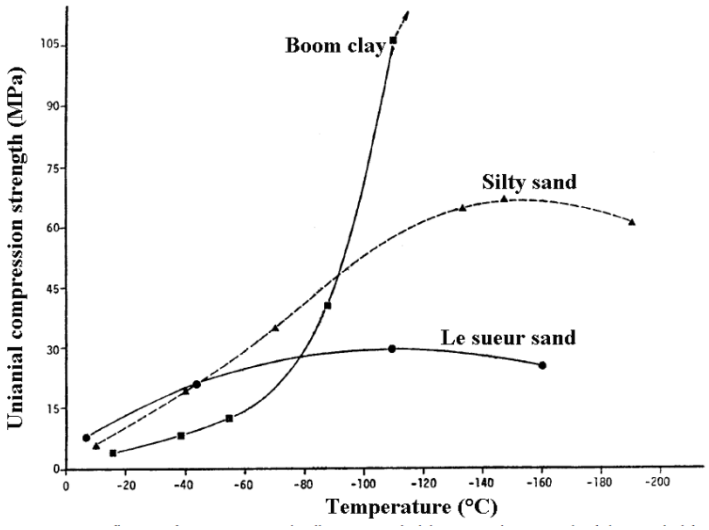

Figure 1. 8: Influence of temperature and soil types on uniaxial compression strength of three typical soils (modified from Andersland and Ladanyi, 2004).

1.4.1 Methods based on wintertime convection to extract heat from embankments

Convective techniques are used to augment wintertime heat extraction to preserve permafrost underneath transportation embankments.

1.4.1.1 Air convection embankment (ACE)

The concept of ACE was first reported in Russia (Vinson et al., 1996), then tested and developed in several countries, such as USA (Alaska), Canada and China. ACE involves the use of a highly porous, poorly graded material with a low fine content to construct the main portion of the embankment (Goering, 2002, 2003, Cheng et al., 2008). During winter, the upper portion of the embankment is cooled by the cold air temperature. The temperature difference between the ACE layer surface and bottom induced unstable air density, which is the reason leading to pore air circulation in ACE layer (Figure 1.9). Natural convection can lead to heat transfer at a rate that may be more than an order of magnitude larger than conduction only. In summer, the air temperature is higher than ground/embankment temperature, no convection can occur as the air in the embankment remains denser and no air convection occurs (Goering, 2003). In those conditions, ACE layer plays the role of a thermal insulation barrier, due to the high porosity and low thermal conductivity (Goering, 2002). Both effects lead to larger wintertime cooling rate and less summertime warming rate.

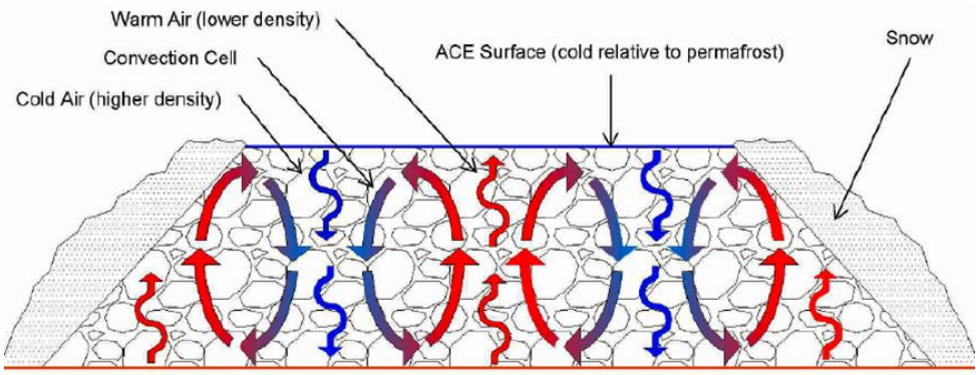

Figure 1. 9: Schematic of wintertime pore air circulation in the ACE (Goering, 2003).

ACE is a good solution to decrease ground temperatures if competent rocks are available around the field site. Although ACE has a good potential to preserve permafrost, in some cases, it cannot stabilize it where a large amount of groundwater flow occurs in permafrost environments. The combination with other techniques, such as insulation, ventilation pipes, and thermosyphons, is a good solution to better stabilizae permafrost(e.g., M-Lepage et al., 2012). Based on previous research, the thermal effectiveness of ACE is closely related to the following factors:

- Different boundary conditions (impermeable and permeable)

There are two types of boundaries: impermeable and permeable boundaries. The air-permeable boundary involves that the ambient air can directly enter the air convection embankment, whereas it cannot enter through the air – impermeable boundary. The selection of impermeable or permeable boundaries heavily depends on the actual conditions of boundaries. In terms of the road surface (asphalt or concrete) and ground surface, they are considered to be impermeable (e.g., Goering, 2002). For the side slope covered by snow, it can be regarded as permeable boundaries. The airflow speed in the snow is small and Darcy's law can be used to characterize the airflow (Shimizu, 1970). The strength of air convection in snow layer also highly depends on the permeability, which closely relates to crystal size and density (Shimizu, 1970; Calonne et al., 2012; Zermatten et al., 2014). The relationship between permeability and crystal size, density can be estimated using a widely used empirical equation (Shimizu, 1970; Wu et al., 2005):

$$\mathrm{K} = 0.077\exp(-0.0078\rho_s)D^2 \tag{1.7}$$

where D and ρ_s are the mean diameter of snow particles and snow density, respectively. It is recommended to place a geotextile layer on top of ACE layer to prevent small soil particles migration into the void, and the rock layer should be placed above the water table to prevent water from filling the voids. It is also highly recommended to leave embankment side slopes open to allow cold air penetration into the ACE during winter.

However, the open ACE cannot preserve “cold” air in ACE in summer, leading to a rapid warming of the layer. This is particularly the case when warm air is forced by wind to enter the ACE layer. One solution is to place a thin gravel layer on side slopes and to install ventilation pipes to connect ACE layer and the atmosphere (Jørgensen et al., 2008).

- Size of stones

If the size of the stones is too small, it will be difficult for the cold air to flow in ACE, having a limited effect on the cooling capacity and maybe no cooling at all. The stone size is directly affecting the permeability of airflow and effective thermal conductivity. In general, the determination of permeability needs three parameters, such as porosity, size gradation, and effective particle diameter d_{10} (Hazen, 1911). One of the common mathematical equations to relate permeability with the three parameters listed above is the Kozeny-Carman equation (Chapuis, 2004):

$$K = \frac{C}{f^2} d_{10}^{\,2} \frac{n^3}{(1-n)^2} \tag{1.8}$$

where f is the specific surface. The constant C depends on the fluid properties and the geometry of the pore channels. For the arrangements of spheres of uniform size, C/f^2 is suggested to be 0.0056 (Côté et al., 2011).

Fair et al. (1993) proposed the equation of permeability considering all the size gradations following the work of Poiseuille on hydraulic flow in materials, cited by Goering (2002):

$$K = \frac{1}{5}\left[\frac{(1-n)^2}{n^3}\left(\frac{\beta}{100}\sum\frac{P}{D_a}\right)\right] \tag{1.9}$$

where K, n, and P are permeability, porosity, and the percentage of stone by weight held between adjacent stone limits, respectively. D_a, β are the geometric mean of stone size, and stone shape factor for irregular stone grain, respectively. The values of β is shown in Table 1.1 (Goering, 2002).

Table 1. 1: Values of shape factor, β (Goering, 2002).

Shape of stone	Shape factor	Ration to spherical factor
Spherical	6.0	1.00
Rounded	6.1	1.02
Worn	6.4	1.07
Sharp	7.0	1.17
Angular	7.7	1.29

In general, permeability increases with the stone size (Goering, 2002; Côté et al., 2011). Lab and field experiments, and also numerical simulations have been carried out to determine its effect on the cooling

capacity (e.g., Goering and Kumar, 1999; Zhang et al., 2007). Since uniform stone size assures maximum permeability, the stones used should have a similar particle size range, as much as possible. For practical engineering application, the ideal ACE is composed of 150-300 mm angular stones (McGregor et al., 2010), assuring a high voids ratio (voids vs. stones) and a better cooling rates during winter.

- Thickness of rock layer

There are two very important parameters, Rayleigh number (Ra) and Nusselt number (Nu) to assess the strength of wintertime air convection. There is a critical Ra triggering the air convection in porous medium, described in Section 2.3. Since ACE does not have the same physical domain and thermal boundaries described above, air convection in ACE occurs at a lower Rayleigh number. In the field site, the critical Rayleigh number drops to as much as 20 or 13 (Saboundjian and Goering, 2003). Increasing ACE thickness provides a larger value of Ra , resulting in stronger natural convection to extract heat from permafrost underneath transportation infrastructure.

- ACE configuration

In current practice, ACE has been used in three different configurations: interlayer or full-width ACE, ACE on side slopes, ACE on toes and U-shape ACE (Figure 1.10). ACE on side slopes is mostly used to cool the ground soil underneath the side slopes, considering the permafrost degradation usually first occurs around the toe of embankments due to the insulation of the snowpack. The overlying sand and gravel directly affect the efficiency of the interlayer ACE. U-shape ACE combines all the benefits of the two other configurations (M-Lepage, 2015). The required embankment thickness should be at least an order of 1.5 m to 2.0 m to obtain adequate wintertime heat extraction (Esch, 1996).

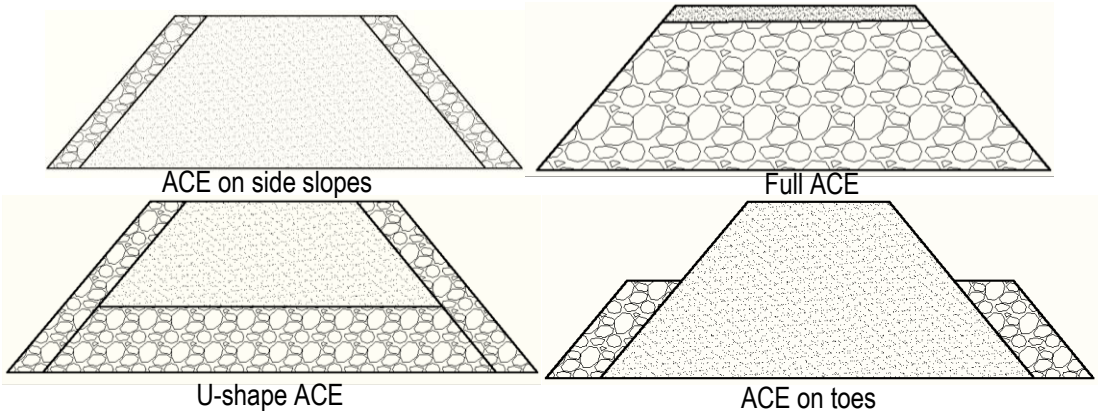

Figure 1. 10: Four ACE configurations.

1.4.1.2 Air duct system

The thermal conductivity of snow is relatively low, compared to that of the soil. Air duct systems (Figure 1.11a) placed in the embankment shoulders, have been used to generate natural convection and promote ground cooling to counteract the insulation of snow cover. In winter, airflow is induced by the temperature difference and air circulation facilitates heat extraction from the ground. In summer, the air inlets and outlets need to be closed to prevent warm air from flowing into the system and warming the surrounding ground. Researches on air duct systems have been carried out as early as the 1980s. Both field experiments at Bonanza Creek (Esch, 1983) and on Alaska Highway near Northway (Zarling et al., 1988) indicate that a bigger diameter seems to have a better heat extraction capacity, and both reduced lateral spreading and cracking problems, but without eliminating those. A more recent experimental test site was constructed at Beaver Creek, Yukon in 2008. The embankment with air duct system has a thickness of about 6.0 m and a length of 54 m. The diameter of the pipes is 0.75 m, and it has a longitudinal length of 18 m and is buried underneath the shoulder. One end of the culvert section is connected to an air inlet buried perpendicular to the embankment alignment towards the toe of the slope, and to the vertical air outlet placed in the shoulder about 2.0 m above the pavement surface. The temperature data collected at the test site from 2008 to 2011 indicates that air duct system has elevated the permafrost table by between 1 and 3 m (Coulombe et al., 2012). It has proven to be one of the most effective techniques used in Beaver Creek (M-Lepage, 2015; Doré et al., 2016).

Airflow is due to the pressure gradient generated by the temperature difference between the air in the longitudinal section of the culvert and the air at the outlet. The net pressure is balanced by velocity pressure and frictional pressure. The velocity is expressed as (Zarling, 1984):

$$V = \left[4gh/(1+ fL_e/D)\left[(T_0 - T_i)/(T_0 + T_i)\right]\right]^{\frac{1}{2}} \tag{1.10}$$

where V, D and L_e are average air velocity, inside duct diameter and equivalent length of duct, respectively. T_0, T_i, f are outside temperature, inside temperature, and Darcy-Weisbach friction factor respectively. h, g are stack height and gravity acceleration, respectively. Based on the Equation (1.10), several main factors affecting the velocity of air flow are listed:

- Duct diameter – The larger diameter decreases the average airspeed, however, it increases the cross section area, which allows more air flow inside the system. Ducts as large as 1.0 to 1.5 m in diameter would have the best useful life cycle and would resist plugging by snow, water or ice (Esch, 1996).
- Duct length - The airspeed can slow down with the length. But for economic considerations, the rational length should be selected.

- Stack height - A taller stack will increase the chimney effect pressure difference, resulting in greater air flow, which was confirmed by field experiments (Zarling et al., 1984)
- Smoothness of air duct inner wall - The airspeed can increase with surface smoothness. For airflow with low velocity, laminar flow dominates.

Another type of ventilation ducts used is the horizontal air ducts transversely embedded in the embankment (Figure 1.11b). This design configuration along Qinghai-Tibet railway takes advantage of the local windy environment. The yearly average wind velocity is about 4.0 m/s with wintertime wind speed much stronger than summertime wind speed (Qin and Zhang, 2013). Both field observations and simulations indicate that air duct system has a great capacity to decrease soil temperatures. Cheng et al. (2008) indicate that the cooling capacity of the air duct system enabled permafrost table to move up close to where the original ground surface used to be. Based on numerical modeling, Lai et al. (2004) indicate that air ducts with 0.4 m diameter and 2.0 m spacing and placed 1.0 m above the natural ground, could compensate the 2.0 °C effect of global warming, and maintain permafrost stability for the next 50 years.

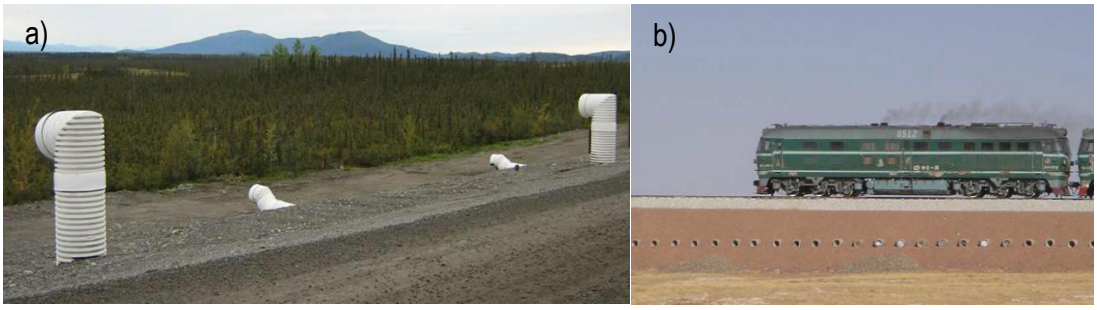

Figure 1. 11: Air duct systems (a) used along Alaska Highway in North America; (b) used along Qinghai-Tibet railway in China.

1.4.1.3 Heat drain

Heat drain, an innovative technique, is proposed by Pavement Engineering Research Group of Laval University in the early 2000s. It uses a 25 mm thick geocomposite with high permeability made of the corrugated plastic core covered on both sides by geotextile (Figure 1.12a). The main purpose of this technique is to promote the winter-time heat extraction in winter by providing one airflow channel in the embankment. The system involves a flat section (2% slope) to collect heat from the ground and a steeper section (45° slope) to create a chimney effect in the drain (Doré et al., 2016) (Figure 1.12b). Heat drain can be placed in the embankment shoulder or underneath the full embankment width. Inlet and outlet pipes are connected to the geocomposite to enable cold air flow into and warm air flow out of the heat drain system in winter.

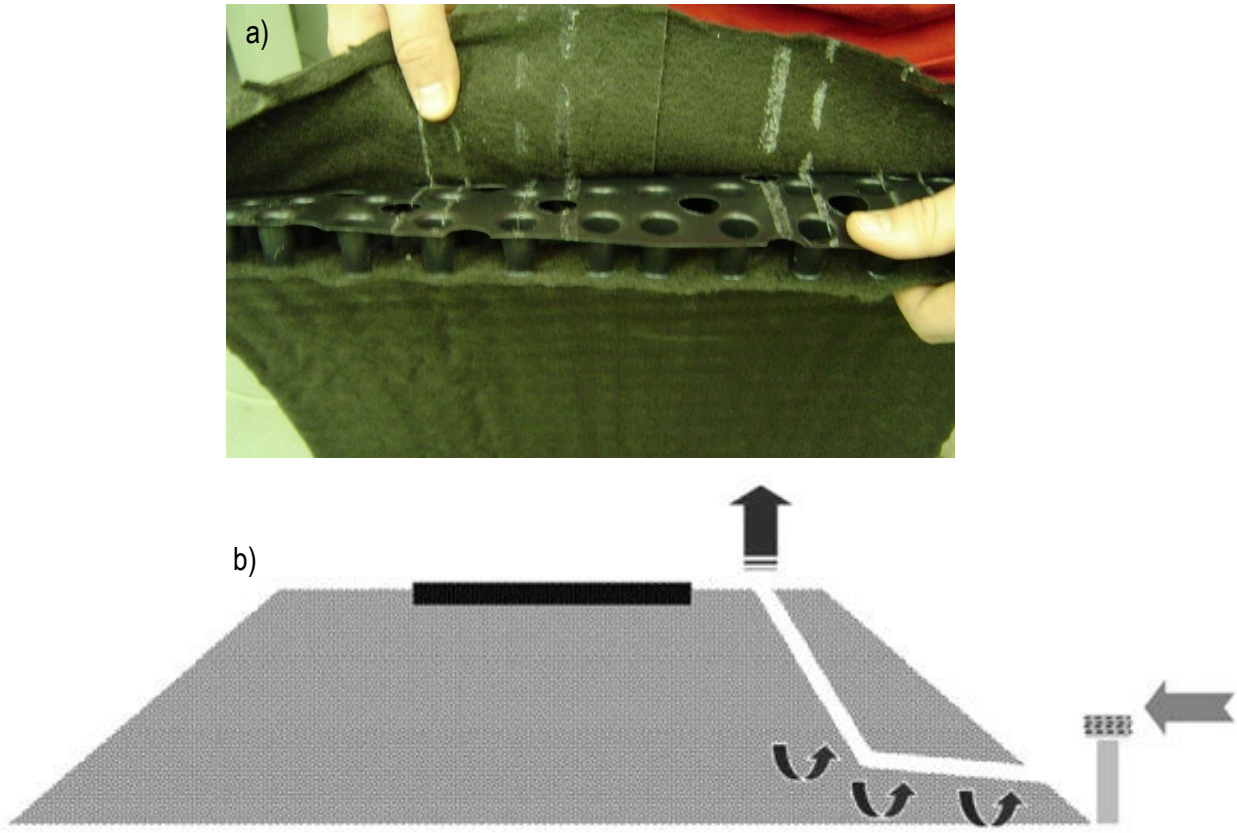

Figure 1. 12: heat drain; a) 25 mm-thick heat drain made of a corrugated plastic core covered by geotextile (Beaulac, 2006); b) Schematic diagram in the shoulder of embankments (Jørgensen et al., 2008).

Field experiments, lab experiments and numerical simulations were carried to test the heat extraction capacity and all the results show that heat drain has a good potential to decrease soil temperatures (Beaulac and Doré, 2006; Jørgensen et al., 2008; Chataigner et al., 2009). Chataigner et al. (2009) carried out 2D numerical simulations for an embankment with heat drain placed in the side slope. The air temperature of -35 °C, bottom temperature of 0 °C and a constant thermal conductivity of k=1.98 W/m-K, were used in the model. Sensitivity analyses were carried out to determine the effect of specific parameters on the thermal effectiveness. The numerical result shows that heat extraction capacity had a close relationship with length, inclination angle, thickness of heat drain and the temperature difference between sub-grade soils and external air temperature. The maximum thickness commercially available (25 mm) appears to be optimal for drain performance, and that thickness is typically used in engineering applications of the heat drain.

The first field application was in 2007 at Tasiuaq airstrip, Northern Quebec (Figure 1.13) with a 50 m long section. The measured data shows that heat drain decreased the ground temperatures both in summer and winter, and raised permafrost table (Jørgensen, 2009). A larger scale application (about 933 m) was carried out at Salluit, Northern Quebec (Figure 1.14). The measurements indicate that it was effective to stabilize the underlying soils during the monitoring period of 3 years (Périer et al., 2016).

Figure 1. 13: Installing heat drain in the shoulder of Tasiujaq airstrip, Northern Quebec, Canada.

Figure 1. 14: Installing heat drain in the shoulder of the embankment at Salluit, Northern Quebec, Canada.

1.4.1.4 Thermosyphons

Thermal conduction, convection, condensation and evaporation, are heat exchange processes used in thermosyphons. It consists of a sealed, fluid-filled tube with an upper part above the ground working as a condenser and a buried part in the ground functioning as an evaporator, utilizing the phase changes of a single fluid/gas system inside the tube. Refrigeration gas typically used are ammonia, carbon dioxide, propane in liquid and gas phase, and different working fluids have different heats of vaporization, vapor, liquid density and liquid thermal properties. The carbon dioxide (CO_2) is the most commonly used working fluid, due to its low maintenance cost, no operation cost and low environmental impact (Forsström et al., 2002). Thermosyphons

work when the ground temperature is at least 1 °C higher than air temperature allowing the refrigeration liquid to boil and change into gas, leading to evaporation in the upper part of the pipe that extends out of the ground and bringing heat along (Calmels et al., 2016). Then, the gas condenses due to the lower air temperature and flows by gravity down into the pipe (Figure 1.15) and, the cycle is repeated. Thermosyphons are dormant when the air temperature is higher than the ground temperature. The radiator should be placed high enough above the snow thickness to take advantage of winter wind. To limit the summertime thawing, it is recommended to combine thermosyphons with an insulation technique (Esch, 1996). There are four types of thermosyphons available, including vertical, sloped, flat-looped thermosyphons and thermopile (Figure 1.16). For the sloped thermosyphons, the inclination of the evaporator pipe should be at least 6% downward near the base of the embankment to facilitate the fluid flow. The evaporator pipe sections should be ideally a little above the top of the underlying permafrost table in the compacted sand or a gravel pad, to help provide thermal effectiveness to raise permafrost table and avoid the difficulty of installing evaporator in the permafrost layer as well (Esch, 1996). Thermosyphons have a limited influence distance, which is highly related to ground soil properties, and the lateral spacing between evaporator pipes should be less than twice the radial freezing distance (Esch, 1996).

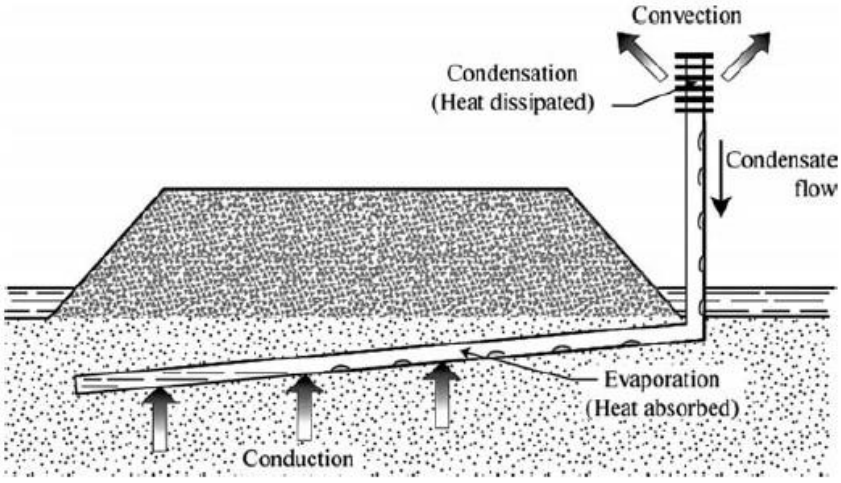

Figure 1. 15: The working principle of thermosyphon (Doré and Zubeck, 2009).

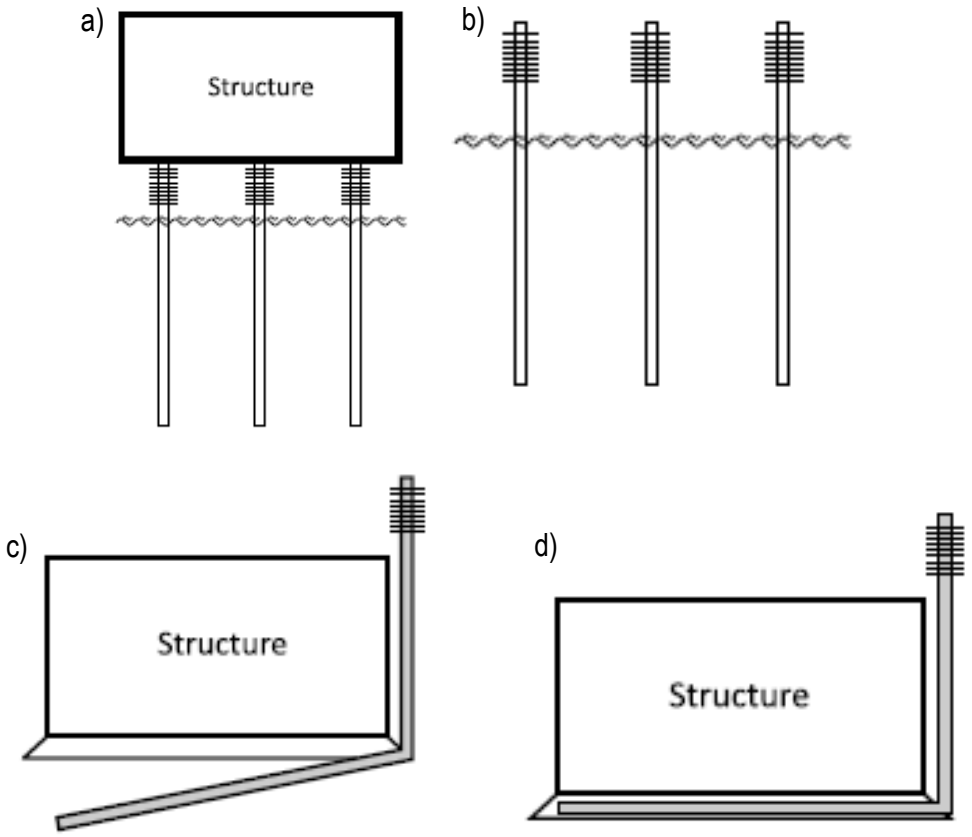

Figure 1. 16: Four types of thermosyphons: a) Thermopile; b) Vertical; c) Sloped; d) Flat looped (Canadian Standards Association, 2014).

Thermosyphons have been studied since the 1950s and it has been wildly applied in Alaska and Canada (M-Lepage, 2015). The application of thermosyphons in China, Russia started in the 1970s (Wu et al., 2010) and 1990s (Popov et al., 2010), respectively. The best-known, largest installation of thermosyphons is the Trans-Alaska Pipeline (completed in 1977) with 124,300 units (Heuer, 1979). The locations of thermosyphons application until 2008, in Alaska, are shown in Figure 1.17. One downside part of thermosyphons is the high cost (typically $1500/unit, Beaulac and Doré, 2006), making it more suitable for severe localized problems (Calmels et al., 2016). In general, for infrastructures such as airports and railways where tolerance for thaw settlement is low, thermosyphons and hairpin thermosyphons maybe one good solution to stabilize embankments (McGregor et al., 2010). To reduce the cost, it is recommended to maximize the length of the evaporator pipe sections (Esch, 1996). The security of road users and aircraft can be affected by the presence of condensers along the infrastructure. A solution is to bury this part underneath the embankment surface using hairpin thermosyphons (McGregor et al., 2010) (Figure 1.18).

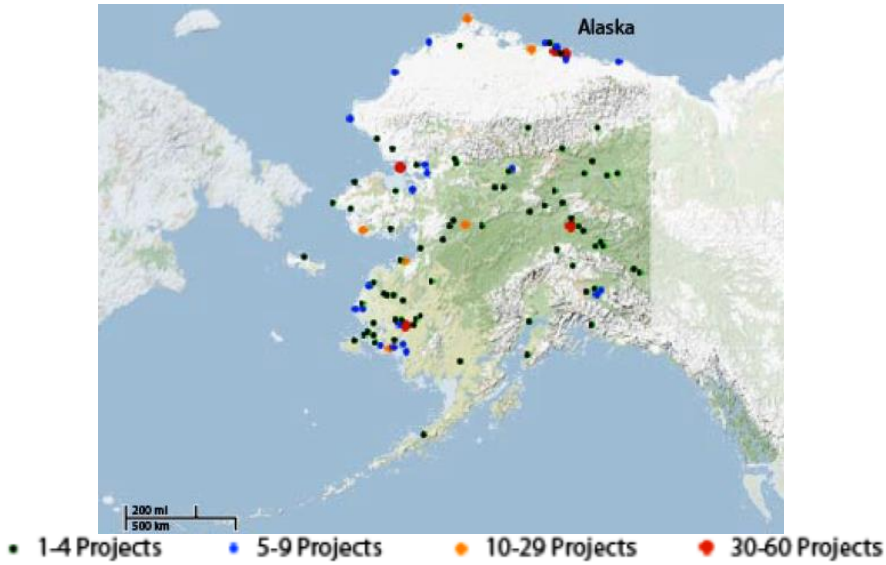

Figure 1. 17: Installation of thermosyphons by Arctic Foundation Inc in Alaska (Wagner, 2014).

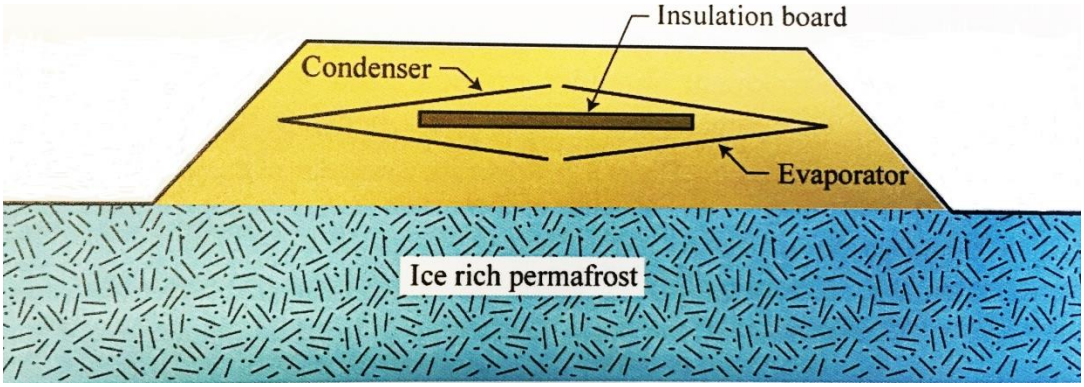

Figure 1. 18: Hairpin thermosyphons (McGregor et al., 2010).

1.4.2 Methods based on reducing heat intake underneath embankments

Solar radiation acting on embankments is one of the main factors causing permafrost degradation (Doré and Zubeck, 2009). These techniques aim to impede the heat transfer through the embankment core, pavement surface and sides slopes and thus reduce the risk of degradation.

1.4.2.1 Insulation

The purpose of insulation is to protect the top part of permafrost (Doré and Zubeck, 2009). The plastic insulation was first initiated in the 1960s by Dow Chemical Company (Esch, 1996). This technique takes advantage of the low thermal conductivity of materials such as polystyrene with a value of 0.03 W/°C and polyurethane with a value of 0.0197 W/°C. It is mainly used to reduce heat intake in summer, while it also impedes heat flowing out of the foundation in winter (Figure 1.19). In cold permafrost regions, reducing wintertime heat flow out of the ground can have a limited effect, but not in warm permafrost regions (Doré and Zubeck, 2009). Insulation may be useless in warm permafrost regions (Nidowicz and Shur, 1998), and it

should be combined with other techniques. It was first tested in Alaska in 1969 in an experimental embankment, and the thaw depth was largely reduced (Esch and Rhode, 1976). Polystyrene is one of the most popularly used insulation materials and it has been used to preserve permafrost along roadways and airstrip since 1970. It would be more effective to reduce thaw depth if placed close to the surface. However, it is susceptible to mechanical damage from cyclic wheel loading. Therefore, it should be installed at a suitable depth, which is mainly determined by the vehicle or aircraft loading, the pavement type, thickness, and its mechanical compressive strength. The recommended minimum depth below the surface ranges from 0.4 m to 1.0 m (Esch, 1996). Polyurethane insulation has the potential to significantly reduce the shipment costs, but it absorbs water and can be compressed in the embankment fill with time (Doré and Zubeck, 2009).

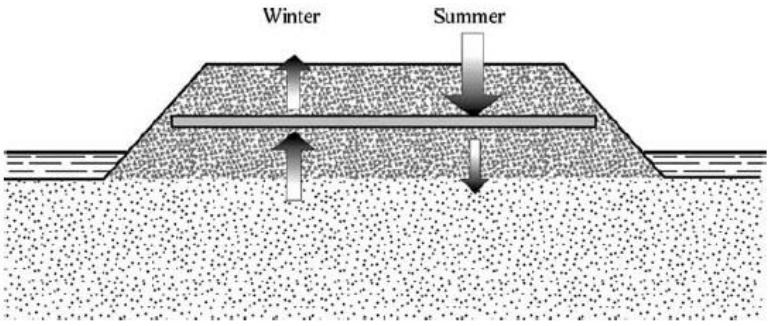

Figure 1. 19: The thermal imped of heat transfer in the embankment fill (Doré and Zubeck, 2009).

Peat is a natural organic insulation material found at most construction sites in arctic regions. The higher latent heat, the larger frozen thermal conductivity (approximately twice) than unfrozen thermal conductivity leads to the faster heat flows out the ground in winter than that flows into the ground in summer, resulting in lower soil temperatures. The peat is generally removed during the construction of transportation infrastructure in most cases. In a field experiment conducted in Alaska, peat was removed from the ground surface and the behavior of the section was compared to an adjacent undisturbed section over a 26-year monitoring period. The results indicate that the permafrost table was lowered by 5.7 m, compared to the undisturbed section (Linell, 1973 cited by M-Lepage, 2015). Another test was done recently along Alaska Highway at Beaver Creek, Yukon in 2008. Grass seed was planted on the side slopes of a 50 m long experimental embankment. The first 2 years of monitoring indicates that the permafrost table has not changed significantly, compared to the important degradation observed at the reference section (M-Lepage, 2015).

1.4.2.2 Increasing embankment thickness

The backfill material has a relatively low thermal conductivity. The most common way to protect embankments against permafrost degradation is to contain the active layer by increasing backfill (gravel) thickness (Zarling et al., 1988). To determine the thickness, site-specific thermal modeling needs to be made or experience-based

judgments need to be used. In the ice-rich, warm permafrost regions, the recommended minimum backfill thickness should be at least 1.5 m to 2.0 m (Doré and Zubeck, 2009). However, the method becomes uneconomical when the mean annual surface temperature is around 0 °C (McGregor et al., 2010).

1.4.2.3 High albedo surface

Albedo is defined as the ratio between the reflected and the incident solar radiation, and it ranges between 0 (perfectly absorbing) and 1.0 (perfectly reflecting). The principle of high albedo surface is to increase the amount of reflected solar radiation. The research (e.g., Alaska Dot, Technical University of Denmark, Université Laval) indicated that high albedo surface a very high potential to preserve permafrost. The benefit of this technique is affected by many factors, such as latitude, cloud cover, wind and traffic speed (Berg, 1985). In general, the values of albedo is 0,15 (0,10-0,18) for a normal bituminous pavement surface, however, it can be increased to around 0,55 (0,40-0,60) for pavement with packed snow on the surface (Doré and Zubeck, 2009). Albedo can be increased on a paved surface by using white paint or other types of high albedo surfacing materials tested in different places, such as Alaska, Greenland Norway and Canada. For example, paint application decreased the average pavement temperature by 1.0 °C on Peger Road in Fairbanks, Alaska (Esch, 1996), and the thaw depth was reduced by 0.4 m along Svalbard airport, Norway (Molmann et al., 1998). The thermal model development using the simplified surface energy balance approach and the measurement of thermal, mechanical properties of high albedo surface have been recently done by the Arquluk program at Université Laval (Dumais and Doré 2016; Richard 2018). Compared to the warming foundation soil at the reference section, high albedo surface decreased the ground temperature by 1.2 °C at the embankment-soil interface and permafrost table was stabilized in the first 3 years' application along Alaska Highway at Beaver Creek, Yukon (M-Lepage, 2015). However, there are many problems, such as high cost associated with the application and the maintenance of the surface as well as safety concerns due to the possible slipperiness of the pavement surface. The albedo of these materials tends to decrease rapidly fast if no annual road maintenance is applied.

1.4.2.4 Sun shed

Sun shed prevent solar radiation from reaching the soil surface and also prevent snow accumulation on the side slope in winter allowing cold air to circulate directly at the ground surface during winter. It can also prevent rainfall from seeping into embankments in summer. Sun shed can be used to decrease the soil temperatures underneath side slopes, and thus avoids cracking and lateral spreading.

Sun sheds were applied on the slopes of an experimental embankment in 1983 at Bonanza Creek, Alaska, located in warm permafrost conditions. The sheds showed a good thermal effect with mean annual slope temperature reduced by 1.7 °C and aggradation of permafrost underneath the side slopes was observed

(Esch, 1996). The effectiveness was also observed along the Alaska Highway at Beaver Creek, Yukon. The active layer thickness was reduced by 1.5 m in the first year after the construction (M-Lepage, 2015). Even though it has a good thermal potential, it is not applied widely due to many problems, such as high-construction cost, high maintenance cost, short-term durability and safety concerns. Sun shed is considered impractical in Alaska, due to safety concerns (Doré and Zubeck, 2009). There are limited applications along Qinghai-Tibet Highway where the radiation is very high and where forced convection due to strong winds can lead to embankment degradation (Ma et al., 2009). Compared to other techniques, the cost of the system is moderate (Beaulac et al., 2004). Some remediation can be better with some specific linear infrastructure. When applying sun shed, guardrails may be required along infrastructure embankments to prevent risks of vehicles accidentally running out of road surfaces. Sun sheds seem more suited for train embankments, as there are not the same types of safety concerns involved.

1.4.3 Methods based on embankment reinforcement

Besides or in addition to the thermal protection described above, mechanical stabilization of embankments can also be considered.

1.4.3.1 Berms and gentle slopes

Several modifications can be made to the embankment cross section to improve the thermal and the mechanical performance of embankments in thaw sensitive permafrost conditions. Lateral berms can be placed at the base of the side slopes to improve material confinement and to improve thermal and mechanical behaviour of the embankment slopes. The berm provides additional granular material protection at the base of embankment slopes reduce snow accumulation and move water away at that critical location of the embankment. The berm has been tested and used in Alaska and is now extensively used in the Yukon. It was first studied at the Bonanza Creek in 1974 with a berm height of 1.8 m, and a temporary (1–3 years) reduction in thaw depth was observed (Esch, 1983). The berm can be constructed using crushed stones in order to take advantage of air convection. The construction of transportation embankments leads to snow accumulation on the side slopes and permafrost underneath side slopes becomes more vulnerable in the following summer. The general slope can be modified to reduce this detrimental effect. Side slope ratio with 1V:2H is generally selected for the design of embankments. Gentle slope can provide protection against temperature variation, reduce the snow accumulation and improve the thermal behavior of embankments (Doré and Zubeck, 2009). A slope with 1V:6H is required to provide cost-effective protection (Hoeve et al., 2004). In 2007, a 50 m-long gentle slope with 1H:8V was constructed at the Tasiujaq airstrip, Northern Quebec. After 3 years of monitoring, the active layer underneath the gentle slope has moved upward by 4.0 m, compared to that at the reference section (Doré et al., 2012). Both berm and general slope are likely to reduce the rotational movement of shoulders, and settlements, crackings on the pavement surface.

1.4.3.2 Geotextiles and geogrids

Geotextiles and geogrids are mainly used to reduce the differential settlements, to prevent lateral spreading and opening of longitudinal cracks in discontinuous permafrost regions. Their mechanical properties are not significantly affected by the freeze-thaw cycles and the installation is low cost (Bell et al., 1984). The danger of sudden failure to the embankment due to the breaking of geosynthetics under repeated vehicle load is a problem, and the strongest material is recommended to resist the progressive forces developed by the thawing of permafrost (Esch, 1996).

1.4.4 Other methods

They include techniques applied during the construction stage, such as pre-thawing, excavation/replacement and intensive maintenance.

1.4.4.1 Pre-thawing

This method is used to thaw the shallow ice-rich frozen soils, prior to the construction of embankments, and it should be avoided for the deep ice-rich permafrost layers. The vegetation is first removed to expose the ground surface to the solar radiation. To help accelerate the thawing process, the thin gravel layer and the asphalt coating are generally used to improve the amount of heat flowing into the ground (Esch, 1996). The problems of this method are that the process is long and labour-intensive. Pre-thawing also involves a complex drainage management and it is not easy to anticipate the final results (Beaulac and Doré, 2006).

1.4.4.2 Extraction/replacement of permafrost

The excavation/replacement is used to replace limited extent massive ice or ice-rich permafrost with non-susceptible soils. It is one of the best methods to reduce thaw settlements (Beaulac and Doré, 2006). This technique is expensive and granular materials need to be available around the construction site.

1.4.4.3 Build and maintain

The most frequently used method is to build an embankment with an adequate structural design but inadequate thermal protection (Doré and Zubeck, 2009). Important embankment movement should be expected and compensated by intensive maintenance.

1.4.4.4 Gravel-surfaced roads

Gravel-surfaced roads have a higher albedo than asphalt-based surfacing materials and absorb less heat from the solar radiation reducing thus permafrost degradation compared to asphalt-paved roads. However, more maintenance is required and the road conditions are also largely affected by vehicle loads, resulting in a lower level of service to road users (Doré and Zubeck, 2009).

1.4.4.5 Snow removal

Snow accumulates along the roadways in winter, which impedes heat to flow out of the ground, leading to permafrost degradation. If the slopes are designed to accommodate maintenance vehicles (gentle slopes or berms), snow-clearing on embankment slopes can be considered as an alternative strategy to protect permafrost. This strategy is however labour-intensive and it needs to be done regularly and maintained over the service life of the embankment to assure effective protection of the permafrost (M-Lepage, 2015).

1.5 Summary of the considerations for method implementation

Engineers select the stabilization methods based on many factors, such as permafrost context, construction/maintenance cost, materials, application conditions and thermal or mechanical benefits, etc. The cost, maintenance, effectiveness, implementation considerations, thickness requirements and strength/durability are summarized in Table 1.2 (McGregor et al., 2010) and Table 1.3 (Calmels et al., 2016). Please note that the cost highly depends on many factors, such as site conditions, available resources and materials availability (Doré and Zubeck, 2009).

Table 1. 2: Applicability, cost and maintenance (McGregor et al., 2010).

Mitigation technique	**Cost of Construction**		**Maintenance**
	Discontinuous permafrost (warm)	Continuous permafrost (cold)	
Air convection embankment	$$$$	$$$$	Low
Heat drain	$$$$	$$$$	Low
Air duct with chimney	$$$$	$$$$	Moderate
Thermosyphons	$$$$$	$$$$$	Moderate
Insulation	$$$	$$$	High
Embankment Thickening	$$	$	NA
High albedo surface	$$$	$$$	High
Sun shed	$$$	$$$	High
Berms and gentle slopes	$$$	$$$	Low
Geotextiles and geogrids	$$$$	$$$$	Low
Pre-thawing	$$$	$$$	NA
Extraction/replacement	$$$	$$	NA
Build and Maintain	$$$	$$	NA
Snow removal	$$$	$$$	NA

Table 1. 3: Effectiveness, implementation considerations, height requirements and strength/durability considerations (Calmels et al., 2016).

Techniques	Effectiveness	Strength / Durability considerations	Implementation Consideration	Embankment height/Depth requirement
Air convection embankment (ACE)	Depends on the design. Rising mean annual ground temperature generates more cooling. Measurable rise of permafrost table and decrease of embankment temperature. Less severe settlements and stabilization over time.	The high strength of the stones makes it suitable for many conditions such as heavy loads and it also provides very low maintenance. If settlement happens, it will lose efficiency but will keep working.	Uncovered ACE is sensitive to intrusion by fine soils. Local availability of suitable aggregates may be problematic. Orientation of embankment with respect to intensity of solar radiation and wind direction should be considered when designing ACE	Minimum height of 2.5 m.
Heat drain	Measurable rise of permafrost table and decrease of embankment temperature.	During installation, a layer of sand must be carefully placed on HD for protection. Must avoid puncture or compression by heavy equipment.	Labour-intensive (manual installation). Avoid installations during windy days. Need to carefully follow the design of heat drain and avoid destroying heat drain during its construction.	Minimum height of 2.0 m.
Air duct with chimney	Measurable decrease of surface temperature around the system. Mainly affect soils around the system.	The pipe makes it susceptible to the damage during the installation.	Susceptible to plugging from snow, debris, surface water and groundwater infiltration. Minimized performance due to thaw settlements, water ponding. The inlet and outlet should be closed in summer. Duct as large as 1.0 m to 1.5 m in diameter.	Minimum height of 2.0 m.

Table 1.3: Effectiveness, implementation considerations, height requirements and strength/durability considerations (Calmels et al., 2016) (Cont.).

Techniques	Effectiveness	Strength / Durability considerations	Implementation Consideration	Embankment height/Depth requirement
Thermosyphons	Measurable rise of permafrost table and decrease of embankment temperature	If a puncture of the tube occurs, the pressurization is lost and the tube will no longer function correctly	Angle of inclination, spacing and length must be adjusted to the site conditions. Susceptible to damage and vandalism	NA
Insulation	Promote thermal stability and delays thawing. May not reverse the global warming trend	Sensitive to mechanical damage. Insulation material has to be installed deep enough to prevent crushing from cyclic wheel loadings and to reduce the risk of differential icing at the surface of the pavement.	Avoid trapping heat in the ground under the insulation layer by implementing in winter/early spring. Relatively easy to construct. Insulation properties may be reduced by the potential for water absorption and compression or breaking of the material. Insulation layer thickness, width, and embedded depth must be adjusted to site conditions.	Depth of insulation varies from 0.5 m above the natural ground surface to 0.8 m below the embankment surface.
Embankment Thickening	Measurable decrease of ground temperature. Slow down the rate of permafrost thawing	NA	Recommend to build a wider embankment to keep the integrity	Minimum height of 1.5 m to 2.0 m in warm permafrost regions
High albedo surface	Measurable decrease of surface temperature.	Durability has a close relationship with the material quality.	Availability of light-colored aggregate may be problematic. High albedo coatings need to respect specification for northern use.	NA

Table 1.3: Effectiveness, implementation considerations, height requirements and strength/durability considerations (Calmels et al., 2016) (Cont.).

Techniques	Effectiveness	Strength / Durability considerations	Implementation Consideration	Embankment height/Depth requirement
Sun shed	Measurable decrease of surface temperature	Easy to install. Short-Term durability and safety concerns could be a problem.	Susceptible to high wind speed. Avoid installations during windy days	NA
Berms and gentle slopes	Reduce spreading, settlements and cracking on the roadway surface.	NA	More efficient if crushed stones available to make air convection occur in berms and general slopes. Granular material needs to be available	NA
Geotextiles and geogrids	Have the potential to prevent longitudinal cracks. Likely to reduce settlement and cracking problems.	Once broken, not useful anymore.	Strong materials are required to resist the forces developed as permafrost thaws and soil consolidates. Material with enough forces maybe problematic. Mainly applied in discontinuous permafrost regions	NA
Pre-thawing	Depend on the thawing methods and soil conditions.	NA	Possible solution if time permits. Difficult to anticipate the final results	NA
Extraction/Replacement of permafrost		NA	To be cost-effective, non frost-sensitive gravel material should be available around the site	NA
Build and Maintain		NA	NA	NA
Snow Removal		NA	Need to design side slopes that can accommodate this method	NA

Note: NA- not applicable.

1.6 Design tools for convective techniques

The prevailing design consideration for embankments and structural design of pavements in permafrost regions is to keep the long-term thermal stability of the underlying permafrost (Doré and Zubeck, 2009). The application of convective techniques may increase the construction cost, compared to that for conventional embankments, however, it decreases the maintenance cost in a long-term period and ensures the infrastructure stability and integrity.

Design procedures are vital to allow for adequate design of protection methods. Overdesign and underdesign of protection systems can lead to expensive construction or poor performance and low level of service of the structure. Optimal design is likely to maintain structural integrity at a reasonable cost. Until now, limited design procedures have been proposed for sound and reliable design of convective techniques. Design procedures for heat drain and air duct systems are currently not available (Doré et al., 2016). Design procedures for thermosyphons have been well developed by Arctic Foundation Inc. and a design thermal analysis software is available. Good knowledge on heat transfer processes involved is needed to design thermosyphons and it is recommended to select a highly experienced engineering company to prepare a report on the technical background, design and construction information to assist designers (Holubec, 2008).

ACE, as indicated above, works as a simple and effective system to extract heat from the ground in winter. A Microsoft Excel spreadsheet (Figure 1.20) has been proposed for the design of ACE by University of Alaska Fairbanks. It is based on the concept of thermal offset, namely the temperature difference between annual average temperatures at the top and at the bottom of an ACE layer. The mean annual surface temperature of a snow-cleared embankment is often above 0 °C and the thermal offset for conventional embankments is generally approximately 0 °C. The design is to ensure the annual average temperature at the bottom of the ACE layer is below freezing point with a sufficiently large thermal offset (McHattie and Goering, 2009). The design objective is to use an ACE layer with sufficient thickness to keep permafrost frozen (McHattie and Goering, 2009). This proposed design spreadsheet presents an user-friendly methodology to design thermal protection using ACE without the need of thermal modeling. However, maintaining the frozen state of soil at the embankment-soil interface cannot ensure permafrost degradation does not happen. Sun et al. (2005) have carried out numerical simulations on the effect of crushed rock layer thickness on the cooling effect of natural convection in the ballast along the Qinghai-Tibet railway, China, however, no model calibration and validation were presented. These models have been specified to use the soil parameters and air temperature on Tibet plateau, and the selected stone sizes are from 2-4 cm, 4-6 cm, 6-8 cm and 8-10 cm, respectively. The convection index is proposed and defined as a cumulative temperature parameter φ in winter to quantify the strength of air convection in an ACE layer. The convection index φ is expressed as (Sun et al., 2005):

$$\varphi = \int_{t_1}^{t_2} (\theta_1 - \theta_2 - \Delta\theta_c) dt \tag{1.11}$$

where θ_1, θ_2 are yearly harmonic temperatures at the top and bottom of embankments, respectively. $\Delta\theta_c$ is the critical temperature difference between the top and bottom of embankments, triggering the air convection in winter (Figure 1.21). The numerical results show that for a range of embankment thickness, the convection index increases quickly with the thickness, however, when the thickness reaches a certain value (approximately 5.0 m), its impact is limited. This research gives us a general idea that increasing ACE layer thickness could be a good solution to increase convection index of ACE, but no information on how to use convection index in the engineering application is given.

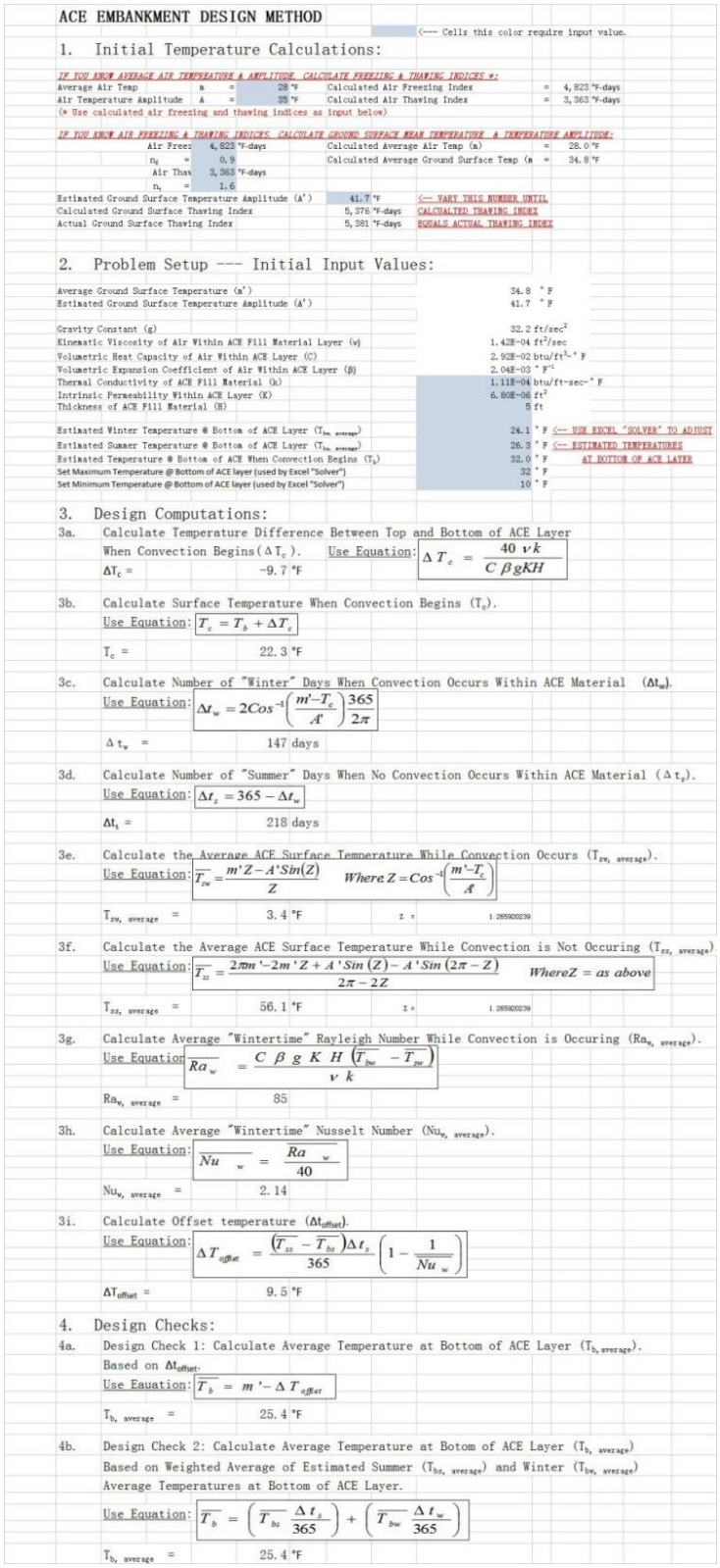

ACE EMBANKMENT DESIGN METHOD

<--- Cells this color require input value.

1. Initial Temperature Calculations:

IF YOU KNOW AVERAGE AIR TEMPERATURE & AMPLITUDE, CALCULATE FREEZING & THAWING INDICES #:

Average Air Temp	n	=	28 °F	Calculated Air Freezing Index	=	4,823	°F-days
Air Temperature Amplitude	A	=	35 °F	Calculated Air Thawing Index	=	3,363	°F-days

(* Use calculated air freezing and thawing indices as input below)

IF YOU KNOW AIR FREEZING & THAWING INDICES, CALCULATE GROUND SURFACE MEAN TEMPERATURE & TEMPERATURE AMPLITUDE:

Air Freez	4,823	°F-days	Calculated Average Air Temp (n)	=	28.0	°F	
n_f =	0.9		Calculated Average Ground Surface Temp (n	=	34.8	°F	
Air Thaw	3,363	°F-days					
n_t =	1.6						
Estimated Ground Surface Temperature Amplitude (A')		41.7 °F	<-- VARY THIS NUMBER UNTIL				
Calculated Ground Surface Thawing Index		5,376 °F-days	CALCULATED THAWING INDEX				
Actual Ground Surface Thawing Index		5,381 °F-days	EQUALS ACTUAL THAWING INDEX				

2. Problem Setup --- Initial Input Values:

Average Ground Surface Temperature (n')	34.8	°F
Estimated Ground Surface Temperature Amplitude (A')	41.7	°F
Gravity Constant (g)	32.2	ft/sec²
Kinematic Viscosity of Air Within ACE Fill Material Layer (ν)	1.42E-04	ft²/sec
Volumetric Heat Capacity of Air Within ACE Layer (C)	2.92E-02	btu/ft³-°F
Volumetric Expansion Coefficient of Air Within ACE Layer (β)	2.04E-03	°F⁻¹
Thermal Conductivity of ACE Fill Material (k)	1.11E-04	btu/ft-sec-°F
Intrinsic Permeability Within ACE Layer (K)	6.80E-06	ft²
Thickness of ACE Fill Material (H)	5	ft
Estimated Winter Temperature @ Bottom of ACE Layer ($T_{bw,\ average}$)	24.1	°F <-- USE EXCEL "SOLVER" TO ADJUST
Estimated Summer Temperature @ Bottom of ACE Layer ($T_{bs,\ average}$)	26.3	°F <-- ESTIMATED TEMPERATURES
Estimated Temperature @ Bottom of ACE When Convection Begins (T_b)	32.0	°F AT BOTTOM OF ACE LAYER
Set Maximum Temperature @ Bottom of ACE layer (used by Excel "Solver")	32	°F
Set Minimum Temperature @ Bottom of ACE layer (used by Excel "Solver")	10	°F

3. Design Computations:

3a. Calculate Temperature Difference Between Top and Bottom of ACE Layer When Convection Begins (ΔT_c). Use Equation: $\Delta T_c = \frac{40\,\nu k}{C\,\beta g K H}$

ΔT_c = −9.7 °F

3b. Calculate Surface Temperature When Convection Begins (T_c).

Use Equation: $T_c = T_b + \Delta T_c$

T_c = 22.3 °F

3c. Calculate Number of "Winter" Days When Convection Occurs Within ACE Material (Δt_w).

Use Equation: $\Delta t_w = 2Cos^{-1}\left(\frac{m' - T_c}{A'}\right)\frac{365}{2\pi}$

Δt_w = 147 days

3d. Calculate Number of "Summer" Days When No Convection Occurs Within ACE Material (Δt_s).

Use Equation: $\Delta t_s = 365 - \Delta t_w$

Δt_s = 218 days

3e. Calculate the Average ACE Surface Temperature While Convection Occurs ($T_{sw,\ average}$).

Use Equation: $\overline{T_{sw}} = \frac{m'Z - A'Sin(Z)}{Z}$ $\quad Where\ Z = Cos^{-1}\left(\frac{m' - T_c}{A'}\right)$

$T_{sw,\ average}$ = 3.4 °F Z = 1.265920239

3f. Calculate the Average ACE Surface Temperature While Convection is Not Occuring ($T_{ss,\ average}$)

Use Equation: $\overline{T_{ss}} = \frac{2\pi m' - 2m'Z + A'Sin(Z) - A'Sin(2\pi - Z)}{2\pi - 2Z}$ $\quad Where Z = as\ above$

$T_{ss,\ average}$ = 56.1 °F Z = 1.265920239

3g. Calculate Average "Wintertime" Rayleigh Number While Convection is Occuring ($Ra_{w,\ average}$).

Use Equation: $\overline{Ra_w} = \frac{C\,\beta\,g\,K\,H\left(\overline{T_{bw}} - \overline{T_{sw}}\right)}{\nu\,k}$

$Ra_{w,\ average}$ = 85

3h. Calculate Average "Wintertime" Nusselt Number ($Nu_{w,\ average}$).

Use Equation: $\overline{Nu_w} = \frac{\overline{Ra_w}}{40}$

$Nu_{w,\ average}$ = 2.14

3i. Calculate Offset temperature (Δt_{offset}).

Use Equation: $\Delta T_{offset} = \frac{\left(\overline{T_{ss}} - \overline{T_{bs}}\right)\Delta t_s}{365}\left(1 - \frac{1}{\overline{Nu_w}}\right)$

ΔT_{offset} = 9.5 °F

4. Design Checks:

4a. Design Check 1: Calculate Average Temperature at Bottom of ACE Layer ($T_{b,\ average}$). Based on Δt_{offset}.

Use Equation: $\overline{T_b} = m' - \Delta T_{offset}$

$T_{b,\ average}$ = 25.4 °F

4b. Design Check 2: Calculate Average Temperature at Botom of ACE Layer ($T_{b,\ average}$) Based on Weighted Average of Estimated Summer ($T_{bs,\ average}$) and Winter ($T_{bw,\ average}$) Average Temperatures at Bottom of ACE Layer.

Use Equation: $\overline{T_b} = \left(\overline{T_{bs}}\frac{\Delta t_s}{365}\right) + \left(\overline{T_{bw}}\frac{\Delta t_w}{365}\right)$

$T_{b,\ average}$ = 25.4 °F

Figure 1. 20: Illustrations of the design Microsoft Excel spreadsheet proposed by University of Alaska Fairbanks.

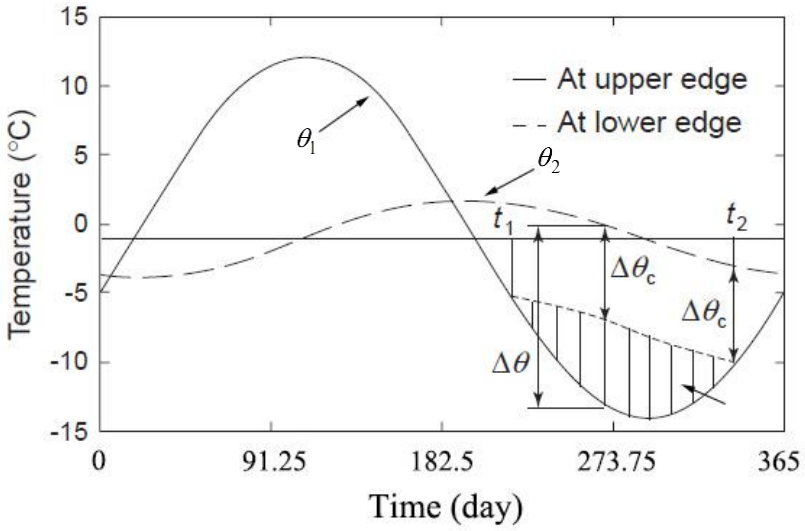

Figure 1. 21: Temperature difference triggering air convection (Sun et al., 2005).

Chapter 2 Research gaps and project objective

Although many promising techniques are available to prevent permafrost from thawing, there is very few sound and practical methods for the design of thermal protection using these techniques for transportation infrastructure in permafrost regions. Also, there is no tool to help engineers select the best technique considering the local context and local needs when permafrost is not stable. As discussed above for the proposed design procedures for ACE, maintaining the frozen state of soil at the embankment-soil interface does not guarantee long-term thermal stability of underlying permafrost.

Thermal stability of permafrost depends on the heat balance at the soil embankment interface, i.e. the total amount of heat flowing into or flowing out of the foundation. In this project, heat balance approach is proposed to help determine the thermal condition of conventional embankments and also allows select suitable techniques to extract at least the amount of extra heat flowing into the foundation for conventional embankments, if instability is observed or estimated.

The main goal of this project is to develop improved engineering design tools for convective techniques, especially ACE and heat drain. The proposed research methodology includes two steps: 1) the development of a heat balance estimation chart for conventional embankments to quickly analyze the thermal stability of infrastructure embankments built over thaw-sensitive permafrost, and 2) the development of heat extraction capacity charts for heat drain and ACE for thermal stabilization of infrastructure embankments in northern regions.

This thesis intends to advance the understanding of permafrost degradation underneath transportation infrastructure and to determine the ability of heat drain and ACE to mitigate the effects of permafrost degradation. More specifically, this project extends the existing knowledge by:

1) Proposing a new analysis framework based on the heat balance approach for conventional embankments.
2) Proposing a new design framework to assess the heat extraction capacity for convection techniques.
3) Proposing practical design charts for ACE and heat drain, for thermal stabilization of embankments on thaw sensitive permafrost.

Chapter 3 Thermal modeling of heat balance through embankments in permafrost regions

Foreword

Xiangbing Kong[1], Guy Doré[1], Fabrice Calmels[2]

[1]Department of Civil and Water Engineering, Laval University, Québec City, Québec, Canada

[2]Yukon Research Centre/Northern Climate ExChange, Yukon College, Whitehorse, Yukon, Canada

State: Published online

Journal: Cold Regions Science and Technique

Résumé

Le pergélisol est largement répandu dans l'hémisphère nord et, dû à plusieurs facteurs, la dégradation de celui-ci a actuellement lieu. Le site d'essais, construit en 2008 le long de l'Alaska Highway, à Beaver Creek au Yukon (Canada), fournit des informations précieuses sur la réponse thermique à long terme du pergélisol sous une infrastructure de transport, suite aux perturbations engendrées par la construction et les changements climatiques. Les données de températures collectées peuvent aussi être utilisées pour calibrer le modèle thermique permettant de mieux comprendre les effets relatifs de différents facteurs sur la sensibilité du régime thermique du sol sous les infrastructures de transport, dans un contexte de changements climatiques. Un modèle 2D à éléments finis de conduction de chaleur, tenant compte du changement de phase eau-glace, a été développé basé sur les caractéristiques et les conditions du site expérimental de Beaver Creek. Pour améliorer la précision du modèle, des paramètres spécifiques au site, tel les propriétés du sol, la température de l'air près de la surface et les dimensions du remblai, ont été mesurés et utilisés comme paramètres d'entrée. Après la calibration du modèle, une analyse de sensibilité de certains paramètres d'entrée, tel la température de l'air, l'épaisseur du remblai et la température du sol, a été faite pour différentes conditions du site. Le modèle a été utilisé pour développer un abaque de conception d'ingénierie permettant d'évaluer le bilan thermique à l'interface entre le remblai et le sol naturel. L'analyse du bilan thermique et l'abaque de conception sont basés sur les résultats de l'analyse de sensibilité et validés en utilisant les données de la piste d'atterrissage de Tasiujaq, Nord du Québec, Canada.

Mots clés: Dégradation du pergélisol; Infrastructure de transport; Alaska Highway; Modélisation thermique; Bilan thermique

Abstract

Permafrost is widely distributed in the northern hemisphere and permafrost degradation underneath transportation infrastructure is on-going due to many factors, such as climate change. The test site, constructed in 2008 along Alaska Highway at Beaver Creek, Yukon, Canada, provides valuable information on the long-term thermal response of permafrost underneath transportation infrastructure, to disturbances induced by constructions and climate change. The temperature data collected can also be used to calibrate thermal models to gain insight into relative effects of different factors on the sensitivity of the ground thermal regime underneath transportation infrastructure to on-going climate change. A finite-element, 2D heat conduction model, taking ice-water phase change into account, was developed based on the Beaver Creek experimental site characteristics and conditions. To increase the accuracy of the model, site-specific parameters, such as soil properties, near surface air temperature, and embankment dimension, were measured and used as input parameters. After calibration of the model, sensitivity analysis of certain input parameters, such as air temperature, embankment thickness and ground temperature, was conducted for different site conditions. The model was used to develop an engineering design chart allowing assessing the heat balance at the interface between embankment and natural ground. The heat balance analysis and the design chart are based on the results of sensitivity analysis and validated using the data from the Tasiujaq airstrip in Northern Quebec, Canada.

Keywords: Permafrost degradation; Transportation infrastructure; Alaska Highway; Thermal modeling; Heat balance

3.1 Introduction

Permafrost, defined as one of six cryospheric indicators of global climate change, refers to soil, rock, ice and organic material, with temperatures at or below 0 °C for at least two consecutive years. In the northern hemisphere, about 24% of exposed land area is underlain by permafrost, and about 17% of permafrost area belongs to the discontinuous regions, which are particularly sensitive to climate change (Brown, 1997; Nelson et al., 2002; Zhang et al., 2008). Physical and mechanical properties of permafrost are highly variable and extremely sensitive to changes in soil temperature. The bearing capacity of permafrost with temperature changing from −4 °C to −1 °C, for example, can decrease to 30% (Cole et al., 1999). In Alaska, permafrost degradation began in the mid-70s (Osterkamp, 2003), and it has been largely documented in Arctic area (e.g., Lachenbruch and Marshall, 1986; Serreze et al., 2000; Jorgenson et al., 2001; Hinzman et al., 2005; Osterkamp, 2007). Several studies on permafrost vulnerability to climate change were conducted as well

(Jorgenson et al., 2001; Lemmen et al., 2008; Grosse et al., 2011; Boyle et al., 2013; Calmels et al., 2015), and they all indicate that permafrost was undergoing severe degradation in response to climate change. Climate change appears to be a long-term trend, regardless of the success of global initiatives to reduce greenhouse gas emission (Lemmen et al., 2008; Pachauri et al., 2014). The global mean surface temperature between 2081 and 2100, compared to the time period between 1986 and 2005, will increase by 2.6 °C to 4.8 °C, and the warming trend is faster in Arctic area (Pachauri et al., 2014). According to Canada's 2010 National Communication to the United Nations Convention on Climate Change, the most significant impact of climate change will happen in Arctic areas, and the increase of winter temperature is expected to be larger than that of summer with increasing reaching 8 °C by 2050. Kaplan and New (2006) indicate that climate change has a serious implication for the Arctic, where the temperature will increase at least 1.5 to 2 times as fast as the global temperature. The warming trend will result in increased active layer thickness, reducing the land area underlain by near-surface permafrost and causing extensive ground settlement in ice-rich permafrost regions (Woo et al., 1992; Nelson et al., 2002).

The effect of climate change on the civil infrastructure integrity has begun since the second half of the 20th century (Cheng and Wu, 2007; Doré et al., 2016). The processes of climate change, with changes in temperatures, precipitation conditions, wind conditions and the occurrence of extreme weather events, can severely disrupt ecosystems and human transportation infrastructures (Jorgenson et al., 2001), and cause serious consequences to land and air transportation service in permafrost regions (Smith and Levasseur, 2002). Extensive evidence of permafrost engineering failures due to many factors, such as climate change, exists along the Alaska Highway, which passes through extensive areas of warm, ice-rich permafrost (M-Lepage, 2015). The engineering failures will increase the maintenance cost for the linear-infrastructure in the Arctic region. The estimated additional maintenance cost to maintain roads in permafrost areas, is about $22,000 (CAD) per year per kilometer in Yukon, Canada (Reimchen et al., 2009). Cole et al. (1999) have estimated that about $12 million (USD) are required to maintain the road network in Alaska. Mueller (2007) estimated that the additional cost related to permafrost degradation will exceed $3 million (CAD) per year by 2055 in North-West Territory, Canada. Although many roads, airports and railways have been designed and constructed in cold regions, little can be found on specific design procedures or guidelines for transportation infrastructure in permafrost conditions. A method based on maintaining the mean annual ground temperature (MAGT) at the base of fill layer below 0 °C was proposed for the design of air convection embankment (Goering, 2002; McHattie and Goering, 2009); however, the permafrost degradation can still happen if a positive thermal gradient exists between MAGT at the base of fill layer and permafrost temperature. Whether permafrost degradation happens or not depends on the total amount of heat flowing into or flowing out of foundation. To maintain permafrost stability under an embankment, the amount of heat flowing out of foundation should be equal or larger than the amount of heat flowing into the foundation during a year. A

relatively new approach, based on the measurement of heat flux between the MAGT at interface between the embankment-soil interface and permafrost temperature, is proposed to analyze heat balance through the interface in one year. The proposed method would allow selecting the suitable mitigation techniques based on the quantity of heat to be extracted and the heat extraction capacity of mitigation techniques. The main objective of this paper is to describe the development of a rational technique to analyze thermal stability of an embankment built over permafrost. More specifically, the paper will include the analysis of the thermal behavior of an embankment in response to climate change, based on the field data in Beaver Creek, Yukon, Canada. It will also include a description of the development of a 2-dimensional heat conduction model, calibrated to the field data from Beaver Creek. The model has then been used to analyze the heat balance through interface with different embankment thickness and site conditions, such as different air temperatures and permafrost temperatures, and to propose an engineering design chart to present the relationship between heat balance and different embankment thicknesses. The engineering design chart has been validated using thermal data from the Tasiujaq airstrip, in Nunavik, Quebec, Canada. The chart is meant to assess permafrost stability under an embankment considering site conditions and to quantify, in unstable cases, the amount of excess heat transferred to permafrost.

3.2 Study site

To better understand permafrost degradation on linear-infrastructure in permafrost regions, 12 experimental sections with and without mitigation techniques were constructed at the Beaver Creek test site. These mitigation techniques mainly include air convection embankment, longitudinal culvert, heat drain, snow/sun shed, snow clearing technique, grass-covered embankment, insulation and high albedo surface. This test site is located at 62^0 20' N, 140^0 50' W, about 8 km south of the community of Beaver Creek and about 30 km south of the Canada-United States border (Figure 3.1). This experimental site is located in an alluvial plain, and has been constructed at km 1865 of the Alaska Highway in 2008. It is located in the extensive discontinuous, warm permafrost region, and the road in this area is experiencing problems related to permafrost thaw.

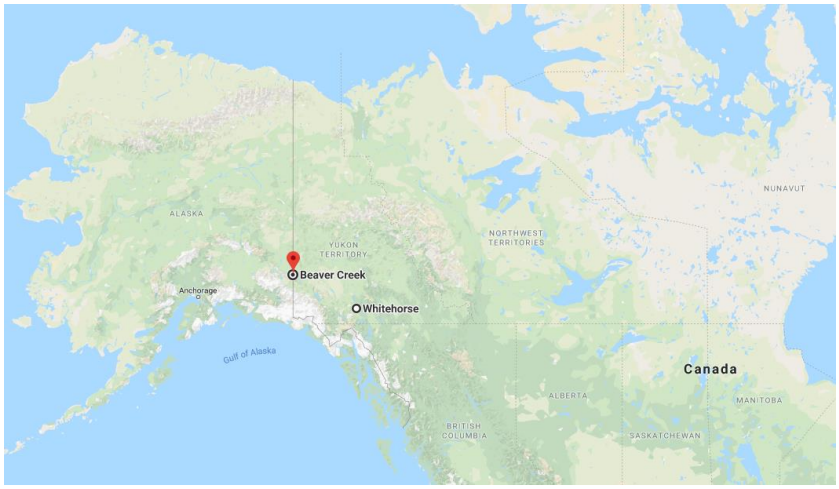

Figure 3. 1: The location of the Beaver Creek experimental site, along the Alaska Highway, Yukon, Canada (Source: GoogleEarth).

The climate is cold continental, with long harsh winters and warm dry short summers (M-Lepage, 2015). Climate records indicated that the mean annual air temperature was about −5.5 °C from 1971 to 2000 (Environment Canada, 2011). Air freezing index and air thawing index are two commonly used climate parameters to quantify the "severity" of winter or summer (Doré and Zubeck, 2009). The average air thawing, freezing index measured at the Beaver Creek weather station between 1971 and 2000 was respectively 1532 °C-day, −3534 °C-day (Environment Canada, 2011).

Mean annual precipitation for the same period is about 419 mm, with 296 mm in the form of water and 123 mm in the form of snow, converted in water equivalent (Environment Canada, 2011). The snowfall begins in September and snowmelt begins in April. Based on the analysis of soil cores obtained from drilling, four types of soils are present at the site: ice-rich peat with volcanic ash, silt, woody peat and silt, and ice-rich diamicton (M-Lepage, 2015).

3.3 Ground thermal regime

In this paper, we focus on the reference section. Thermistors strings were installed in 15.5 m deep boreholes in 2008. Thermistors were spaced by a distance of 0.3 m to 1.0 m. Since then, temperatures were measured automatically six times per day, and the data were transmitted by satellite every 4 h to the computer server in Whitehorse, Yukon. The temperature probes, produced by LogTag Recorders Company, have an operating range from −40 °C to 85 °C with a standard recording accuracy of ±0.1 °C. The thermistor strings were installed under the centerline (BH1), under the center of the side slope (BH2) and in the natural ground at the toe of the slope (BH3). Availability of temperature data collected 6 times per day along three 15.5 m holes across the embankment allows analyzing 2-D temperature variations with time. Figure 3.2 illustrates temperatures variations under the centerline of the reference section (BH1) for a four year period from

December 2008 to December 2012. The interface between the embankment and the foundation soil is used as the reference level (0 m). From this figure, it can be seen that the embankment thickness of 5.5 m did not prevent the thawing front to penetrate into the natural ground with the thawing depths reaching around 1.0m underneath the natural ground surface in summer. The 0 °C isotherm reached the interface between embankment and foundation around mid-July.

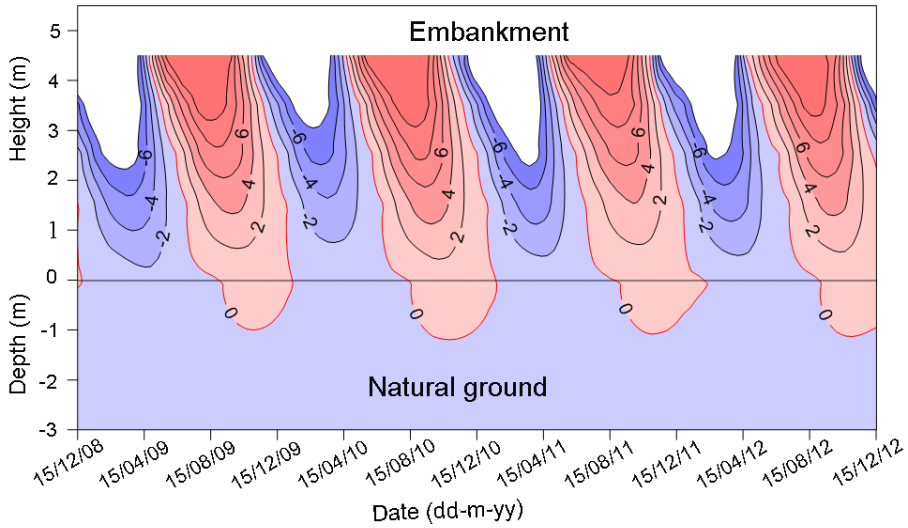

Figure 3. 2: Thermal behavior of the Beaver Creek experimental embankment under the centerline of the reference section (BH1).

Another approach proposed to assess thermal stability of permafrost is to quantify the gradient of MAGT as a function of depth in soils (Batenipour et al., 2010). A positive mean annual thermal gradient is an indication of warming and degrading permafrost. Figure 3.3 gives an example of a thermal regime for BH1 with a gentle positive thermal gradient showing unstable permafrost conditions.

Figure 3.4 illustrates MAGT profiles as a function of depth at the centerline of the reference section during the monitoring period from 2009 to 2012. Figure 3.4 shows that the all the mean annual ground thermal gradients in the natural ground were positive, indicating more heat flowing into the permafrost layer from 2009 to 2012. In the embankment, the trend of mean annual temperature variation was irregular with the depth, and the mean annual temperature had the maximum values in 2010, compared to other three years.

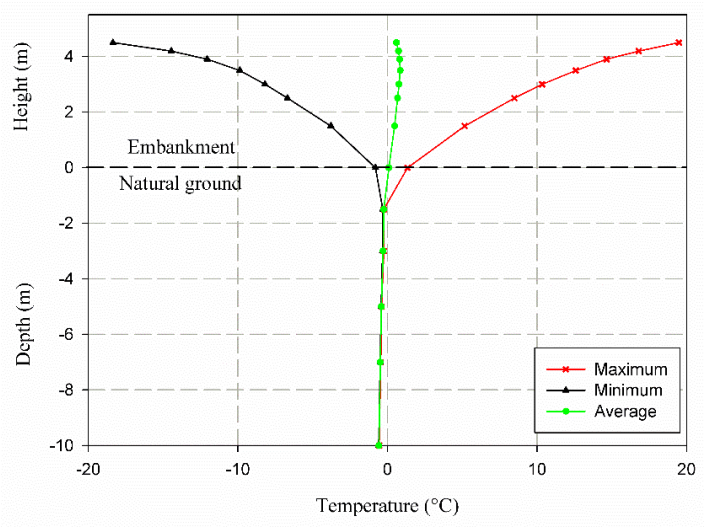

Figure 3. 3: Mean annual ground temperature (MAGT) envelope under the centerline of the reference section (BH1) in 2010.

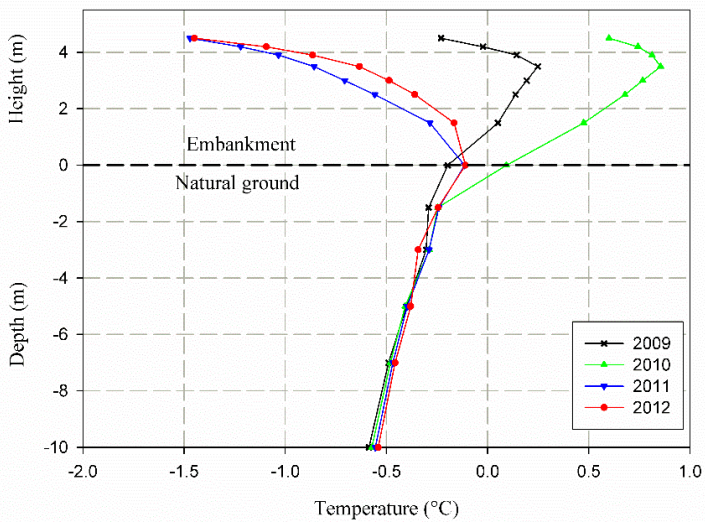

Figure 3. 4: Mean annual ground temperature (MAGT) profiles with depth under the centerline of the reference section (BH1) from 2009 to 2012.

The maximum thaw depth is observed around the beginning of November. Figures 3.5 and 3.6 show the temperature profiles with depth in the side slopes (BH2) and at the toe of the embankment (BH3) respectively, on every November 5th during monitoring years 2009 to 2012. Figure 3.5 shows that temperature increased in the embankment from 2009 to 2012, with the temperature reaching 1.1 °C and 2.5 °C at the interface in 2009 and 2012, respectively.

The effect of seasonal air temperature variations decreases with increasing depth in the ground, and from 2009 to 2012, temperatures remained the same 2.3 m below the original ground surface. Figure 3.5 shows an increase of the temperatures in the side slopes as well as an increase in thaw depth. The thickness of active layer increased by 1.13m over the monitoring period, going from 0.75 m to 1.88 m under the interface between

the embankment and the foundation soil from 2009 to 2012. The gradual increase of active layer thickness in the side slopes has affected the embankment integrity and, as a result, longitudinal cracks have appeared along embankment edges.

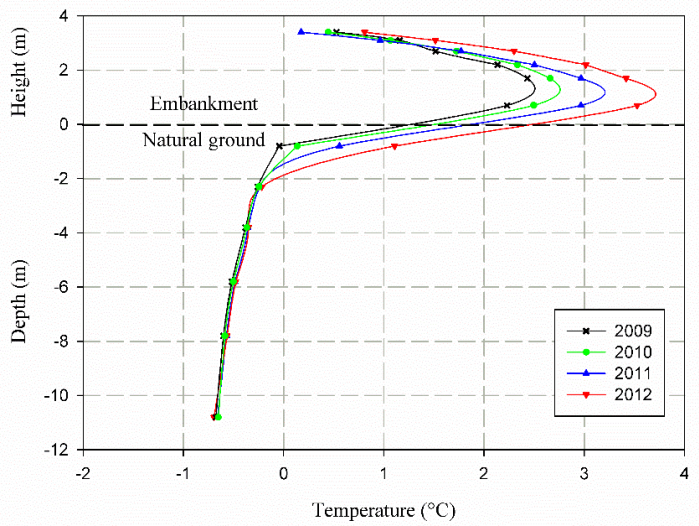

Figure 3. 5: Temperature profiles on November 5th along the depth in the side slopes of the reference section (BH2) from 2009 to 2012.

Figure 3.6 illustrates the temperature profile in soil at the toe of the embankment slope. It shows that below the first two meters in the natural ground, the temperature increased steadily from 2009 to 2012. The maximum difference of temperature reached 0.22 °C at the depth of 5.2 m below the natural ground surface. The thickness of active layer showed a slight increase as well, going from 1.54 m to 2.38 m from 2009 to 2012.

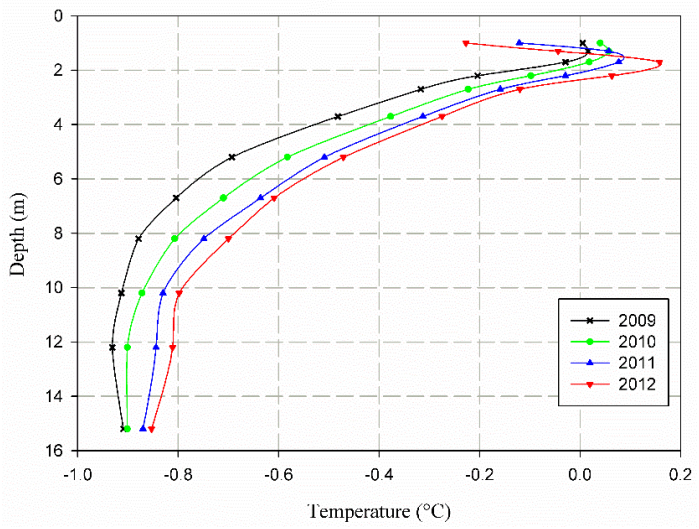

Figure 3. 6: Temperature profiles on November 5th along the depth at the toe of the reference section (BH3) from 2009 to 2012.

3.4 Numerical simulation

A numerical model was built using the SVHeat geothermal modeling software to simulate the case of the reference embankment at the Beaver Creek test site. Actual geometry of embankment and soil properties were used to build the model, which was then calibrated using 4 years of temperature data collected at the site.

3.4.1 Physics, governing equations and input parameters

The physical domain consists of a normal embankment and foundation soil. The whole domain is used for numerical simulation (Figure 3.7), due to the fact that physical domain is not symmetrical. The physical domain represents an area 44.2 m wide from the centerline of the embankment and a depth of 16.0 m underneath the centerline from road level. In the physical domain, part ① is the embankment fill, which consists of 50% gravel, 30% sand, and 10% silt; part ② is the saturated silt with water content 36% (de Grandpré et al., 2012).

Heat conduction is the main heat transfer mode if water flow is not considered in soils, and the equation governing two-dimensional, non-linear heat flow in soils can be expressed as (Newman and Wilson, 1997):

$$\frac{\partial}{\partial x}(k_x \frac{\partial T}{\partial x}) + \frac{\partial}{\partial y}(k_y \frac{\partial T}{\partial y}) = C\frac{\partial T}{\partial t} - L_f \frac{\rho_i}{\rho_w}\frac{\partial \theta_i}{\partial t} \tag{3.1}$$

where t is the time (s), T is the temperature (°C), k is the thermal conductivity (J/(s-m-°C)), C is the volumetric heat capacity (J/(m^3-°C)), L_f is the volumetric latent heat of fusion of water, which equals to 3.34×10^8 J/m^3, x, y are coordinates (m). ρ_i, ρ_w are the ice density and water density (kg/m^3), respectively.

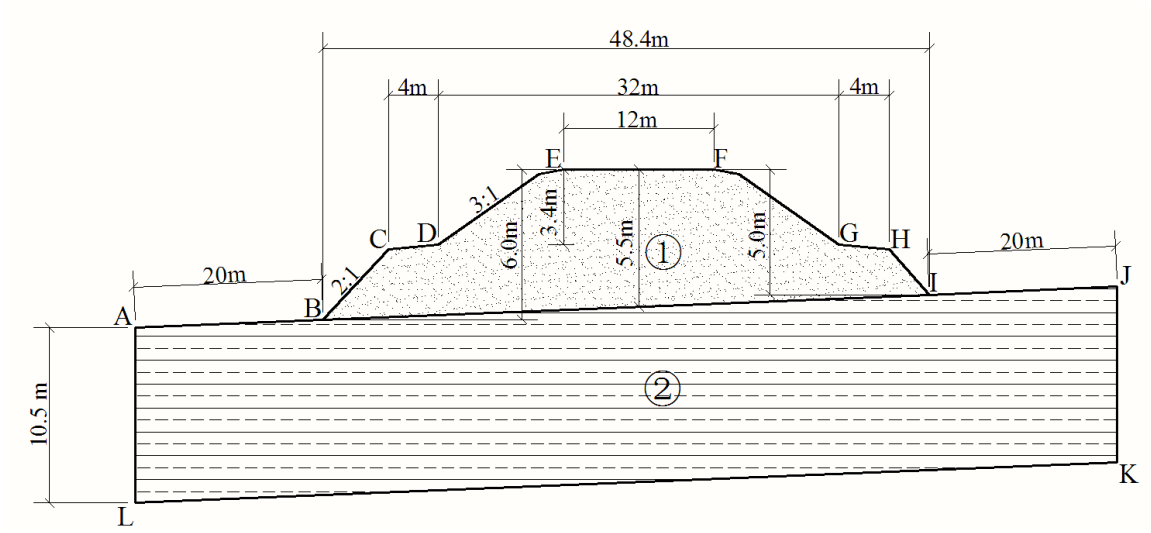

Figure 3. 7: The physical domain of the embankment and foundation.

In the model, the unfrozen water content in frozen soils varies with soil types and temperature, and the relationship between unfrozen water content and temperature can be expressed as (Tice et al., 1976; Farouki, 1986):

$$\theta_u = \begin{cases} \theta_w & \text{if } T \geq T_f \\ \frac{\rho_d}{\rho_w} a|T|^{-b} & \text{else} \end{cases} \tag{3.2}$$

where θ_u is the volumetric unfrozen water content (m^3/m^3), θ_w is the volumetric water content of unfrozen soil (m^3/m^3), T_f is the soil freezing point (°C), ρ_d is the soil dry density (kg/m^3), ρ_w is the water density (kg/m^3). a, b are the experimental parameters, whose values are shown in Table 3.1. An example of unfrozen water content versus temperature using published experimental parameters (Andersland and Ladanyi, 2004) is shown in Figure 3.8a. The unfrozen water content has a large effect on the volumetric heat capacity, C, which is calculated based on the following equation (Farouki, 1986):

$$C = \rho_d \left(c_s + c_w w_u + c_i w_i \right) \tag{3.3}$$

where c_s, c_w and c_i are the mass-specific heat of solids, water, and ice, respectively. The values of c_w, c_i are 4184 J/(kg-°C) and 2100 J/(kg-°C), respectively (Farouki, 1986). w_u is the gravimetric unfrozen water content of the soil, and w_i is the gravimetric ice content of the soil.

Table 3. 1: The values of experimental parameters.

Media	Embankment fill	Silt
a	0.021	0.048
b	0.408	0.326

The measured thermal parameters of foundation soil (silt) from laboratory testing are shown in Table 3.2 (de Grandpré et al., 2012). The values of thermal conductivity are given in unfrozen state and frozen state with no unfrozen water content varying outside the phase change zone. In this paper, the calculation of thermal conductivity in the phase change zone is done following the method proposed by Johansen (1975). The thermal functions for thermal conductivity and thermal capacity of silt used in this paper are shown in Figure 3.8b.

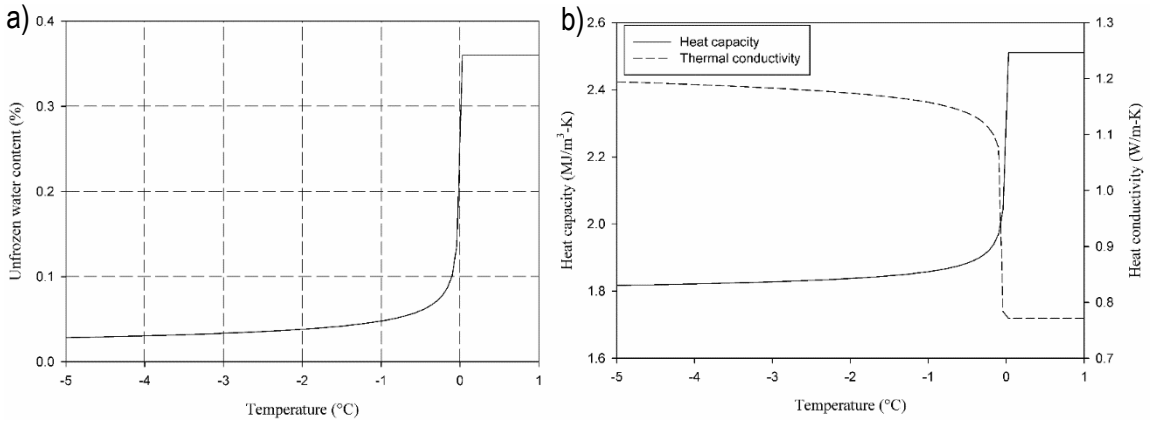

Figure 3. 8: Thermal functions used in the model: (a) unfrozen water content versus temperature for silt; (b) thermal conductivity and heat capacity for silt (Johansen, 1975).

Table 3. 2: Physical parameters measured in the foundation soil at Beaver Creek (de Grandpré et al., 2012).

Physical variable	k_f (W/m · K)	k_u (W/m · K)	C_f (MJ/m3 · °C)	C_u (MJ/m3 · °C)	θ (m3/m3)	S_r (%)
Silt	1.21	0.76	1.73	2.51	0.36	100

The soil parameters of embankment fill directly affect the temperature distribution in the embankment and, based on laboratory testing, the measured water content of embankment fill in summer varies from 2.3% to 7.2% in different positions of embankment fill (Doré et al., 2007).

The calculation of thermal conductivity, volumetric heat capacity in frozen state and unfroze state for embankment fill, can be estimated using empirical equations for coarse-grained soils (Kersten, 1949):

$$k = \begin{cases} 0.01442 \times (0.7 \log w + 0.4)(10)^{0.6243\rho_d} & \text{if } T \geq T_f \\ 0.01096 \times (10)^{0.8116\rho_d} + 0.00461 \times (10)^{0.9115\rho_d} w & \text{else} \end{cases} \quad (3.4)$$

$$C = \begin{cases} \left(\frac{\rho_d}{\rho_w}\right)\left(0.17 + 1.0\frac{w_u}{100}\right)C_{vw} & \text{if } T \geq T_f \\ \left(\frac{\rho_d}{\rho_w}\right)\left[\left(0.17 + \frac{1.0w}{100}\right) + 0.5\left(\frac{w - w_u}{100}\right)\right]C_{vw} & \text{else} \end{cases} \quad (3.5)$$

where ρ_d is soil dry density (kg/m^3), C_{vw} is volumetric water heat capacity, whose value is 4.187 MJ/(m^3-°C). w is the total gravimetric water content. The subscripts, u and f, mean respectively unfrozen state, and frozen state in soils.

The near-surface temperature is applied on the top boundaries of the physical domain. In general, the approximate sinusoidal curves or cosine curves with a thermal modifier (n-factor) fitting the observed air

temperature is often used in numerical simulations. A weather station installed at the site provides detailed information on the air temperature. Air freezing index represents the summation of average daily air temperatures below 0 °C. The air thawing index is the summation of temperatures above 0 °C (Andersland and Ladanyi, 2004). To ensure the accuracy of the thermal simulation, the simulated air freezing and thawing indices should approximate reasonably the indices calculated from measured air temperature. The average calculated field thawing, freezing air index are 1604 °C-day, −3023 °C-day from 2009 to 2013, and the simulated thawing, freezing air index are 1551.5 °C-day, −3025 °C-day. The difference between the calculated and simulated air index is<4%, and as a result, the simulated air temperature can be used reliably for the simulation (Figure 3.9).

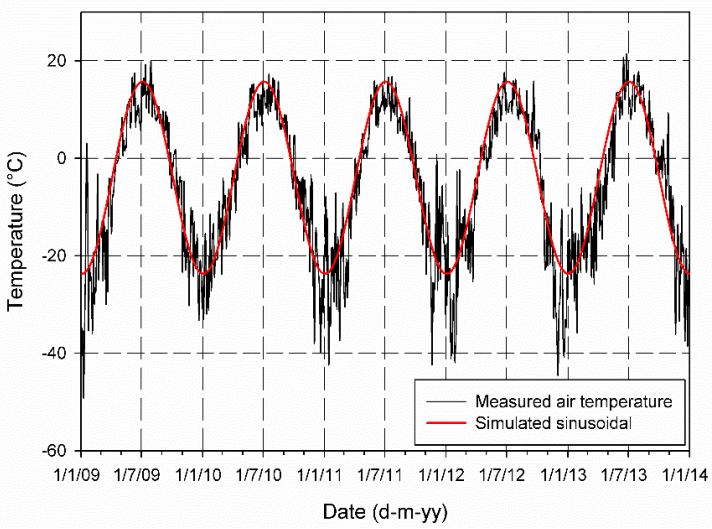

Figure 3. 9: Graphical comparison between measured air temperature and simulated sinusoidal temperature.

The n-factor is very sensitive to many factors, such angle of incidence of solar radiation, cloud cover, precipitation and vegetation. On a yearly basis, the freezing n-factor has been observed to vary between 10 and 30% in Yukon Territory (Karunaratne and Burn, 2003). However, to simplify the simulation, constant annual freezing n-factor and annual thawing n-factor are given on the thermal boundaries of numerical models. This assumption involves that the surface conditions, such as vegetation cover, precipitation, wind speed and snow cover, do not vary on a yearly basis. Constant temperature boundary at the bottom of the model can provide a more efficient computing time, comparing to heat flux boundary (Alfaro et al., 2009). Moreover, considering that the model is not used to assess long-term evolution of permafrost temperature, a fixed temperature condition can thus be applied at the bottom of the model. The measured permafrost temperature of −0.56 °C is therefore applied along the boundary KL. The near-surface temperatures with a modifier (n-factor) are applied on the top boundaries of the physical domain (ABCDE and FGHIJ), and the lateral boundaries (AL and JK) are assumed to be adiabatic.

3.4.2 Models calibration

The computational domain, shown in Figure 3.7, was divided into 3104 nodes and 1473 triangular finite elements, with a greater element density in the embankment fill and natural ground surface layer underneath the embankment to obtain a better solution for the active layer and the top part of permafrost.

A detailed calibration procedure was carried out using 4 years of temperature data to try to reproduce the ground thermal regime underneath the embankment. Table 3.3 is the summary of the iterations that were done to calibrate the model. Based on the field temperature data, the ground thermal regime changed from 2009 to 2013 due to many factors, such as the variation of air temperature, wind speed, relative humidity and precipitations. In order to average the variation of contributing factors on the ground thermal regime, the average 4-years record of temperature distribution was selected as the reference to calibrate the model.

Table 3. 3: Summary of model iterations.

Iteration	Comments
I1	Steady-state analysis for the initial temperature regime, based on field data
I2	Initial model iterations: simulated over a 25-year period model with thawing, freezing n-factor from literature for different thermal boundaries.
I2a	Revise I2 using adjusted n-factor for embankment surface to make the MAGT along the centerline in the embankment, close to measured field data
I2b	Revise I2a using adjusted n-factor in the side slopes to make the MAGT at the interface close to field data
I2c	Revise I2b, and add a layer (0.5 m thickness) with higher water content above the interface to improve accuracy

The simulated sinusoidal air temperature (Figure 3.9), measured embankment dimension (Figure 3.7) and measured soil parameters (Table 3.2), were used in the model iterations. In the following discussion, each experimental model iteration was labeled with "I". The validation process began with I1 and ended in I2c. The first step in the modeling was to determine the initial ground temperatures, which were applied in the following transient steps. I1 represented the steady state analysis, which was used to generate the initial ground temperature for the next analysis. In I1, the temperature boundaries for steady state analysis were obtained from the monitored ground temperature at different depths.

One thing to note is that the measured unfrozen thermal conductivity is about 1.40 J/(s-m-°C) in the shallow part of the embankment fill, and the thermal conductivity should be consistent with this value to react to the field thermal parameters. Through the above equation (3.4), the water content 3% and density 1800 kg/m^3 were assigned for the whole embankment fill in the initial model iteration in I1.

I2 was built upon I1, and all the model iterations were 25 year-long to obtain a stable annual cycle, which responded to the given thermal boundaries and material properties of soils. The time of model iterations was 5 years longer than that used in the previous models (Buteau et al., 2004).

The model was ran, using automatic time steps chosen by the finite element software in the first 20 years to save time and to avoid numerical crashing, and after the 20 years period, time step was set to 1.0 day, with results saved every day. The numerical results for the final year for all the following model iterations were exported for the future temperature analysis.

Air temperature and n-factor are the most critical driving input parameters for the ground thermal regime, comparing to other parameters, such as the thermal properties of foundation soil (Darrow, 2011). The n-factor used in I2 are given in Table 3.4. I2a, was similar to I2, except that the embankment surface n-factor was adjusted to improve the quality of the fit between the modeled and observed ground temperature regime. Through sensitivity analysis, the adjusted embankment surface thawing (n_t), freezing n-factor (n_f) are 1.4 and 1.0, respectively. Snow depth and density strongly affect ground temperature (e.g., Jorgenson et al., 2001). The temperature at the base of the embankment and in subgrade soils is controlled by embankment surface boundary and side slopes boundary conditions. I2b was built on I2a, adjusting the nt, nf on the side slopes through sensitivity analysis. The n_t, n_f in the side slopes obtained from the analysis were 1.2, and 0.97, respectively. The values of n_t and n_f chosen for different thermal boundaries are given in Table 3.5.

Table 3. 4: N-factor used in I2.

Surface type	n_t	n_f
Natural ground surface	0.5	0.5
Embankment surface	1.8	1.0
Embankment side slopes	1.1	0.5

Values obtained from literature (Goering, 2003; Andersland and Ladanyi, 2004; Zottola et al., 2012).

Table 3. 5: Final determined n-factor for different thermal boundaries.

Surface type	n_t	n_f
Natural ground surface	0.50[a]	0.50[a]
Embankment surface	1.4[b]	1.0[b]
Embankment side slopes	1.2[b]	0.97[b]

[a] Values obtained from the literature (Goering, 2003; Zottola et al., 2012); [b]Values obtained through sensitivity analysis.

MAGT profile with depth is a good indication of heat flow direction across the interface between embankment and subgrade soil in one year (Batenipour et al., 2010). It is also a good indicator for model fit to measured temperature data.

Mean annual vertical temperature profiles under the centerline of the embankment generated using the three models described above are shown in Figure 3.10. The average temperature profile measured at the site is also shown in the figure for comparison. For I2, comparison between the modeled temperatures and the measured field temperatures as a function of depth indicates that temperature discrepancy decreases with depth. In addition, the modeled temperatures are typically 0.04 °C to 0.75 °C warmer than the measured temperature in the subgrade soil.

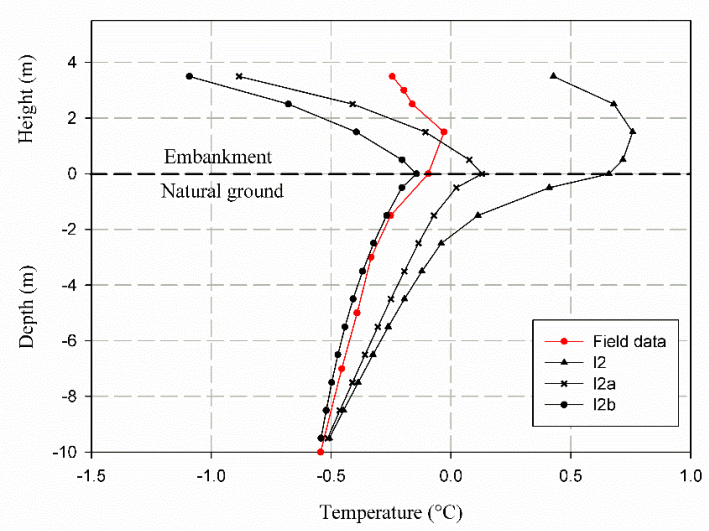

Figure 3. 10: Comparison of 4-year average temperature profiles with depth at the centerline of the embankment measured at the site and obtained with simulations I2, I2a, and I2b.

With the adjusted n-factor on the embankment surface in I2a, a significant difference of temperatures still existed in the 4 m below embankment surface. However, soil temperatures in the natural ground are closer to the measured temperatures, typically within 0.2 °C of the measured average temperature below the interface, with the biggest temperature difference at the interface between embankment and subgrade soil. For I2b, the modeled temperatures matched the measured temperatures within 0.06 °C in the subgrade soil. The results for I2c, were similar to I2b, with a better fit in the embankment fill, close to the interface. The measured water content ranges from 2.3% to 7.2% in embankment fill, and in I2c, a 0.5-m thick layer of embankment with a higher water content was specified at the bottom of the embankment improving the accuracy of the simulation. The final calibrated results of I2c simulation including maximum, minimum and average temperature profiles at the centerline is shown in Figure 3.11.

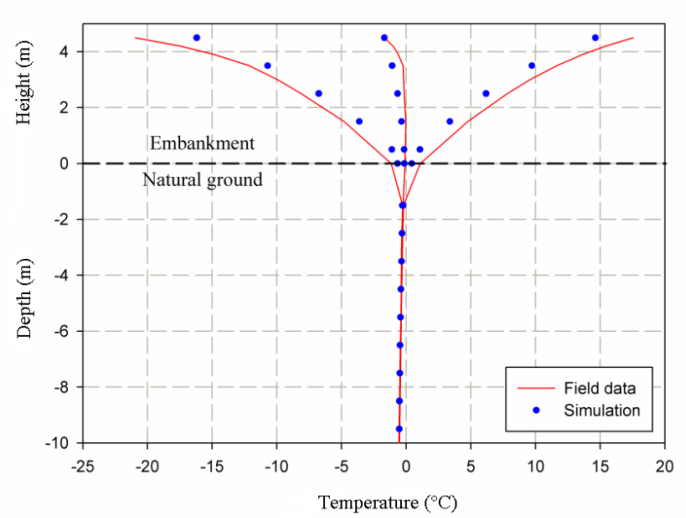

Figure 3. 11: Comparison of maximum, minimum and average temperature profiles with depth at the centerline between field data and numerical simulation I2c.

The results indicate that the modeled average temperature was typically 0.05 °C to 0.85 °C colder than the measured temperature in the embankment. Below the embankment-soil interface, the modeled temperature fitted the measured temperature well, and the maximum temperature difference was<0.1 °C. Comparison between the modeled maximum temperature with the measured maximum temperature indicates that the temperature difference decreased with the depth in the embankment with the temperature difference of 0.66 °C occurring at the embankment-soil interface. Below the embankment-soil interface, the maximum temperature difference was<0.1 °C. For the minimum temperature, the modeled temperature was warmer than the measured temperature in the embankment, and the difference was 0.48 °C at the embankment-soil interface.

3.5 Analysis, validation and discussion

Heat balance is the summation of all negative and positive heat fluxes passing through a plane during a year. M-Lepage et al. (2012) have proposed the use of two indices, the induction index, and extraction index, to quantify heat balance at the interface between an embankment and subgrade soils. Heat balance equals to induction index plus extraction index, which are expressed as:

$$H_x = k_{frozen} \times \frac{T_1 - T_2}{\Delta z} \times \Delta t \tag{3.6}$$

$$H_i = k_{unfrozen} \times \frac{T_1 - T_2}{\Delta z} \times \Delta t \tag{3.7}$$

where H_x, H_i are the extraction index and induction index, respectively. T_1, T_2 are the ground temperatures at depth of h_1, h_2 under the interface. Δz is the absolute difference between h_1 and h_2. k_{frozen}, $k_{unfrozen}$ are the thermal conductivity at frozen and thawing states in the surface ground layer. In this paper, Δz, Δt are specified to be 10.5 m and 1.0 day, respectively.

After the model was calibrated by the measured field temperature data at Beaver Creek, sensitivity analyses were carried out to quantify heat balance through the soil-embankment interface at the centerline for different embankment thicknesses and site conditions. The analysis was done with the model calibrated using four years of data collected at the test site and is considered to be representative of thermal conditions for those four years. Thus, it does not consider the effect of long-term climate change at the top thermal boundaries of models.

In the sensitivity analysis, the permafrost temperature was set at -1 °C and different values of mean annual air temperature and embankment thickness were used to obtain different thermal gradients between the interface and bottom boundary to simulate the different thermal conditions for different embankment thicknesses and site conditions. Thermal gradients were calculated based on the MAGT at the interface and constant bottom temperature in the model.

To obtain the constant thermal gradient between the interface and bottom boundary, a time length for every sensitivity analysis was set to be 60 years. MAGT was plotted as function of time and when temperature became stable, the full temperature variation in that year was used for the sensitivity analysis. The relationships between heat balance through interface and embankment thickness, thermal gradient, were obtained through statistical regression (Table 3.6) using data points obtained by numerical simulation. The results of the quantification of heat balance through the embankment-soil interface at the centerline of the embankment for different embankment thicknesses and air temperatures are shown in Figure 3.12. From the figure, it can be seen that heat balance increases with thermal gradient for all embankment thickness and nonlinearity is obvious for the thicker embankments. For example, with a thermal gradient of 0.1 °C/m, the corresponding heat balances were -2.4×10^6 J/m^2, 1.0×10^6 J/m^2, 2.5×10^6 J/m^2, 3.1×10^6 J/ m^2 for embankment thickness 1.0 m, 2.5 m, 4.0 m and 5.5 m, respectively. Increasing embankment thickness is considered as an effective method to protect permafrost by improving thermal resistance. However, for thicknesses >4.0 m, the effectiveness of this method decreases significantly.

Table 3. 6: Regression equations between heat balance at the embankment-soil interface, embankment thickness and thermal gradient.

Embankment thickness (m)	Regression equation	Coefficient of determination (R^2)
1.0	$Q = 3.06 \times 10^7 \times x - 5.34 \times 10^6$	> 0.99
2.5	$Q = 3.17 \times 10^7 \times x - 2.22 \times 10^6$	> 0.99
4.0	$Q = -0.55 \times 10^6 + 3.31 \times 10^7 \times x - 2.56 \times 10^7 \times x^2$	> 0.99
5.5	$Q = 0.028 \times 10^6 + 3.42 \times 10^7 \times x - 3.81 \times 10^7 \times x^2$	> 0.99

x is the thermal gradient (°C/m) between the MAGT at interface and permafrost temperature; Q is the heat balance (J/m^2) through the interface.

The model was calibrated using observed maximum, minimum and average temperature profiles with depth at the centerline of the embankment. However, the temperature profiles did not include the detailed information on temperature changes with time in 1 year, which was required to calculate heat balance through the interface. The calculated mean annual heat balance based on field data over the period from 2009 to 2013, was 1.1 MJ/m^2 and the value obtained from Figure 3.12 was around 1.4 MJ/m^2. The difference of 0.3 MJ/m^2 between the modeled results and the measured heat balance can be attributed to the fact that the measured temperature along the centerline at the interface had a larger range varying between −1.16 °C and 1.09 °C, while the modeled temperature range was between -0.68 °C and 0.43 °C. For each embankment thickness, the critical thermal gradient corresponding to zero heat balance through the interface can be obtained from Figure 3.12. As shown in Figure 3.13, critical thermal gradient are generally above 0 °C/m and vary between 0.175 °C/m and -0.003 °C/m for different embankment thicknesses. The critical thermal gradient decreases with embankment thickness following a non-linear relationship. Above the critical thermal gradient, heat balance is positive, which means permafrost underneath transportation infrastructure is undergoing degradation and is unstable.

Engineers pay much attention to the thermal state of permafrost underneath transportation infrastructure, and Figure 3.13 can help make a preliminary assessment based on measured or estimated temperature underneath transportation infrastructure.

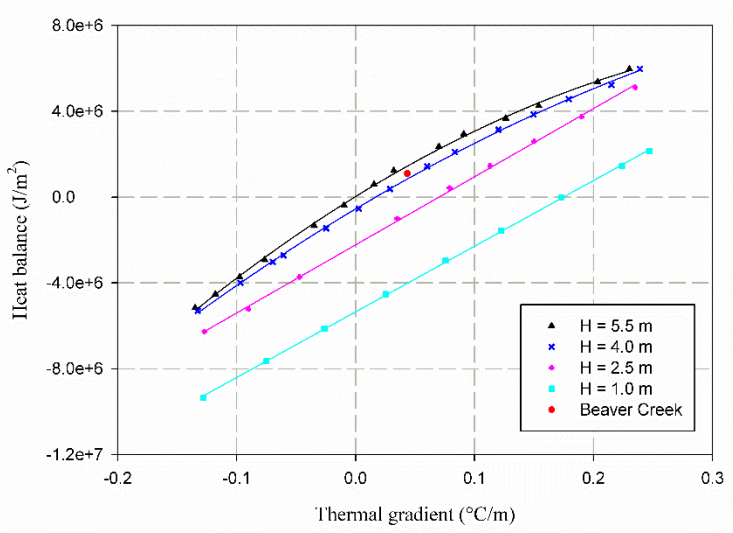

Figure 3. 12: Heat balance at the embankment-soil interface as a function of embankment thickness (H) and thermal gradient.

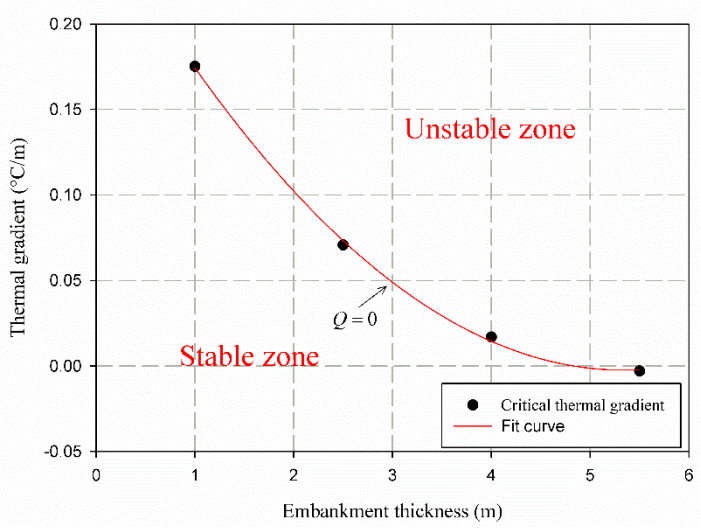

Figure 3. 13: Critical thermal gradient as a function of embankment thickness.

The proposed engineering design chart has been developed based on the model built and calibrated using data from the Beaver Creek test site. It needs to be validated using data from other field sites to improve its reliability. Additional validation data was obtained from the Tasiujaq airstrip in Nunavik, Quebec, Canada. The construction of the airstrip in Tasiujaq was completed in 1990 and the site is located in a extensive discontinuous permafrost zone. The permafrost underneath the airport is ice-rich and thaw-sensitive. Differential settlements had been observed along the length of the runway (Doré et al., 2007). The thickness of the embankment at the location of the instrumentation is 2.45 m and the subgrade soils underneath embankment are medium coarse sand (0 – 1.45 m) overlying ice-rich silty sand (1.45m – 5.20 m), coarse

sand and gravel (5.20 m – 9.70 m) and silty clay (9.70 m – 27 m) (Allard et al., 2009). Two thermistor cables were installed at the centerline of the runway, at 5.4 m and 13.5 m depth.

The temperature data at the interface and permafrost temperature at the depth of 13.5 m, available on a daily basis, were used to calculate the thermal gradient and associated heat balance through the interface. In Equations (3.6) and (3.7), heat balance highly depends on the frozen and unfrozen soil conductivities. For a different type of soils, the heat balance chart cannot be used directly. It can, however, be corrected by multiplying the heat balance by the ratio between thermal conductivity of the new soil and of the soil used in the model. The heat balance, at Tasiujaq, has been calculated and is plotted into the engineering design chart for the period going from 2011 to 2014 as shown in Figure 3.14. The results indicate that the annual heat balance is in good agreement with the heat balance curve for an embankment thickness of 2.5 m.

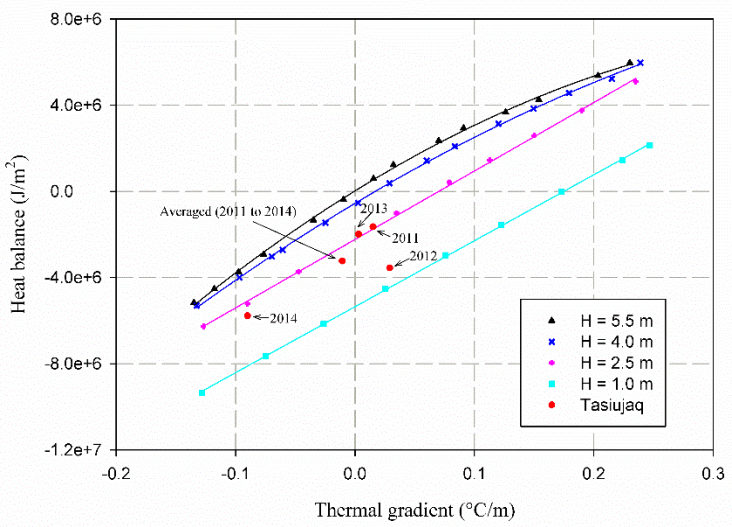

Figure 3. 14: Validation of heat balance using Tasiujaq airstrip temperature data.

Also, the averaged and annual heat balances from 2011 to 2014 are negative, which suggest permafrost degradation underneath embankment did not happen from 2011 to 2014. This is confirmed by the decreasing active layer thickness from 2011 to 2014 (Figure 3.15) and by decreasing temperature at the depth of 9.0 m below embankment surface at the centerline from 2011 to 2014 (Figure 3.16).

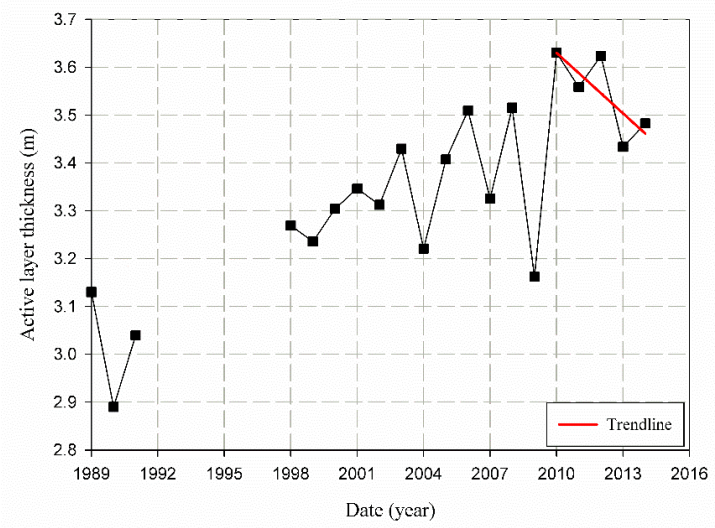

Figure 3. 15: Evolution of the active layer thickness with time at the centerline of Tasiujaq airstrip.

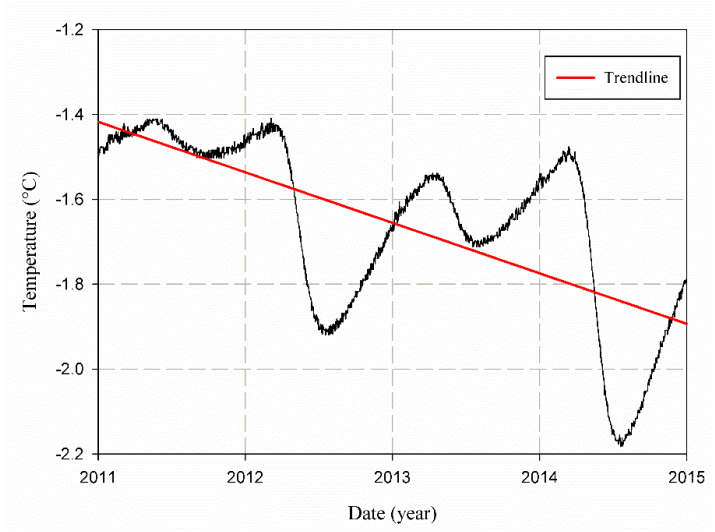

Figure 3. 16: Evolution of ground temperature at the depth of 9.0 m below embankment surface at the centerline of Tasiujaq airstrip.

In summary, the engineering design chart has been successfully validated by the calculated heat balance using temperature data from the Tasiujaq airstrip. The design chart should be used with caution when applied to different soils. Heat balance can be corrected by multiplying the ratio between thermal conductivity of subgrade soils at the site considered and of the soil used in the development of the model.

Climate warming will lead to the warming of soils, and the warming rate of soils decrease with depth underneath the natural ground surface. As a result, the mean annual thermal gradient between the embankment- soil interface temperature and permafrost temperature is likely to increase for a given site depending on site conditions and embankment thickness. Based on the expected change of the mean annual thermal gradient and using Figure 3.12, it is possible to assess the amount of extra heat flowing into the

subgrade soil due to climate warming and to estimate when the embankment is likely to become unstable based on the characteristic of the changing thermal gradient and a selected scenario of climate warming at the site.

3.6 Conclusion

The beaver Creek test site, built along Alaska Highway at Beaver Creek, Yukon, Canada, provided valuable information on the long-term thermal response of permafrost underneath transportation infrastructure in the northern regions. In response to both disturbance induced by constructions and climate change, the increase in ground temperature and active layer thickness were observed at this field site. A 2D, thermal conduction model, taking ice-water phase change into account, was developed and calibrated using the monitored field data from the reference section of the test site. To increase the accuracy of the model, site-specific parameters, such as soil properties, near surface air temperature, and embankment dimension, were measured and used as input parameters into the 2D model. A detailed calibration procedure was proposed, and the final numerical results over the period of 25 years were in a good agreement with temperature data monitored at Beaver Creek, although neglecting the complex effect of uneven snow accumulation on the side slopes in the model.

A relatively new method based on the calculation of heat balance at the embankment-soil interface, has been used in this study. The proposed method allows to determine if permafrost degradation underneath transportation infrastructure is happening or will happen, based on a given site conditions and embankment thickness. An engineering design chart, to estimate heat balance at the embankment-soil interface, was developed based on the calibrated model and has been successfully validated using the data from the Tasiujaq airstrip, in Nunavik, Quebec, Canada. The numerical results indicated that for all embankment thicknesses considered, the relationships between heat balance and thermal gradient have similar trends with heat balance increasing with thermal gradients, and embankment thickness. For the same thermal gradient, the increase in embankment thickness has much more effect on heat balance for thin embankments than for thick embankments. For each embankment thickness, one critical thermal gradient corresponding to zero heat balance can be obtained from the design chart. Above the critical thermal gradient, the embankment is thermally unstable and permafrost degradation is likely to occur. The critical thermal gradient decreases with increasing embankment thickness following a non-linear trend.

The effect of climate warming can be integrated into the proposed procedure by increasing the mean annual thermal gradient between the embankment-soil interface and permafrost considering a climate change scenario selected by the designer. The expected change in air temperature can be used to estimate the change in average yearly temperature at the embankment-soil interface and consequently, the change in

temperature gradient. It would thus be possible to predict the time when permafrost underneath transportation infrastructure is likely to become unstable, if currently stable.

The numerical results were obtained based on the heat conduction model. For future work involving numerical modeling, it is suggested to 1) consider the effect of possible water flow in the active layer on heat balance at the embankment-soil; 2) calibrate thermal models, by comparing the modeled ground temperatures with observed ground temperature and by comparing heat balance with active layer thickness evolution and temperature data history at selected depths.

Acknowledgements

The authors would like to acknowledge the financial support of the Natural Sciences and Engineering Research Council of Canada as well as the technical and financial support of public and private partners of the permafrost engineering research program ARQULUK for this project. The contribution of the Center for Northern Studies of Laval University, who provided data for model validation, is also gratefully acknowledged.

3.7 References

Alfaro, M.C., Ciro, G.A., Thiessen, K.J., Ng, T. (2009). Case study of degrading permafrost beneath a road embankment. Journal of Cold Regions Engineering, 23 (3), 93–111.

Allard, M., Doré, G., L'Hérault, E., Sarrazin, D., Verreault, J.(2009). Investigations géotechniques, caractérisation du pergélisol et stratégie d'adaptation pour les aéroports du MTQ au Nunavik. In: Rapport d'étape. Vol. 2. Centre d'études Nordiques, Université Laval, Quebec, Canada, pp. 1–83.

Andersland, O.B., Ladanyi, B.(2004). Frozen ground engineering. John Wiley & Sons.

Batenipour, H., Kurz, D., Alfaro, M., Graham, J., Kalynuk, K. (2010). Results from an instrumented highway embankment on degraded permafrost. In: Proceedings of the 63rd Canadian Geotechnical Conference and 6th Canadian Permafrost Conference. Calgary, Alberta, Canada, pp. 512–519.

Boyle, J., Cunningham, M., Dekens, J. (2013). Climate Change Adaptation and Canadian Infrastructure. International Institute for Sustainable Development (IISD), Winnipeg, Manitoba, Canada, pp. 1–40.

Brown, J. (1997). Disturbance and recovery of permafrost terrain. Disturbance and Recovery in Arctic Lands: An Ecological Perspective, 167–178.

Buteau, S., Fortier, R., Delisle, G., Allard, M. (2004). Numerical simulation of the impacts of climate warming on a permafrost mound. Permafrost and Periglacial Processes, 15 (1), 41–57.

Calmels, F., Roy, L., Laurent, C., Pelletier, M., Kinnear, L., Benkert, B., Horton, B., Pumple, J. (2015). Vulnerability of the North Alaska Highway to Permafrost Thaw: A Field Guide and Data Synthesis. Northern Climate ExChange, Yukon Research Centre. Yukon College, Canada, pp. 1–120.

Cheng, G., Wu, T. (2007). Responses of permafrost to climate change and their environmental significance, Qinghai-Tibet Plateau. Journal of Geophysical Research: Earth Surface, 112 (F2).

Cole, H., Colonell, V., Esch, D. (1999). The economic impact and consequences of global climate change on Alaska's infrastructure: assessing the consequences of climate change for Alaska and the Bering sea region. In: Workshop Proceedings Summarized for the US Global Change Research Program. University of Alaska Fairbanks, USA, pp. 43–56.

Darrow, M.M. (2011). Thermal modeling of roadway embankments over permafrost. Cold Regions Science and Technology, 65 (3), 474–487.

Doré, G., Niu, F., Brooks, H. (2016). Adaptation methods for transportation infrastructure built on degrading permafrost. Permafrost and Periglacial Processes, 27 (4), 352–364.

Doré, G., Pierre, P., Juneau, S., Lemelin, J. (2007). Expérimentation de méthodes de mitigation des effets de la fonte du pergélisol sur les infrastructures du Nunavik: aéroport de Tasiujaq, Rapport d'étape 1– Compte rendu des travaux d'instrumentation et de supervision de construction des planches expérimentales de l'aéroport de Tasiujaq, description des planches construites et de l'instrumentation installée. GRINCH, Université Laval, Quebec, Canada.

Doré, G., Zubeck, H.K. (2009). Cold regions pavement engineering. McGraw-Hill, New York.

Environment Canada (2011). Canadian Climate Normals 1971–2000 [Online]. Available from. http://www.climat.meteo.gc.ca (accessed on July 4 2011).

Farouki, O.T. (1986). Thermal properties of soils. In: seres of Rock and Soil Mechanics. 11. Trans Tech Publications, Clausthal-Zellerfeld, Germany, pp. 1-136.

Goering, D.J. (2002). Convective cooling in open rock embankments. In: Proceedings of the 11th International Conference on Cold Regions Engineering, Anchorage, Alaska, USA, pp. 629–644.

Goering, D. (2003). Passively cooled railway embankments for use in permafrost areas. Journal of Cold Regions Engineering, 17 (3), 119–133.

de Grandpré, I., Fortier, D., Stephani, E. (2012). Degradation of permafrost beneath a road embankment enhanced by heat advected in groundwater 1. Canadian Journal of Earth Sciences, 49 (8), 953–962.

Grosse, G., Romanovsky, V., Jorgenson, T., Anthony, K.W., Brown, J., Overduin, P.P. (2011). Vulnerability and feedbacks of permafrost to climate change. Eos, Transactions American Geophysical Union, 92 (9), 73–74.

Hinzman, L.D., Bettez, N.D., Bolton, W.R., Chapin, F.S., Dyurgerov, M.B., Fastie, C.L., Griffith, B., Hollister, R.D., Hope, A., Huntington, H.P. (2005). Evidence and implications of recent climate change in northern Alaska and other arctic regions. Climatic Change, 72 (3), 251–298.

Johansen, Ø. (1975). Thermal conductivity of soils. Ph.D thesis, University of Trondheim. (in Norwegian). Translated in U.S. Army, Cold Regions Research and Engineering Laboratory, Translation 637.

Jorgenson, M.T., Racine, C.H., Walters, J.C., Osterkamp, T.E. (2001). Permafrost degradation and ecological changes associated with a warming climate in Central Alaska. Climatic Change, 48 (4), 551–579.

Kaplan, J.O., New, M. (2006). Arctic climate change with a 2°C global warming: timing, climate patterns and vegetation change. Climatic Change, 79 (3–4), 213–241.

Karunaratne, K., Burn, C. (2003). Freezing n-factors in discontinuous permafrost terrain, Takhini river, Yukon Territory, Canada. In: Proceedings of the 8th International Conference on Permafrost, pp. 519–524 University of Zurich, Switzerland.

Kersten, M.S. (1949). Laboratory research for the determination of the thermal properties of soils. Research Laboratory Investigations, Engineering Experiment Station, University of Minnesota, Minneapolis. Technical Report 23.

Lachenbruch, A.H., Marshall, B.V., 1986. Changing climate: geothermal evidence from permafrost in the Alaskan Arctic. Science 234, 689–697.

Lemmen, D.S., Warren, F.J., Lacroix, J., Bush, E. (2008). From Impacts to Adaptation: Canada in a Changing Climate. Government of Canada, Ottawa, Canada, pp. 448.

McHattie, R.L., Goering, D.J. (2009). Air convection embankment (ACE) design guide. Alaska. Department of Transportation. Report, FHWA-AK-RD-09-06.

M-Lepage, J. (2015). Experimentation of mitigation techniques to reduce the effects of permafrost degradation on transportation infrastructures at Beaver Creek experimental road site (Alaska Highway, Yukon). Mater's thesis, Laval University, Quebec, Canada.

M-Lepage, J., Doré, G., Fortier, D., Murchison, P. (2012). Thermal performance of the permafrost protection techniques at Beaver Creek experimental road site, Yukon, Canada. In: Proceedings of the 10th International Conference on Permafrost, Salekhard, Russia, pp. 261.

Mueller, B. (2007). Climate change and transportation in the NWT. Department of Transportation-Planning, Government of the NWT 06–6855-5000. pp. 1–96.

Nelson, F.E., Anisimov, O.A., Shiklomanov, N.I. (2002). Climate change and hazard zonation in the circum-Arctic permafrost regions. Natural Hazards, 26 (3), 203–225.
Newman, G.P., Wilson, G.W. (1997). Heat and mass transfer in unsaturated soils during freezing. Canadian Geotechnical Journal, 34 (1), 63–70.
Osterkamp, T. (2003). A thermal history of permafrost in Alaska. In: Proceedings of the 8th International Conference on Permafrost, University of Zurich, Switzerland, pp. 863–868.
Osterkamp, T. (2007). Characteristics of the recent warming of permafrost in Alaska. Journal of Geophysical Research: Earth Surface (F2), 112.
Pachauri, R.K., Allen, M.R., Barros, V.R., Broome, J., Cramer, W., Christ, R., Church, J.A., Clarke, L., Dahe, Q., Dasgupta, P. (2014). Climate Change 2014: Synthesis Report. Intergovernmental Panel on Climate Change IPCC, Geneva, Switzerland, pp. 151.
Reimchen, D., Doré, G., Fortier, D., Walsh, R. (2009). Cost and constructability of permafrost test sections along the Alaska Highway, Yukon. In: Proceedings of the Transport Association of Canada Annual Conference. Vancouver, B.C, Canada, pp. 1–20.
Serreze, M., Walsh, J., Chapin, F.S., Osterkamp, T., Dyurgerov, M., Romanovsky, V., Oechel, W.C., Morison, J., Zhang, T., Barry, R. (2000). Observational evidence of recent change in the northern high-latitude environment. Climatic Change, 46 (1–2), 159–207.
Smith, O.P., Levasseur, G. (2002). Impacts of Climate Change on Transportation Infrastructure in Alaska. The Potential Impacts of Climate Change on Transportation. pp. 151–160.
Tice, A.R., Anderson, D.M., Banin, A. (1976). The Prediction of Unfrozen Water Contents in Frozen Soils from Liquid Limit Determinations. U.S. Army Cold Regions Research and Engineering Laboratory. CRREL, Report 76–8.
Woo, M.-k., Lewkowicz, A.G., Rouse, W.R. (1992). Response of the Canadian permafrost environment to climatic change. Physical geography, 13 (4), 287–317.
Zhang, T., Barry, R., Knowles, K., Heginbottom, J., Brown, J. (2008). Statistics and characteristics of permafrost and ground-ice distribution in the Northern Hemisphere. Polar Geography, 31 (1–2), 47–68.
Zottola, J., Darrow, M., Daanen, R., Fortier, D., de Grandpré, I. (2012). Investigating the effects of groundwater flow on the thermal stability of embankments over permafrost. Cold Regions Engineering 2012: Sustainable Infrastructure Development in a Changing Cold Environment. pp. 601–611.

Chapter 4 Modeling the thermal response of air convection embankment in permafrost regions

Foreword

Xiangbing Kong[1], Guy Doré[1], Fabrice Calmels[2], Chantal Lemieux[1]

[1]Department of Civil and Water Engineering, Laval University, Québec City, Québec, Canada

[2]Yukon Research Centre/Northern Climate ExChange, Yukon College, Whitehorse, Yukon, Canada

State: Submitted to review (should be accepted with minor modifications required from the editor)

Date of Submission: 09 December 2018

Journal: Cold Regions Science and Technology

Résumé

La dégradation du pergélisol sous les infrastructures de transport résulte souvent en tassements différentiels dus au dégel du sol de fondation riche en glace. Les changements climatiques sont associés aux problèmes d'ingénierie liés au pergélisol. Les remblais à convection d'air (ACE) sont une méthode efficace pour prévenir le dégel du pergélisol, en réponse aux changements climatiques. Des granulats de dimension uniforme sont utilisés pour faciliter la circulation d'air dans un ACE durant l'hiver lorsque le gradient de densité de l'air est instable. Une section d'essai à grande échelle d'un ACE a été construite en 2008 le long de l'Alaska Highway, à Beaver Creek au Yukon (Canada), pour étudier la capacité d'extraction de chaleur des remblais à convection d'air. Des forages ont été faits et instrumentés en pied et dans l'épaulement du remblai, ainsi qu'au centre de la chaussée. Les données de températures collectées à ce site ont été utilisées pour étudier la performance thermique d'un ACE et pour calibrer le modèle thermique 2D basé sur le site d'essai de Beaver Creek. Pour améliorer la précision du modèle développé, des paramètres spécifiques au site, tel la température de l'air, les propriétés du sol de fondation et les dimensions du remblai, ont été mesurés et utilisés comme paramètres d'entrée. Une nouvelle approche basée sur le bilan thermique à l'interface remblai/sol a été proposée pour étudier la capacité d'extraction de chaleur des remblais à convection d'air. Suite à la calibration du modèle au site de Beaver Creek, un abaque de conception d'ingénierie été développé et est proposé pour évaluer le bilan thermique à l'interface remblai/sol pour différentes épaisseurs de remblai et conditions du site.

Mots clés: Dégradation du pergélisol; Alaska Highway; Remblai à convection d'air (ACE); Bilan thermique

Abstract

Permafrost degradation under transportation infrastructure often results in thaw settlement due to thawing of the ice-rich subgrade. Climate change is associated with permafrost-related engineering problems. Air convection embankments (ACE) have been proven to be an effective method to prevent permafrost thawing, in response to climate change. Poorly-graded aggregates are used to facilitate the air flow in an ACE, especially during winter when the air density gradient is unstable. A large-scale ACE test section was constructed along the Alaska Highway in 2008 at Beaver Creek, Yukon, Canada, to investigate the heat extraction capacity of ACEs. Boreholes under the toe, the side slope and the centerline were drilled and instrumented. Temperature data collected at this site were used to investigate the thermal performance of the ACE and to calibrate a 2D thermal model that was developed based on the Beaver Creek experimental site. Specific site characteristics, such as air temperature, foundation soil properties and embankment dimensions, were measured and used as input parameters to improve the accuracy of the 2D model developed. A relatively new approach based on heat balance at the embankment-soil interface has been proposed to investigate the heat extraction capacity of ACEs. After satisfactory calibration of the model at the Beaver Creek site, an engineering design chart has been developed and is proposed to assess the heat balance at the embankment-soil interface for different embankment thicknesses and site conditions.

Keywords: Permafrost degradation; Alaska Highway; Air convection embankment (ACE); Heat balance

4.1 Introduction

Permafrost refers to soil, rock, ice and organic material, with temperatures at or below 0 °C for at least two consecutive years. Permafrost is widespread and it underlies approximately 24% of exposed land surface in the Northern Hemisphere (Brown and Haggerty, 1998; Davis, 2001). About half of Canadian permafrost is qualified of “warm permafrost”, with temperatures ranging between -2 °C and 0 °C (Smith, 2011).

Permafrost underlying transportation infrastructure supports the load of embankments and traffic; thus any mechanical failure can directly affect the normal operations, reduce the ride quality and increase the potential risks for users. Permafrost degradation mainly results in increased thaw settlements, reduced ground bearing capacity, and degradation of drainage systems leading to most engineering problems for permafrost transportation infrastructure. The degradation of permafrost is caused by many complex factors; the most important being: changes in surface characteristics caused by removal of vegetation and use of low albedo surfacing materials; embankment geometry, causing snow accumulation on the side slopes and modification to

surface and sub-surface water flow; and expected climate change, increasing of air temperature and precipitation (Doré, et al., 2016).

Temperatures in Arctic areas have drastically increased due to climate change and will continue to in future (Serreze et al., 2000). Projections of future climate change suggest that a large proportion of transportation infrastructure is located in a high hazard region in the Northern Hemisphere (Anisimov et al., 1997; Nelson et al., 2002). Recent studies (e.g., M-Lepage, 2015; Darrow and Jensen, 2016) recommend air convection embankments (ACE) to prevent permafrost degradation under transportation infrastructure. It is a relatively new method compared to other mitigation methods, such as air duct systems, high albedo surfaces and thermosyphons. The concept of ACE was first reported in Russia (Vinson et al., 1996), and later tested and developed in several other countries, such as United States, Canada and China.

ACEs involve the use of a highly porous, poorly-graded granular material to construct the main portion of the embankment (e.g., Goering, 2002, 2003). During winter, low ambient air temperatures cool the surface and upper portion of the embankment, while the temperature at the bottom remains relatively warm due to the heat accumulation in the ground during summer and warm permafrost temperatures in the fall. This results in a natural convection system, as an unstable air density gradient within the pore space of the ACE causes cold air in the upper portion to sink to the bottom where it is replaced by warm air moving upward, which accelerates the heat transfer from the bottom to the upper portion of the ACE. This system enhances winter heat transfer in a porous embankment with sufficient air permeability. During summer, the atmospheric air temperature warms the upper portion of the ACE, while air is relatively cold at the bottom, resulting in a stable air density gradient and natural convection does not occur. Since air has a much lower thermal conductivity than coarse-grained embankment fill, ACEs also act as an insulation layer to prevent heat from flowing into foundation soils during summer (Goering, 2002).

Current knowledge of fluid flow through a porous medium facilitated the development of ACEs (Bear, 1972; Segerlind, 1976; Lunardini, 1981; Nield and Bejan, 1992). A significant amount of research on the heat extraction capacity of ACEs in permafrost regions, including field and lab experiments, as well as numerical simulations, has been carried out, and the results show that heat extraction capacity heavily depends on several main factors, such as crusher rock layer thickness (e.g., McHattie and Goering, 2009; Sun et al., 2005; Doré et al., 2016), boundary conditions (e.g., Goering and Kumar, 1996; Goering, 1998; Goering 2002, 2003; Jørgensen et al., 2008; Doré et al., 2016), stone size (e.g., Esch, 1996; Goering and Kumar, 1996; Goering, 2002), and embankment configuration (e.g., Goering and Saboundjian, 2004; Xu and Goering, 2008; Doré et al., 2012; Gaumond et al., 2012).

The Alaska Highway links Alaska to the rest of the continent U.S, via Yukon Territories and British Columbia, and it passes through extensive areas of warm and ice-rich discontinuous permafrost, highly sensitive to degradation. It is a crucial road for the economic development of northwestern Canada and the United States. Permafrost degradation related failures, such as differential settlements, longitudinal cracks and sinkholes, have been observed along the Alaska Highway (M-Lepage, 2015).

To investigate the heat extraction capacity of an ACE to protect permafrost from thawing, a large-scale ACE section was constructed along the Alaska Highway in 2008 at Beaver Creek, Yukon, Canada. Using the available research and data from this site, the primary goals of the research reported here are to: 1) assess the thermal performance of the large-scale ACE in response to global warming observed on the Alaska Highway at Beaver Creek; 2) develop a 2D thermal model, calibrated to the measured data from Beaver Creek; 3) apply a relatively new method based on heat balance, to assess the heat extraction capacity of an ACE layer; and 4) propose an engineering design tool to optimize the thickness of ACE layer as a function of heat extraction requirement for specific site conditions.

4.2 Site description and ground thermal regime

The Beaver Creek test site is located on the Alaska Highway at 62°20' N, 140°50' W, about 30 km south of the Canada-United States border (Figure 4.1). This site is located in a warm, thaw-sensitive, discontinuous permafrost region, with a dry continental climate (Brown, 1967). Mean annual precipitation from 1971 to 2000 is 419 mm, of which 123 mm is snow and 296 mm is rain (Environment Canada, 2011). The summers are warm, dry and short while the winters are long and cold (M-Lepage, 2015). The mean annual air temperature is -5.5 °C and annual average range of air temperature is 36.8 °C based on climate data recorded between 1971 and 2000 (Environment Canada, 2011).

The 3.3 m thick ACE section at the Beaver Creek test site is underlaid mainly by ice-rich mixture of silt and peat. Thermistor strings, with a standard recording accuracy of ± 0.1 °C, were installed in three 15.5 m deep boreholes located at the toe, the side slope and the centerline of the ACE (Figure 4.2a). Photos of the ACE during construction and after construction with grass growing on the side slope are shown in Figure 4.2b and Figure 4.2c, respectively. To prevent warm air to enter in the convection material in the summer, a geotextile was laid out above the ACE layer and a 30 cm-thick layer was added on the geotextile and the side slope during the construction of the ACE. The sensors have a spacing varying from 0.1 m to 1.0 m. The temperature data, collected automatically every 4 hours since October 2008, were analyzed to assess the effects of the ACE on the thermal state of the permafrost underlying the road, in response to climate change.

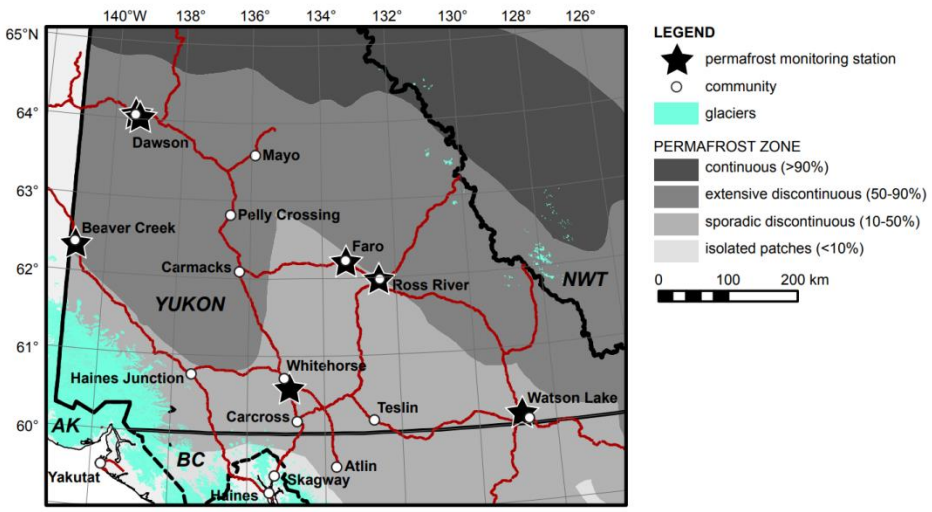

Figure 4. 1: The location of the Beaver Creek experimental site, along the Alaska Highway, Yukon, Canada (Lipovsky, 2015).

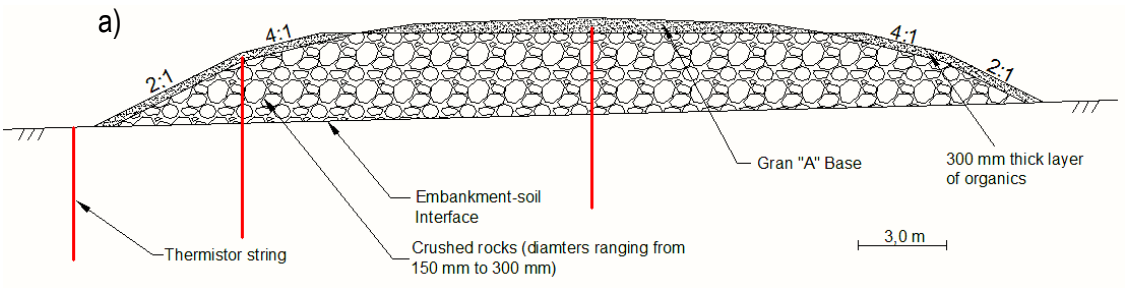

Figure 4. 2: Air convection embankment (ACE) at Beaver Creek, Yukon: a) diagram of the ACE; b) during the construction of the ACE; c) after the construction of the ACE.

Figure 4.3 illustrates temperature variations under the centerline of the embankment over a five year period from December 2008 to December 2013. The embankment-soil interface is used as the reference level (0 m), and below the reference level, it is the natural ground with negative values of depth along the y-axis. Figure 4.3 shows that an embankment thickness of 3.3 m (under the centerline) did not prevent the thaw front from penetrating into the natural ground. Nevertheless, in the summer of 2009, one year after the construction of the ACE, the permafrost table was around 2.25 m under the embankment-natural ground interface, and it gradually moved up by a small magnitude of nearly 0.15 m over the five year period from 2009 to 2013. This confirms that the ACE succeeded in stabilizing the active layer thickness under the centerline. In contrast, the permafrost table deepened at the control section of this experimental site (Coulombe et al., 2012; M-Lepage, 2015).

During winter, the ACE layer across the embankment showed a strong passive cooling influence by reducing the ground temperatures. This is due to the air convection in the ACE layer, enhancing the heat transfer in winter. The -1 °C isotherm, for instance, lowered into the ground during the winter period from 2009 (-3.33 m) to 2013 (-7.30 m) (Figure 4.3). It is also possible to observe that the cooling zone, -1 °C isotherm for example, was getting bigger with time, which means that heat is effectively being removed from the soil underneath the embankment. The warm zone (≥ 0 °C), is stable over the monitoring period. As a result, more heat was extracted from the ground, and soil temperatures generally decreased with time.

Figure 4.4 shows the variation of natural ground temperature with time at a depth of -2.5 m under the centerline. The temperature generally decreased during winter with minimum temperatures reaching -2.5 °C in 2009 and -5.1 °C in 2013. By contrast, the change in the maximum yearly ground temperatures was limited in the summer, with the temperature difference less than 0.2 °C.

Under the side slope, isotherms with positive temperature values can quickly reach the natural ground underneath the embankment-soil interface, and the permafrost table reached a greater depth than that under the centerline, mainly due to the reduced embankment thickness and thermal boundaries (Figure 4.5). During summer 2009, the permafrost table was -2.84 m under the side slope of the embankment, and as under the centerline, it showed little change in the following four years. However, the ground temperatures did not show a continuous decrease in the winter. The lowest position of the -0.5 °C isotherm, for instance, moved up during the period from 2009 (-2.24 m) to 2011 (-0.95 m), then moved back down with the position reaching -2.23 m in 2013, probably due to the combined effects of yearly atmospheric temperature and snow thickness on the side slope.

The comparison between the winter thermal regime for the centerline and the side slope suggests that heat extraction of the ACE mainly occurred under the traffic lanes and did not have much effect under the side slope of the embankment.

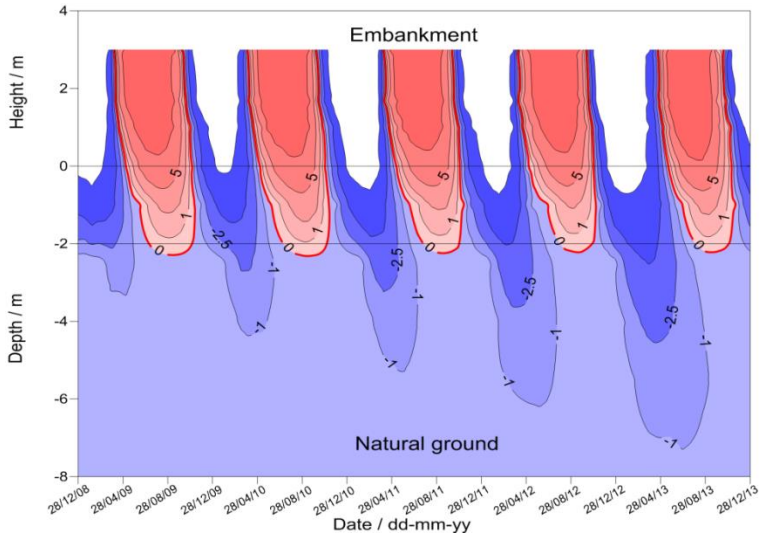

Figure 4. 3: Evolution of embankment and ground temperature with time under the centerline for the ACE section at the Beaver Creek experimental site.

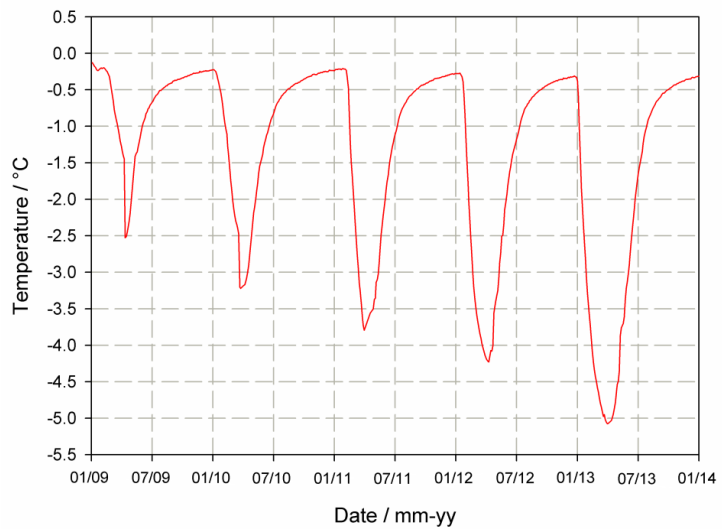

Figure 4. 4: Natural ground temperatures variation with time at -2.5 m under the centerline of the ACE section.

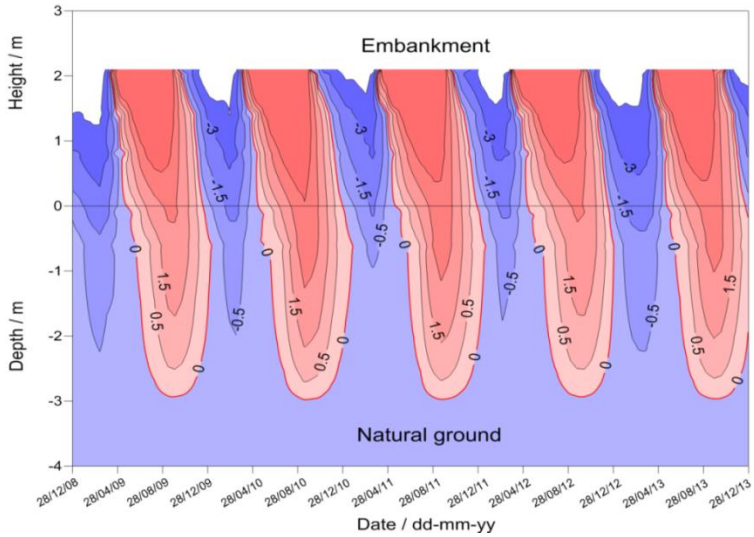

Figure 4. 5: Evolution of embankment and ground temperature with time under the side slope for the ACE section at the Thermal behavior of the Beaver Creek experimental site.

4.3 Thermal modeling

The thermal model was developed to simulate the case of the ACE section at the Beaver Creek test site in Yukon. The coupled software SVHEAT for thermal conduction and SVAIR for density-driven air convection, 2D/3D finite element program from SoilVision, were used for modeling. Site-specific parameters, such as near-surface air temperature, thermal properties of foundation soil and embankment dimensions, were used to improve the accuracy of the 2D model developed. After calibration of the model, it was used to develop an engineering design chart to assess the heat extraction capacity of the ACE for different embankment thicknesses and site conditions.

4.3.1 Governing equations and physical domains

Considering the air density in a crushed rock embankment is very unstable in the winter, Darcy's law can be used to determine the air flow due to pressure, neglecting water content and inertial forces at the surface of the crushed rocks. The governing equations for mass, momentum and energy can be expressed as follows (Goering and Kumar, 1996, cited from Nield and Bejan, 1992):

Continuity:

$$\frac{\partial q_y}{\partial y} + \frac{\partial q_x}{\partial x} = 0 \tag{4.1}$$

Momentum:

$$q_y = -\frac{K}{\mu} \bullet (\frac{\partial P}{\partial y} + \rho_a g) \tag{4.2}$$

$$q_x = -\frac{K}{\mu} \bullet \frac{\partial P}{\partial x} \tag{4.3}$$

$$\rho_a = \rho_0 [1 - \beta (T - T_0)] \tag{4.4}$$

Energy:

$$\frac{\partial}{\partial x}(k_x \frac{\partial T}{\partial x}) + \frac{\partial}{\partial y}(k_y \frac{\partial T}{\partial y}) - (C_a q_x{}^a) \frac{\partial T}{\partial x} - (C_a q_y{}^a) \frac{\partial T}{\partial y} = C \frac{\partial T}{\partial t} \tag{4.5}$$

where t is the time (s); T is the temperature (°C); k is the thermal conductivity (W/m-°C)); K is the intrinsic permeability of the porous medium (m^2); P is the pressure (Pa); C is the volumetric heat capacity of porous medium (J/(m^3-°C)); L_f is the volumetric latent heat of fusion of water, which is equal to 3.34×10^8 J/m^3; x and y are the coordinates (m); C_a and q^a are the volumetric heat capacity of air (J/(m^3-°C)) and pore-air flow velocity (m/s), respectively; θ_u is the volumetric unfrozen water content at a given negative temperature (m^3/m^3); μ and β are the kinematic viscosity (kg/m-s) and the coefficient of thermal expansion for air, respectively; and, ρ_0 and T_0 are the reference air density (kg/m^3) and the reference temperature (°C), respectively.

For the foundation soil, neglecting the convection due to water and air flow, conduction is the main heat transfer mode. The equation governing two dimensional, non-linear heat flow can be expressed as (Newman and Wilson, 1997):

$$\frac{\partial}{\partial x}(k_x \frac{\partial T}{\partial x}) + \frac{\partial}{\partial y}(k_y \frac{\partial T}{\partial y}) = C\frac{\partial T}{\partial t} - L_f \frac{\rho_i}{\rho_w}\frac{\partial \theta_i}{\partial t} \tag{4.6}$$

where ρ_i and ρ_w are the ice density and water density (kg/m^3), respectively; and θ_i is the volumetric ice content (m^3/m^3).

The modeled physical domain represents an area 20 m wide from the toe of the embankment and 30 m beneath the original ground surface (Figure 4.6). In the physical domain, part ① is the porous medium with a high permeability, consisting of crushed rocks; part ② is the saturated ice-rich mixture of silt and peat with a volumetric water content of 36%; part ③ is the 300 mm thick layer of organics covering the side slope of the ACE and; part ④ is the crushed base course aggregate. The measured embankment thickness is 3.3 m under the centerline.

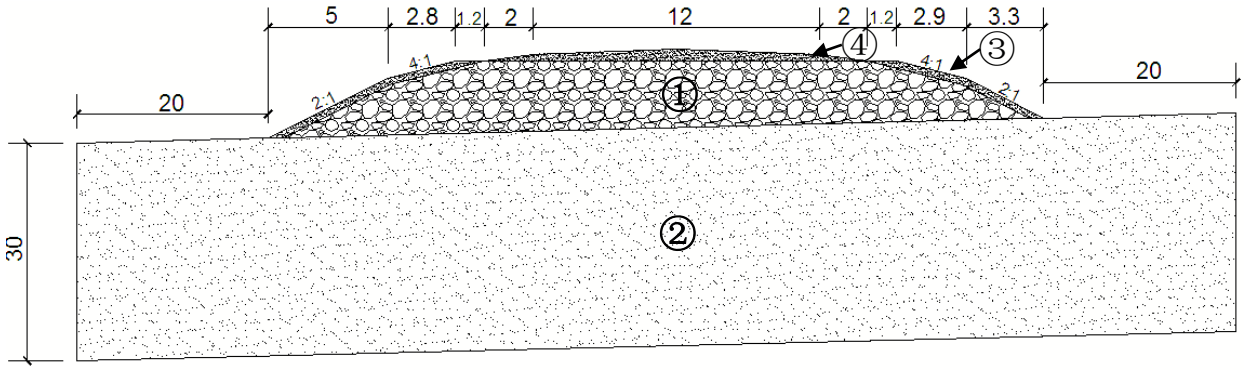

Figure 4. 6: Physical domain of the embankment and foundation (unit: m).

4.3.2 Material properties and boundary conditions

In soils with a small particle size, such as clays and silts, thermal conduction is the main heat transfer mechanism. However, with increasing particle size, heat radiation should be considered in the heat transfer process (Johansen, 1975). Experiments using a particle size of 20 mm indicated that heat radiation contributed up to 10% of total heat transfer at normal temperatures (Wakao and Kato, 1969). For crushed rocks with an equivalent particle size ranging from 90 mm to 100 mm, heat radiation was about two times greater than heat conduction (Fillion et al., 2011). Previous numerical simulations on the heat extraction capacity of an ACE did not consider the effects of the thermal radiation properties of crushed rocks on net heat extraction (e.g., Goering and Kumar, 1996; Sun et al., 2005; Darrow and Jensen, 2016). Neglecting heat radiation will underestimate the rate of heat transfer in the ACE layer. The thermal conductivity of crushed rocks considering heat radiation was estimated using the equation developed through lab experiments (Fillion et al., 2011):

$$k_e = \frac{(k_{2p}\lambda_s - \lambda_f)(1-n) + \lambda_f}{1 + (k_{2p} - 1)(1-n)} + 4Ed_{10}\sigma T^3 \tag{4.7}$$

$$k_{2p} = 0.29(15\lambda_f / \lambda_s)^{\varphi} \tag{4.8}$$

where k_e is the effective thermal conductivity (W/m-K); λ_s is the thermal conductivity of a solid (W/m-K); λ_f is the thermal conductivity of a fluid (air); φ is the empirical factor accounting for structure, n is the porosity of the porous medium; E is the exchange factor; σ is the Stefan-Boltzmann constant and is equal to 5.67E-8 W/m^2-K^4; T is the temperature (K); and d_{10} is the particle diameter (10% of the whole matieral mass has particles smaller than d_{10}) in a nonuniform porous medium (m). On the right side of Equation 4.7, the second term represents the radiation component.The embankment aggregate consists of a dry crushed rock material with diameters ranging from 150 mm to 300 mm. ACEs generally have a porosity of about 40% to form interconnected, convection cells (Doré et al., 2016), and the porosity of crushed rocks was assumed to be 0.4 in the model. The thermal conductivity function used in the model for the crushed rock material including thermal radiation is shown in Figure 4.7.

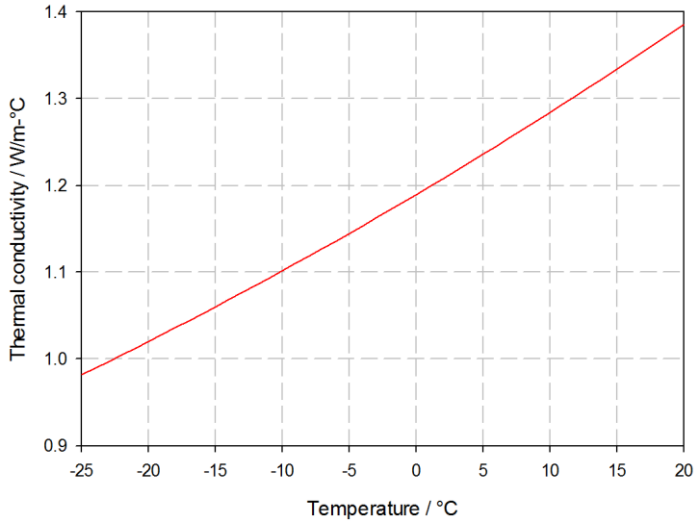

Figure 4. 7: Thermal conductivity of crushed rocks, considering thermal radiation.

The unfrozen water content has a large effect on the volumetric heat capacity (C), which can be calculated with the following equation (Farouki, 1986):

$$C = \rho_d\left(c_s + c_w w_u + c_i w_i\right) \tag{4.9}$$

where c_s, c_w and c_i are the mass-specific heat of solids, water, and ice, respectively; and w_u is the gravimetric unfrozen water content of the soil, and w_i is the gravimetric ice content of the soil. The values of c_w, c_i are 4184 J/(kg-°C) and 2100 J/(kg-°C), respectively (Farouki, 1986). The water content of crushed rocks is assumed to be zero, considering the crushed rock size and high permeability. With a negligible water content, a specific heat capacity of 755.5 J/(kg-°C) and a solid dry density of 2440 kg/m^3, the volumetric heat capacity is 1.098 MJ/m^3. This value is similar to that used by Goering (2003) (C=1.02 MJ/m^3) for the thermal modeling of an ACE, which was composed of crushed rocks with a porosity of 0.35 and a dry density of 1625 kg/m^3.

One of the most difficult variables to obtain is the intrinsic permeability, and it generally increases as mean particle size increases and the size distribution becomes more uniform (Saboundjian and Goering, 2003). Theoretical and empirical relations have been developed to estimate the intrinsic permeability of coarse-grain materials and different forms of equations have been proposed (Côté et al., 2011). In the thermal model, a Kozeny-Carman equation modified by Chapuis (2004) was used to obtain intrinsic permeability:

$$K = 1.25(10^{-4})\alpha^{0.7825} \tag{4.10}$$

$$\alpha = \frac{d^2{}_{10}}{(1-n)^2} n^3 \tag{4.11}$$

where d_{10} and n are the effective particle size (m) and the porosity of crushed rocks, respectively. The ACE was constructed using 150 mm to 300 mm crushed rocks with a negligible water content. The permeability of the ACE layer is estimated to be $K = 2.61\times10^{-6}$ m^2, based on the assumed porosity of 0.4 and the effective particle size of 200 mm for the crushed rocks in the ACE layer.

The foundation soil is a uniform ice-rich mixture of silt and peat with a volumetric water moisture content of 36% based on the summer drilling program and thermal properties of foundation soil, which were measured in the laboratory. Air flow and water flow were restricted in the foundation soil by setting the water flux to zero and the air permeability to an arbitrary value of 1×10^{-10} m/day. The air permeability was set to a much smaller value than that used by Darrow and Jensen (2016) (3.05×10^{-6} m/day) for the foundation soil in the model of the ACE. Table 4.1 is the summary of material properties used in the thermal model.

Table 4. 1: Material properties for the ACE layer and foundation soil.

Material type	k_f (W/m-°C)	k_u (W/m-°C)	C_f (MJ/m^3-°C)	C_u (MJ/m^3-°C)	K (m^2)	θ (m^3/m^3)
ACE layer	---	---	1.098	1.098	2.61×10^{-6}	≈ 0
Foundation soil	1.337	0.907	1.73	2.51	≈ 0	0.36

The water content of the 30 cm-thick soil layer (part ③, Figure 4.6) and crushed base course aggregate (part ④, Figure 4.6) was assumed to be 3%, based on laboratory testing of the shallow portion of the embankment soils in the control section (Doré et al., 2007). The thermal properties are estimated using Kersten's equations, as the most commonly used reference for the thermal conductivity, for coarse and fine-grained soils (Kersten, 1949).

There are two types of air flow boundaries: impermeable and permeable boundaries. The air-permeable boundary indicates that the ambient air can directly enter the ACE, but is unable to for the air-impermeable boundary. The selection of impermeable or permeable boundaries depends on the actual site conditions. Due to the fact that the road surface was covered by asphalt and the side slope was covered by soils, impermeable boundaries were applied in the thermal model. Zero air flow flux boundary was applied on the embankment surface, natural ground surface and side slope to prevent atmospheric air from flowing into or out of embankment and foundation.

The thermal boundary conditions consisted of temperature functions applied to the embankment and natural ground, and a constant heat flux boundary was applied to the bottom, right and left boundaries. At the left-hand and right-hand boundaries, a zero heat flux was applied, considering the negligible temperature variation. The geothermal gradient varies on the different sites in Northern Canada, and it generally ranges from 0.009 m/°C to 0.033 m/°C (Brown, 1963). At the bottom of the thermal model, the geothermal heat flux of 0.03 W/m^2 was applied, considering its limited effect on the permafrost temperature in the model.

At the upper boundaries of the physical domain, exposed to the environment, the approximate temperature curve with a thermal modifier (n-factor) was used in the analysis, due to the unavailable data such as air relative humidity and net radiation, for the calculation of a more accurate surface energy balance boundary. Air temperature data for Beaver Creek, Yukon indicated an average air freezing index of -3023 °C-day and average air thawing index of 1604 °C-day from 2009 to 2013 (Figure 4.8). The simulated air freezing and air thawing index from the approximate sinusoidal curve were -3025 °C-day and 1551.5 °C-day, respectively, which is close to the measured ones. Therefore, the simulated approximate temperature curve was reliable for the numerical simulation (Figure 4.8). The air temperature with modified n-fatcor is the most critical input parameter for the model results (Darrow, 2011). The yearly n-factor was assumed to be constant, neglecting

the yearly change due to variable factors, such as solar radiation, cloud cover, wind speed, snow cover, surface vegetation and precipitation. These environmental factors and soil surface conditions are considered to be the same during the numerical simulation.

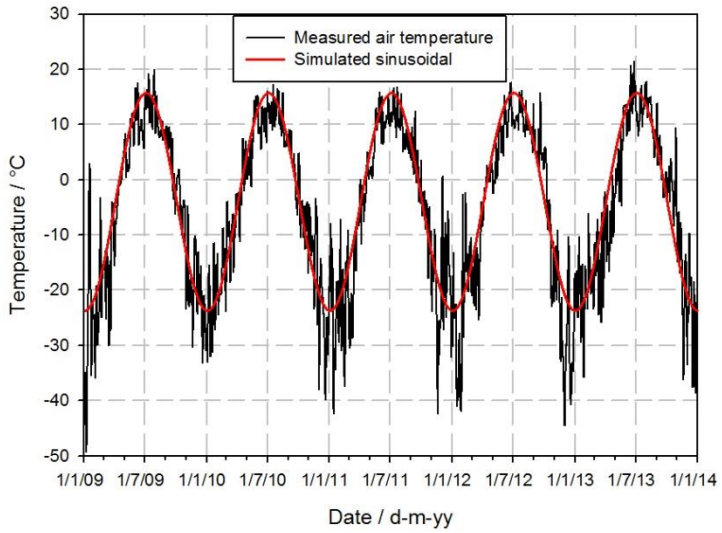

Figure 4. 8: Comparison between measured air temperature and simulated sinusoidal temperature.

Snow accumulation on the side slope of the embankment and natural ground insulates and prevent heat extraction from the underlying ground in the winter, resulting in warm permafrost and a thicker active layer (Johnston, 1981). A field investigation was done to assess the snow accumulation on the side slope of the ACE and the adjacent natural ground surface along profiles parallel and perpendicular to the road alignment during the winter season of 2010. Based on field measurements, the average snow cover thickness was 42 cm to 45 cm on the side slope and on the adjacent natural ground surface (Stephani, 2013). The value of the n-factor with a snow cover on the side slope of the embankment was selected based on the logarithmic relationship between the n-factor value and the snowpack thickness, developed by Lanouette et al. (2015). The thawing n-factors for the embankment surface and side slope were initially 1.9 and 1.7, respectively, based on published values (Goering and Kumar, 1996). The values were slightly adjusted based on the model calibration to ensure that the simulated active layer thickness and ground temperatures were similar to the measured field data. Table 4.2 summarizes all the n-factors used in the model.

Table 4. 2: Summary of n-factor values used in the thermal model.

Surface type	n_t	n_f
Natural ground surface	0.37[a]	0.29[a]
Embankment surface	1.95[b]	1.0[a]
Embankment side slopes	1.85[b]	0.30[a]

[a]Values obtained from the literature (Lunardini 1978; Andersland and Ladanyi, 2004; Lanouette et al., 2015); [b]Values obtained through a sensitivity analysis.

4.3.3 Modeling stage and time step

The physical domain consists of a roadway embankment and an underlying foundation, shown in Figure 4.6. Due to the asymmetry, the whole physical domain was used to carry out the simulation. The first step for the transient analysis was to develop the initial temperature field for the model. The simulated temperature field including a steady analysis and a transient analysis or the measured temperature data can be both applied as the initial temperature field. The measured temperature data for the control section was available and as a result, applied as the initial temperature field for the 2D model of the ACE.

The grid resolution could affect the numerical results, and case studies with different meshing densities have been done to confirm that the selected resolutions had limited effects on the heat transfer process in the model developed. Numerical simulation was carried out with a finite element grid consisting of 4127 triangular elements and 8460 nodes. The grid was not uniform, with an element size ranging from less than 0.32 m in the embankment to approximately 2 m at the bottom of the foundation. To better simulate the active layer, a higher element density was automatically set near the embankment and the shallow portion of the foundation. The ACE was constructed in 2008 and the temperature data from 2009 to 2013 were analyzed. Due to the non-linear effect of the air convection mechanism in the ACE layer, an automatic step less of than 0.2 days was used with a total simulation time of 5 years in order to compare the simulated results with available field data. The daily ground temperatures taken at various depths were exported for future analysis during the 5-year simulation. In previous research, the winter air flow characteristics and thermal regime of an ACE layer are largely documented (e.g., Goering and Kumar, 1996; Goering, 1998; Sun et al., 2005; Darrow and Jensen, 2016); however, the main interest of this project is to explore the heat extraction capacity of an ACE layer to decrease ground temperatures.

4.3.4 Results from the calibrated model

The soil temperature varies annually in the shallow portion of the foundation due to the atmospheric air temperature and, in general, soil temperature profiles at various depths at a given time cannot directly indicate the annual effect of atmospheric air temperature. Batenipour et al., (2010) suggest that the average annual soil temperature gradient is a good indicator of net heat flow through the ground surface in one year.

Figure 4.9 and Figure 4.10 indicate the measured and simulated mean annual soil temperature profiles at various depths under the centerline and under the side slope in 2009 and 2013, respectively. Note that the foundation soil contains the peat, which is likely to induce a thermal offset underneath the embankment. From Figure 4.9, it can be seen that the simulated mean annual ground temperatures at various depths were higher than the measured ones except at -5.5 m below the natural ground surface in 2009. In the embankment, the temperature difference between simulated mean annual soil temperatures and measured mean annual soil

temperatures ranged from 0.01 °C to 1.0 °C above the embankment-soil interface, however, a smaller range of 0.09 °C to 0.24 °C was observed in the foundation. In 2013, the temperature difference was typically 0.01 °C to 0.58 °C above the embankment-soil interface. Below the embankment-soil interface, the simulated mean annual ground temperatures came closer to the measured mean annual ground temperatures with a maximum temperature difference of 0.14 °C at a depth of -5.5 m in 2013.

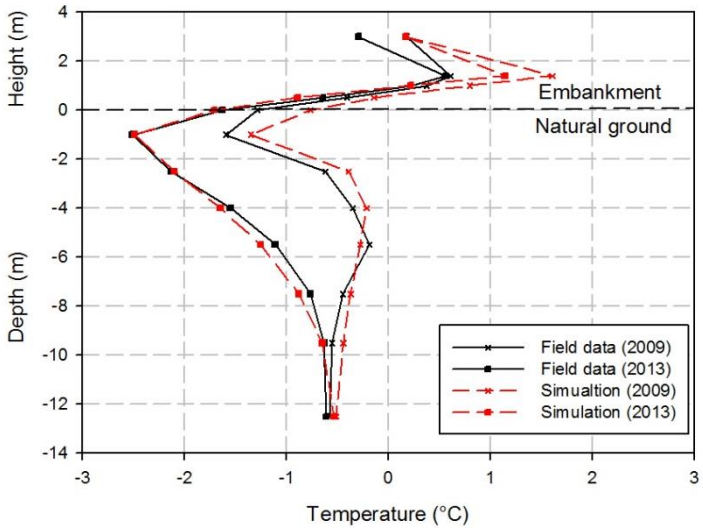

Figure 4. 9: Comparison of measured mean annual soil temperatures and simulated mean annual soil temperatures under the centerline of the ACE in 2009 and 2013.

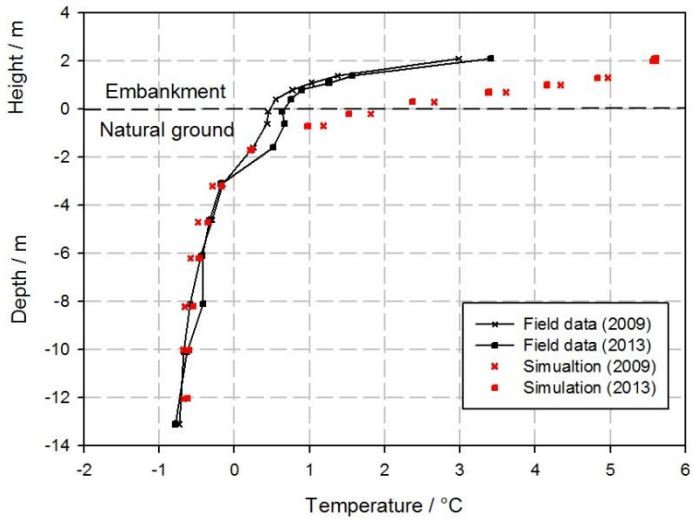

Figure 4. 10: Comparison of measured mean annual soil temperatures and simulated mean annual soil temperatures under the side slope of the ACE in 2009 and 2013.

Under the centerline, the simulated mean annual ground temperatures came closer to the measured mean annual ground temperatures in the first 4 m below the embankment-soil interface in 2013, compared to in 2009. This was probably due to the fact that the construction of the ACE affected the ground temperature

distribution in the first year. Lingnau (1985) indicated that re-establishing the thermal regime is necessary since stabilization requires 3 and 5 years in areas of summer and winter construction, respectively. With time, the calibrated model improved its ability to estimate thermal regime changes of underlying permafrost in the foundation.

Under the side slope, measured mean annual ground temperatures illustrated a limited variation with a maximum temperature difference less than 0.27 °C between 2009 and 2013, indicating less heat extraction than under centerline (Figure 4.10). The simulated mean annual soil temperatures and the measured mean annual soil temperatures had a similar trend of temperature decreasing with depth, and the simulated mean annual soil temperature was typically 1.62 °C to 3.60 °C higher than the measured mean annual soil temperatures in the embankment in the two selected years. The n-factor is a crucial input parameter for the thermal model, which directly affects the temperature distribution of foundations (Darrow, 2011). Based on field measurements, the snowpack thickness on the side slope changed with time in the winter at this experimental site (Lanouette et al., 2015). The discrepancy between the simulated mean annual soil temperatures and the measured mean annual soil temperatures is likely attributed to the simplified n-factor, neglecting the monthly and yearly variation of snowpack thickness on the side slope. Below 1.6 m in the ground, the simulated mean annual ground temperatures was more accurately estimating the measured mean annual ground temperatures with a maximum temperature difference less than 0.2 °C.

Natural convection and heat conduction are the primary heat transfer mechanisms in the ACE layer in the winter and summer, respectively. Figure 4.11a and Figure 4.11b compare the measured soil temperatures and the simulated soil temperatures under the centerline of the ACE in December and July 2013, respectively. Figure 4.11a indicates the ground temperatures increased with depth in December, with measured minimum temperatures and simulated minimum temperatures in the top portion of the ACE layer reaching -20.5 °C, -18.3 °C, respectively. The difference between measured soil temperatures and simulated soil temperatures decreased with depth in the ground, except at a depth of -1.0 m where the temperature difference was 1.32 °C. The maximum temperature difference reached 4.78 °C in the embankment. At the embankment-soil interface, the temperature difference was 0.38 °C. In general, the simulated ground temperature came closer to the field data in July, with a maximum temperature difference reaching 0.67 °C at the embankment-soil interface (Figure 4.11b). Larger temperature differences were observed in the top portion of the embankment.

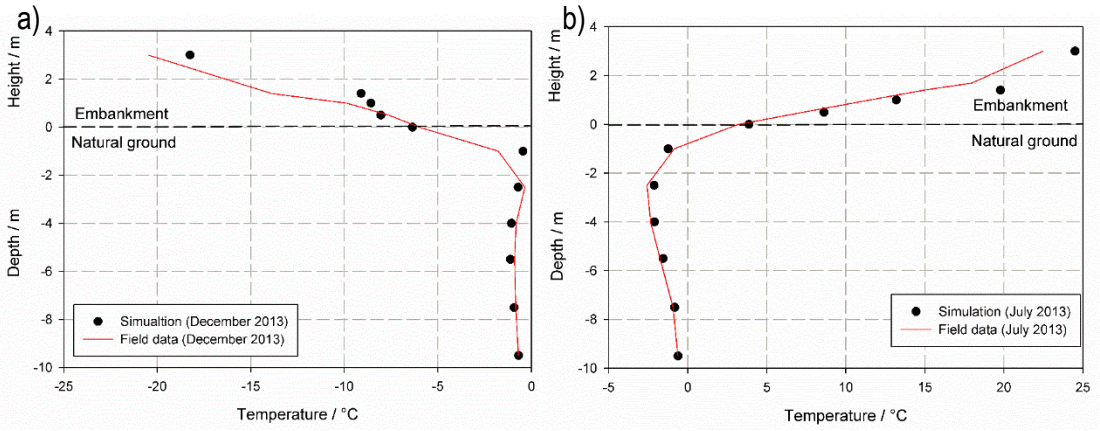

Figure 4. 11: Comparison of measured soil temperatures and simulated soil temperatures under the centerline of the ACE in: a) December 2013; and b) July 2013.

Figure 4.12a and Figure 4.12b compare the simulated soil temperatures and measured soil temperatures under the side slope in December and July 2013, respectively. The results indicate that the simulated ground temperatures beneath the embankment came closer to the measured ground temperatures in July, with a maximum temperature difference reaching 1.31 °C at -0.2 m. Below this depth, the temperature difference decreased significantly, with the maximum temperature difference reaching 0.44 °C. In December, in the first 2 m below the embankment-soil interface, the simulated ground temperatures were around the measured ground temperatures, with a maximum temperature difference less than 0.3 °C. Below -2 m, the simulated ground temperatures more accurately matched the measured ground temperatures with a maximum temperature difference less than 0.04 °C.

In summary, the simulated soil temperatures accurately estimated the measured soil temperatures in the ground under the side slope and under the centerline in the two selected months, supporting the choice of material properties, thermal boundaries and developed model.

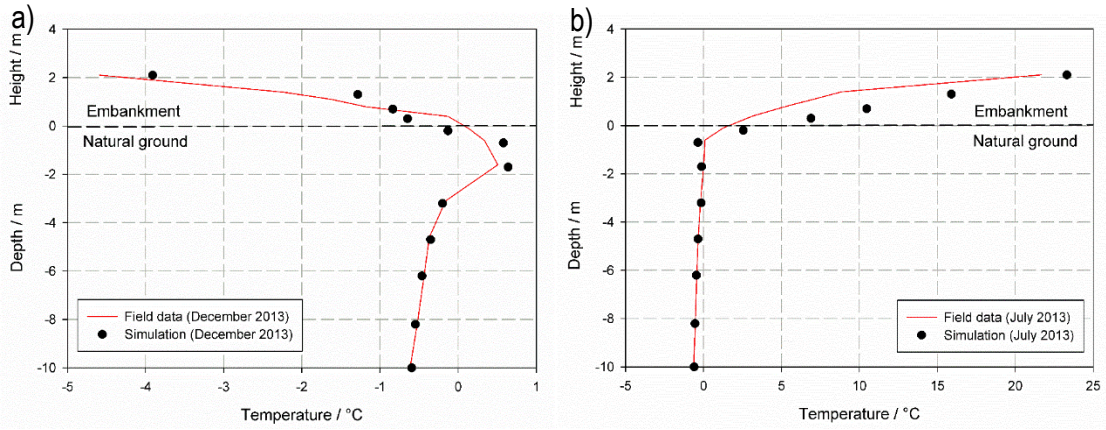

Figure 4. 12: Comparison of measured soil temperatures and simulated soil temperatures under the side slope of the ACE in: a) December 2013; and b) July 2013.

Heat balance is a relatively new method to assess the heat budget through an embankment-soil interface, based on the heat flux measurements at the embankment-soil interface over one year. Heat balance is the summation of the heat extraction index (H_x) and the heat induction index (H_i) for one year, which can be expressed as (M-Lepage et al., 2012):

$$H_x = k_{frozen} \times \frac{T_1 - T_2}{\Delta z} \times \Delta t \tag{4.12}$$

$$H_i = k_{unfrozen} \times \frac{T_1 - T_2}{\Delta z} \times \Delta t \tag{4.13}$$

where H_x , H_i are the heat extraction index and heat induction index, respectively; T_1 , T_2 are the ground temperatures at the interface and at the depth of h_1 under the interface; Δz is the absolute difference between the interface and h_1 ; k_{frozen} and $k_{unfrozen}$ are the thermal conductivity in frozen and thawed states in the surface ground layer (Table 4.1), respectively. Heat balance with positive values indicates that more heat flows into the foundation than out of the foundation, therefore the thermal state of the permafrost underlying transportation infrastructure is unstable. The temperature profile obtained from the calibrated model matched the measured temperature profile (Figure 4.9~4.11), however, the detailed variation of ground temperatures with time cannot be seen in these figures, but are required to calculate the heat balance. Under the centerline, the heat balance was calculated from the interface to the depth of 12.5 m with approximately zero annual amplitude (Figure 4.9) and Δt was specified to be 1.0 day (Equations (4.12) and (4.13)).

The comparison between the simulated heat balance and the calculated heat balance based on the measured field data under centerline during the period from 2009 to 2013, is shown in Figure 4.13. From this figure, it can be seen that the heat balance based on the field data followed the yearly change of measured air freezing index, and it showed a variation with a maximum value and minimum value reaching -3.35×10^6 J/m^2 and -8.07×10^6 J/m^2, respectively. The 5-year average air temperature was applied on the top boundaries of the model, without considering the changing air freezing index. Heat balance from the calibrated model to reproduce the ground thermal regime after the construction of ACE, showed a continuously decreasing trend with a decreasing cooling rate, indicating that the foundation soil was approaching a stable state after a few years. The yearly change of heat balance from the developed model decreased with time, with the heat balance difference reaching 1.26×10^6 J/m^2 and 0.23×10^6 J/m^2 between 2009 and 2010 and between 2012 and 2013, respectively. The average five-year heat balance from the calibrated model and field data are respectively -5.30×10^6 J/m^2, -5.94×10^6 J/m^2, and the discrepancy was around 10%.

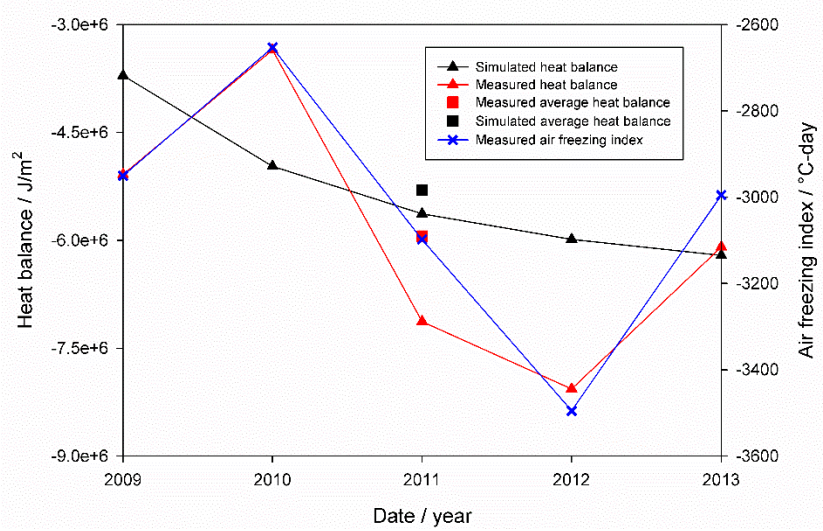

Figure 4. 13: Comparison of heat balance based on the calibrated model and field data under the centerline.

4.3.5 Development of a design chart for thermal stabilization of embankments on permafrost

After the model was well calibrated using the data from the Beaver Creek test site, sensitivity analyses were carried out to explore the heat extraction capacity of an ACE layer through the embankment-soil interface along the centerline with different embankment thickness and site conditions.

The Rayleigh number is a parameter influencing heat exchange in ACE in winter. The adimensional number is proportional to the embankment thickness and temperature difference between top and bottom of an ACE layer for a given form of crushed rocks (Goering, 2002). Heat conduction is the main heat transfer form in subgrade soils if convective heat transfer from water flow is neglected. Considering one-dimensional heat transfer, permafrost temperature is mainly affected by soil temperature at embankment-soil interface and soil properties in the subgrade. The amount of heat transfer by conduction increased as the thermal gradient increased between mean annual winter air temperature (MAWAT) and permafrost temperature. Thus, embankment thickness and temperature difference (ΔT) between MAWAT and permafrost temperature were selected as key parameters to investigate heat extraction capacity of the ACE.

The results of the simulations were sensitive to the thermal boundaries and initial temperature conditions. 30 years of simulations were used in order to eliminate the effects of the assumed initial temperature distribution and to obtain a stable annual cycle in response to the given air temperature and embankment thickness. The 30-year simulation period used is 3~10 years longer than periods used in the previous thermal models for ACE (Goering and Kumar, 1996; Goering, 2003; Darrow and Jensen, 2016). The ground temperatures, at 20th, 25th and 30th year for the same day, were compared to ensure the numerical simulation reached a stable

annual cycle. The numerical simulation results for the final year were exported for the calculation of heat balance for different embankment thicknesses and site conditions.

The relationship between heat extraction capacity through the embankment-soil interface, embankment thickness and temperature difference (ΔT) between MAWAT and permafrost temperature, were obtained through statistical regression using the data points obtained by the sensitivity analysis (Table 4.3). Figure 4.14 indicates the results of the quantification of heat extraction capacity through the embankment-soil interface along the centerline of embankment for different embankment thickness and site conditions. From this figure, it can be seen that heat extraction capacity increases with embankment thickness, non-linearly to approximately linearly with lower ΔT.

The thermal performance of ACE varies for different site conditions. Heat extraction capacity is strongly affected by ΔT. For example, for an embankment thickness of 3.0 m, the corresponding heat extraction capacity, obtained from Figure 4.14, were -2.33×10^6 J/m^2, -6.64×10^6 J/m^2, -1.05×10^7 J/m^2 with ΔT =-14.8 °C, -16.1 °C, -17.1 °C, respectively. The effect of embankment thickness on the heat extraction capacity is however stronger for lower ΔT. This indicated that increasing the thickness of the ACE layer is considered more effective for heat extraction from the foundation in the regions where there is a large difference between MAWAT and permafrost temperature. In the ACE layer, the effective thermal conductivity (including thermal radiation effects) is much larger than that only with pure thermal conductivity (paths through contacting solid crushed rocks). The model developed has been calibrated using 150-300 mm angular crush rock material used at Beaver Creek, Yukon and thus, heat extraction capacity with other types of crushed rocks might differ from the proposed design chart (Figure 4.14) in this paper.

The heat balance chart for conventional embankment has been developed in the previous research (Kong et al., 2019) and through the chart, the amount of extra heat flowing into the subgrade can be estimated. As indicated in the example below, the engineering design chart presented in this paper (Figure 4.14) can assist designers to determine the ACE embankment thickness required to extract a sufficient amount of heat to stabilize the embankment considering the effect of climate change.

Note that in the calculation of heat balance for conventional embankments (Kong et al., 2019) and for the ACE, Δz was set to be 10.5 m and 12.5 m, respectively (Equations 4.12 and 4.13). To directly use these two charts together, Δz was set to be 12.5 m for both equations. The heat balance chart for conventional embankments was corrected by multiplying the ratio between the selected depths, shown in Figure 4.15a. For example, a 2.5 m thick embankment with a 0.2 °C/m thermal gradient located in an environment where the temperature difference (ΔT) between MAWAT and permafrost temperature is -14.8 °C would require at least a 5.6 m thick ACE layer to extract the 4×10^6 J/m^2 excess heat affecting the embankment, (Figure 4.15b).

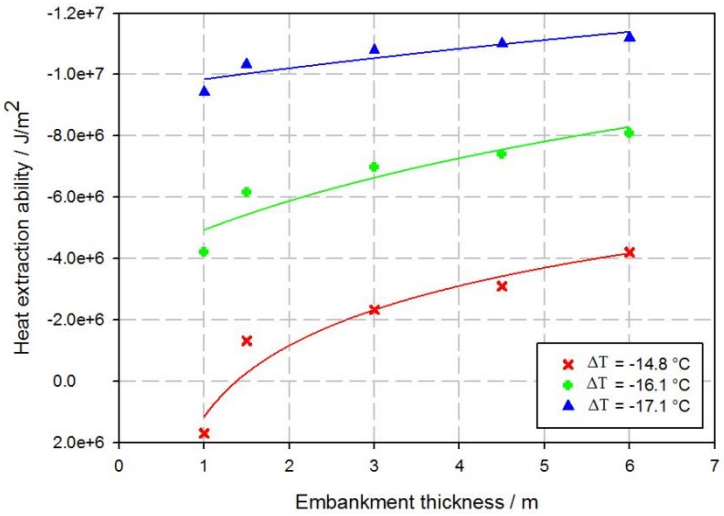

Figure 4. 14: Heat extraction capacity of the ACE at the embankment-soil interface as a function of embankment thickness and temperature difference (ΔT) between MAWAT and permafrost temperature.

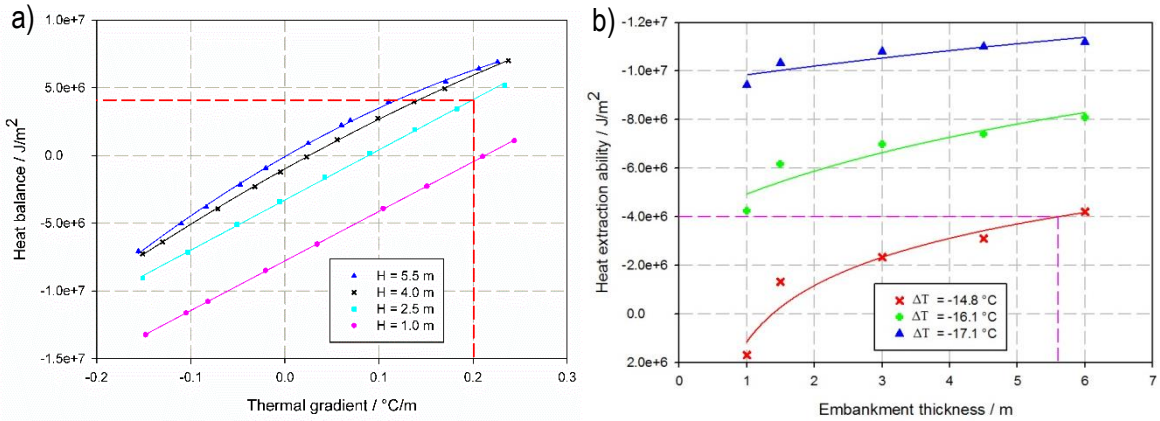

Figure 4. 15: Heat balance chart at the embankment-soil interface as a function of embankment thickness (H) and thermal gradient in the ground (a); Heat extraction capacity chart for the ACE at the embankment-soil interface as a function of embankment thickness and temperature difference (ΔT) between MAWAT and permafrost temperature (b).

Table 4. 3: Relationships between heat extraction capacity at the embankment-soil interface, embankment thickness and temperature difference (ΔT) between MAWAT and permafrost temperature.

ΔT (°C)	Regression equation	Coefficient of determination (R^2)
-17.1	$Q = -4.110 \times 10^6 \times \ln(x + 9.96)$	> 0.80
-16.1	$Q = -3.853 \times 10^6 \times \ln(x + 0.259)$	> 0.85
-14.8	$Q = -2.415 \times 10^6 \times \ln(x - 0.38)$	> 0.90

x is embankment thickness (m); Q is the heat extraction capacity (J/m^2) at the embankment-soil interface. It is important to consider that for similar delta T conditions, the heat extraction capacity of an air convection layer is the same in warm or in cold permafrost conditions. However, due to the presence of an important quantity of unfrozen water in warm permafrost, thermal stabilization in those conditions will be much longer due to the large quantity of latent heat to be extracted to refreeze the soil.

4.4 Conclusion

The air convection embankment (ACE), built along the Alaska Highway at the Beaver Creek test site in Yukon, Canada, provided much information on the thermal response of the ACE layer since 2008. The analysis of measured field temperature data indicated that the ACE layer induced significant air convection movement during winters, and heat extraction due to the ACE mainly occurred under traffic lanes with limited effect under the side slope of the embankment. Under the centerline of the ACE, mean annual ground temperatures showed a continuous decreasing trend between -2.0 m and -10.0 m in the ground over the period from 2009 to 2013. However, the mean annual ground temperatures indicated a very limited variation under the side slope, compared to that under the centerline.

A coupled heat conduction and convection 2D thermal model was developed and well calibrated using five years of measured soil temperature data under the centerline and under the side slope of the ACE. The maximum temperature differences were less than 0.25 °C between measured and simulated mean annual ground temperatures under the centerline in 2009 and 2013. For the side slope, the maximum temperature difference was less than 0.2 °C below 1.6 m in the ground. A relatively new approach based on the calculation of heat balance at the embankment-soil interface, can be used to quantify the heat to be extracted for thermal stabilization of permafrost underneath an embankment. The difference between measured and simulated average heat balance during the period from 2009 to 2013 was about 10%. Both the comparisons of mean annual ground temperatures and averaged heat balance between the field data and model indicated the reasonable accuracy of the 2D model developed and supported the selections made for the thermal properties, intrinsic permeability of ACE layer and surface boundaries. After the model was well calibrated, sensitivity analysis were carried out to investigate heat extraction capacity of the ACE across the embankment-soil interface for different embankment thickness and site conditions.

The proposed relationship between heat extraction capacity, embankment thickness and temperature difference (ΔT) between MAWAT and permafrost temperature indicated that heat extraction capacity increased with embankment thickness following a non-linear trend. Increasing embankment thickness had less effect on heat extraction capacity in high ΔT conditions. For example, with the ΔT of -17.1 °C, the heat extraction capacities with embankment thickness 6.0 m was 8.2% larger than that with embankment thickness 3.0 m, however, it was 79.0% for the site condition with the ΔT of -14.8 °C.

The atmospheric air temperature was one key factor affecting the heat extraction capacity of the ACE, and global warming can reduce the air convection movement in one ACE layer in winter. The effect of global warming was integrated into the proposed procedure by decreasing ΔT, considered by the designer using the site-specific climate change scenario during the service life of transportation infrastructure. It would thus be

possible to quickly assess the heat extraction capacity using the proposed heat extraction capacity curve for the ACE during the service life for one ACE thickness for a given site condition. The heat balance chart for conventional embankments to determine the amount of extra heat flowing into the subgrade was proposed in a previous publication (Kong et al., 2019). ACE should extract at least the estimated amount of extra heat to ensure the thermal stability of subgrade underneath transportation infrastructure.

The proposed engineering design charts for the ACE and the conventional embankments should be used together to determine the suitable embankment thickness to extract the estimated amount of extra heat to prevent permafrost underneath transportation infrastructure from thawing. In summary, this paper describes the development of a rational method to design ACE for thermal stabilization of transportation infrastructure in northern regions.

Acknowledegments

The authors would like to acknowledge the financial support of the Natural Sciences and Engineering Research Council of Canada, the 2013-2020 Climate Change Action Plan and Transports Québec, as well as the technical and financial support of public and private partners of the permafrost engineering research program ARQULUK for this project.

4.5 References

Andersland, O. B., Ladanyi, B., 2004. Frozen ground engineering. John Wiley, Hoboken, N. J.

Anisimov, O. A., Shiklomanov, N. I., Nelson, F. E. (1997). Global warming and active-layer thickness: results from transient general circulation models. Global and Planetary Change, 15(3-4), 61-77.

Batenipour, H., Kurz, D., Alfaro, M., Graham, J., Kalynuk, K., 2010. Results from an instrumentedhighway embankment on degraded permafrost. In: Proceedings of the 63rd Canadian Geotechnical Conference and 6th Canadian Permafrost Conference. Calgary, Alberta, Canada, pp. 512–519.

Bear, J., 1972. Dynamics of fluids in porous media. Elsevier, New York.

Brown, J., Haggerty, C. (1998). Permafrost digital databases now available. Eos, Transactions American Geophysical Union, 79(52), 634-634.

Brown, R. (1967). Permafrost in Canada. Geological Survey of Canada Map 1246a and Division of Building Research Map NRC-9769. Natural Resources Council of Canada, Ottawa, ON.

Brown, W. G. (1963). Graphical determination of temperature under heated or cooled areas on the ground surface. Technical Paper of the Division of Building Research NRC, 163.

Chapuis, R. P. (2004). Predicting the saturated hydraulic conductivity of sand and gravel using effective diameter and void ratio. Canadian Geotechnical Journal, 41(5), 787-795.

Côté, J., Fillion, M.-H., Konrad, J.-M. (2011). Intrinsic permeability of materials ranging from sand to rock-fill using natural air convection tests. Canadian Geotechnical Journal, 48(5), 679-690.

Coulombe, S., Fortier, D., Stephani, E. (2012). Using air convection ducts to control permafrost degradation under road infrastructure: Beaver Creek experimental site, Yukon, Canada. Cold Regions Engineering 2012: Sustainable Infrastructure Development in a Changing Cold Environment, pp. 21-31.

Darrow, M. M. (2011). Thermal modeling of roadway embankments over permafrost. Cold Regions Science and Technology, 65(3), 474-487.

Darrow, M. M., Jensen, D. D. (2016). Modeling the performance of an air convection embankment (ACE) with thermal berm over ice-rich permafrost, Lost Chicken Creek, Alaska. Cold Regions Science and Technology, 130, 43-58.

Davis, T. N. (2001). Permafrost: a guide to frozen ground in transition: University of Alaska Press, Fairbanks, pp. 351.

Doré, G., Ficheur, A., Guimond, A., Boucher, M. (2012). Performance and cost-effectiveness of thermal stabilization techniques used at the Tasiujaq airstrip. Cold Regions Engineering 2012: Sustainable Infrastructure Development in a Changing Cold Environment, pp. 32-41.

Doré, G., Niu, F., Brooks, H. (2016). Adaptation methods for transportation infrastructure built on degrading permafrost. Permafrost and Periglacial Processes, 27(4), 352-364.

Doré, G., Pierre, P., Juneau, S., Lemelin, J. (2007). Expérimentation de méthodes de mitigation des effets de la fonte du pergélisol sur les infrastructures du Nunavik: aéroport de Tasiujaq, Rapport d'étape 1– Compte rendu des travaux d'instrumentation et de supervision de construction des planches expérimentales de l'aéroport de Tasiujaq. Groupe de recherche en ingénierie des chaussées. Département en génie civil, Université Laval, Québec, Canada, pp. 28.

Environment Canada, 2011. Canadian Climate Normals 1971–2000 [Online]. Available from. http://www.climat.meteo.gc.ca (accessed on July 4 2011).

Esch, D. C. (1996). Roads and airfield design for permafrost conditions. In Roads and airfields in cold regions: a state of practice report, pp. 121-149.

Farouki, O.T. (1986). Thermal properties of soils. In: seres of Rock and Soil Mechanics. 11. Trans Tech Publications, Clausthal-Zellerfeld, Germany, pp. 1-136.

Fillion, M.-H., Côté, J., Konrad, J.-M. (2011). Thermal radiation and conduction properties of materials ranging from sand to rock-fill. Canadian Geotechnical Journal, 48(4), 532-542.

Gaumond, F., Doré, G., Guimond, A. (2012). Monitoring the thermal and mechanical behaviours of Puvirnituq airstrip, Nunavik, Northern Quebec Cold Regions Engineering 2012: Sustainable Infrastructure Development in a Changing Cold Environment , pp. 52-61.

Goering, D., Saboundjian, S. (2004). Design of passive permafrost cooling system for an interior Alaska roadway. In: Proceedings of the Cold Regions and Construction Conference, ASCE/CSCE/IWCSEAA, Edmonton, Alberta, Canada.

Goering, D. J. (1998). Experimental investigation of air convection embankments for permafrost-resistant roadway design. In: Proceedings of 7th International Conference on Permafrost. Yellowknife, NWT, Canada, pp. 319–326.

Goering, D. J. (2002). Convective cooling in open rock embankments. In: Proceedings of the 11th Cold Regions Engineering: Cold Regions Impacts on Transportation and Infrastructure, Anchorage, AK, pp. 629-644.

Goering, D. J. (2003). Passively cooled railway embankments for use in permafrost areas. Journal of cold regions engineering, 17(3), 119-133.

Goering, D. J., Kumar, P. (1996). Winter-time convection in open-graded embankments. Cold Regions Science and Technology, 24(1), 57-74.

Johansen, Ø., (1975). Thermal conductivity of soils. Ph.D thesis, University of Trondheim. (in Norwegian). Translated in U.S. Army, Cold Regions Research and Engineering Laboratory, Translation 637.

Johnston, G. H. (1981). Permafrost: engineering design and construction: J. Wiley, pp. 540.

Jørgensen, A. S., Doré, G., Voyer, É., Chataigner, Y., Gosselin, L. (2008). Assessment of the effectiveness of two heat removal techniques for permafrost protection. Cold Regions Science and Technology, 53(2), 179-192.

Kersten, M.S. (1949). Laboratory research for the determination of the thermal properties of soils. Research Laboratory Investigations, Engineering Experiment Station, University of Minnesota, Minneapolis. Technical Report 23.

Kong, X.B., Doré, G., Calmels, F. (2019). Thermal modeling of heat balance through embankments in permafrost regions. Cold Regions Science and Technology, 158, 117-127.

Lanouette, F., Doré, G., Fortier, D. (2015). Influence of snow cover on the ground thermal regime along an embankment built on permafrost: In-situ measurements. In: Proceedings of the 68th Canadian Geotechnical Conference and the 7th Canadian Permafrost Conference, Quebec, Canada, pp. 7.

Lingnau, B. (1985). Observation of the design and performance of the Dempster Highway. Master's Thesis, University of Alberta, Department of Civil Engineering.

Lipovsky, P.S. (2015). Summary of Yukon Geological Survey permafrost monitoring network results, 2008-2013. In: Yukon Exploration and Geology 2014, K.E. MacFarlane, M.G. Nordling and P.J. Sack (eds.), Yukon Geological Survey, pp. 113-122.

Lunardini, V. J. (1978). Theory of n-factors and correlation of data. In: Proceedings of the 3rd International Conference on Permafrost. National Council of Canada: Ottawa, pp. 40–46.

McHattie, R.L., Goering, D.J. (2009). Air convection embankment (ACE) design guide. Alaska. Department of Transportation. Report, FHWA-AK-RD-09-06.

McGregor, R., Hayley, D., Wilkins, G., Hoeve, E., Grozic, E., Roujanski, V., Jansen, A., Dore, G. (2010). Guidelines for development and management of transportation infrastructure in permafrost regions. Transportation Association of Canada, Ottawa, Ontario.

Lunardini, V. J. (1981). Heat transfer in cold climates. Van Nostrand Reinhold: New York.

M-Lepage, J., Doré, G., Fortier, D., Murchison, P. (2012). Thermal performance of the permafrost protection techniques at Beaver Creek experimental road site, Yukon, Canada. In: Proceedings of the 10th International Conference on Permafrost, Salekhard, Russia, pp. 261.

M-Lepage, J. (2015). Experimentation of mitigation techniques to reduce the effects of permafrost degradation on transportation infrastructures at Beaver Creek experimentalroad site (Alaska Highway, Yukon). Mater's thesis, Laval University, Canada.

Nelson, F. E., Anisimov, O. A., Shiklomanov, N. I. (2002). Climate change and hazard zonation in the circum-arctic permafrost regions. Natural Hazards, 26(3), 203-225.

Newman, G. P., Wilson, G. W. (1997). Heat and mass transfer in unsaturated soils during freezing. Canadian Geotechnical Journal, 34(1), 63-70.

Nield, D. A., Bejan, A. (1992). Convection in porous media: Springer-Verlag, New York.

Saboundjian, S., Goering, D. (2003). Air convection embankment for roadways: Field experimental study in Alaska. Transportation Research Record: Journal of the Transportation Research Board, pp. 20-28.

Segerlind, L. J. (1976). Applied finite element analysis. Wiley, New York.

Serreze, M., Walsh, J., Chapin, F. S., Osterkamp, T., Dyurgerov, M., Romanovsky, V., Oechel, W. C., Morson, J., Zhang, T., Barry, R. G. (2000). Observational evidence of recent change in the northern high-latitude environment. Climatic change, 46(1-2), 159-207.

Smith, S. L. (2011). Trends in permafrost conditions and ecology in northern Canada. Technical Thematic Report, Canadian Councils of Resource Ministers, pp. 22.

Stephani, E. (2013). Permafrost geosystem assessment at the Beaver Creek Road experimental site (Alaska Highway, Yukon, Canada). Mater's thesis, University of Alaska Fairbanks, USA.

Sun, B. X., Xu, Z. Z., Lai, Y. M., Fang, M.X. (2005). Evaluation of fractured rock layer heights in ballast railway embankment based on cooling effect of natural convection in cold regions. Cold Regions Science and Technology, 42(2), 120-144.

Vinson, T. S., Rooney, J. W., Haas, W.H. (1996). Roads and airfields in cold regions: a state of the practice report. ASCE Publications 0–7844–0191-8, Technology and Engineering, 321p.

Wakao, N., Kato, K. (1969). Effective thermal conductivity of packed beds. Journal of Chemical Engineering of Japan, 2(1), 24-33.

Xu, J., Goering, D. J. (2008). Experimental validation of passive permafrost cooling systems. Cold Regions Science and Technology, 53(3), 283-297.

Chapter 5 Field and numerical studies on the thermal performance of air convection embankment to protect side slopes in permafrost environments

Foreword

Xiangbing Kong[1], Guy Doré[1], Fabrice Calmels[2], Chantal Lemieux[1]

[1]Department of Civil and Water Engineering, Laval University, Québec City, Québec, Canada

[2]Yukon Research Centre/Northern Climate ExChange, Yukon College, Whitehorse, Yukon, Canada

State: Submitted to review

Date of Submission: 16 April 2019

Journal: Cold Regions Science and Technology

Résumé

Les remblais à convection d'air installés dans l'épaulement (ACE) sont adéquats pour limiter l'effet de l'accumulation de neige sur les pentes des remblais des infrastructures de transport nordique. Toutefois, il y a peu d'informations disponibles sur les procédures de conception. L'objectif de cet article est de proposer de nouvelles lignes directives et un abaque de conception d'ingénierie pour quantifier la capacité d'extraction de chaleur des ACE installés dans l'épaulement. L'ACE dans l'épaulement construit en 2018 sur la section d'essai de l'Alaska Highway à Beaver Creek, au Yukon, a fourni des données importantes pour l'évaluation de la performance sur le terrain et du modèle développé. Des câbles à thermistances ont été installés au centre de la chaussée et sous la pente du remblai. Les mesures ont indiqué un refroidissement significatif du sol, principalement sous les épaulements, durant la période de suivi de 2009 à 2013. Les données collectées ont également servi à calibrer un modèle couplé de conduction-convection pour reproduire les conditions thermiques et l'évolution des températures dans le sol de fondation. Un abaque de conception d'ingénierie a été développé basé sur le modèle calibré et a été validé avec succès en utilisant les données thermiques de la piste d'atterrissage de Puvirnituq au Nord du Québec, Canada.

Mots clés: Dégradation du pergélisol; Alaska Highway; Remblai à convection d'air (ACE); Procédures de conception; Capacité d'extraction de chaleur

Abstract

Shoulder air convection embankments (ACEs) are sufficient to counter the effect of snow accumulation on side slopes of northern transportation infrastructure. However, little information is available for the design procedure. This paper aims to propose new design guidelines and an engineering design chart to quantify the heat extraction capacity of shoulder ACEs. The tested shoulder ACE, constructed on the Alaska Highway at Beaver Creek, Yukon, in 2008, provided valuable data for the assessment of field performance and model development. Thermistor strings were installed under the centerline and under the side slope. Measurements indicated that the cooling of ground soils was significant mainly under the side slope during the monitoring years from 2009 to 2013. The data collected were also used to calibrate a coupled conduction-convection model to reproduce the thermal conditions and the changing temperature trend in the subgrade. An engineering design chart was developed based on the well-calibrated model, and was successfully validated using the thermal data from the Puvirnituq airstrip in Northern Quebec, Canada.

Keywords: Permafrost degradation; Alaska Highway; Air convection embankment (ACE); Design procedures; Heat extraction capacity

5.1 Introduction

Physical and mechanical properties of permafrost are highly variable and extremely sensitive to changes in soil temperature, which is a key parameter in permafrost engineering. Transportation infrastructures, such as roadways and airstrips, are crucial to socio-economic activities and are often built on permafrost in northern regions (Goering and Kumar, 1996). The stability and thermal state of frozen soils under infrastructures are closely related, especially in discontinuous permafrost environments (Regehr et al., 2012). The construction of embankments modifies ground surface characteristics and disturbs the ground surface energy balance, often increasing the temperature of the underlying permafrost (Goering, 2003; Doré et al., 2016). In addition, climate change has been significantly affecting embankments constructed on permafrost since the second half of the 20th century (Doré et al., 2016). Other factors, such as snow accumulation and ponding of surface water, amplify permafrost degradation, resulting in instability and embankment failure (Doré et al., 2016). Permafrost degradation makes the driving conditions of roads hazardous and increases the maintenance cost of road networks in permafrost conditions (Reimchen et al., 2009; Nelson et al., 2002). To counteract the problems resulting from permafrost degradation, many mitigation techniques, such as heat drains, air convection embankments (ACEs) and snow/sun sheds were proposed to maintain the thermal stability of embankments.

Poorly graded rocks (idealy 150-300 mm angular rocks) with a high porosity are used to facilitate convection in an ACE. Winter temperatures cool the embankment surface and the upper portion of the embankment, while the temperature at the base remains relatively warm due to heat accumulation in the ground in summer. The temperature difference between the surface and the base of an ACE results in an unstable air density gradient, which is balanced by the air circulation in the pore space. This phenomenon enhances winter-time heat transfer in an ACE with sufficient air permeability. In summer, the embankment air density gradients are stable and air circulation does not occur (Goering, 2002). ACEs have been applied and tested in the USA, China and Canada (Goering, 1988; Ma et al., 2006; Doré et al., 2016). A lot of research based on numerical simulations, laboratory experiments and full-scale field studies, has been done to provide information on material properties, effectiveness and optimization of ACEs (e.g., Goering, 1998; Goering and Kumar, 1999; Beaulac and Doré, 2006; Darrow and Jensen, 2016; Jorgensen et al., 2008; Sun et al., 2011; M-Lepage et al., 2012; Doré et al., 2012). Design procedures are necessary to construct a performing ACE. McHattie and Goering (2009) proposed design procedures for ACEs to ensure the average annual temperature at the bottom of an ACE layer is below the freezing point by determining sufficient ACE thickness. However, maintaining the frozen state of soils at the embankment-soil interface cannot ensure that permafrost degradation will not occur.

Given the limitations of the current design procedures, the main objective of this paper is to define the field of application and to propose new design procedures for the use of ACEs in embankment shoulders. The full-scale shoulder ACE built on the Alaska Highway at Beaver Creek, Yukon in 2008, was used to develop the new design tools. More specifically, the thermal performance of shoulder ACEs was first analyzed based on the temperature measured from 2009 to 2013. Then, a numerical model was developed and calibrated to the field data measured at the Beaver Creek experimental site. The heat balance approach was used to quantify the heat extraction capacity of the shoulder ACE with respect to site conditions and embankment thickness. Finally, an engineering design chart was developed to determine the ACE thickness required for long-term thermal stability of the embankment. The design chart was successfully validated using the Puvirnituq airstrip field data in Northern Quebec, Canada. This research product enhances the ability of shoulder ACEs to preserve northern transportation infrastructure underlain by permafrost, and thus contributes to the social-economic development in permafrost environments.

5.2 Field site and ground thermal regime

The experimental site is located on the Alaska Highway, 8 km south of the Beaver Creek municipality and about 30 km south of the Canada-United States border, at 62° 20' N, 140° 50' W (Figure 5.1). The test site is representative of roadway conditions in discontinuous permafrost environments. The climate is continental with a mean annual air temperature (MAAT) of -5.5 °C from 1971 to 2000 (Environment Canada, 2011). The mean

annual precipitation is 419 mm, with 296 mm falling as rain and 123 cm falling as snow (Environment Canada, 2011).

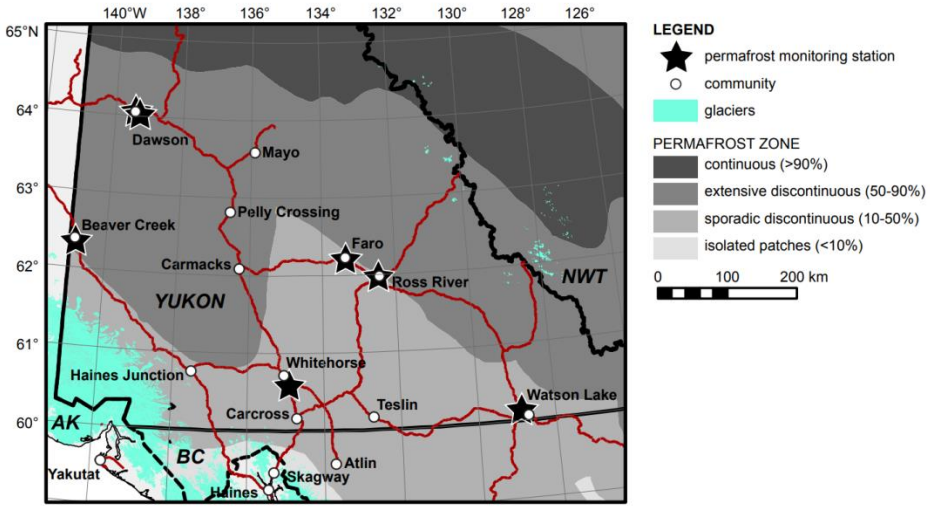

Figure 5. 1: The location of the Beaver Creek experimental site, Yukon, Canada (Lipovsky, 2015).

In order to improve the understanding of the impact of permafrost degradation on transportation infrastructure and to evaluate the potential solutions to limit permafrost degradation, 12 experimental sections were constructed in 2008 at Beaver Creek. Many mitigation techniques were tested: snow/sun shed, heat drain, high albedo surface, grass-covered embankment, longitudinal culvert, snow clearing maintenance techniques and ACEs with different configurations. The Beaver Creek site is divided into twelve 50 m long experimental sections. This paper focuses on the shoulder ACE test section (Figure 5.2a). Crushed rocks with particle diameters ranging from 150 to 300 mm were used in order to create effective convection cells (Figure 5.2b). Thermistor cables were placed under the centerline (BH1) and under the side slope (BH2) to measure ground temperatures. Thermistor string was installed around 15.5 m in BH1 and BH2, in 2008. Thirteen thermistors with a standard recording accuracy of ±0.1 °C were spaced at a distance of 0.3 m to 3.0 m. None of the boreholes reached the bedrock. A meteorological station was installed on the site, recording the wind speed, wind direction and air temperature since October 2008.

Figure 5. 2: The shoulder ACE section at Beaver Creek, Yukon. (a) General view; (b) Typical rock diameter.

Figure 5.3 and Figure 5.4 illustrate temperature variations under the side slope (BH2) and under the centerline (BH1) of the embankment, respectively, for a five-year period from December 2008 to December 2013. The interface between the embankment and the subgrade was used as the reference level (0 m), meaning all positive values along the y-axis refer to a position inside the embankment fill. From Figure 5.3, it can be seen that the ACE did not prevent the thawing front from penetrating into the subgrade but the top of permafrost (the bottom of active layer) slightly moved upward from -0.80 m in 2009 to -0.71 m in 2013. The top of the permafrost reached -0.82 m in 2010, -0. 78 in 2011 and -0.70 m in 2012. This suggests that the ACE was successful in stabilizing the permafrost table, considering permafrost degradation was observed in the reference section during the same period. The thermal analysis of reference section was not included in this study. During winter, significant ground cooling was observed under BH2. The average ground temperature at a depth of -2.45 m, for example, decreased from -0.4 °C to -1.4 °C from 2009 to 2013. The negative temperature isotherms showed an obvious change. The -1 °C isotherm, for instance, moved downward from 2010 to 2013 with the positions reaching -1.19 m, -6.29 m in 2010 and 2013, respectively. It is worth mentioning that the -1 °C isotherm position was lower reaching -2.66 m in 2009, compared to 2010, mainly due to lower winter air temperatures in 2009. MAAT reached -5.3 °C in 2009 and -4.4 °C in 2010.

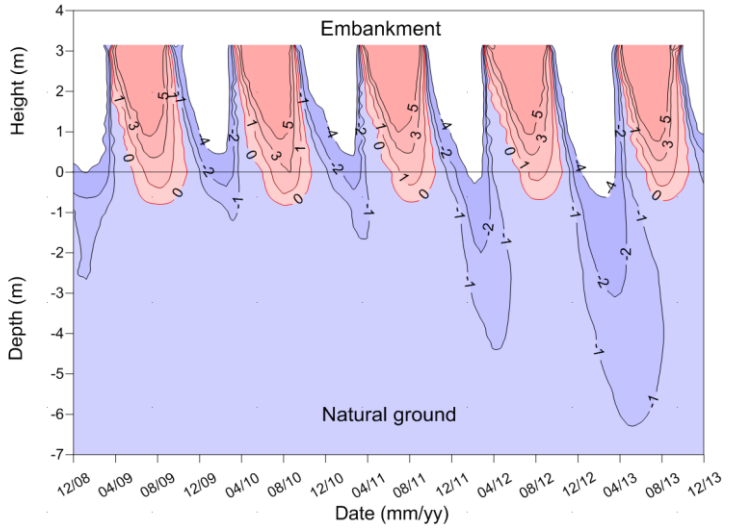

Figure 5. 3: Thermal behavior of the Beaver Creek experimental embankment under the side slope of the embankment (BH2).

Under BH1, the permafrost table reached a greater depth in the subgrade than it did under BH2 (Figure 5.4). The permafrost table was -1.21 m below the embankment-soil interface in 2009, and was at almost the same depth in the following four years. There was limited change in the ground temperature from 2009 to 2013. The average ground temperatures at a depth of -2.80 m, for instance, were -0.6 ° C in 2009 and -0.4 °C in 2013. Overall, the shoulder ACE effectively decreased ground temperatures under BH2, but not under BH1.

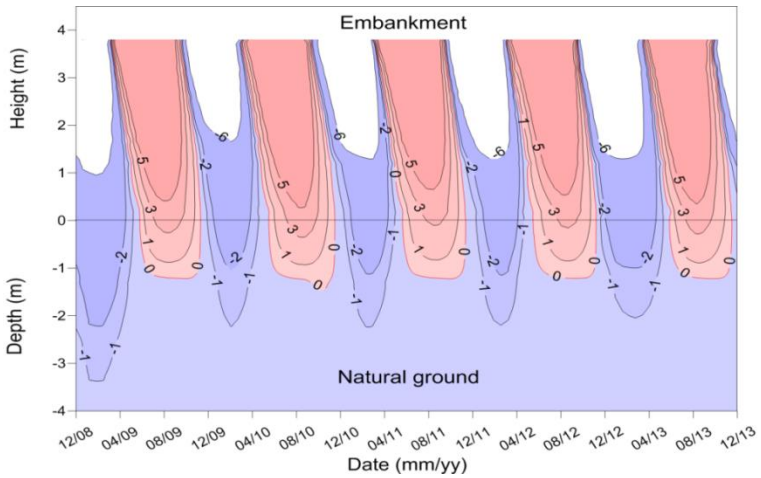

Figure 5. 4: Thermal behavior of the Beaver Creek experimental embankment under the centerline of the embankment (BH1).

Figure 5.5 and Figure 5.6 illustrate the mean monthly ground temperature (MMGT) at the interface under the side slope (BH2) and under the centerline (BH1), respectively. The yearly maximum MMGT under BH2 was consistently lower than it was under BH1. This is mainly due to the low thermal conductivity of the high-porosity ACE layer. Under BH2, the maximum MMGT exceeded 3.0 °C in 2010, and then decreased to 1.7 °C,

1.4 °C and 1.9 °C in the following three years, respectively. The yearly maximum MMGT was consistently in September from 2009 to 2012, however, it was one month ahead in 2013 due to the complex weather conditions in Yukon. The yearly minimum MMGT decreased by 2.4 °C from 2010 to 2013, indicating significant winter-time air convection in the ACE (Figure 5.5). Under BH1, all the yearly maximum MMGTs exceed 3.0 °C. The maximum MMGT of 4.2 °C was recorded under BH1 in 2010, which was the same year the maximum MMGT under BH2 was recorded. The yearly minimum MMGT varied around -3.5 °C from 2009 to 2013 under BH1 (Figure 5.6).

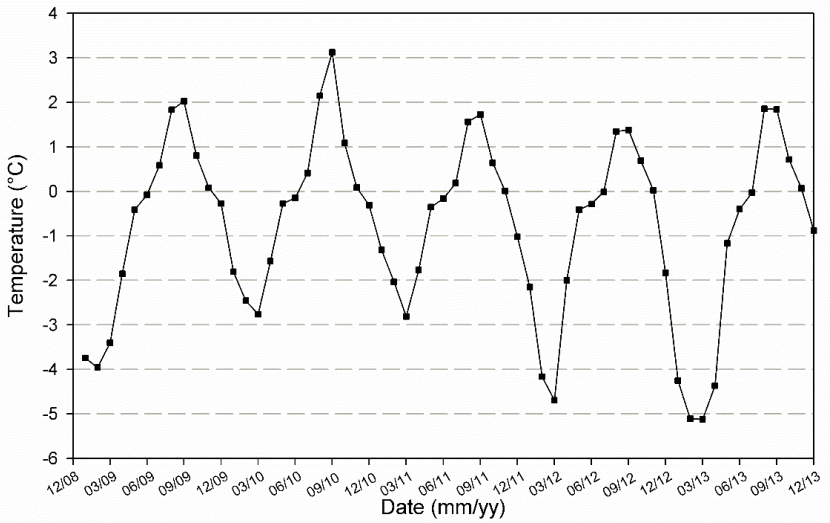

Figure 5. 5: Mean monthly ground temperature at the embankment-soil interface under the side slope of the embankment (BH2).

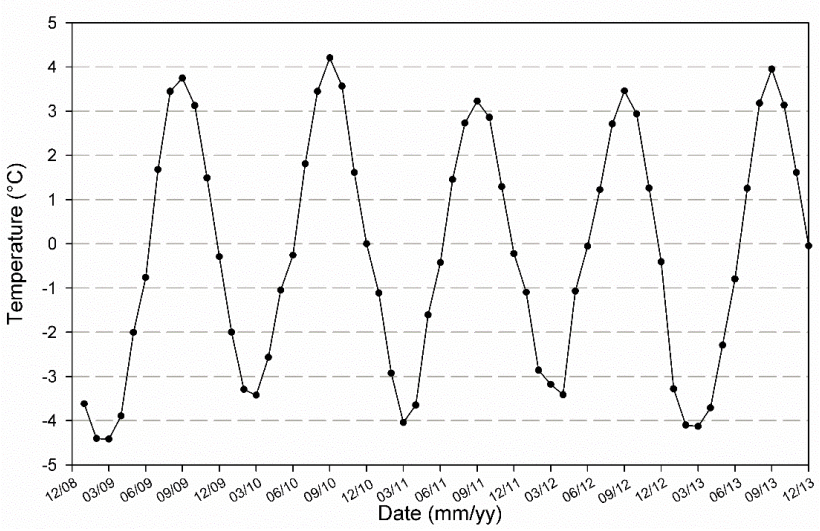

Figure 5. 6: Mean monthly ground temperature at the embankment-soil interface under the centerline of the embankment (BH1).

5.3 Thermal modeling

A 2D finite element model was developed to simulate the shoulder ACE at the Beaver Creek test site, using two modules from the SoilVision software suite: SVHeat for conductive heat flow and SVAir-flow for density-driven air convection. The two modules were coupled to simulate the air convection within the rock layer and the conductive heat transfer within the foundation soil and embankment fill.

The left half of the physical domain was chosen due to the symmetry of the embankment. The difference of snow conditions due to the variation of snow drift from one side to another, was not considered in this model. The embankment thickness is 4.1 m. The computational domain was extended for 15 m from the toe of the embankment, and the lower boundary was located 30 m beneath the ground surface. In the computational domain, part ① is the ACE layer. Its porosity was assumed to be 0.4 and the intrinsic permeability of 6.0×10^{-7} m^2 was used; part ② is the embankment fill with a composition of 50% gravel, 30% sand and 10% silt; part ③ is the foundation soil (silt) with the volumetric water content 36%. The permafrost temperature is -0.8 °C. The thermal properties of the foundation soil were measured in the lab (de Grandpré, 2011. Cited by M-Lepage, 2016). The thermal properties of embankment fill were estimated through the Kersten's equations (1949), and the water content was uniformly assumed to be 4.0%, considering the measured water contents varying from 2.3% to 7.2% at different locations in the embankment fill (Doré et al., 2007). The water flow within both the non-rock layer and the rock layer and the airflow within the non-rock layer were restricted. Table 5.1 lists the thermal properties of the different materials used in the model.

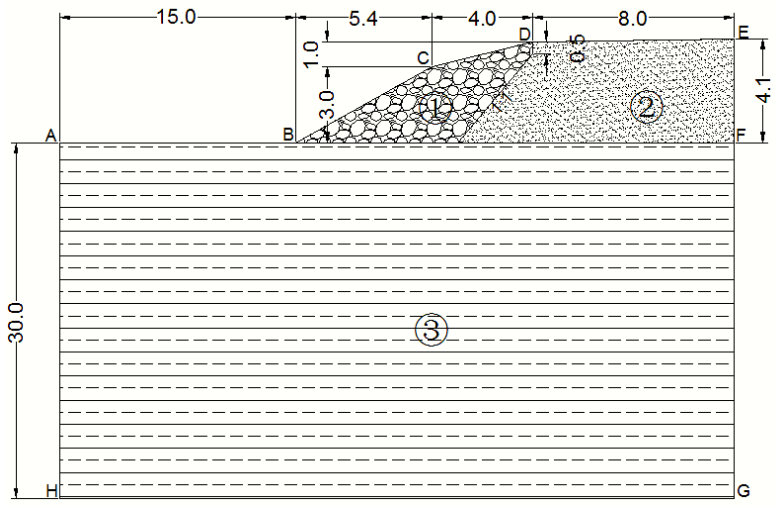

Figure 5. 7: Physical domain of the embankment and subgrade (unit: m).

Table 5. 1: Material properties for the rock layer and non-rock layer.

Material type	k_f (W/m-°C)	k_u (W/m-°C)	C_f (MJ/m^3-°C)	C_u (MJ/m^3-°C)	K (m^2)
Rock layer	0.35	0.35	1.098	1.098	6.0×10^{-7}
Embankment fill	1.134	1.443	1.430	1.580	≈ 0
Foundation soil	1.337	0.907	1.73	2.51	≈ 0

Note: k_f = the frozen thermal conductivity; k_u = the unfrozen thermal conductivity; C_f = the frozen volumetric heat capacity; C_u = the unfrozen volumetric heat capacity; K = the intrinsic permeability.

The thermal boundary conditions consisted of variable temperature functions at the top of the domain and the heat flux at other boundaries. At the left-hand boundary (AH) and right-hand boundaries (EF and FG), zero heat flux was applied, considering the negligible thermal effect of the embankment on the left-hand boundary and the symmetry of the embankment along the right-hand boundary. A heat flux of 0.03 W/m^2 was applied at the bottom (GH), considering the geothermal gradient ranges from 0.009 W/°C to 0.033 W/m^2 in Northern Canada (Brown, 1963). Temperature functions were applied to the embankment surface, the side slopes and the natural ground surface. In numerical models, the simulated harmonic temperature with a thermal modifier (n-factor), is generally employed. At this experimental site, the air temperature was measured every four hours from 2009 to 2013, and the harmonic temperature was derived from the measured air freezing index, air thawing index and MAAT (Figure 5.8).

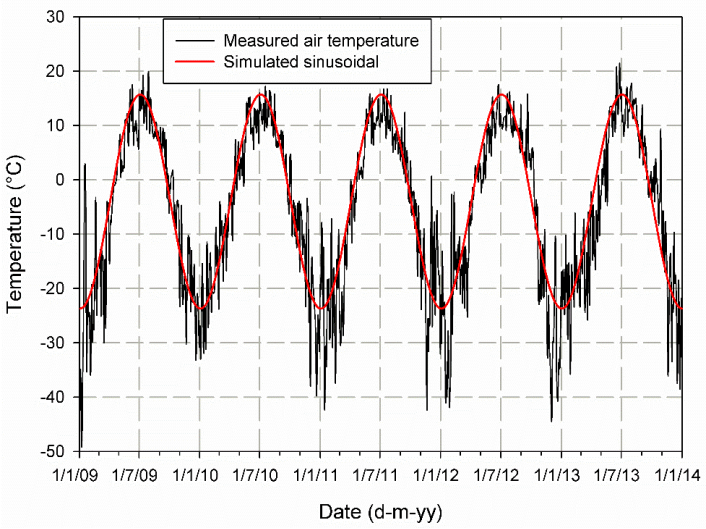

Figure 5. 8: Comparison between the measured air temperature and simulated sinusoidal temperature.

The n-factor is the ratio of air temperature to surface temperature. This ratio varies in time, from month to month and from year to year at a given site (Lunardini, 1978). However, constant summer and winter n-factors for all the temperature boundaries were applied in the model, due to unavailable and insufficient data to predict the yearly changes of the n-factor. The published values of 0.37 for the thawing n-factor (n_t) and 0.29 for the freezing n-factor (n_f), were applied on the natural ground surface (Andersland and Ladanyi, 2004). We

initially used the published values of 1.1 and 0.6 for the n_t and n_f, respectively, on the side slope (Goering and Kumar, 1999; Darrrow, 2011). We also initially used the published values of 1.72 and 1.0 for the n_t and n_f, respectively, on the embankment surface (Berg and Aitken, 1973; Zarling and Braley, 1986). Only thawing n-factor values for the embankment surface and side slopes were slightly adjusted to ensure that the modelled active layer thickness and ground temperatures were representative of the measured field data. The final n-factors were summarized in Table 5.2. The embankment surface (DE), the side slope (CD) and the natural ground surface (AB) were assumed to be impermeable to prevent the atmospheric air from flowing into or out of the embankment and the subgrade. The side slope (BC) was assumed to be permeable, as it was uncovered and directly exposed to the atmospheric air.

Table 5. 2: Summary of n-factor used in the model.

Surface type	n_t	n_f
Natural ground surface	0.37[a]	0.29[a]
Embankment surface	1.6[b]	1.0[a]
Embankment side slopes	1.05[b]	0.6[a]

[a]Values obtained from the literature (Berg and Aitken, 1973; Zarling and Braley, 1986; Goering and Kumar, 1999; Andersland and Ladanyi, 2004; Darrow, 2011); [b]Values obtained through sensitivity analysis.

The computational domain, shown in Figure 5.7, was divided into 2292 triangular elements and 4715 nodes, with an element size ranging from less than 0.3 m in the embankment to approximately 2.5 m in the subgrade. The grid resolution has been optimized to confirm that the selected resolutions had limited effect on the heat transfer process in soils. For the transient thermal analysis, the first step is to apply the initial temperature field for the 2D model. We used the measured temperature data at the reference section, as the initial temperature field, to better reproduce the temperature distribution.

The measured data from 2009 to 2013 were available and used for model calibration. The model was run for five years and an automatic step of less than 0.2 days was used to prevent the model from crashing due to the characteristics of non-linear air convection in the rock layer. The results from each step were saved, and daily temperatures were exported for future analysis.

The comprehensive effects of winter-time air convection and summer-time heat conduction in the rock layer can be assessed by the mean annual ground temperature (MAGT) along the depth. Figure 5.9 shows the modelled MAGT profile and measured MAGT profile as a function of depth under the side slope (BH2) in 2009 and 2013. This figure clearly shows that the measured MAGT and modelled MAGT decreased from 2009 to 2013. Generally, the modelled MAGT corresponded to the measured MAGT in 2009 with the maximum temperature difference less than 0.4 °C and 0.2 °C in the embankment and in the subgrade, respectively. At the interface, the measured MAGT and modelled MAGT were -0.68 °C and -0.70 °C, respectively. In 2013, the

measured MAGT was lower than the modelled MAGT below the depth of -0.95 m with the maximum temperature difference reaching -0.11 °C at a depth of -2.45 m. However, there was a larger temperature difference of 0.47 °C at the interface in 2013, compared to 0.02 °C in 2009. This was likely due to the field surface water flow, which was excluded to simplify the model.

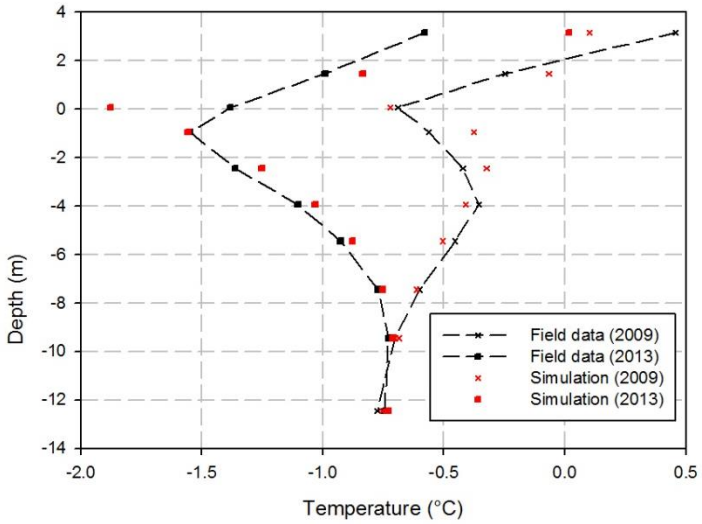

Figure 5. 9: Comparison of MAGT profile and modeled MAGT profile with depth under the side slope (BH2) in 2009 and 2013.

Natural convection and heat conduction were the main heat transfer modes in the rock layer in winter and in summer, respectively. Figure 5.10a and Figure 5.10b present the measured temperature profile and modelled temperature profile as a function of depth under the side slope (BH2) at the beginning of January and at the end of July 2012. These periods were selected to represent the coldest and warmest air temperatures in one year. Figure 5.10a indicates the measured temperature and modelled temperature increased with depth above the depth of -0.95 m and then decreased below that depth in January. The maximum temperature differences were 0.79 °C and 0.31 °C in the embankment and in the subgrade, respectively. In summer, a similar trend with higher measured ground temperatures than the modelled ones was also observed at the top of the natural ground with the maximum temperature difference reaching 0.72 °C at a depth of -0.95 m.

Heat conduction was the main mode of heat transfer under the centerline in winter and in summer, neglecting the possible advective effect of water flow in the subgrade. Figure 5.11a and Figure 5.11b compare the measured temperature profile and modelled temperature profile as a function of depth under the centerline at the beginning of January and at the end of July 2012. In the subgrade, the modelled temperatures and measured temperatures were closely matched in both winter and summer, with both maximum temperature differences less than 0.12 °C below the depth of -2.8 m.

The modelled temperatures beneath the embankment matched the measured field data with reasonable accuracy and validated the selection of material properties and model boundaries.

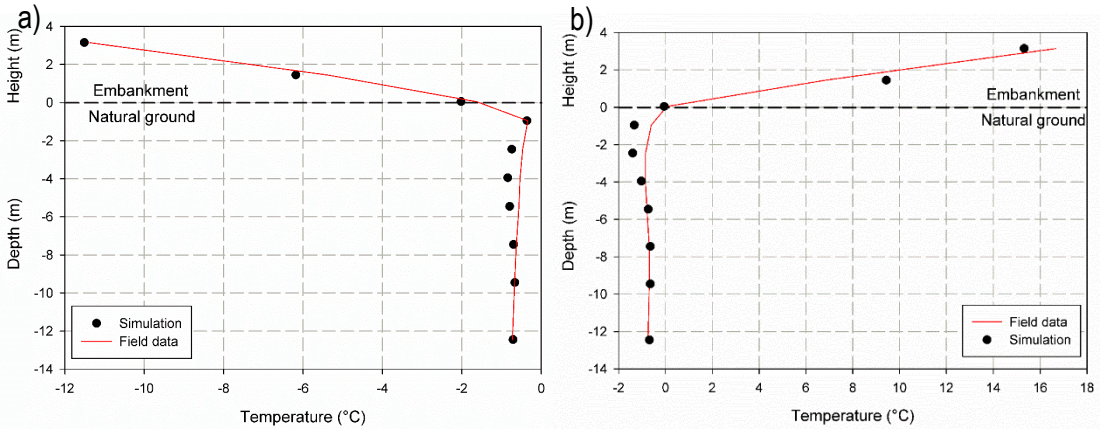

Figure 5. 10: Comparison of measured temperature profile and modeled temperature profile with depth under the side slope (BH2) in: a) January 2012; b) July 2012.

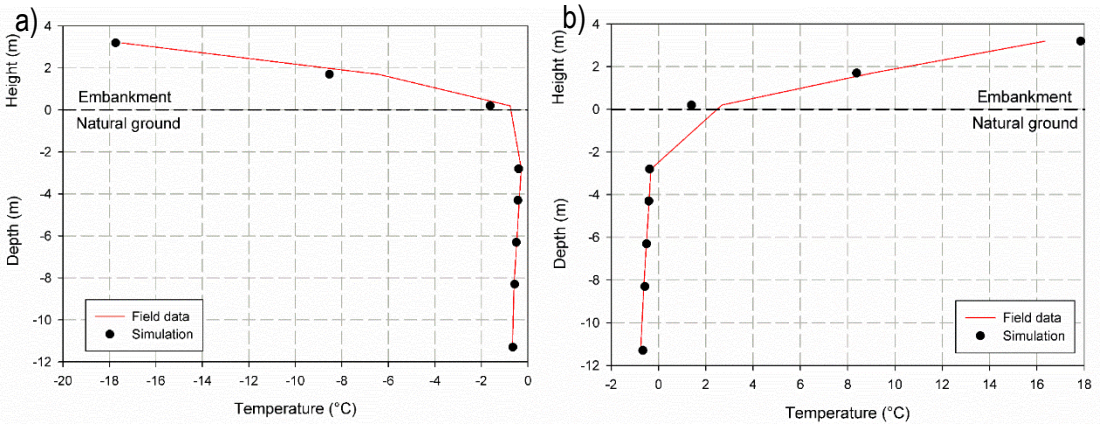

Figure 5. 11: Comparison of measured temperature profile and modeled temperature profile under the centerline (BH1) in: a) January 2012; b) July 2012.

5.4 Analysis, validation and discussion

Heat balance is used to quantify the heat budget through the interface in one year. It equals to the summation of extraction index and induction index. A negative heat balance indicates that more heat is extracted than induced. The extraction index and induction index are expressed as (M-Lepage et al., 2012):

$$H_x = k_{frozen} \times \frac{T_1 - T_2}{\Delta z} \times \Delta t \tag{5.1}$$

$$H_i = k_{unfrozen} \times \frac{T_1 - T_2}{\Delta z} \times \Delta t \tag{5.2}$$

where Q is the heat balance. H_x, H_i are the extraction index with negative values and heat induction with positive values in one year, respectively (Figure 5.12). T_1 is the temperature at the interface and T_2 is the permafrost temperature. k_{frozen} and $k_{unfrozen}$ are the thermal conductivity at frozen and thawing states in the surface ground layer, respectively (Table 5.1). A negative heat balance indicates that more heat is extracted than induced, indicating that the ground is cooling. This approach is used to help determine the thermal condition of conventional embankments and to select a suitable mitigation technique to extract a sufficient amount of heat from the ground to stabilize the permafrost. In this paper, the heat balance under the side slope was calculated from the interface to the depth of 12.5 m with the limited seasonal ground temperature change (Δz = 12.5 m) (Figure 5.9). Δt was specified to 1.0 day.

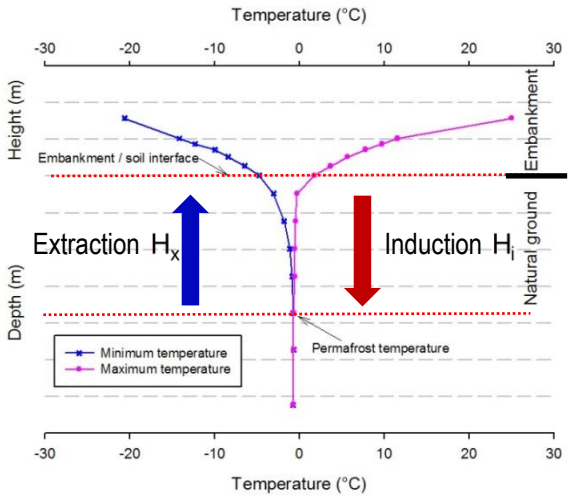

Figure 5. 12: Schematic of heat extraction index and induction index in the ground in one year.

After the thermal model was calibrated using the temperature data measured at Beaver Creek, sensitivity analyses were carried out to quantify the heat extraction capacity of the shoulder ACE through the embankment-soil interface underneath the mid-length of the side slope for different embankment thickness and site conditions. The physical properties of crushed rocks, such as the thermal conductivity, heat capacity and intrinsic permeability, were kept constant for all simulations. The thickness of an ACE layer should be at least 1.5 m to create an efficient convection movement in the rock layer (Esch, 1996). Thus, the embankment thickness of 1.5 m was selected as the minimum and the thickness was increased by 1.5 m increments to a maximum thickness of 6.0 m. The movement of air was induced by the temperature difference between the top and base of the rock layer in the winter. Therefore, the temperature difference (ΔT) between the mean annual winter air temperature (MAWAT) and permafrost temperature was selected as another control parameter, considering the climate conditions, thermal conditions in the subgrade and the practical use of it for engineers. In the simulations, the varying parameters included the MAWAT and embankment thickness. The main interest

was to quantify the heat extraction capacity of the shoulder ACE under the side slope in long-term conditions. Goering (1996) discussed the simulated characters of airflow and temperature fields for a 2.5 m-thick ACE in the long-term state with a total simulation time of 25 years. Darrow and Jension (2016) reported the field data and numerical data for an average 2.0 m-thick ACE to demonstrate the long-term cooling effect with a total simulation time of 27 years. In this paper, a time step of less than 0.2 days was used for each simulation with a total simulation time of 60 years to eliminate the effects of assumed initial temperature field and to obtain the periodic annual cycle in response to the given boundary conditions and given MAWAT. Considering the various embankment thicknesses and site conditions used in this research, the simulation time of 60 years was longer than that used in previous research. The average daily temperatures for the final year of the simulation were exported for the calculation of heat balance (Equations 5.2 and 5.3).

The relationships between the heat extraction capacity through the embankment-soil interface underneath the mid-length of the side slope, the embankment thickness and ΔT, were obtained through the statistical regression (Table 5.3) using the data points obtained by numerical simulations. Figure 5.13 shows the relationship between the heat extraction capacity, the embankment thickness and ΔT. From this figure, it can be seen that the heat extraction capacity increases with the embankment thickness and with ΔT. For example, with an ΔT of -14.6 °C, the corresponding heat extraction capacities were -1.06×10^6 J/m^2, -3.33×10^6 J/m^2, -4.63×10^6 J/m^2, $-5.54\times\times10^6$ J/m^2 for embankment thicknesses of 1.5 m, 3.0 m, 4.5 m and 6.0 m, respectively. The larger absolute value of negative ΔT tended to induce a stronger winter-time convection in the rock layer and a larger heat extraction capacity was generated. However, the rate of increase is reduced. For example, for the embankment thickness of 3.0 m, the corresponding heat extraction capacities were -3.33×10^6 J/m^2, -5.37×10^6 J/m^2, -6.86×10^6 J/m^2 for ΔT of -14.6 °C, -16.1 °C, -17.4 °C, respectively.

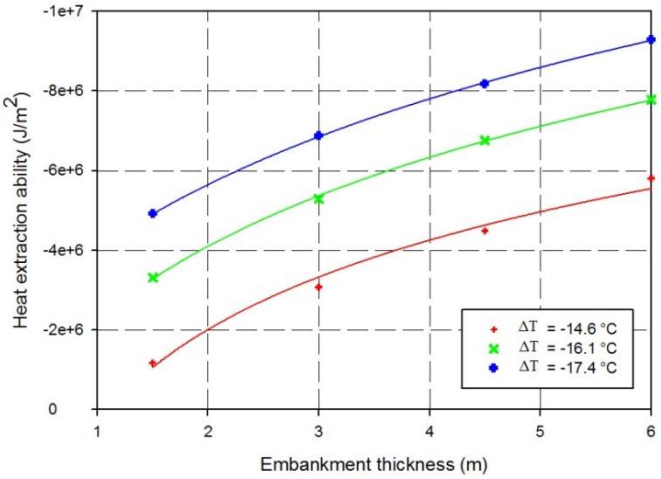

Figure 5. 13: Heat extraction capacity of shoulder ACE through the embankment-soil interface as a function of embankment thickness and temperature difference (ΔT) between MAWAT and permafrost temperature.

Table 5. 3: Regression equations between heat extraction capacity of shoulder ACE at the embankment-soil interface, embankment thickness and temperature difference (ΔT) between MAWAT and permafrost temperature.

ΔT (°C)	Regression equation	Coefficient of determination (R^2)
-17.4	$Q = -4.63 \times 10^6 \times \ln(x + 1.39)$	> 0.99
-16.1	$Q = -4.07 \times 10^6 \times \ln(x + 0.74)$	> 0.99
-14.6	$Q = -3.12 \times 10^6 \times \ln(x - 0.09)$	> 0.97

x is embankment thickness (m); Q is the heat extraction capacity (J/m^2) of shoulder ACE through the mid-length of the side slope.

Before applying the shoulder ACE, it is necessary to determine the thermal condition of permafrost underneath conventional embankments during the service life. This heat extraction capacity chart through the interface under side slopes (Figure 5.13) should be used together with the heat balance chart through the interface under side slopes for conventional embankments (Figure 5.14). The heat balance chart was developed based on the thermal model calibrated in the first part of this research project (Kong et al., 2019). Figure 5.14 shows the minimum amount of extra heat underneath side slopes that should be extracted through the application of shoulder ACEs for the thermal stabilization of permafrost underneath the side slopes. There are two suggested ways that can be used to obtain the thermal gradient in the subgrade for conventional embankments: 1) the preferred way for existing embankments is to use instrumentation to obtain directly the site-specific information. Alternatively, if the information is available on a similar embankment at a nearby site, it can be used to assess the required input data; 2) for planned embankments or for existing embankments where it is impractical to measure the temperature, the input data can be obtained using numerical models.

The relationships between the heat balance through the interface, the embankment thickness and the thermal gradient, were also obtained through the statistical regression (Table 5.4) using data points obtained by numerical simulations. The embankment thickness is a key factor in determining the thermal effectiveness of shoulder ACEs and it is one crucial parameter to obtain enough heat extraction to keep the stability of underlying permafrost. The embankment thickness required to achieve the desired heat extraction capacity could be obtained through Figure 5.13.

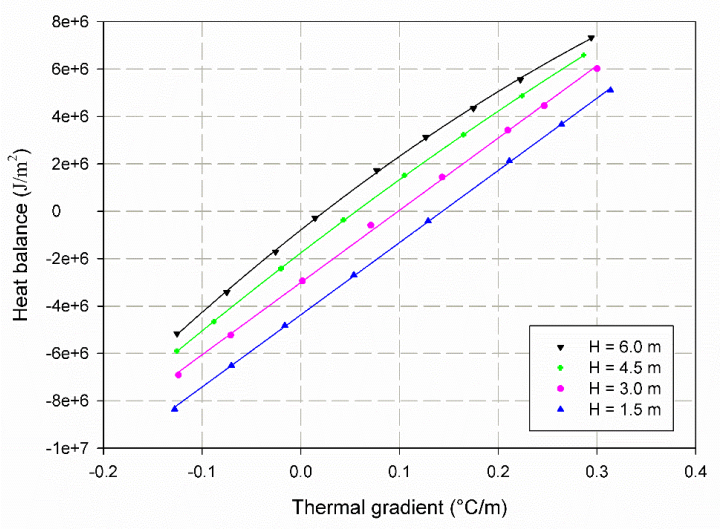

Figure 5. 14: Heat balance at the embankment-soil interface as a function of the embankment thickness (H) and thermal gradient.

Table 5. 4: Regression equations between heat balance at the embankment-soil interface, embankment thickness and thermal gradient for conventional embankments.

Embankment thickness (m)	Regression equation	Coefficient of determination (R^2)
1.5	$Q = 3.05\times10^{7}\times x - 4.37\times10^{6}$	> 0.99
3.0	$Q = 3.05\times10^{6}\times x - 3.01\times10^{6}$	> 0.99
4.5	$Q = -1.75\times10^{6} + 3.19\times10^{7}\times x - 9.89\times10^{6}\times x^{2}$	> 0.99
6.0	$Q = -0.78\times10^{6} + 3.29\times10^{7}\times x - 1.85\times10^{7}\times x^{2}$	> 0.99

x is the thermal gradient (°C/m) between the average annual temperature at interface and permafrost temperature; Q is the heat balance (J/m^2) through the interface.

The proposed engineering design chart (Figure 5.13) was developed based on the model built and calibrated using the measured data at Beaver Creek. The model was validated using the data from the Puvirnituq airstrip, Quebec, Canada. The Puvirnituq airstrip is located in a continuous permafrost region (Gaumond, 2014) and was constructed using an embankment reaching a thickness of 6.0 m. After the construction of the Puvirnituq airstrip, large settlements were observed and to stabilize the airstrip, an ACE was constructed in both shoulders to protect a 150 m long section of the runway in later summer, 2009. Thermistor strings were installed under the side slope, under the centerline and at the toe of the embankment. Temperature data were available before and after the construction of the ACE. The field data, including the MAWAT, the permafrost temperature and the mean annual soil temperature at the embankment-soil interface, were used to determine the heat extraction capacity, based on Figure 5.13. The measured data were used to calculate the heat balance before the construction of the ACE as well. The calculated heat balance and estimated heat extraction capacities were 7.2×10^{6} J/m^2, -7.8×10^{6} J/m^2 before and after the construction of the ACE. The net heat budget

with -0.6×10^6 J/m^2 was confirmed by the decreasing temperature at the depth of 2.5 m below the interface from 2012 to 2014 (Figure 5.15).

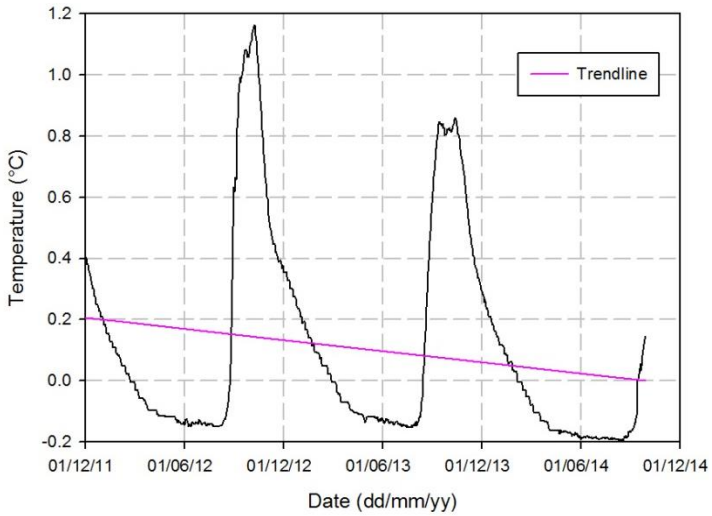

Figure 5. 15: Evolution of ground temperature at the depth of 2.5 m below the ground surface at Puvirnitup airstrip, Northern Quebec, Canada.

5.5 Conclusion

The shoulder ACE at Beaver Creek, Yukon, provided much information on the thermal capacity of ACEs to decrease the ground temperature. Measured temperature data indicated that under the side slope, the mean annual ground temperature (MAGT) experienced a decreasing trend down to a depth of 10 m in the ground. The MAGT decreased by 0.70 °C at the embankment-soil interface during 5 years of experimentation. However, the MAGT at the interface showed limited cooling, reaching -0.45 °C in 2009 and -0.41 °C in 2013, under the centerline. This suggests that the ACE performed well in winter and also supported the application of the shoulder ACE to protect permafrost effectively underneath the side slopes, where engineering problems usually occur.

The main objective of this project is to propose new design procedures and an engineering design chart using numerical models. The coupled software modules SVHeat for the conductive heat transfer and SVAir-flow for the natural convection were used to develop a 2D model. Through fieldwork and lab testing, detailed information including the embankment dimension, thermal properties of soils and air temperature were obtained to feed the model. The measured and modelled MAGT and soil temperatures with depths at selected months were compared and discussed in detail. The reproduction of the ground thermal regime supported the reasonable accuracy of the developed model.

Heat balance approach was employed to determine the thermal conditions for conventional embankments and to assess the heat extraction capacity of stabilization methods. The heat extraction capacity chart through the embankment-soil interface under mid-length of the side slope with different embankment thicknesses and site conditions was developed and successfully validated using the measured data from the Puvirnituq airstrip, Northern Quebec, Canada. The results indicated that the heat extraction capacity increased with the embankment thickness and the temperature difference (ΔT) between the MAWAT and the permafrost temperature. The chart can assist engineers in determining the shoulder ACE thickness required to extract a sufficient amount of extra heat flowing into the foundation of conventional embankments if thermal instability is observed or expected.

In summary, this research developed design procedures or guidelines for the thermal stabilization of northern transportation infrastructure built on thaw-sensitive permafrost. Design tools for shoulder ACEs were also developed and validated to support the design and management of infrastructure. Results of this research can impact the quality of northern transportation infrastructure by improving our current ability to design shoulder ACEs in a way that preserves unstable permafrost in the context of global warming.

Acknowledgements

The authors would like to acknowledge the financial support of the Natural Sciences and Engineering Research Council of Canada, the 2013-2020 Climate Change Action Plan and Transports Québec, as well as the technical and financial support of public and private partners of the permafrost engineering research program ARQULUK for this project.

5.6 References

Andersland, O. B., Ladanyi, B. (2004). Frozen ground engineering: John Wiley & Sons.

Beaulac, I., Doré, G. (2006). Airfields and access roads performance assessment in Nunavik, Quebec, Canada Current Practices in Cold Regions Engineering, pp. 1-12.

Berg, R. L., Aitken, G. W. (1973). Some passive methods of controlling geocryological conditions in roadway construction. Permafrost: The North American Contributions to the Second International Conference. National Academy of Sciences,Washington, DC, pp. 581–586.

Brown, W. G. (1963). Graphical determination of temperature under heated or cooled areas on the ground surface. Ottawa, Canada: Division of Building Research, National Research Council, Canada.

Darrow, M. M. (2011). Thermal modeling of roadway embankments over permafrost. Cold Regions Science and Technology, 65(3), 474-487.

Darrow, M. M., Jensen, D. D. (2016). Modeling the performance of an air convection embankment (ACE) with thermal berm over ice-rich permafrost, Lost Chicken Creek, Alaska. Cold Regions Science and Technology, 130, 43-58.

Doré, G., Ficheur, A., Guimond, A., Boucher, M. (2012). Performance and cost-effectiveness of thermal stabilization techniques used at the Tasiujaq airstrip Cold Regions Engineering 2012: Sustainable Infrastructure Development in a Changing Cold Environment, pp. 32-41.

Doré, G., Niu, F., Brooks, H. (2016). Adaptation methods for transportation infrastructure built on degrading permafrost. Permafrost and Periglacial Processes, 27(4), 352-364.

Doré, G., Pierre, P., Juneau, S., Lemelin, J. (2007). Expérimentation de méthodes de mitigation des effets de la fonte du pergélisol sur les infrastructures du Nunavik: aéroport de Tasiujaq, Rapport d'étape 1– Compte rendu des travaux d'instrumentation et de supervision de construction des planches expérimentales de l'aéroport de Tasiujaq, description des planches construites et de l'instrumentation installée. GRINCH, Université Laval, Canada, pp. 28.

De Grandpré, I. 2011. Impacts de l'écoulement souterrain sur la dégradation du pergélisol, mémoire de maîtrise, département de géographie, faculté des Arts et Sciences, Université de Montréal, pp.132 .

Environment Canada. (2011). Canadian climate normals 1971–2000 [online]. Available from http://www.climat.meteo.gc.ca (accessed on July 4 2011).

Esch, D. C. (1996). Road and airfield design for permafrost conditions. In Roads and Airfields in Cold Regions: an ASCE Monograph, Vinson TS, Rooney JW, Haas WH (eds). American Society of Civil Engineers: New York, New York, USA; 121-149.

Gaumond, F. G. (2014). Suivi des comportements thermique et mécanique du remblai de la piste de Puvirnituq. Mater's thesis, Laval University, Quebec, Canada.

Goering, D. J. (1998). Experimental investigation of air convection embankments for permafrost-resistant roadway design. In: Proceedings of 7th International Conference on Permafrost, Yellowknife, Canada, Collection Nordicana, pp. 319–326.

Goering, D. J. (2002). Convective cooling in open rock embankments Cold Regions Engineering: Cold Regions Impacts on Transportation and Infrastructure, pp. 629-644.

Goering, D. J. (2003). Passively cooled railway embankments for use in permafrost areas. Journal of cold regions engineering, 17(3), 119-133.

Goering, D. J., Kumar, P. (1996). Winter-time convection in open-graded embankments. Cold Regions Science and Technology, 24(1), 57-74.

Goering, D. J., Kumar, P. (1999). Permeability effects on winter-time natural convection in gravel embankments. Advances in Cold-Region Thermal Engineering and Science. 533: 455- 464.

Goering, D. J.(1998). Experimental investigation of air convection embankments for permafrost-resistant roadway design. In: Proceedings of the 7th International Conference on Permafrost, Yellowknif, NWT, Canada, pp.319-326.

Jørgensen, A., Doré, G., Voyer, É., Chataigner, Y., Gosselin, L. (2008). Optimization of the characteristics of two heat removal techniques for permafrost protection. Cold Regions Science and Technology, 53(2), 179-192.

Kersten, M.S., 1949. Laboratory research for the determination of the thermal properties of soils. Research Laboratory Investigations, Engineering Experiment Station, University of Minnesota, Minneapolis. Technical Report 23.

Kong, X., Doré, G., Calmels, F. (2019). Thermal modeling of heat balance through embankments in permafrost regions. Cold Regions Science and Technology, 158, 117-127.

Lipovsky, P.S. (2015). Summary of Yukon Geological Survey permafrost monitoring network results, 2008-2013. In: Yukon Exploration and Geology 2014, K.E. MacFarlane, M.G. Nordling and P.J. Sack (eds.), Yukon Geological Survey, pp. 113-122.

Lunardini, V. J. (1978). Theory of n-factors and correlation of data. In Proceedings of the 3rd International Conference on Permafrost, Edmonton, Alta. National Research Council of Canada, pp. 40–46.

Ma, W., Shi, C.H., Wu, Q.B., Zhang, L.X., Wu, Z.J., 2006. Monitoring study on technology of the cooling roadbed in permafrost region of Qinghai–Tibet Plateau. Cold Regions Science and Technology 44, 1–11.

McHattie, R.L., Goering, D.J., 2009. Air convection embankment (ACE) design guide. Alaska. Department of Transportation. Report, FHWA-AK-RD-09-06.

M-Lepage, J. (2016). Experimentation of mitigation techniques to reduce the effects of permafrost degradation on transportation infrastructures at Beaver Creek experimental road site (Alaska Highway, Yukon). Mater's thesis, Laval University, Quebec, Canada.

M-Lepage, J., Doré, G., Fortier, D., Murchison, P. (2012). Thermal performance of the permafrost protection techniques at Beaver Creek experimental road site, Yukon, Canada. In: Proceedings of the 10th International Conference on Permafrost, Salekhard, Russia, pp. 261.

Nelson, F. E., Anisimov, O. A., Shiklomanov, N. I. (2002). Climate change and hazard zonation in the circum-Arctic permafrost regions. Natural Hazards, 26(3), 203-225.

Regehr, J. D., Milligan, C. A., Montufar, J., Alfaro, M. (2012). Review of effectiveness and costs of strategies to improve roadbed stability in permafrost regions. Journal of Cold Regions Engineering, 27(3), 109-131.

Reimchen, D., Doré, G., Fortier, D., WALSH, R. (2009). Cost and constructability of permafrost test sections along the Alaska Highway, Yukon. In: Proceedings of Transport Association of Canada Annual Conference, Vancouver, Canada, pp.1-20.

Sun, B., Yang, L., Liu, Q., Wang, W., Xu, X. (2011). Experimental study on cooling enhancement of crushed rock layer with perforated ventilation pipe under air-tight top surface. Cold Regions Science and Technology, 68(3), 150-161.

Zarling, J. P., Braley, W. A. (1986). Thaw stabilization of roadway embankments constructed over permafrost: Alaska Department of Transportation and Public Facilities, pp.1-34.

Chapter 6 Investigation on the heat extraction capacity of the heat drain for thermal stabilization of embankments on thaw sensitive permafrost

Foreword

Xiangbing Kong[1], Guy Doré[1], Fabrice Calmels[2], Chantal Lemieux[1]

[1]Department of Civil and Water Engineering, Laval University, Québec City, Québec, Canada

[2]Yukon Research Centre/Northern Climate ExChange, Yukon College, Whitehorse, Yukon, Canada

State: Submitted to review

Date of Submission: 15 July 2019

Journal: Cold Regions Science and Technology

Résumé

La construction d'infrastructures de transport cause souvent la dégradation du pergélisol et les changements climatiques amplifient ce phénomène. Le drain thermique, basé sur la convection naturelle en hiver, est une nouvelle technique de mitigation et est conçu pour limiter ou éviter le dégel du pergélisol. Durant l'hiver, l'extraction de chaleur est accentuée par la convection naturelle d'air dans les pores du matériel, générée par l'instabilité de la densité de l'air dans le drain thermique. Pour effectuer le suivi de l'efficacité de cette technique, un drain thermique a été construit à l'été 2007, dans l'épaulement de la piste d'atterrissage de Tasiujaq, dans le Nord du Québec (Canada). Des thermistances ont été installées sous l'épaulement pour mesurer les températures du sol. Une bonne performance thermique a été observée et a permisde stabiliser le pergélisol. Un modèle thermique a été développé basé sur les caractéristiques et les conditions du site expérimental de Tasiujaq. Le modèle a aussi été calibré aux données collectées à Tasiujaq. Un ensemble d'abaques de conception a été développé par le modèle et a été validé en utilisant les données mesurées à Salluit, au Nord du Québec (Canada), où un drain thermique est installé depuis 2012.

Mots clés: Infrastructure de transport; Dégradation du pergélisol; Drain thermique; Abaques de conception

Abstract

Construction of transportation infrastructure often results in permafrost degradation and global warming amplifies this phenomenon. Heat drain, based on winter-time natural convection, is a new mitigation technique and is designed to limit or avoid the thawing of permafrost. In winter, heat extraction is enhanced by the buoyancy-driven convection of the pore-air due to unstable air density in the heat drain. To monitor the efficiency of this technique, an heat drain was constructed in the shoulder of Tasiujaq airstrip in Northern Quebec, Canada, in the summer 2007. Thermistors were installed beneath the side slopes to measure ground temperatures. A good thermal performance was observed resulting in thermal stabilization of the underlying permafrost. A thermal model was developed based on the Tasiujaq experimental site characteristics and conditions. The model was also calibrated to the field data collected at Tasiujaq. A set of design charts was developed through the model and were successfully validated using the measured data from Salluit, Northern Quebec, Canada, where an heat drain is installed since 2012.

Keywords: Transportation infrastructure; Permafrost degradation; Heat drain; Design charts

6.1 Introduction

Transportation infrastructure is essential to the socio-economic development of the local communities and, in northern regions, it is usually built on the widely distributed permafrost. Permafrost is often ice-rich, making it prone to thaw settlements when the thermal equilibrium is disturbed. The construction of transportation embankments modifies the pre-existing surface conditions by compressing or removing the organic layer, and often results in the thawing of permafrost and infrastructure instability, leading to expensive maintenance and repairs (Jørgensen et al., 2008; Goering and Kumar, 1996). Global warming is ongoing at a greater rate than observed in the past few decades, and amplifies the degradation of permafrost (Doré et al., 2016).

Since the 1960s, various mitigation techniques have been developed and tested in Alaska, Canada, China and Russia to limit permafrost degradation underneath transportation infrastructure. Those techniques can be categorized into three main groups: (i) limiting the heat transfer from the atmosphere into permafrost; (ii) enhancing the winter-time heat extraction to cool permafrost; and (iii) reinforcing the embankment (Doré et al., 2016). The prevailing consideration for the structural design of linear transportation is to keep the long-term thermal stability of the underlying permafrost (Doré and Zubeck, 2009). Method from the last category (iii) is mainly used to improve the mechanical stability, and thus, is not widely applied (Calmels et al., 2016). Methods from category (i) include embankment insulation (e.g., Esch, 1983), snow/sun sheds (e.g., Zarling and Braley, 1986; M-Lepage et al., 2012), increase of the embankment thickness (e.g., Zarling et al., 1988) and high albedo surface (e.g., Berg and Aitken, 1973; Dumais and Doré, 2016). Air convection embankment (ACE), thermosyphons and air ducts from category (ii) have been used to decrease ground temperatures. Goering

(1998) studied the field efficiency of ACE built in warm permafrost regions. Zarling et al. (1984) reported the field application of air ducts in Bonanza Creek, Alaska. Hayley et al. (1983) monitored thermosyphons installed along the fen to peat plateau transitions of the Hudson Bay Railway.

Heat drain, based on the method from category (ii), is an innovative technique developed by Université Laval in the early 2000s. It consists of a 25 mm thick, drainage geocomposite with high permeability to promote convective heat exchange in the embankment shoulder or across the full embankment width (Doré et al., 2016). The drainage geocomposite is made of a corrugated plastic core covered on both sides by geotextile (M-Lepage, 2015). In winter, the instability of pore-air density draws cold air through inlets at the base of the shoulder, which then flows through the geocomposite, cooling the ground soil. A “flat” section with a slope angle of approximately 2% is needed to collect ground heat and a steep section with a 45° slope is required in order to facilitate the airflow in the heat drain (Doré et al., 2016).

Heat drain is lightweight and easy to transport to construction sites and this is a good solution when granular materials to construct ACE are not available (M-Lepage, 2015). Both the numerical simulations (Chataigner et al., 2009; Jørgensen et al., 2008) and lab experiments (Beaulac and Doré, 2006) indicated the thermal efficiency of heat drain to decrease soil temperatures. To test the performance on a full-scale site, in 2007, an heat drain was installed on the shoulder of Tasiujaq airstrip embankment in Nunavik, Northern Quebec, Canada.

Thermal stability of permafrost depends on the heat balance across the embankment-soil interface, i.e. the total amount of heat flowing in and out of the foundation. To maintain permafrost thermal stability underneath transportation embankments, the annual heat balance should be equal or less than 0. Heat balance approach is a rational way to determine the thermal state of conventional embankments and to select the suitable stabilization method to extract at least the amount of extra heat flowing into the foundation.

The principal objective of this paper is to propose a set of engineering design charts, developed using numerical simulations, to investigate the heat extraction capacity with different embankment thickness and site conditions, in permafrost environments. More specifically, the field performance of heat drain installed at Tasiujaq was firstly analyzed. Then, a two-dimensional model was developed and well calibrated to the field data collected at Tasiujaq airstrip. Finally, a set of engineering design charts based on heat balance approach were developed and validated using the available measured thermal data from Salluit road, Northern Quebec, Canada.

The design charts provide engineers a thermal assessment of the capacity of the heat drain to mitigate the effects of permafrost degradation underneath transportation embankments for a specific site. The design

charts are easy to use and special knowledge on finite element modeling and heat transfer process are not required.

6.2 Study site and temperature data measured

The village of Tasiujaq is located in the southeastern part of Ungava Bay (58° 71' N and 69° 82' W), several kilometers north of tree line in a continuous permafrost zone (Figure 6.1). The Tasiujaq airstrip is the only transportation infrastructure connecting the village all year long with the outside world. The runway was built on a terrace of fluvial origin with a total length of 1190 m along a north-east/south-west axis (Allard et al., 2007). A significant amount of ice with a maximum ice content of approximately 50% was found in the ground, making it vulnerable to permafrost thawing (Allard et al., 2009). The rate of thaw settlement was between 20 mm/year and 70 mm/year, with an average of 35 mm/year, which was considered to be high (Doré et al., 2007). Degradations, such as settlements and crackings were observed at several locations along the airstrip (Allard et al., 2007). Intensive maintenance is needed to keep a reasonable service level (Doré et al., 2012).

Figure 6. 1: The location of Tasiujaq experimental site, Northern Quebec, Canada (Doré et al., 2007).

Snow accumulation on the embankment slope impedes heat extraction from the ground in winter, leading to higher soil temperatures the following summer. The snowpack thickness were respectively 60-175 cm and 25-105 cm on the east and west side slopes of Tasiujaq airstrip on April 2005 (Allard et al., 2007). Due to climate change, permafrost degradation is expected to intensify in the future (Allard et al., 2007). In that context, three adaptation methods, including a heat drain, an air convection embankment (ACE) and a gentle slope (8H:1V), were applied in the shoulder of the airstrip embankment to assess the feasibility of construction and the efficiency of the techniques to stabilize the infrastructure (Doré et al., 2012).

This paper focuses on the heat drain (Figure 6.2a). To minimize the thermal disturbance of construction on the underlying permafrost, 50 m long heat drain was installed in September 2007, immediately after the excavation (Figure 6.2b) to limit the impact of heat flowing into the soil. To prevent any damages to the drain by the backfill, two thin layers of sand were placed under and above it (Figure 6.2c). A vertical thermistor string, reaching a depth of 3.15 m in the natural ground, was installed in the side slope to measure ground temperatures. Also, two thermistors were placed in the air inlet and air outlet.

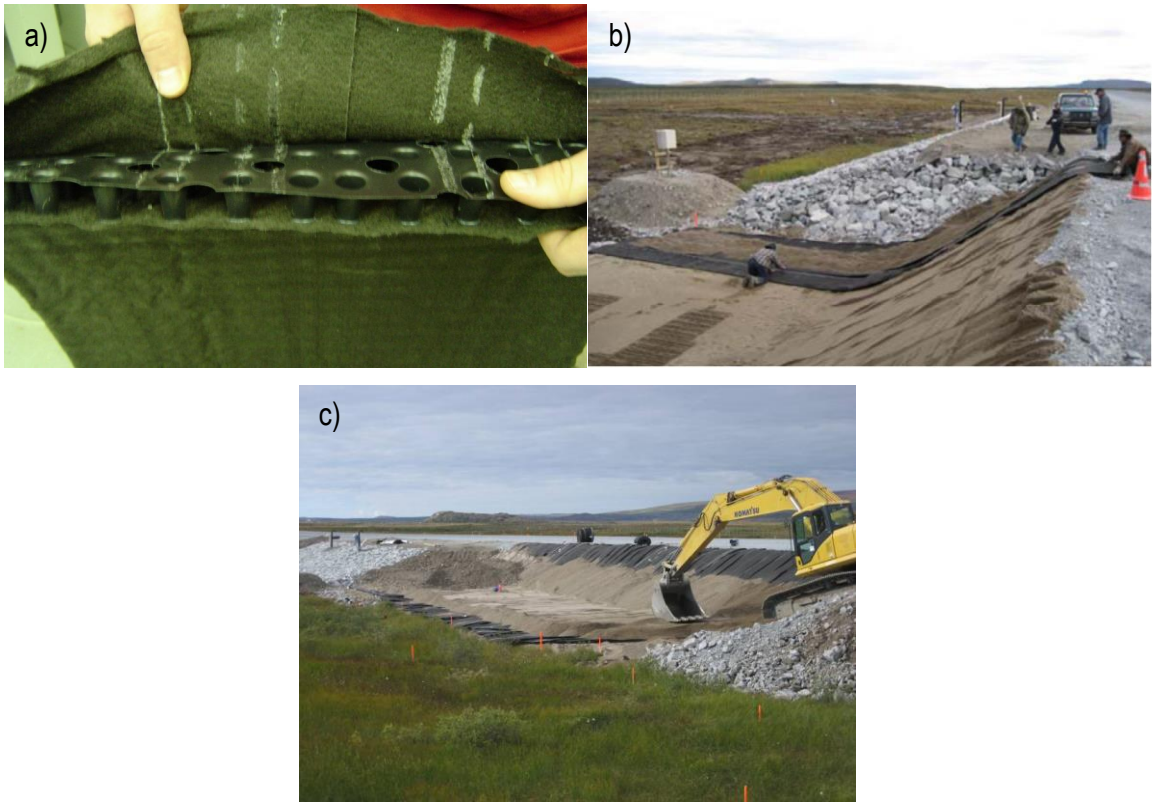

Figure 6. 2: Heat drain installed at Tasiujaq airstrip, Northern Quebec, Canada. (a) heat drain; (b) during the installation; (c) layers of sand under and above.

The atmospheric temperature has a direct effect on the thermal behavior of the ground. Air thawing index and air freezing index are used to quantify the "severity" of site conditions in summer and winter seasons, respectively (Doré and Zubeck, 2009). The net air index, the addition of air thawing and freezing indices, at Tasiujaq airstrip over the period of 2008 to 2011, is shown in Figure 6.3. The net air index increased slightly from -1953 °C-day in 2008 to -1896 °C-day in 2009, however, a dramatic increase is observed in 2010 with a net air index reaching -612 °C-day. In 2011, the net air index was much smaller than the one in 2010 but still larger than in 2008 and 2009. The measured mean annual air temperature (MAAT) from 2008 to 2011 had a similar trend as the measured net air index.

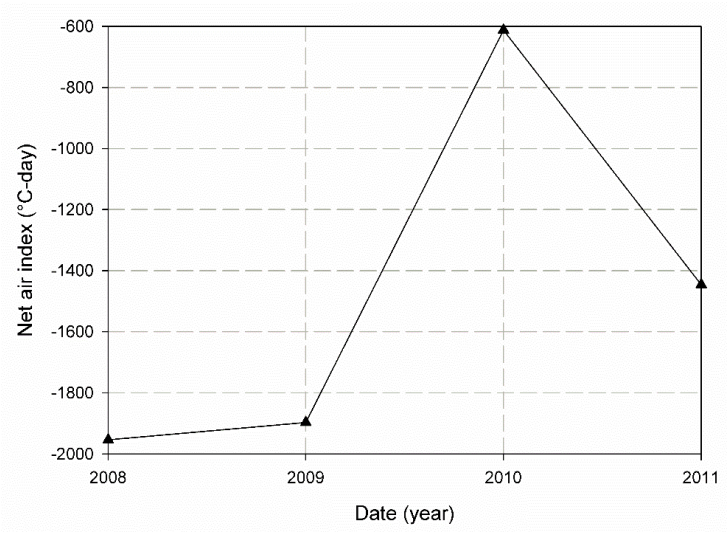

Figure 6. 3: Net air index measured from 2008 to 2011 at Tasiujaq airstrip, Northern Quebec, Canada.

The winter air temperature in the air inlet followed the atmospheric temperature, and the one from the air outlet was higher. The analysis of the air temperature difference between the outlet and inlet is a good indicator of the seasonal movement of air in the heat drain, even if the speed of air flow was not measured. The positive values of air temperature difference indicated the air was warmed in the heat drain, implying heat was extracted from the ground. The monthly averaged temperature difference (MATD) in 2009 is shown in Figure 6.4. The MATD continually decreased from 7.1 °C in January to 1.6 °C in May, indicating that the heat extraction was strongest in January and decreased in the following four months. As the soil around the drain becomes lower during winter, the temperature difference between soil and air diminishes, reducing thus the effectiveness of the heat drain. MATD fluctuated of ±1.3 °C around 0 °C from June to November, indicating a limited motion of air in the heat drain compared to the one during winter-time. The negative temperature difference in summer, was prossibily due to the forced wind effect. In December, MATD reached 1.8 °C, which was similar to the value in May.

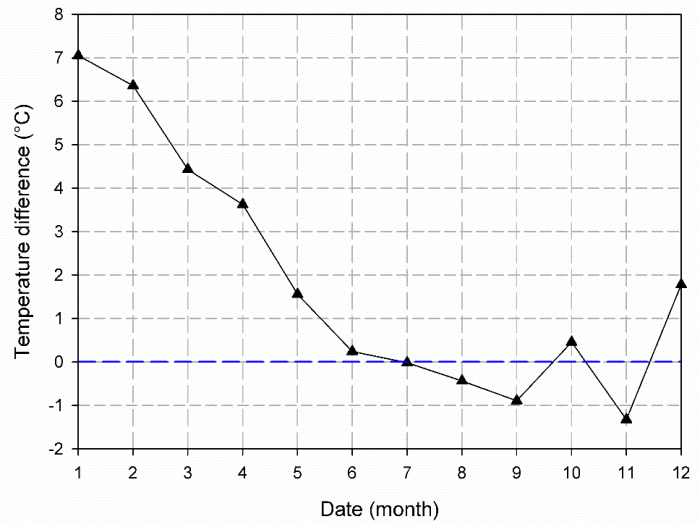

Figure 6. 4: Monthly averaged temperature difference between air outlet and inlet from January to December 2009.

The ground temperature varies with time due to many factors, such as solar radiation, soil depth, and air temperature. Figure 6.5 shows the temperature profiles with depth for selected mid-months in the shoulder of the embankment, in 2009. The top thermistor, located 0.3 m below the surface in the side slope, was used to measure the near-surface temperature. The temperature profiles demonstrate a temperature range of 15.5 °C in the shallow part of the side slope, with the minimum, maximum temperatures reaching -7.9 °C and 7.6 °C, respectively. The ambient air temperature only affected a certain depth of ground soil. For example, the ground temperature at the depth of -3.15 m was almost constant with a value of -0.86 °C.

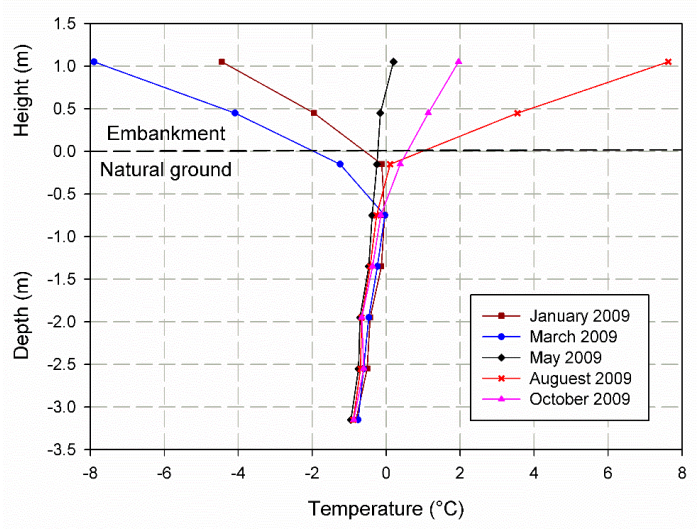

Figure 6. 5: Measured temperature profiles with depth under the side slope in 2009.

The higher near-surface temperature on the side slopes during summer and lower one during the winter were attributed to the effects of exposed gravel surface (summer) and snow accumulation (winter). The temperature

in the shallow part of the side slope was -4.4 °C in January and decreased in the following two months, with a minimum temperature reaching -7.9 °C in March. This resulted in cold temperatures quickly moving deeper in the embankment. A small temperature difference, less than 0.1 °C, was measured at the depth of -1.35 m. From March to May, a warming trend of near-surface temperature was observed, reaching 0.2 °C in May, then the heat moved into the embankment until the winter time. The ground temperatures in the selected months indicated small changes below the depth of -0.75 m. For example, the seasonal soil temperature variation decreased from 0.34 °C at the depth of -0.75 m to 0.20 °C at the depth of -3.15 m in the ground.

Figure 6.6 illustrates temperature variation under the side slope for a four years' period, from January 2008 to January 2012. The interface between the embankment and the natural ground is used as the reference level (0 m). The thaw front penetrated into the natural ground in the summertime from 2009 to 2011 even though an heat drain was installed in the shoulder. The air temperature followed a complex pattern, and it changed from 2009 to 2011. The measured difference of MAAT in 2008 and 2009 was less than 0.2 °C, however, global warming was observed in the following year (2010) with a MAAT around 3.5 °C larger than the previous two years. In 2011, MAAT was lower than 2010 but still higher than 2008 and 2009. The active layer thickness decreased from 1.43 m below the interface in 2008 to 1.12 m in 2009, due to the winter-time heat extraction of heat drain and the possible change of surface conditions. The measured ground temperatures at different depths indicated a decreasing trend from 2008 to 2009. For example, MAGT at the depth of -1.35 m decreased from -0.28 °C to -0.38 °C. Since 2009, ground temperatures did not show a continuous decreasing trend, mainly due to the warmer climate. The active layer thickness were -1.54 m in 2010 and -1.47 in 2011.

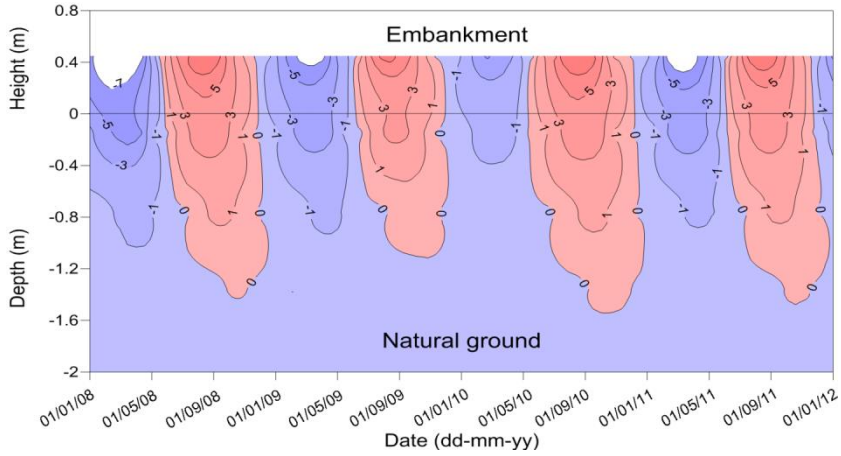

Figure 6. 6: Thermal behavior of the embankment fill and foundation soil under the side slope.

6.3 Numerical simulation

A model was developed to reproduce the temperature distribution in the embankment and in the subgrade soil. Site-specific characteristics, such as air temperature and embankment dimensions, were measured and used

as input parameters to improve the accuracy of the model. In the numerical modeling, two modules from the SoilVision software suite were used. SVHeat simulated the conductive heat transfer, taking ice-water phase change into account, in fine-grained and coarse-grained soils. SVAir-flow simulated the airflow due to unstable air density in the heat drain. The coupled finite-element program SVHeat and SVAir-flow were used together to model heat transfer due to density-driven air convection within the heat drain and conductive heat transfer within the embankment fill and foundation soil.

6.3.1 Governing equations

The equations governing the unsteady energy transport and motion of air in the coupled model are shown in this section.

SVHeat uses the following governing differential equation to describe the two-dimensional conductive heat flow in soils:

$$\frac{\partial}{\partial x}(k_x \frac{\partial T}{\partial x}) + \frac{\partial}{\partial y}(k_y \frac{\partial T}{\partial y}) + Q = C \frac{\partial T}{\partial t} - L_f \frac{\rho_i}{\rho_w} \frac{\partial \theta_i}{\partial t} \tag{6.1}$$

where k is the thermal conductivity of the porous medium (soils), which was held constant in the x, y directions; T is the temperature; C is the heat capacity; Q is the applied boundary flux; L_f is the volumetric latent heat of fusion of water, which equals to 3.34×10^8 J/m^3, x, y are coordinates. ρ_i, ρ_w are the ice density and water density, respectively.

The SVAir-flow module can be jointly utilized with the SVHeat module to simulate fluid flow in the porous medium. In the model developed, only the airflow was considered, neglecting the presence of moisture in the heat drain, considering the high permeability of the drain and its position in the embankment above standing water in the ground. Thus, the latent heat in the drain was thus assumed to be approximately zero. Darcy's law was employed to relate air pressure and interstitial air velocity. The governing equation for mass, momentum, and energy with air density as a function of temperature are expressed as (Goering and Kumar, 1999):

Continuity:

$$\frac{\partial v_y}{\partial y} + \frac{\partial v_x}{\partial x} = 0 \tag{6.2}$$

Momentum:

$$q_y = -\frac{K}{\mu} \bullet (\frac{\partial P}{\partial y} + \rho_a g) \tag{6.3}$$

$$q_x = -\frac{K}{\mu} \bullet \frac{\partial P}{\partial x} \tag{6.4}$$

$$\rho_a = \rho_0 [(1 - \beta (T - T_0)] \tag{6.5}$$

Energy:

$$\frac{\partial}{\partial x}(k_x \frac{\partial T}{\partial x}) + \frac{\partial}{\partial y}(k_y \frac{\partial T}{\partial y}) - (C_a v_x)\frac{\partial T}{\partial x} - (C_a v_y)\frac{\partial T}{\partial y} = C\frac{\partial T}{\partial t} \tag{6.6}$$

where C_a, v are the volumetric heat capacity of air and pore-airflow velocity, respectively. μ and β are the kinematic viscosity and the coefficient of thermal expansion for air, respectively. P is the air pressure. ρ_0 and T_0 are reference air density and reference temperature, respectively.

6.3.2 Physical domain, material properties and boundary conditions

The physical domain consists of the runway trapezoidal cross section and underlying foundation soil. To maximize the modeling efficiency and to reduce the computing time, half of the physical domain is chosen for the simulation (Figure 6.7). The physical domain represents an area of 65.8 m wide from the centerline of the embankment and a depth of 30.0 m underneath the original natural ground surface. The embankment fill material is 4.3 m deep at the centerline. In the physical model, part ① is the heat drain installed in the shoulder. Its porosity is assumed to be 0.65, considering the volume occupied by the corrugated plastic core to support the drainage geocomposite. The air conductivity of 0.47 m/s^2 is used, based on the sensitivity analysis and the moisture content is assumed to be zero in the heat drain. Part ② is the embankment fill with a low water content. The thermal properties are estimated using the empirical equations for coarse-grained soils with the assumed water content of 3% (Kersten, 1949); part ③ is the saturated silt with a water content of 30%, based on the measurements made on soil sampled at the test site. The water flow in the whole computational domain is restricted by setting water flux to be zero. The thermal properties of heat drain and foundation soil are summarized in Table 6.1.

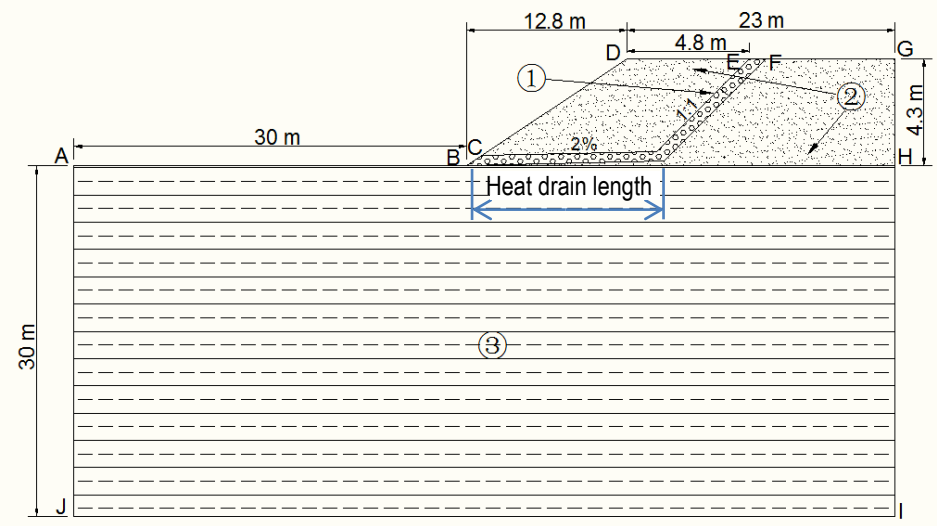

Figure 6. 7: The physical domain of the embankment and foundation.

Table 6. 1: Thermal properties used in the model.

Material type	k_f (W/m-°C)	k_u (W/m-°C)	C_f (MJ/m3-°C)	C_u (MJ/m3-°C)
Heat drain	0.09	0.09	0.09	0.09
Subgrade soil	1.19	0.86	1.72	2.11

The pressure and thermal conditions at each edge of the physical domain (Figure 6.7) were required for the thermal modeling, in addition to the governing equations described above. The boundaries, BC and EF, were set to be open and the pressure based on the surrounding ambient air mass was specified. Zero air flux was set on the side slope (CD) and embankment surface (DE and FG), considering that they were covered by soils and no air could flow inside. The foundation soil has typically a very small air permeability (Goering and Kumar, 1999), thus it provided an impermeable barrier (zero air flux) at the right boundary (HI), left boundary (AJ) and bottom boundary (IJ). Zero air flux was also set along the centerline (GH) of the embankment. The thermal boundary consisted of zero heat flux on the right boundary (GHI), left boundaries (AJ) and geothermal heat flux of 0.03 W/m2 at the bottom boundary (IJ), and temperature functions with thermal modifiers (n-factor) applied on the embankment surface, side slopes and natural ground surface.

The daily air temperature was measured at the local weather station. Instead of directly using measured air temperature with thermal modifiers (n-factor) in the model, a sinusoidal air temperature function (Figure 6.8) based on the measured air freezing index, air thawing index and MAAT was adopted for the simulations. Note that the simulated sinusoidal temperature function was derived from the temperature data collected in 2008, 2009 and 2011. Data collected in 2010 was not included in the model due to the exceptional air temperatures

recorded during that year, and the air temperature in 2010 still had an impact on the gorund thermal regime in the following year 2011, used in the model calibriation.Three temperature functions with thermal modifiers (n-factor) were used to simulate the near-surface temperatures: on the natural ground surface, on the gravel embankment surface where snow is plowed in winter and on the gravel side slope where snow accumulates in winter. Snow accumulation impedes heat extraction from the ground in the winter, resulting in a lower freezing n-factor, compared to snow plowed surface. The insulation effect is related to several factors, such as snow thickness and snow density, and to simplify the model, the yearly snow variation on the side slope was not considered in the model. The measured snow thickness on the side slope of Tasiujaq airstrip varied from 20 cm to 105 cm (Allard et al., 2009). Lanouette et al. (2015) developed a logarithmic relation between freezing n-factor and snowpack thickness, based on the in-situ measurement. To simply the simulation, the snowpack thickness was assumed to be the same on the side slope in the model. We initially set the freezing n-factor (n_f) to be 0.39, based on the assumed snowpack thickness of 40 cm. Also, values of 1.1 for thawing n-factor (n_t) on the gravel embankment surface, gravel side slopes and 0.8 for n_f on the gravel embankment surface were used for the simulations. The selected values were in the proposed range for gravel surface materials (Doré and Zubeck, 2009; Andersland and Ladanyi, 2004). The n_f and n_t for the natural ground were selected from the published values (Andersland and Ladanyi, 2004). The values of n_f for the side slope was slightly adjusted to make sure the modeled ground temperatures fit the measured temperatures well under the side slope. Table 6.2 summaries all the final determined n-factors used in the model.

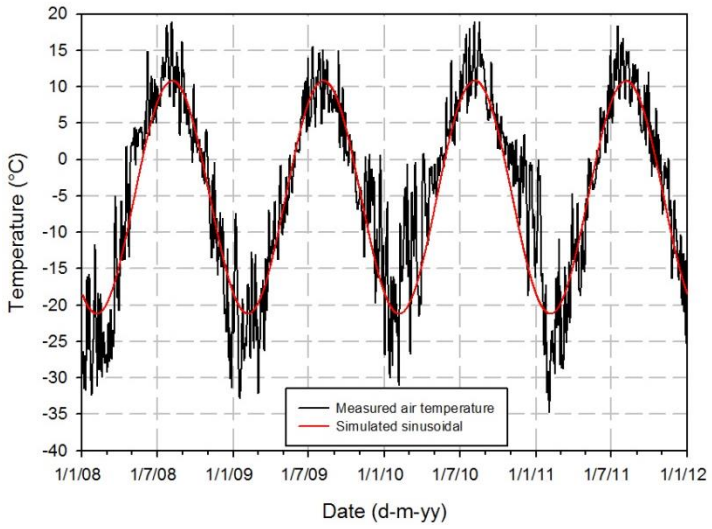

Figure 6. 8: Comparison between measured air temperature and simulated sinusoidal temperature.

Table 6. 2: Summary of n-factor used in the model.

Surface type	n_t	n_f
Natural ground surface	0.37	0.29
Embankment surface	1.1	0.8
Embankment side slopes	1.1	0.43

6.3.3 Model meshing

The meshing consisted of 14,410 triangular finite elements and 29,273 nodes, with the element size ranging from less than 1.0 m in the embankment fill to approximately 3.0 m in the subgrade, covering the domain shown in Figure 6.7. More meshing was generated for heat drain with the element size less than 0.05 m, due to its thin thickness and winter-time airflow characteristic in heat drain. Also, a density meshing was generated at the natural ground surface layer to obtain a better solution of the active layer and the top part of permafrost.

6.3.4 Analysis, validation and discussion

Heat drain was installed at Tasiujaq in the summer of 2007, and 4 years of data were available from 2008 to 2011. The corresponding total simulation time of 4 years was set. Note that the 3 years of data (2008, 2009 and 2011) were selected and averaged data for the model calibration. The model was run using time steps less than 0.1 day, automatically chosen by the finite element software to prevent it from crashing. The numerical results for the daily temperature were saved and then exported for future analysis, such as maximum, minimum and average temperature profiles.

The heat extraction capacity can be assessed by examining the mean annual ground temperature (MAGT) at the interface. Figure 6.9 shows the measured MAGT and modeled MAGT at the interface over the period of 2008-2011. Heat drain worked well to extract heat from the ground in winter (Figure 6.4) and this could help explain the reasonability of the modeled thermal efficiency with the unchanged simulated air temperature applied on the model boundaries, to continually decrease MAGT from 2008 to 2011 (Figure 6.9). The measured MAGT was higher than the modeled MAGT in 2010, mainly due to the higher temperature than the one used in the model. Also, the measured averaged MAGT and modeled MAGT in 2008, 2009 and 2011 were -0.14 °C and -0.13 °C, respectively. Figure 6.10 compares the modeled and measured maximum, minimum, average temperature profiles with depth in the side slope in 2009. The results indicate that the modeled average temperature was larger than the measured temperature with a maximum temperature difference of 0.45 °C in the embankment. Below the interface, the modeled average temperature fitted well the measured average temperature with a maximum temperature difference of 0.20 °C at the depth of -1.95 m. For the maximum temperature, the modeled temperature was higher than the measured temperature in the embankment and subgrade with a maximum temperature difference of 1.96 °C occurring at 0.45 m above the

interface. Below the depth of -0.75 m in the ground, the temperature difference was less than 0.50 °C. Comparison between the modeled minimum temperature and measured minimum temperature indicates that the biggest temperature difference of 2.34 °C occurred at 1.05 m above the interface. The modeled minimum temperatures just above and below the interface were higher than the measured temperatures, and the temperature difference was 0.52 °C at the interface. The modeled temperature was a little lower than the measured temperature with the maximum temperature difference less than 0.1 °C between the depths of -1.35 m and -2.55 m. As a whole, the developed model was judged reasonable and satisfactory to reproduce the thermal regime underneath the heat drain.

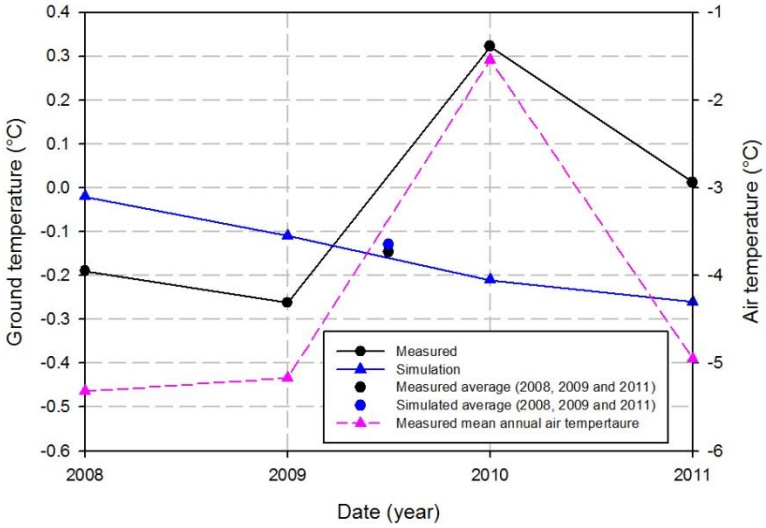

Figure 6. 9: Measured mean annual ground temperatures and modeled mean annual ground temperatures at the embankment-soil interface, from 2008 to 2011.

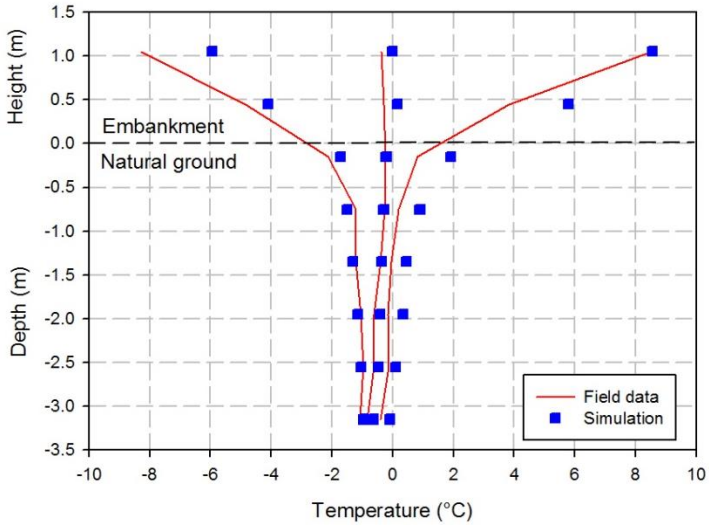

Figure 6. 10: Comparison between the field data and numerical simulation of the maximum, minimum and average temperature profiles with depth, in the side slope, in 2009.

After the model was well calibrated, a set of simulations were carried out to simulate the heat extraction capacity for different embankment thickness and site conditions. The heat extraction capacity was assessed by heat balance, which includes two parts, namely extraction index and induction index, expressed as (M-Lepage et al., 2012):

$$H_x = k_{frozen} \times \frac{T_1 - T_2}{\Delta z} \times \Delta t \tag{6.7}$$

$$H_i = k_{unfrozen} \times \frac{T_1 - T_2}{\Delta z} \times \Delta t \tag{6.8}$$

where H_x H_i are the extraction index and induction index, respectively. T_1, T_2 are the temperatures at the interface and permafrost temperature, respectively. Δz is the vertical length between the interface and the depth with permafrost temperature. k_{frozen}, $k_{unfrozen}$ are the thermal conductivity at frozen and thawing states in the surface ground layer. A positive heat balance indicates that less heat is extracted than induced.

The soil properties, thermal modifiers (n-factor) and mesh setting obtained from the calibrated model described above, were utilized in the following simulations. Stack height affects the thermal efficiency with a taller stack height enhancing the chimney effect (Calmels et al., 2016). It was directly quantified by the embankment thickness, which was an important factor for the practical engineering design. The optimized slope angle of 45° was kept constant in the design of heat drain, considering the balance between reasonable construction conditions and thermal efficiency. The motion of air was induced by unstable air density in the geocomposite layer in winter, which was heavily affected by the temperature difference (ΔT) between mean annual winter air temperature (MAWAT) and the ground temperature. In addition to that, the thermal efficiency was heavily affected by the length of the horizontal section (heat drain length) of the heat drain (Chataigner et al., 2009). In summary, three controlling parameters, including ΔT, embankment thickness and heat drain length, were selected to quantify the heat extraction capacity. To investigate its long-term thermal efficiency on preserving the underlying permafrost, a total time length of 25 years was used in models, in response to the given boundary conditions and material properties. The embankment thickness were set to be 2.0 m, 4.0 m and 6.0 m, considering the usual embankment thickness in most cases of northern regions.

The results of the quantification of heat extraction capacity through the interface in the mid-heat drain length for different embankment thicknesses and site conditions are shown in Figure 6.11. Each graph is valid for one specific ΔT, ranging from -14.3 °C to -12.5 °C. For a constant ΔT, the heat extraction capacity increases non-linearly with embankment thickness. For a selected embankment thickness, drain effectiveness increase with decreasing heat drain length. Longer heat drain tends to lose effectiveness due to heat accumulation in

the flat portion of the drain. For example, with a ΔT of -13.3 °C and the embankment thickness of 4.0 m, the corresponding heat extraction capacity are -2.42×10^6 J/m^2, -1.28×10^6 J/m^2, -1.73×10^5 J/m^2 for heat drain lengths of 3.0 m, 6.0 m and 9.0 m, respectively.

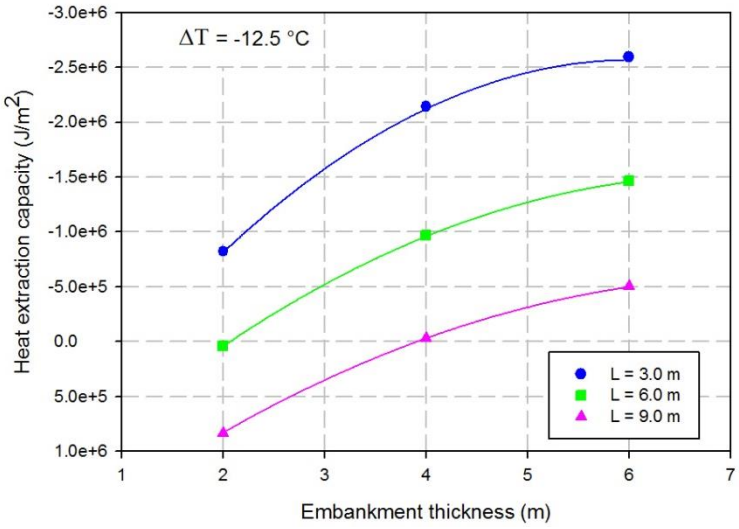

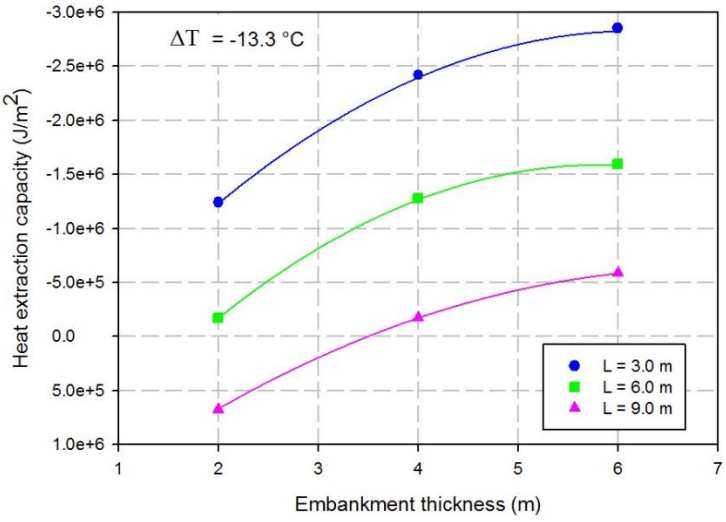

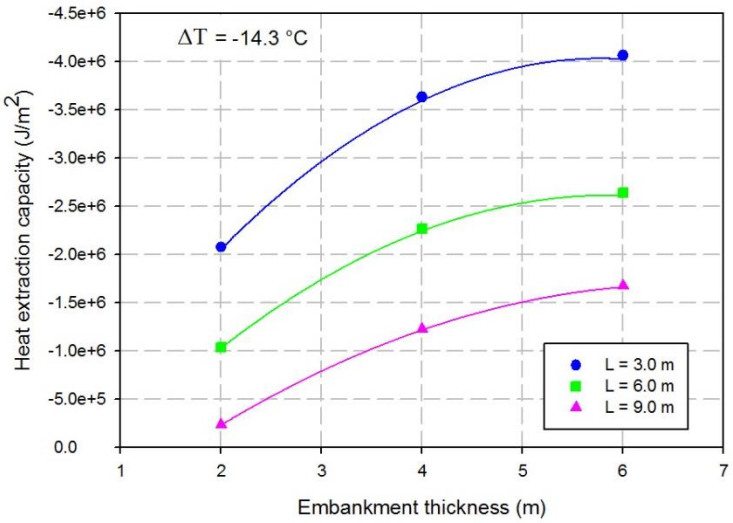

Figure 6. 11: Heat extraction capacity of heat drain at the embankment-soil interface as a function of the embankment thickness, heat drain length (L) and temperature difference (ΔT) between MAWAT and permafrost temperature.

The design charts were validated using data from Salluit, Northern Quebec, Canada. A 1000 m long section of the road connecting the northern communities of Salluit to the airport, is built on a thaw-sensitive clay deposit, and rapid degradation was observed (Périer et al., 2015). To limit the thawing of permafrost and to raise permafrost table, 933 m long heat drain was applied in the shoulder of the embankment in summer 2012 (Figure 6.12). The embankment thickness was 2.5 m and the length of the flat portion of the heat drain was about 3.0 m.

Figure 6. 12: The view of the roadway with heat drain installed in the shoulder at Salluit, Northern Quebec, Canada, providing the validation data.

The construction of embankments during summer is inducing heat into the ground, leading to warming and thawing the underlying permafrost; therefore re-establishing the thermal regime requires approximately three years (Lingnau, 1985). Thus, the measured data available from 2013 to 2015 were still in the period of re-establishing the thermal regime, but were close to the final thermal stabilization as the period suggested by

Lingnau (1985). The MAGT at the interface decreased faster than permafrost temperature due to the natural convection in the heat drain. The thermal gradient became more and more negative in the ground, meaning more heat is extracted than intake, before a new thermal regime was reached, which was required to calculate the heat balance (Equations (6.7) and (6.8)). Thus, the modeled long-term heat extraction capacity is larger than the measured one from 2013 to 2015 (Figure 6.13). The measured heat extraction capacity in 2015, close to the final thermal stabilization of foundation soil, is plotted into the developed design chart with the ΔT of -13.3 °C, as shown in Figure 6.14. The results indicate that the measured heat extraction capacity has a good agreement with the modeled heat extraction capacity for the embankment thickness of 2.5 m and heat drain length of 3.0 m.

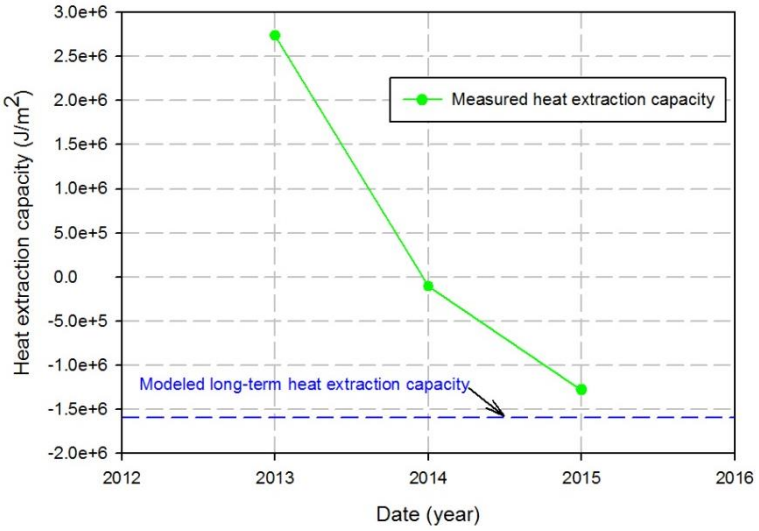

Figure 6. 13: Comparison of modeled long-term heat extraction capacity and measured three years' heat exaction capacity of heat drain, in the shoulder of the road embankment of Salluit.

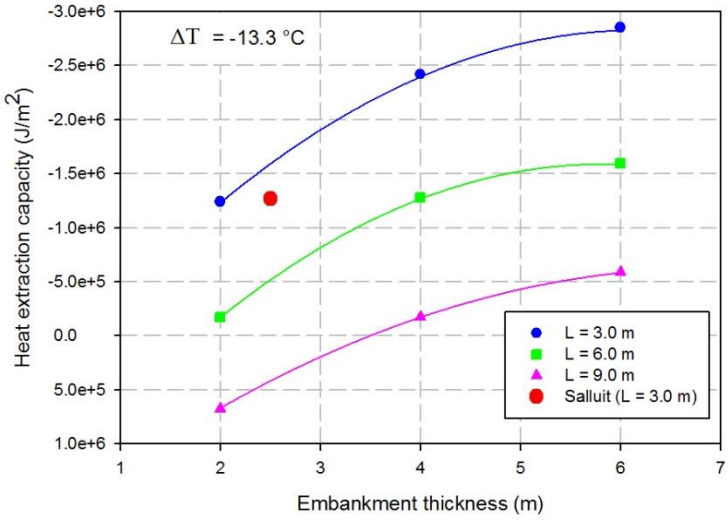

Figure 6. 14: Validation of heat extraction capacity using Salluit temperature data.

In addition to the validation using the measured thermal data, a model was also built to represent the road embankment before the construction of heat drain to determine the heat balance across the interface at Salluit road. The site-specific parameters, such as near-surface air temperature, embankment dimensions and ground temperatures, were measured and used as input parameters. Since the main interest of this paper is to propose engineering design charts for heat drain and the thermal modeling process for conventional embankments was largely documented (e.g., Alfaro et al., 2009; Darrow 2011), the detailed information on the model development at Salluit is not given. Based on the modeling results, the calculated heat balance is 1.17×10^6 J/m^2. The heat extraction capacity, obtained from Figure 6.11, is -1.59×10^6 J/m^2, and thus, the net heat balance is -0.42×10^6 J/m^2. This suggested that permafrost degradation did not happen after the construction of heat drain, which was confirmed by the decreasing temperature at the depth of 3.0 m below the interface, under the side slope from 2012 to 2015 (Figure 6.15). In summary, the design charts have been well validated using the measured data at Salluit and additional modeling results.

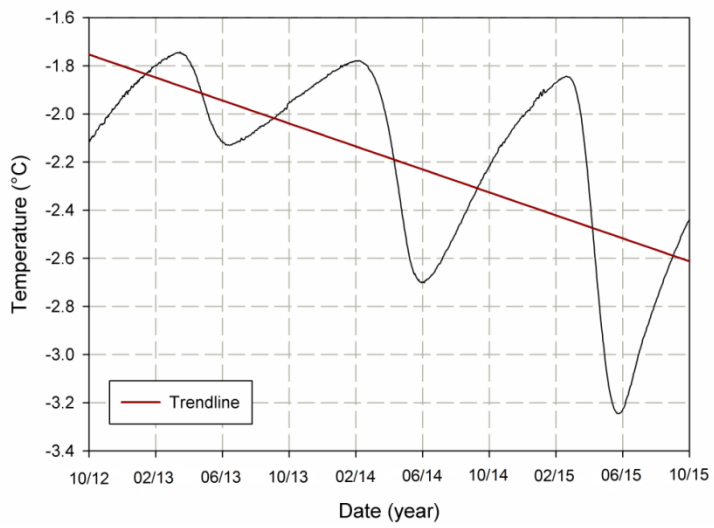

Figure 6. 15: Evolution of ground temperature at the depth of 3.0 m below the embankment-soil interface under the side slope of embankment at Salluit, Northern Quebec, Canada.

6.4 Conclusion

Heat drain is a new thermal stabilization method, which is lightweight and can be easily transported to field sites. It provides another solution to avoid or limit permafrost degradation underneath roadways and airstrips. In 2007, a full-scale experimental site was constructed at Tasiujaq airstrip. The measured data proved the thermal efficiency of heat drain to stabilize permafrost during the 4 years study period. The paper focused on the design of the heat drain to assure thermal effectiveness and particular emphasis was placed on the heat drain installed in the shoulder of roadways. A model was developed to reproduce the thermal regime of ground temperatures underneath the heat drain and it was calibrated using the measured data at Tasiujaq airstrip. The difference between the modeled temperature profiles and the measured temperature profiles with depth

may be caused by simplifications used in the model such as the simplified uniform foundation soils, unchanged simulated air temperature and the simplified n-factor on the side slope (Figure 6.10). However, the modeled average 3-years ground temperature matched the measured average 3-years record temperature at the embankment-soil interface closely with the temperature difference of 0.01 °C, supporting the reasonable accuracy of developed model. After a satisfying calibration of the model, numerical simulations were carried out to develop a set of engineering design charts, with different heat drain length, embankment thickness and the temperature difference (ΔT) between mean annual winter air temperature (MAWAT) and permafrost temperature. The numerical results indicated that the heat extraction capacity increased non-linearly with embankment thickness and decreased with heat drain length. The design charts have been successfully validated using data from Salluit. Additional validation was also provided using the comparison between modeled heat balance before the construction of heat drain at Salluit and the heat extraction capacity obtained from the design charts (Figure 6.11). A negative net heat balance was obtained, which was confirmed by the measured decreasing ground temperature underneath the heat drain at Salluit. These validations support the reliability of developed charts.

These charts allow designers to quickly determine the suitable design of heat drain to avoid the current or future permafrost degradation, by extracting at least the amount of extra heat flowing into the foundation for conventional embankments, if currently or estimated unstable. Heat balance charts, to determine the thermal conditions for conventional embankments, were developed and successfully validated in the previous research (Kong et al., 2019). Future research should focus on the thermal efficiency of heat drain across the whole embankment. In some cases, heat drain could be combined with other stabilization methods to extract more heat from thaw-sensitive permafrost underneath transportation infrastructure.

Acknowledgements

The authors would like to acknowledge the financial support of the Natural Sciences and Engineering Research Council of Canada, the 2013-2020 Climate Change Action Plan and Transports Québec, as well as the technical and financial support of public and private partners of the permafrost engineering research program ARQULUK for this project.

6.5 References

Alfaro, M. C., Ciro, G. A., Thiessen, K. J., Ng, T. (2009). Case study of degrading permafrost beneath a road embankment. Journal of cold regions engineering, 23(3), 93-111.

Allard, M., Doré, G., L'Hérault, E., Sarrazin, D., Verreault, J.(2009). Investigations géotechniques, caractérisation du pergélisol et stratégie d'adaptation pour les aéroports du MTQ au Nunavik. In: Rapport d'étape. Vol. 2. Centre d'études Nordiques, Université Laval, Quebec, Canada, pp. 1–83.

Allard, M., Fortier, R., Calmels, F., Savard, C., Guimond, A., Tarussov, A. (2007). L'évaluation de l'impact du réchauffement climatique sur la stabilité des pistes d'atterrissage au Nunavik: première étape vers une stratégie d'entretien. Congrès annuel de 2007 de L'Association des transports du Canada.

Andersland, O. B., Ladanyi, B. (2004). Frozen ground engineering. Hoboken, N.J: Wiley.

Beaulac, I., Dore, G. (2006). Development of a new heat extraction method to reduce permafrost degradation under roads and airfields. In: Proceedings of the 13th International Conference on Cold Regions Engineering, Orono, Maine, USA.

Berg, R. L., Aitken, G. W. (1973). Some passive methods of controlling geocryological conditions in roadway construction. Permafrost: The North American Contributions to the Second International Conference. National Academy of Sciences, Washington, DC, pp. 581–586.

Calmels, F., Doré, G., Kong., X, Roy, LP., Lemieux, C., Horton, B. (2016). Vulnerability of the north Alaska Highway to permafrost thaw: Design options and climate change adaptation. Whitehorse: Northern Climate Exchange, Yukon Research Centre, Yukon College, pp. 132.

Chataigner, Y., Gosselin, L., Doré, G. (2009). Optimization of embedded inclined open-ended channel in natural convection used as heat drain. International Journal of Thermal Sciences, 48(6), 1151-1160.

Darrow, M. M. (2011). Thermal modeling of roadway embankments over permafrost. Cold Regions Science and Technology, 65(3), 474-487.

Doré, G., Pierre, P., Juneau, S., Lemelin, J. (2007). Expérimentation de méthodes de mitigation des effets de la fonte du pergélisol sur les infrastructures du Nunavik: aéroport de Tasiujaq, Rapport d'étape 1– Compte rendu des travaux d'instrumentation et de supervision de construction des planches expérimentales de l'aéroport de Tasiujaq, description des planches construites et de l'instrumentation installée. GRINCH, Université Laval, Canada.

Doré, G., Ficheur, A., Guimond, A., Boucher, M. (2012). Performance and cost-effectiveness of thermal stabilization techniques used at the Tasiujaq airstrip. Cold Regions Engineering 2012: Sustainable Infrastructure Development in a Changing Cold Environment , pp. 32-41.

Doré, G., Niu, F., Brooks, H. (2016). Adaptation methods for transportation infrastructure built on degrading permafrost. Permafrost and Periglacial Processes, 27(4), 352-364.

Doré, G., Pierre, P., Juneau, S., Lemelin, J. (2007). Expérimentation de méthodes de mitigation des effets de la fonte du pergélisol sur les infrastructures du Nunavik: aéroport de Tasiujaq, Rapport d'étape 1– Compte rendu des travaux d'instrumentation et de supervision de construction des planches expérimentales de l'aéroport de Tasiujaq, description des planches construites et de l'instrumentation installée. GRINCH. Département en génie civil, Université Laval, Québec, Canada, pp. 28.

Doré, G., Zubeck, H. K. (2009). Cold regions pavement engineering. McGraw-Hill, New York.

Dumais, S., Doré, G. (2016). An albedo based model for the calculation of pavement surface temperatures in permafrost regions. Cold Regions Science and Technology, 123, 44-52.

Esch, D. (1983). Design and performance of road and railway embankments on permafrost. In: Proceedings of the the 4th International Conference on Permafrost, Fairbanks, Alaska, pp. 23-30.

Goering, D. J., Kumar, P. (1996). Winter-time convection in open-graded embankments. Cold Regions Science and Technology, 24(1), 57-74.

Goering, D. J. (1998). Experimental investigation of air convection embankments for permafrost-resistant roadway design. In: Proceedings of the 7th International Conference on Permafrost, Yellowknife, Canada, pp. 319-326.

Goering, D. J., Kumar, P. (1999). Permeability effects on winter-time natural convection in gravel embankments Advances in cold-region thermal engineering and sciences. In: Proceedings of the 6th International Symposium Held, Darmstadt, Germany, pp. 455-464.

Hayley, DW., Roggensack, WD., Jubien, WE., Johnson, PV. (1983). Stabilization of sinkholes on the hudson bay railroad. In: Proceedings of the 4th International Conference on Permafrost, Fairbanks, Alaska, pp. 468 – 473.

Jørgensen, A. S., Doré, G., Voyer, É., Chataigner, Y., Gosselin, L. (2008). Assessment of the effectiveness of two heat removal techniques for permafrost protection. Cold Regions Science and Technology, 53(2), 179-192.

Kersten, M.S. (1949). Laboratory research for the determination of the thermal properties of soils. Research Laboratory Investigations, Engineering Experiment Station, University of Minnesota, Minneapolis. Technical Report 23.

Kong, X., Doré, G., Calmels, F. (2019). Thermal modeling of heat balance through embankments in permafrost regions. Cold Regions Science and Technology, 158, 117-127.

Lanouette F., Doré G., Fortier D., and Lemieux C. (2015). Influence of snow cover on the ground thermal regime along an embankment built on permafrost: In-situ measurements. In: Proceedings of the 68th Canadian Geotechnical Conference and 7th Canadian Permafrost Conference, Quebec City, Canada.

Lingnau, B. (1985). Observation of the design and performance of the Dempster Highway. Master's thesis University of Alberta, Canada.

M-Lepage, J., Doré, G., Fortier, D., Murchison, P. (2012). Thermal performance of the permafrost protection techniques at Beaver Creek experimental road site, Yukon, Canada. In: Proceedings of the 10th International Conference on Permafrost, Salekhard, Russia, pp. 261

M-Lepage, J. (2015). Experimentation of mitigation techniques to reduce the effects of permafrost degradation on transportation infrastructures at Beaver Creek experimental road site (Alaska Highway, Yukon). Mater's thesis, Laval University, Canada

Périer, L., Lemieux, C., Lamontagne, V., Roger, J., Doré, G., Allard, M. (2015) Suivi du comportement thermique et mécanique de la route d'accès de Salluit et expérimentation d'une méthode de détection de la dégradation du pergélisol le long des structures linéaires. Rapport GCT-2015, Ministère des transports du Québec.

Zarling, J. P., Braley, W. A. (1986). Thaw stabilization of roadway embankments constructed over permafrost: Alaska Department of Transportation and Public Facilities, Research Section.

Zarling, J. P., Connor, B., Goering, D. J. (1984). Air duct systems for roadway stabilization over permafrost areas. Technical report. U.S. Department of Transportation Federal Highway Administration.

Zarling, J.P., Braley, W.A., Esch, D.C. (1988). Thaw stabilization of roadway embankments, In: Proceedings of the 5th International Conference on Permafrost, Trondheim, Norway, pp. 1352 – 1357.

Chapter 7 Thermal stabilization of embankments built on thaw sensitive permafrost

Foreword

Xiangbing Kong, Guy Doré

Department of Civil and Water Engineering, Laval University, Québec City, Québec, Canada

State: Submitted to review

Date of Submission: 29 May 2019

Journal: Journal of Cold Regions Engineering

Résumé

En raison des changements climatiques et des techniques de conception peu adaptées aux conditions du pergélisol, la dégradation thermique du pergélisol sous les infrastructures de transport mènent à l'instabilité de l'infrastructure et à l'augmentation des couts d'entretien. Des méthodes de stabilisation ont été développées pour limiter les effets de la dégradation du pergélisol; toutefois, peu d'information sur les procédures de conception est disponible. L'objectif de cet article est de proposer une nouvelle approche de stabilisation des remblais construits sur pergélisol sensible au dégel et de présenter des abaques développés grâce à des simulations numériques. Les modèles thermiques ont été développés à partir de sites expérimentaux spécifiques et sont bien calibrés aux données de températures mesurées. Les abaques ont été validés en utilisant les données additionnelles du Yukon et du Nunavik (Canada) pour améliorer leur robustesse et leur fiabilité. Les abaques de conception ont été développés pour les techniques de mitigation prometteuses, incluant la pente douce, les surfaces à albédo élevé, le remblai à convection d'air (ACE) et le drain thermique.

Mots clés: Infrastructure de transport; Dégradation du pergélisol; Méthodes de stabilisation; Outils de conception

Abstract

As a result of climate change and design techniques poorly adapted to permafrost conditions, thermal degradation of permafrost underneath transportation infrastructure is leading to infrastructure instability and the increase of maintenance cost. Stabilization methods have been developed to counter the effects of

permafrost degradation; however, little information on the design procedures is available. The objective of this paper is to propose a new approach for thermal stabilization of embankments built on that sensitive permafrost and to present design charts developed using numerical simulations. Thermal models have been built based on specific field sites and they are well calibrated to the measured temperature data. The charts have been validated using the additional data in Yukon and Nunavik, Canada to improve their robustness and their reliability. Design charts have been developed for promising mitigation techniques, including gentle slope, high albedo surface, air convection embankment (ACE) and heat drain.
Keywords: Transportation infrastructure, Permafrost degradation, Stabilization methods, Design tools

7.1 Introduction

Transportation infrastructure plays a vital role in the social and economic developments in northern regions. The construction of infrastructure embankments modifies the pre-existing surface conditions by compressing or removing the organic layer, and by changing snow and water accumulation patterns, resulting in a warmer ground surface. The problem is exacerbated by global warming and increased precipitations resulting from global climate changes. Signs of road and runway degradation are becoming increasingly evident in Northern Canada, and maintaining stable and safe transportation infrastructure is an important engineering challenge. Long-term stability of an embankment built on thaw-sensitive permafrost relies heavily on favorable ground thermal conditions and the prevailing consideration for embankment and structural design is to maintain a stable thermal state of permafrost (Doré and Zubeck, 2009). Thermal stabilization methods, such as high albedo surface, gentle slope and heat drain, have been developed to preserve permafrost. All these methods need to be carefully designed to ensure long-term thermal and mechanical stability of embankments; however, limited information on the thermal design of those techniques is available. The objective of this paper is to describe the development of two rational design methods and to present several easy-to-use design charts to assist the designers for thermal stabilization of embankments built on thaw-sensitive permafrost.

7.2 Methodology

The first thermal stabilization method proposed is based on the quantification of the thermal gradient between mean annual ground temperature (MAGT) at the embankment-soil interface and permafrost temperature (Batenipour et al., 2010). A positive thermal gradient generally indicates a net heat flow into the foundation and, as a result, leads to an unstable warming permafrost. As illustrated in Figure 7.1, the proposed approach, referred to as the “interface temperature correction (ITC)” method, is to achieve the required thermal shift to obtain a zero temperature gradient in the ground by decreasing the soil temperature at the interface using stabilization methods. The minimum required ITC is defined as:

$$\mathrm{ITC} = \mathrm{T}_{\mathrm{interface}} - \mathrm{T}_{\mathrm{permafrost}} + \mathrm{SM} \tag{7.1}$$

where $T_{interface}$ is the mean annual ground temperature (MAGT) at the soil-embankment interface; $T_{permafrost}$ is the permafrost temperature at the zero temperature variation depth and SM is a safety margin to account for global warming during the design life of the structure. All the parameters are in °C. This approach can be used to modify the relevant design parameters, such as surface albedo and embankment slope (V:H), based on empirical relationships, to stabilize permafrost.

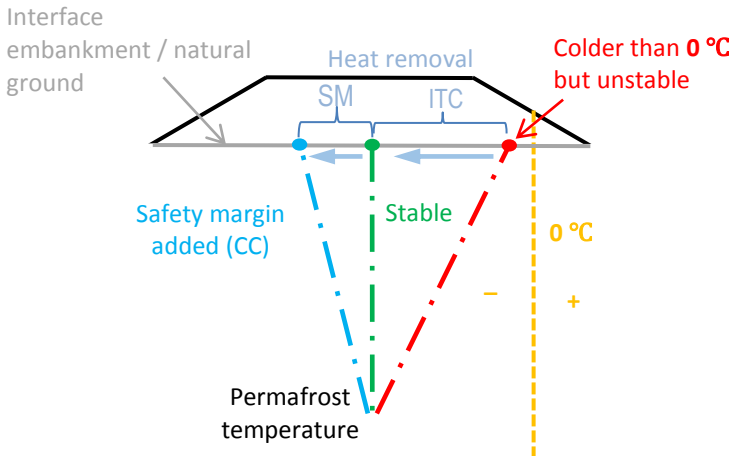

Figure 7. 1: Principle of thermal stabilization.

The second thermal stabilization method proposed is based on the calculation of the heat balance at the interface between the embankment and natural ground. Heat balance is the summation of heat induction index and heat extraction index, which are expressed as (M-Lepage et al., 2012):

$$H_x = k_{frozen} \times -\frac{\partial T}{\Delta z} \times \Delta t \tag{7.2}$$

$$H_i = k_{unfrozen} \times \frac{\partial T}{\Delta z} \times \Delta t \tag{7.3}$$

where H_x, H_i are the heat extraction index and heat induction index, respectively. $k_{unfrozen}$, k_{frozen} are the thermal conductivity at the unfrozen and thawing states in the surface ground layer. $\partial T / \partial z$ is the thermal gradient between MAGT at the interface and permafrost temperature. A positive heat balance indicates that more heat is induced in the soil than heat is extracted. The thermal state of soil is therefore unstable leading to permafrost degradation. This approach is proposed to help determine the thermal state of conventional embankments and to help select suitable mitigation techniques to extract a sufficient amount of heat to assure permafrost stability during the design life of the embankment.

7.3 Development of analysis and design charts for embankment built on thaw sensitive permafrost

The thermal finite element analysis softwares TEMP/W from the GeoStudio geotechnical suite and SVHeat from the Soil Vision suite have been used for the 2D simulation of embankments with high albedo surface and with gentle slopes. The Finite element software SVHeat for thermal conduction coupled with SVAirflow for density-driven air convection from the SoilVision software suite, have been used to investigate the heat balance across the interface for an unprotected embankment as well as for embankments protected using ACE and heat drains. For each modeling case, thermal data from several instrumented field sites were used for model calibration and validation.

7.3.1 Design of gentle slopes using the ITC approach

Snow accumulation on the embankment slope prevents heat to be extracted from the ground in winter. Standard embankments, typically designed with slopes of 2H:1V, tend to cause turbulence on the down-wind side of the embankment causing snow accumulation against the embankment slope. Previous research work (Lanouette et al., 2015; Doré et al., 2012) and experience have shown that the modification of the slope can help reduce snow accumulation for embankments built across dominant wind direction and, as a result, can mitigate permafrost degradation underneath the embankment shoulder. Work done by Doré et al. (2012) based on the monitoring of a test sections with the gentle slope (8H:1V) in Tasiujaq, Nunavik clearly demonstrated the effectiveness of a gentle slope to reduce snow accumulation and to create stable thermal conditions underneath an embankment slope in permafrost conditions (Figure 7.2). Lanouette et al. (2015) instrumented and monitored another test section at the Tasiujaq airstrip and developed a framework for the design of embankment slope for permafrost protection.

Figure 7. 2: Experimental gentle slope built on the Tasiujaq airstrip in Nunavik, Quebec.

Based on the work done by these authors, a thermal model has been developed using SV-Heat and validated based on the data collected on the two test sections. The modeled maximum, minimum, average temperatures profiles with depth are in good agreement with the measured maximum, minimum, average temperatures profiles with depth, confirming a reasonable accuracy for the 2D models developed (Figure 7.3).

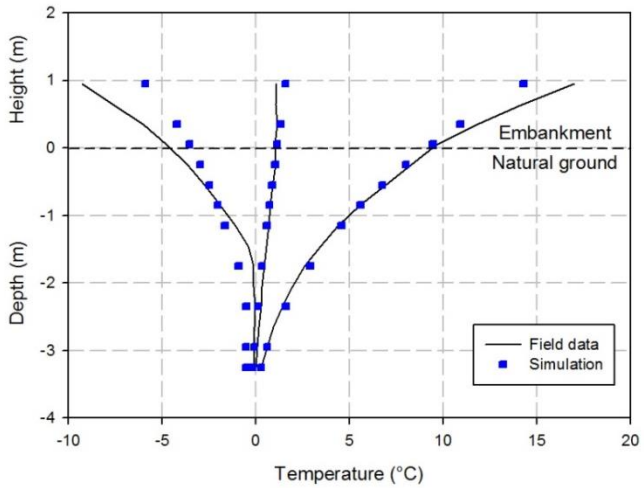

Figure 7. 3: Calibration of a 2D thermal model using thermal data collected at the Tasiujaq test site.

The model was used afterward to quantify the effect of several geometric and climatic factors. Figure 7.4 illustrates the recommended slope embankment as a function of the required interface temperature correction (ITC) at the mid-length of the side slope. Numerical results indicate that for embankment thicknesses lower than 3,5 m, ITC is not affected significantly by the embankment thickness and the chart developed (Figure 7.4) has been well validated using the thermal data at the nearby field embankment as well. From Figure 7.4, it can be seen that the recommended slope (V:H) decreases non-linearly with required ITC with the maximum ITC of 4.4 °C obtained for the slope (6H:1V). The effect of decreasing the slope down to 4:1 is moderate while strong interface temperature corrections can be achieved using slopes more gentle than 4:1.

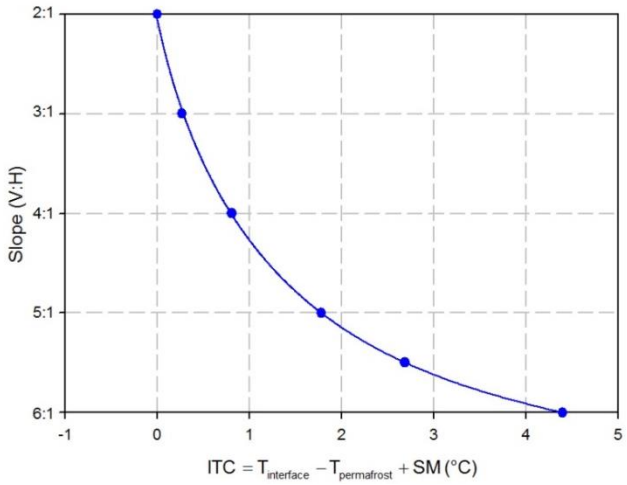

Figure 7. 4: Design chart for the selection of embankment slope for thermal stabilization under the center of the slope using the ITC method.

The thermal model was also used to estimate the required safety margin (SM) required as a function of expected change in the mean annual air temperature (MAAT) during the design life of the embankment according to the global warming model and reliability level selected by the designer. As shown in Figure 7.5, SM increases linearly with the increase in MAAT for the standard embankment.

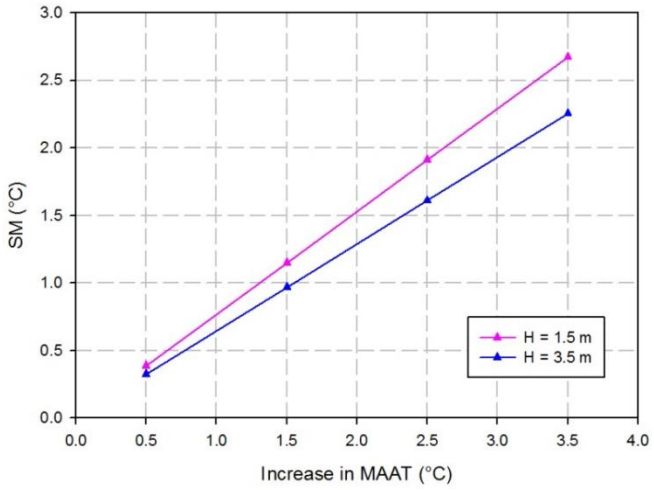

Figure 7. 5: SM (safety margin) as a function of the increase in mean annual air temperature (MAAT).

7.3.2 Design of high albedo surfaces based on the ITC approach

Albedo is a property of the surface of an object defined as the ratio between the reflected and the incident solar radiation. This property can thus be used to reduce heat absorption by an embankment surface and therefore promote thermal stability of the embankment. The use of high-albedo surfacing materials has been studied by several researchers (CRREL, Alaska DoT, Technical University of Denmark, Laval University, etc.) and all these studies have concluded that the technique has a very high potential to contribute to the thermal stability of embankments, more specifically in the case of paved surfaces. Despite the evidence of good thermal performance, only one full-scale project has been treated using a high albedo surfacing material: the Thule air base airstrip. The slipperiness of painted surfaces and the maintenance required to maintain the integrity of the protective surface have impeded a wider use of high albedo surfacing materials for permafrost protection. New asphalt-based or resin –based products well adapted for road applications have recently become available and open new perspectives for albedo treatment to promote thermal stability of embankments built on permafrost. As part of the Arquluk permafrost engineering research program, two projects (Dumais and Doré 2016; Richard 2018) involving the development of simplified surface energy balance models as well as the monitoring of thermal and mechanical performance of three different high-albedo surfacing materials at four different test sites have allowed to develop design tools and guidelines for the use of these materials (Figure 7.6).

Figure 7. 6: High albedo surface with the cool gray colour on bituminous surface treatment (BST) on a test site on the Alaska highway in Yukon.

A numerical thermal model has been developed using the surface energy balance as main input of the model. The maximum, minimum, average temperatures profiles with depth predicted with the model are in good agreement with the observations made at the Beaver Creek test site (Yukon, Canada) (Figure 7.7). The model has afterward been validated using temperature data and albedo measurements from other test sites, confirming a reasonable accuracy for the 2D model developed. Figure 7.8 illustrates the recommended surface albedo as a function of the required ITC for different embankment thicknesses (Richard 2018). As shown in Figure 7.8, the required albedo increases linearly with ITC for all embankment thicknesses.

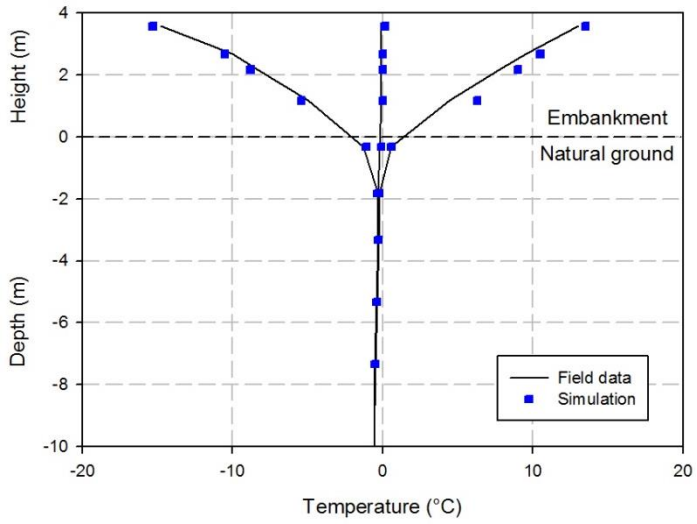

Figure 7. 7: Comparison between the field data and numerical simulation for maximum, minimum and average temperature profiles with depth for high albedo surfaces.

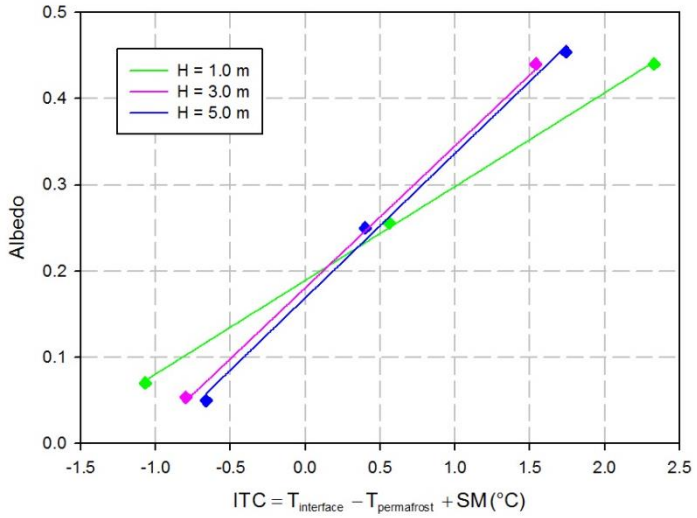

Figure 7. 8: Albedo required to stabilize permafrost as a function of embankment thickness (H) and required ITC (Richard 2018).

The relationships between SM (safety margin) and the increase in mean annual air temperature (MAAT) in 30 years for the albedo surface is shown in Figure 7.9. SM increases linearly with the increase in MAAT and the change of embankment thickness has a larger effect on SM for the high albedo surface, compared to that for the low albedo surface (Figure 7.9). For example, for the increase of MAAT of 3.5 °C, SM between embankment thickness 1.0 m and 5.0 m, is 1.14 °C for the albedo 0.45, however, it is 0.78 °C for the albedo 0.05. For the selected albedo, SM is always larger for thin embankment than that for thick embankments.

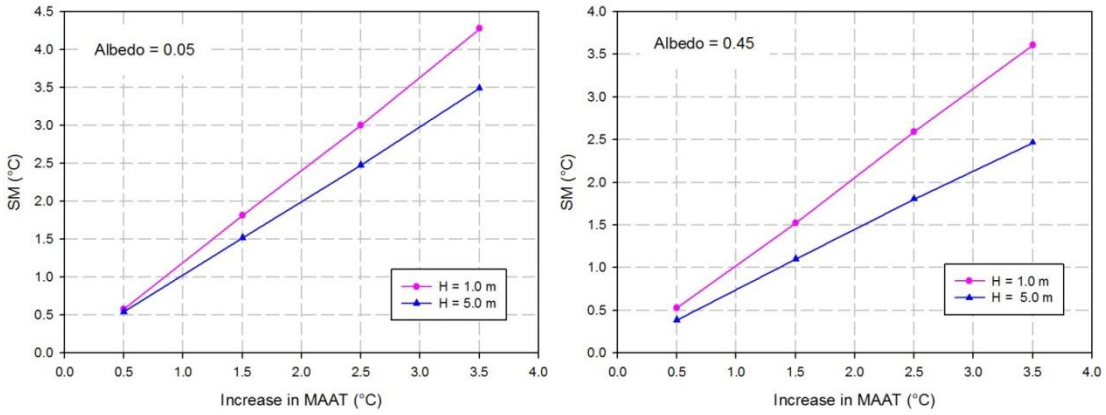

Figure 7. 9: SM (safety margin) as a function of the increase in mean annual air temperature (MAAT) and embankment thickness (H) for the albedo surface.

7.3.3 Thermal stabilization using an air convection embankment (ACE)

During winter, heat extraction can be strongly increased by the density-driven natural convection in air convection embankment (ACE). Two different configurations of ACEs, namely full-width ACE and ACE applied on side slopes (Figure 7.10), were constructed at the Beaver Creek experimental site, Yukon in 2008. The site-

specific parameters, such as soil properties, near-surface air temperature and embankment dimension, have been measured at Beaver Creek and used as input parameters to improve the model accuracy.

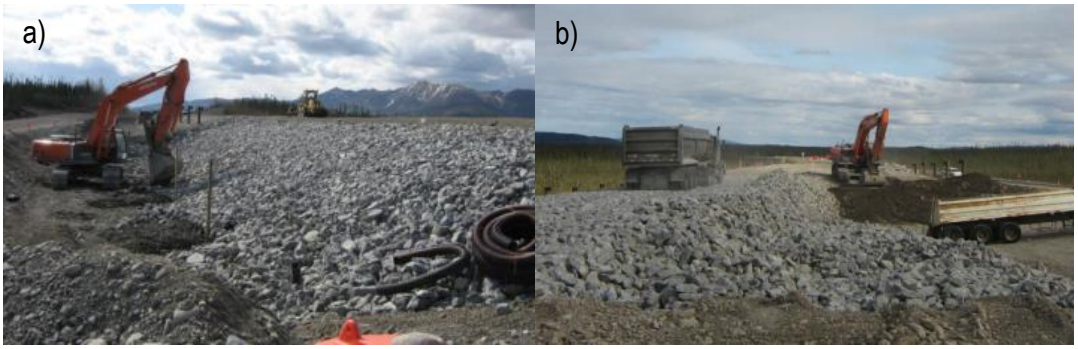

Figure 7. 10: ACEs at the Beaver Creek experimental site: a) ACE on side slopes uncovered; b) Full-width ACE during construction.

Two models have been developed for the two types of ACE application. The two models have proved to reproduce satisfactorily the ground thermal regime with depth (Figure 7.11).

Convective heat transfer in ACE occurs in winter and Rayleigh number is used to assess the strength of winter air convection. Rayleigh number increase with embankment thickness and the temperature difference between the top and bottom of an ACE layer (Goering, 2002). In the foundation beneath ACE, heat conduction is the main heat transfer mode, if the convective water flow is not considered and the amount of heat transfer by thermal conduction in winter is mainly controlled by the temperature difference (ΔT) between mean annual winter air temperature (MAWAT) and permafrost temperature. Thus, two key parameters, including embankment thickness and the temperature difference (ΔT) between MAWAT and permafrost temperature, have been selected to investigate the heat extraction capacity of the ACE layer in winter. Figure 7.12a and Figure 7.12b illustrate the relationships between heat extraction capacity of the ACE layer through the soil-embankment interface, embankment thickness and temperature difference (ΔT) between MAWAT and permafrost temperature. The heat extraction capacity is estimated under the centerline for the full-width ACE and under the center of the side slope for the slope application. As shown in Figure 7.12a and Figure 7.12b, the heat extraction capacity increases non-linearly with embankment thickness for both types of ACE applications. ΔT has a larger effect on heat extraction capacity for full-width ACE than that for ACE applied on side slopes. For example, for an embankment thickness of 3.0 m, the heat extraction with a ΔT of -16.1 °C is 185.3% larger than that with a ΔT of -14.8 °C for full-width ACE, while it is 61.2% larger with ΔT decreasing from -14.6 °C to -16.1 °C for ACE on side slopes.

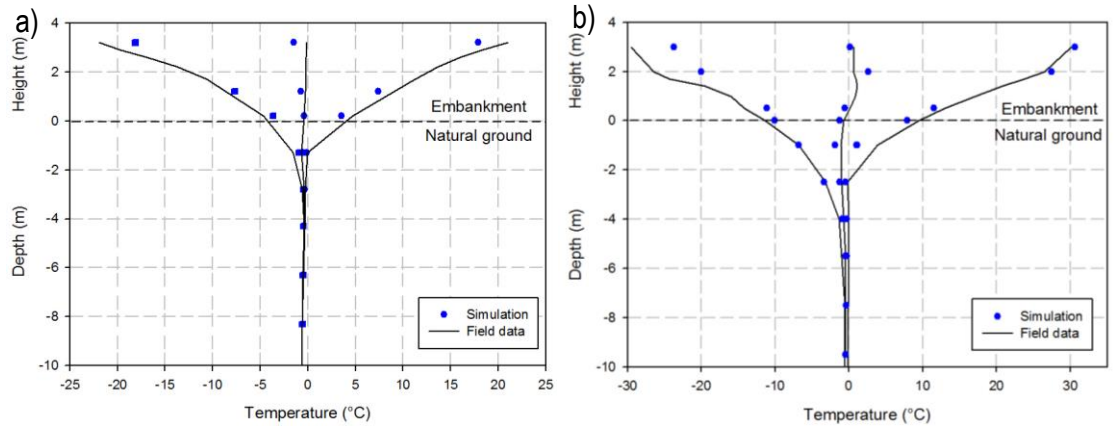

Figure 7. 11: Comparison of maximum, minimum and average temperature profiles with depth between the field data and numerical simulation for: a) Full-width ACE under the centerline; b) ACE on side slopes uncovered under the side slope.

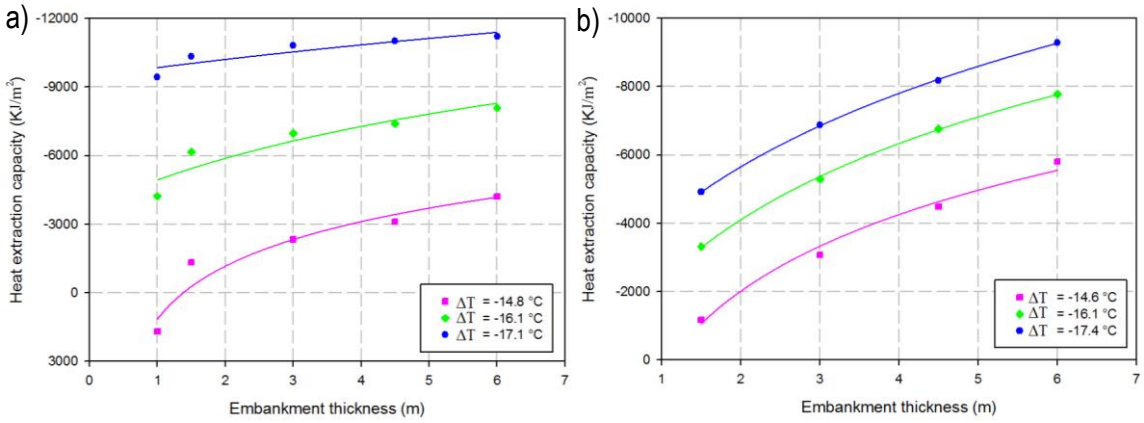

Figure 7. 12: Heat extraction capacity at the embankment-soil interface as a function of embankment thickness and temperature difference (ΔT) between MAWAT and permafrost temperature for: a) Full-width ACE under the centerline; b) ACE on side slopes under the center of the slope.

7.3.4 Heat drain

Heat drain is an innovative technique developed at Laval University in the early 2000s. It uses a 25 mm-thick drainage geocomposite with high permeability to induce convection in the embankment shoulder (Figure 7.13a). The geocomposite is made of the corrugated plastic core covered on both sides by geotextile (Figure 7.13b). Natural convection is generated by density instability in heat drain, to promote the heat extraction in winter. A slope of 2% in the "flat" section and a 45^0 slope have been optimized to allow air movement inside heat drain and to maintain reasonable construction conditions (Doré et al., 2016).

To investigate the thermal effectiveness, heat drain was installed in the shoulder of Tasiujaq airstrip, Nunavik in 2007 (Figure 7.13c), and thermistors were installed in the side slope to monitor the thermal performance of the system. The model developed reproduced satisfactorily the measured temperature profiles with depth underneath heat drain (Figure 7.14). As for the ACE, the heat extraction capacity of heat drain is controlled by embankment thickness and the temperature difference (ΔT) between MAWAT and permafrost temperature. In

addition to these two parameters, air flow in heat drain is much affected by the heat drain length (the flat section) (Chataigner et al., 2009).

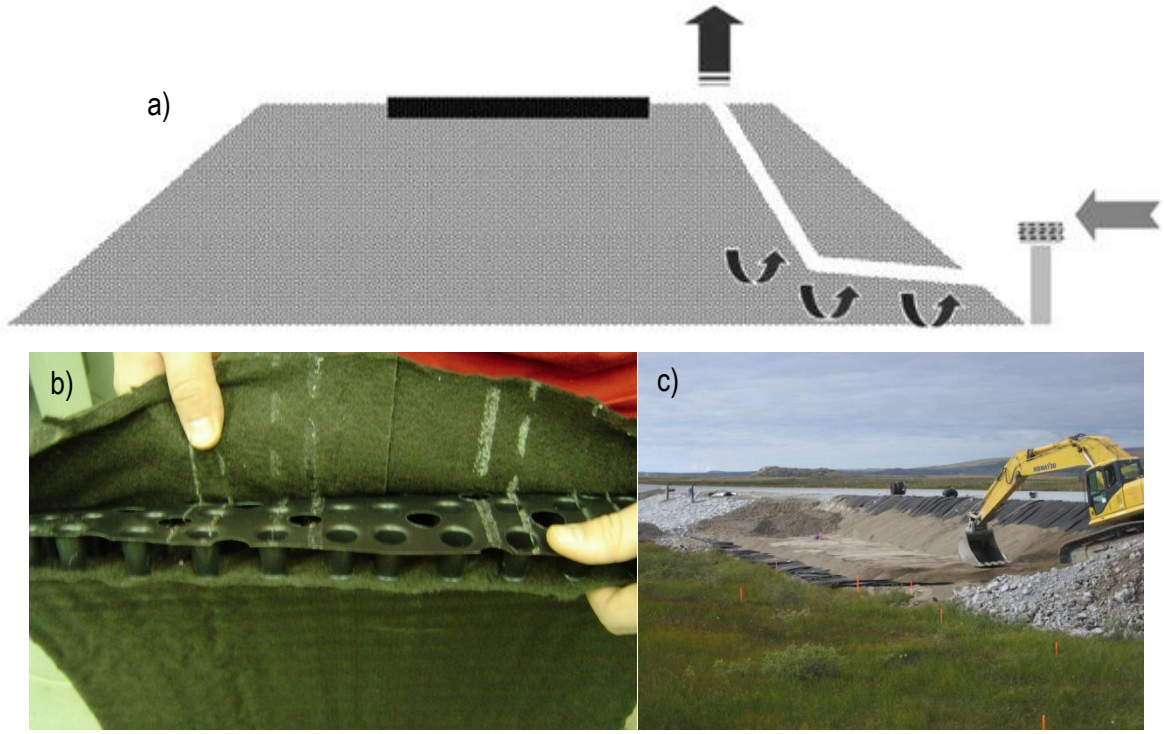

Figure 7. 13: Heat drain: a) placed in the shoulder of an embankment (Beaulac, 2006); b) the geocomposite used to drain heat; c) under construction in the shoulder of the Tasiujaq airstrip, Northern Quebec, Canada.

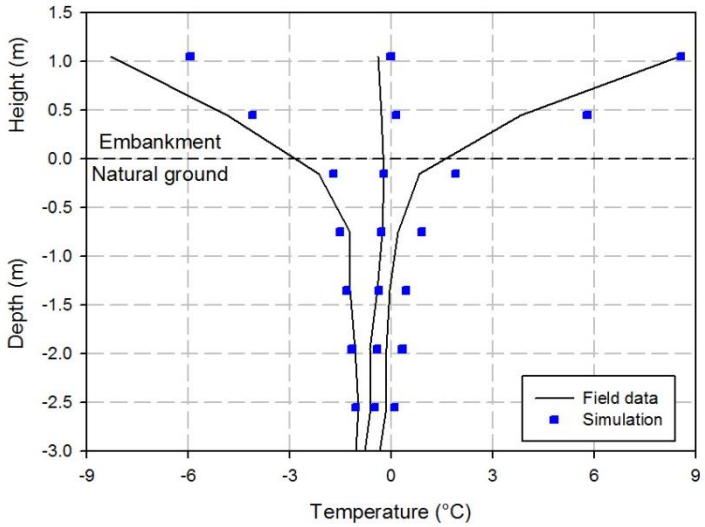

Figure 7. 14: Comparison of maximum, minimum and average temperature profiles with depth between the field data and numerical simulation under the side slope.

Figure 7.15 illustrates the relationships between heat extraction capacity through the soil-embankment interface, embankment thickness and the temperature difference (ΔT) between MAWAT and permafrost

temperature for different lengths of the flat portion of the drain. The figure shows that the heat extraction capacity increases non-linearly with embankment thickness, and the length of the flat portion of the heat drain tends to reduce the cooling capacity per unit area. For example, with an embankment thickness of 5.0 m and a ΔT of -12.5 °C, the corresponding heat extraction capacities, are -374.7 KJ/m^2, -1523.9 KJ/m^2 and -2942.8 KJ/m^2 for heat drain length 9.0 m, 6.0 m, and 3.0 m, respectively.

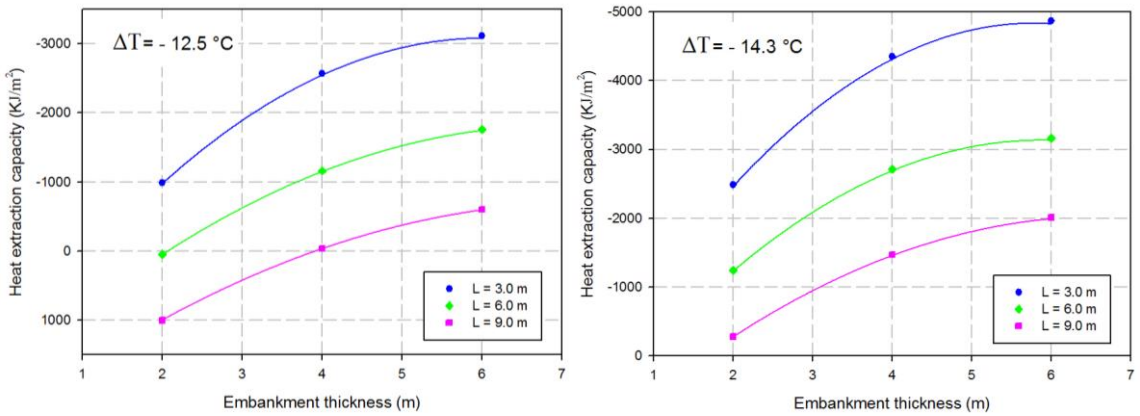

Figure 7. 15: Heat extraction capacity of the heat drain at the embankment-soil interface as a function of embankment thickness, length of the flat portion of the heat drain (L) and temperature difference (ΔT) between MAWAT and permafrost temperature.

7.4 Practical engineering application

The design charts proposed in (Figure 7.4 and Figure 7.8) and using the interface temperature correction (ITC) approach, can assist the designer in determining the surface albedo and the slope (V:H) required to stabilize permafrost, based on the embankment thickness and field conditions. The heat balance analysis charts for unprotected embankment proposed in Kong et al. 2019 (Figure 7.16a) combined with the heat extraction capacity charts for ACE and heat drain, provide a sound basis for thermal stabilization of embankments built on thaw sensitive permafrost. For example, a 1.5m thick embankment with a 0.27 °C/m thermal gradient in the permafrost conditions where the temperature difference (ΔT) between MAWAT and permafrost temperature is -14.6 °C with global warming anticipated during the design life of the structure, would require at least a 3.7 m thick ACE layer to extract the 4000 KJ/m^2 excess heat affecting the embankment (Figure 7.16b).

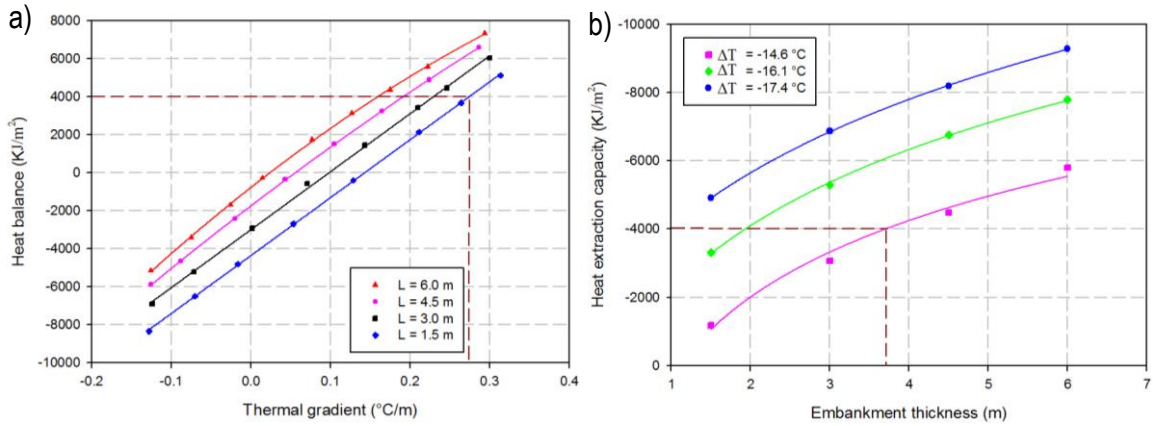

Figure 7. 16: Example of thermal analysis of embankment stability under the side slope: a) heat balance assessment chart for conventional embankments; b) heat extraction capacity chart for ACE on side slopes.

The application of the method requires information on air temperature, generally available from local weather stations. Other key parameters, including permafrost temperature and MAGT at the interface, are also required to use the charts. The information can be obtained by: 1) using measured data observed at the site or estimated from data observed at a nearby field site or, 2) using numerical thermal simulation based on available site information. The effect of global warming is integrated into the design procedure by changing the controlling parameters of charts, such as thermal gradient in the ground, the temperature difference between MAGT at interface and permafrost temperature, and the temperature difference between MAWAT and permafrost temperature, considering the climate change scenario selected by the designer.

The proposed design methods were built using sound physical heat transfer principles, but were prepared in a format to facilitate application in practical engineering. The calibration of the thermal analysis models used for the development was done using reliable thermal data collected at several test sites in Northern Canada and the design charts were all satisfactorily validated on test sites other than the one used for their development. The design methods are considered to be reliable but have some limitations:

- Due to the scarcity of instrumented test sites in permafrost environments, calibration and validation of the models are based on a limited number of observations. The models and the design tools develop therefore need to be further validated to improve their robustness.
- The design methods for convective thermal stabilisation techniques are valid for ACE and Heat drain materials used in the development of the method. The heat extraction capacity of stabilisation techniques using other types of materials may differ significantly from the estimations published in this paper.
- The effect of advective heat from lateral ground-water movements and wind is not considered in the proposed analysis. In cases where significant heat transfer is expected from these

mechanisms, the design should include an additional safety margin. There is however currently no way to estimate the required SM to fully compensate these effects.

7.5 Conclusion

Permafrost degradation affects transportation stability and increases maintenance cost. In this research, two new approaches, namely the interface temperature correction (ITC) approach and the heat balance approach, have been proposed to help design thermal stabilization methods. Several design charts have been developed for different site conditions and for different mitigation techniques using numerical simulations. Thermal data measured at field sites provide valuable information on the thermal effectiveness of the mitigation techniques, and allow for model calibrations and validations. Research done as part of the Arquluk research program has allowed developing tools, methods, and guidelines for thermal analysis and thermal stabilization of embankments built on thaw sensitive permafrost in the context of climate change. These research products will help improve our current capacity to adapt to climate changes and contribute to social and economic sustainability in northern regions.

Acknowledgements

The authors would like to acknowledge the financial support of the Natural Sciences and Engineering Research Council of Canada, the 2013-2020 Climate Change Action Plan and Transports Québec, as well as the technical and financial support of public and private partners of the permafrost engineering research program ARQULUK for this project.

7.6 References

Batenipour, H., Kurz, D., Alfaro, M., Graham, J., Kalynuk, K. (2010). Results from an instrumented highway embankment on degraded permafrost. Paper presented at the Proceedings 63rd Canadian Geotechnical Conference and 6th Canadian Permafrost Conference, Calgary AB, Canada.

Beaulac, I. (2006). Impacts de la fonte du pergélisol et adaptations des infrastructures de transport routier et aérien au Nunavik, Master's thesis, Laval University, Canada.

Chataigner, Y., Gosselin, L., Doré, G. (2009). Optimization of embedded inclined open-ended channel in natural convection used as heat drain. International Journal of Thermal Sciences, 48(6), 1151-1160.

Doré, G., Ficheur, A., Guimond, A., Boucher, M. (2012). Performance and cost-effectiveness of thermal stabilization techniques used at the Tasiujaq airstrip Cold Regions Engineering 2012: Sustainable Infrastructure Development in a Changing Cold Environment, pp. 32-41.

Doré, G., Niu, F., Brooks, H. (2016). Adaptation methods for transportation infrastructure built on degrading permafrost. Permafrost and Periglacial Processes, 27(4), 352-364.

Doré, G., Zubeck, H.K. (2009). Cold regions pavement engineering. McGraw-Hill, New York.

Dumais, S., Doré, G. (2016). An albedo based model for the calculation of pavement surface temperatures in permafrost regions. Cold Regions Science and Technology, 123, 44-52.

Goering, D.J. (2002). Convective cooling in open rock embankments. In: Proceedings of the 11th International Conference on Cold Regions Engineering, Anchorage, Alaska, USA, pp. 629–644

Kong, X., Doré, G., Calmels, F. (2018). Thermal modeling of heat balance through embankments in permafrost regions. Cold Regions Science and Technology, 158, 117-127.

Lanouette F., Doré G., Fortier D., and Lemieux C. (2015). Influence of snow cover on the ground thermal regime along an embankment built on permafrost: In-situ measurements. In: Proceedings of the 68th Canadian Geotechnical Conference and 7th Canadian Permafrost Conference, Quebec City, Canada.

M-Lepage, J., Doré, G., Fortier, D., Murchison, P. (2012). Thermal performance of the permafrost protection techniques at Beaver Creek experimental road site, Yukon, Canada. In: Proceedings of the 10th International Conference on Permafrost, Salekhard, Russia, pp. 261.

Richard, C. (2018). Stabilisation thermique des infrastructures routières construites sur pergélisol sensible au dégel à l'aide de surface à albédo élevé". Master's thesis, Laval University, Canada.

Chapter 8 Discussion

The purpose of this project was to develop improved engineering tools for convective stabilization techniques, focussing on air convection embankment (ACE) and heat drain. The heat balance approach is proposed to help determine the thermal condition of conventional embankments and to allow select suitable mitigation techniques to extract the amount of excess heat flowing into the foundation of an unstable embankment. Four thermal models have been built and calibrated using measured temperature data from experimental sites. A heat balance chart for conventional embankments and, several heat extraction capacity charts for ACE and heat drain have been developed using numerical simulations and validated using data from test sites in Yukon and Northern Quebec, Canada. A discussion on the limitations of the models and the design tools developed, on their application and on future research needed to refine them is proposed in the following sections.

8.1 Research critical review

The design charts have been developed using a sound approach based on numerical simulations, and several assumptions were made:

1) The foundation soil is assumed uniform (one soil layer, taking ice-water phase change into account). The properties of the uniform layer were obtained through the most characteristics of representative field sample cores or through numerical simulations. In the modeling, one common way to infer soil thermal properties is based on the characteristics of measured soil temperatures between the top and the bottom of the uniform soil layer.

2) The results are sensitive to the thermal boundaries. The climate conditions change from one year to another, and to average the effects, the averaged air temperature during the monitoring years is applied. The n-factor, as an empirical approach, is widely used since the 1950s, providing a simple, reliable method to determine the thermal boundaries. At the field site, the snowpack thickness along the side slopes are not the same, thus, the freezing n-factors are different. However, a uniform n-factor is employed, and its value is obtained through a sensitivity analysis to make the modeled soil temperature fit the measured soil temperature. To some extent, this leads to an inaccurate active layer thickness under side slopes.

3) ACE has a larger permeability to allow pore-air flow in winter. From personal conversations, several engineers (e.g., G. Doré, project supervisor; D. J. Goering, University of Alaska Fairbanks) suggest the sand inside the ACE layer, due to the construction or maintenance practice, could lead to a large loss of heat extraction from the ground in winter. This is confirmed by the ACE uncovered on side slopes at the Beaver Creek experimental site. The sand decreases the permeability of the ACE layer. For full-width ACE, a geotextile has been laid out above the ACE layer to prevent the sand from filling voids inside the ACE layer.

Radiation accounts for a significant proportion of heat transfer in full-width ACE with a large porous area. Thus, for full-width ACE, radiation is taken into account and the intrinsic permeability is estimated using a Kozeny-Carman equation modified by Chapuis (2004). For ACE on side slopes uncovered, radiation is not considered and permeability is estimated using sensitivity analysis, instead of empirical equations.

4) Groundwater affects permafrost stability. Large-scale structures, such as roads, railways and airstrip, may cross surface and subsurface water flow paths, and thus intercepts or concentrates water. The effect of water flow in the active layer is not considered in the models developed as part of the project. To some extent, this assumuption would lead to lower estimated ground temperature in the model.

5) The heat balance (or heat extraction capacity) is not the same with different positions at the embankment-soil interface. Taking heat drain as an example, the cold air flowing inside the heat drain becomes warmer along the airflow channel, compared to the air at the entrance of the drain. In the analysis cases using numerical approach, the middle-side slope was considered representing the average values of heat balance. Therefore, the use of the middle-side slope as the reference position in the analysis of the embankment-soil interface, is considered to be reasonable.

6) The calculation of heat balance has a close relationship with thermal properties of soil. The heat balance charts and heat extraction charts can be corrected by multiplying the ration between the frozen thermal conductivity of subgrade soils at the field sites considered and of the soil used in the model development. This simplification is reasonable, considering the active layer does not go deep underneath the embankment (except under side slopes) and it leads to an overestimation of the heat induced during summer, which leads to a conservative design.

7) The models were developed and calibrated on specific test sites conditions (mostly Beaver Creek, Yukon) and are therefore valid for the conditions of these sites. Use of the models to conditions of other sites using different materials can lead to some design errors.

8.2 Additional research

The work done as part of this doctoral project has some limitations including those described above and thus future research is recommended to extend this project.

1) Snow is an important factor affecting the ground thermal regime. Additional boreholes under the side slope could help determine the ground thermal conditions and more accurate freezing n-factors through sensitivity analysis; thus improving developed models, mostly if the research focus is to determine the detailed thermal regime under the side slopes. It is recommended to measure the snowpack thickness and near-

surface soil temperatures on side slopes.

2) Water flow should be integrated into models to better reflect site conditions. Future numerical simulations and field observations are needed to examine its influence on the heat balance across the interface, if water flow is observed or expected at field sites.

3) Whether permafrost degradation happens or not depends on the heat balance across the interface embankment/natural ground. With a larger positive heat budget, thaw settlements will happen. Engineers pay much attention to thaw settlements, which is the main reason to cause engineering problems. A negative heat balance would freeze soils back and thus reduce the active layer thickness. Therefore, the relationship between thaw settlements and heat balance is of great interest. Furthermore, it is pretty interesting to associate such recommended research with risk assessments, which has been done by Dr. Heather Brooks at Université Laval.

4) U-shape ACE combines all the benefits of the full width and the shoulder application of ACE. That may enable U-shape ACE to have the best thermal performance, which would be interesting to apply in the field site. Therefore, investigation on the design charts of the U-shape ACE should be a great interest.

5) Measurements indicate that heat drain installed in the shoulder, has been proved to decrease ground temperatures under the side slope, and it has limited thermal effectiveness under the centerline of embankments. This is because wintertime airflow in heat drain occurs in the side slope. It is recommended to apply heat drain across the whole embankment width in the field site to monitor its performance under the centerline and under the side slope. It is also interesting to build additional models to reproduce the ground thermal regime and to propose the associated heat extraction capacity charts.

6) No single engineering solution could be applied to all problems sites and a better stabilization option often appears to be a combination of techniques. Heat drain, as a new technique, has a good potential to cool the ground. Therefore, the combination of heat drain with others, such as insulation and high albedo surface, is of great interest.

7) The design frameworks proposed in this project, can be applied to other promising techniques, such as air duct system and sun shed.

8) The proposed design charts have been developed using data from a few test sites and validated using thermal data at a limited number of test sites other than the one used for the model development. To improve their robustness, design charts should be validated using more instrumented sites when these become available in the future.

8.3 Practical application

Heat balance approach is sensitive to thermal conductivity of soils. The proposed heat balance curves are based on the thermal conductivity of soils present at the test sites used for the model calibration. These curves can be corrected by multiplying the heat balance obtained from the chart by the ratio between thermal conductivity of subgrade soils at the site considered and of the soil used in the development of the model.

In the design charts, different controlling parameters are required to determine the thermal conditions for conventional embankments and heat extraction capacity for ACE, heat drain. The controlling parameters are:

1) Thermal gradient in the foundation and embankment thickness for conventional embankments.

2) Temperature difference between mean annual winter air temperature and permafrost temperature, embankment thickness for ACE.

3) Temperature difference between mean annual winter air temperature and permafrost temperature, heat drain length and embankment thickness for heat drain.

In general, the air temperature data can be found from the local weather stations or Environment Canada (https://weather.gc.ca/canada_e.html). The thermal gradient and permafrost temperature are required to use the charts. There are two suggested ways that can be used to obtain that information: 1) The preferred way for existing embankments is by using instrumentation to obtain directly the site-specific information. Alternatively, if information is available on a similar embankment at at a nearby site, it can be used to assess the required input data; 2) For planned embankment or for existing embankment where it is impractical to measure temperature, the input data can be obtained using numerical models. Commercial finite element software, such as SVoffice, Comsol and GeoStudio (TEMP/W and SEEP/W) are available. The detailed information about the model development, such as thermal boundaries, meshing and governing equations, for conventional embankments, ACE and heat drain has been described in Chapters 5 to 7, which could provide valuable information for the modeling purpose.

Global warming can lead to more heat flow into the foundation and reduce the heat extraction capacity of convective techniques. The effect of global warming has been integrated into to the procedure, by reducing the thermal gradient in the ground for conventional embankments and the temperature difference between the mean annual winter temperature and permafrost temperature for convective techniques, considered by the designers using the site-specific climate change scenario during the service life of transportation infrastructure.

The heat balance charts and heat extraction capacity charts should be used together by designers. For example, a 1.5m thick embankment with a 0.28 °C/m thermal gradient in the permafrost conditions where the temperature difference (ΔT) between mean annual winter air temperature and permafrost temperature is -14.6 °C, would require at least a 3.8 m thick ACE layer to extract the 4000 KJ/m^2 excess heat affecting the embankment (Figure 8.1).

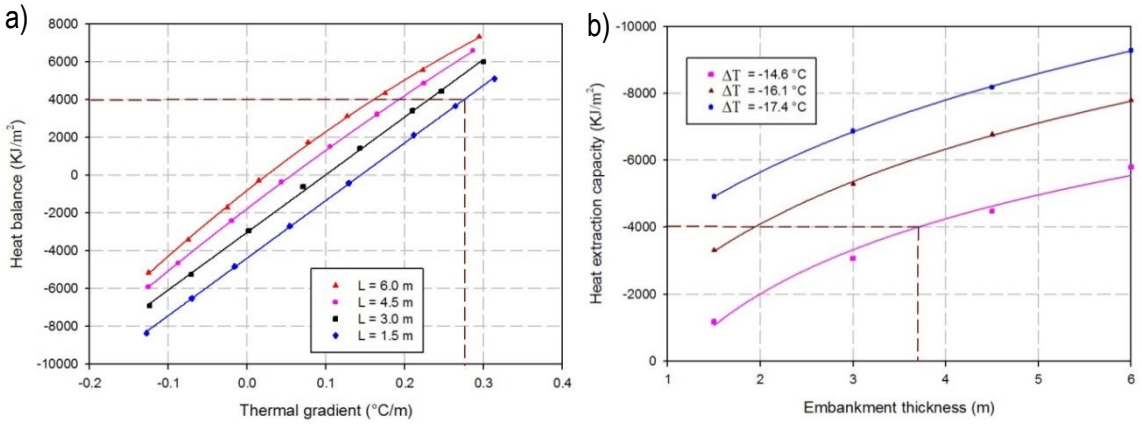

Figure 8. 1: Engineering design charts under the side slope: a) heat balance chart for conventional embankments; b) heat extraction capacity chart for ACE on side slopes.

Conclusion

Transportation infrastructure is vital to economic and social developments for the northern communities. About half the Canadian landmass is characterized by the presence of permafrost, which can be sensitive to thawing. Permafrost degradation underneath transportation embankments reduces the level of infrastructure serviceability, increases the maintenance cost as well as the risks for users, and can even lead to embankment failure in some cases. Given these conditions, tools are needed to assist engineers in maintaining the mechanical and the thermal stability of the existing and future transportation infrastructure in permafrost environments.

This project is part of the ARQULUK engineering research program, which aims at the development of improved engineering design tools for convective techniques to mitigate permafrost instabilities under transportation infrastructure in a climate change context. The main conclusions obtained from this project, are the following:

1) To achieve this objective, a new analysis framework based on the heat balance analysis for conventional embankments and a new design framework to assess the heat extraction capacity for convective techniques have been developed;

2) 2-D finite element models developed using the SVOffice (SVHeat and SVAir flow modules) from SoilVision were used to simulate the heat transfer process at the field sites in Yukon and Northern Quebec, Canada. With the assistance of numerical simulations, design tools to quantify the heat extraction capacity of convection techniques, especially heat drain and air convection embankment (ACE), have been developed and validated using the additional temperature data. Heat extraction capacity calculated using other types of soil materials may differ from the estimations proposed in this thesis;

3) The heat balance estimation chart to analyze the thermal stability of conventional embankments built on thaw-sensitive permafrost have been proposed and validated as well; Three controlling parameters consisting of thermal conductivity of subgrade soils, embankment thickness and thermal gradient in the subgrade, were used;

4) The effect of global warming has been integrated into the design procedures by changing the controlling parameters of heat balance estimation charts/heat extraction capacity charts: 1) increase the thermal gradient for conventional embankments; 2) decrease the temperature difference at the embankment/soil interface between mean annual winter air temperature and permafrost temperature, for the

heat extraction capacity of convective techniques. The site-specific climate change scenario should be selected by designers;

5) The design tools have been developed and validated based on a limited number of observations in Yukon and Northen Quebec, and additional validations are required to increase the robustness and to expand the engineering usefulness;

6) The proposed design charts, based on the heat balance approach, were developed considering the heat conduction as the main heat transfer mode and neglecting possible advective heat transfer from wind and water flow. In the case of significant advective heat transfer at the field sites, an additional safety margin should be included in the design by engineers. There is however currently no way to estimate the required safety margin to fully compensate these effects;

7) Despite the limitations of design charts, this project improved the understanding of the analysis of thermal stability using sound physical heat transfer principles and the understanding of the capacity of heat drain and ACE to extract the amount of extra heat flowing into the subgrade to stabilize the embankment;

In summary, this research project has allowed developing methods and guidelines for thermal analysis, thermal stabilization of transportation infrastructure built on thaw-sensitive permafrost and design tools have been developed, validated to support the design and the management of northern transportation infrastructure. Results of this project improved the design capacity of convective techniques to preserve permafrost, with a high potential to have a significant impact on the quality of northern roads, runways and airstrips.

Bibliographie

Allard, M., Doré, G., L'Hérault, E., Sarrazin, D., Verreault, J.(2009). Investigations géotechniques, caractérisation du pergélisol et stratégie d'adaptation pour les aéroports du MTQ au Nunavik. In: Rapport d'étape. Vol. 2. Centre d'études Nordiques, Université Laval, Quebec, Canada, pp. 1–83.

Assessment, A.C.I. (2004). Impacts of a warming Arctic-Arctic climate impact assessment, UK: Cambridge University Press, pp.144.

Beaulac, I., Dore, G. (2006). Development of a new heat extraction method to reduce permafrost degradation under roads and airfields. In: Proceedings of the 13th International Conference on Cold Regions Engineering, Orono, Maine, USA.

Beaulac, I., Doré, G., Shur, Y., Allard, M. (2004). Permafrost thawing impacts on road and airfields: problem assessment and review of possible solutions. In: Proceedings of the Cold Regions Engineering and Construction Conference, Edmonton, Alberta, Canada

Bell, J.R., Allen, T., Vinson, T.S. (1984), Properties of geotextiles in cold regions application. In: Proceedings of 4th International Conference on Permafrost, Washington, pp. 51-56.

Berg, R. L. (1985). Effect of color and texture on the surface temperature of asphalt concrete pavements. In: Proceedings of the 4th international Conference on Permafrost, Washington, pp. 57-61.

Brown, J. (1997). Disturbance and recovery of permafrost terrain. Disturbance and Recovery in Arctic Lands: An Ecological Perspective, 167-178.

Calmels, F., Doré, G., Kong., X, Roy, LP., Lemieux, C., Horton, B. (2016). Vulnerability of the north Alaska Highway to permafrost thaw: Design options and climate change adaptation. Whitehorse: Northern Climate Exchange, Yukon Research Centre, Yukon College, pp. 132.

Calonne, N., Geindreau, C., Flin, F., Morin, S., Lesaffre, B., Du Roscoat, S. R., Charrier, P. (2012). 3-D image-based numerical computations of snow permeability: links to specific surface area, density, and microstructural anisotropy. The Cryosphere, 6, 939-951.

Canadian Standards Association. (2014). Thermosyphon foundations for building in permafrost regions, in National Standard of Canada, CAN/CSA-S500-14. Mississauga, Canada.

Chapuis, R. P. (2004). Predicting the saturated hydraulic conductivity of sand and gravel using effective diameter and void ratio. Canadian Geotechnical Journal, 41(5), 787-795.

Chataigner, Y., Gosselin, L., Doré, G. (2009). Optimization of embedded inclined open-ended channel in natural convection used as heat drain. International Journal of Thermal Sciences, 48(6), 1151-1160.

Cheng, G., Sun, Z., Niu, F. (2008). Application of the roadbed cooling approach in Qinghai–Tibet railway engineering. Cold Regions Science and Technology, 53(3), 241-258.

Côté, J., Fillion, M.-H., Konrad, J.-M. (2011). Intrinsic permeability of materials ranging from sand to rock-fill using natural air convection tests. Canadian Geotechnical Journal, 48(5), 679-690.

Coulombe, S., Fortier, D., Stephani, E. (2012). Using air convection ducts to control permafrost degradation under road infrastructure: Beaver Creek experimental site, Yukon, Canada Cold Regions Engineering 2012: Sustainable Infrastructure Development in a Changing Cold Environment, pp. 21-31.

Davis, T. N. (2001). Permafrost: A guide to Frozen Ground in Transition. University of Alaska Press, Fairbanks, pp.351.

De Vries, D. (1958). Simultaneous transfer of heat and moisture in porous media. Eos, Transactions American Geophysical Union, 39(5), 909-916.

Doré, G.,Pierre, P., Juneau, S. (2008). Expérimentations de techniques de mitigation des effets de la fonte du pergélisol sur les infrastructures du Nunavik : aéroport de Tasiujaq. Université Laval, pp.1-39.

Doré, G., Ficheur, A., Guimond, A., Boucher, M. (2012). Performance and cost-effectiveness of thermal stabilization techniques used at the Tasiujaq airstrip. Cold Regions Engineering 2012: Sustainable Infrastructure Development in a Changing Cold Environment, pp. 32-41.

Doré, G., Ficheur, A., Guimond, A., Boucher, M. (2012). Performance and cost-effectiveness of thermal stabilization techniques used at the Tasiujaq airstrip. Cold Regions Engineering 2012: Sustainable Infrastructure Development in a Changing Cold Environment, pp. 32-41.

Doré, G., Niu, F., Brooks, H. (2016). Adaptation methods for transportation infrastructure built on degrading permafrost. Permafrost and Periglacial Processes, 27(4), 352-364.
Doré, G., Zubeck, H. K. (2009). Cold regions pavement engineering. McGraw-Hill, New York.
Dumais, S., Doré, G. (2016). An albedo based model for the calculation of pavement surface temperatures in permafrost regions. Cold Regions Science and Technology, 123, 44-52.
Esch, D. (1983). Design and performance of road and railway embankments on permafrost. In: Proceedings of the 4th International Conference on Permafrost, Fairbanks, Alaska, pp. 23-30.
Esch, D. C. (1996). Roads and airfield design for permafrost conditions. In Roads and airfields in cold regions: a state of practice report, pp. 121-149.
Fair, G. M., Hatch, L. P., Hudson, H. E. (1933). Fundamental factors governing the streamline flow of water through sand. Journal-American Water Works Association, 25(11), 1551-1565.
Farouki, O. (1981). Thermal properties of soils. Hanover, N.H: U.S. Army Corps of Engineers, Cold Regions Research and Engineering Laboratory.
Ficheur, A., Doré, G. (2010). Expérimentation de techniques de mitigation des effets de la fonte du pergélisol sur les infrastructures de transport du Nunavik : Aéroport de Tasiujaq, Rapport final, Université Laval, pp.1-177.
Ficheur, A. (2011). Expérimentation de techniques de mitigation des effets de la fonte du Pergelisol sur les infrastructures de transport du Nunavik: Aéroport de Tasiujaq. Mater's thesis, Laval University, Canada.
Forsström, A., Long, E. L., Zarling, J. P., Knutsson, S. (2002). Thermosyphon cooling of chena hot springs road Cold Regions Engineering: Cold Regions Impacts on Transportation and Infrastructure, pp. 645-655.
Goering, D. (2003). Thermal response of air convection embankments to ambient temperature fluctuations. In: Proceedings of the 8th International Conference on Permafrost, Zurich, pp. 291-296.
Goering, D. J. (1998). Experimental investigation of air convection embankments for permafrost-resistant roadway design. In: Proceedings of the 7th International Conference on Permafrost, Yellowknife, Canada, pp. 319-326
Goering, D. J. (2002). Convective cooling in open rock embankments Cold Regions Engineering: Cold Regions Impacts on Transportation and Infrastructure, pp. 629-644.
Goering, D. J., Kumar, P. (1999). Permeability effects on winter-time natural convection in gravel embankments Advances in cold-region thermal engineering and sciences. In: Proceedings of the 6th International Symposium Held, Darmstadt, Germany, pp. 455-464.
Jørgensen, A. S., Doré, G., Voyer, É., Chataigner, Y., Gosselin, L. (2008). Assessment of the effectiveness of two heat removal techniques for permafrost protection. Cold Regions Science and Technology, 53(2), 179-192.
L'Hérault E., M. Allard, C. Barrette, G. Doré, et D. Sarrazin (2012). Investigations géotechniques, caractérisation du pergélisol et stratégie d'adaptation dans un contexte de changements climatiques pour les aéroports d'Umiujaq, Inukjuak, Puvirnituq, Akulivik, Salluit, Quaqtaq, Kangirsuk et Tasiujaq, Nunavik. Rapport final. Réalisé pour le compte du ministère des Transports du Québec. Québec, Centre d'études nordiques, Université Laval, pp. 1-224.
McHattie, R.L., Goering, D.J. (2009). Air convection embankment (ACE) design guide. Alaska. Department of Transportation. Report, FHWA-AK-RD-09-06.
Heuer, C. E. (1979). The application of heat pipes on the Trans-Alaska pipeline. Special Report 79-26, United States Army Corps of Engineers.
Goodrich, L.E., 1982. The influence of snow cover on the ground thermal regime. Canadian Geotechnical Journal, 19(4), pp.421-432.
Hazen, A. (1911). Discussion of "Dams on sand formations". Transactions of the American Society of Civil Engineers, 73: 199–203.
Hinzman, L.D., Bettez, N.D., Bolton, W.R., Chapin, F.S., Dyurgerov, M.B., Fastie, C.L., Griffith, B., Hollister, R.D., Hope, A., Huntington, H.P. (2005). Evidence and implications of recent climate change in northern Alaska and other arctic regions. Climatic Change, 72(3), 251-298.

Hoeve, T., Seto, J., Hayley, D. (2004). Permafrost response following reconstruction of the Yellowknife Highway. In: Proceedings of the Cold Regions Engineering and Construction Conference, Edmonton, Alberta.

Holubec, I. (2008). Flat loop thermosyphon foundations in warm permafrost. In: Proceedings of the 9th International Conference on Permafrost, Fairbanks, Alaska.

Johansen, O. (1975). Thermal conductivity of soils. Retrieved from soils. Ph.D thesis, University of Trondheim. Translated in U.S. Army, Cold Regions Research and Engineering Laboratory, Translation 637.

Jørgensen, A. S. (2009). Assessment of three mitigation techniques for permafrost protection. Ph.D thesis,Technical University of Denmark (DTU), Denmark.

Jørgensen, A. S., Doré, G., Voyer, É., Chataigner, Y., Gosselin, L. (2008). Assessment of the effectiveness of two heat removal techniques for permafrost protection. Cold Regions Science and Technology, 53(2), 179-192.

Kaplan, J. O., New, M. (2006). Arctic climate change with a 2°C global warming: Timing, climate patterns and vegetation change. Climatic change, 79(3-4), 213-241.

Klene, A. E., Nelson, F. E., Shiklomanov, N. I., Hinkel, K. M. (2001). The n-factor in natural landscapes: variability of air and soil-surface temperatures, Kuparuk River Basin, Alaska, USA. Arctic, Antarctic, and Alpine Research, 33(2), 140-148.

Kondratiev, V. (2010). Some geocryological problems of railways and highways on permafrost of Transbaikai and Tibet. In: Proceedings of the 63rd Canadian Geotechnical Conference and the 6th Canadian Permafrost Conference, Calgary, Alberta.

Lai, Y., Wang, Q., Niu, F., Zhang, K. (2004). Three-dimensional nonlinear analysis for temperature characteristic of ventilated embankment in permafrost regions. Cold Regions Science and Technology, 38(2-3), 165-184.

Lebeau, M., Konrad, J.-M. (2009). Natural convection of compressible and incompressible gases in undeformable porous media under cold climate conditions. Computers and Geotechnics, 36(3), 435-445.

Linell, K. A. (1973). Long-term effects of vegetative cover on permafrost stability in an area of discontinuous permafrost. Permafrost: North American Contribution to the 2rd International Conference, pp. 688-693.

Lingnau, B. (1985). Observation of the design and performance of the Dempster Highway. Master's thesis University of Alberta, Canada.

Lunardini, V. J. (1981). Heat transfer in cold climates. Nostrand Reinhold, New York.

Wa, W., Cheng, G.D., Wu, Q.B. (2009). Construction on permafrost foundations: lessons learned from the Qinghai–Tibet railroad. Cold Regions Science and Technology, 59(1), 3-11.

M-Lepage, J., Doré, G., Fortier, D., Murchison, P. (2012). Thermal performance of the permafrost protection techniques at Beaver Creek experimental road site, Yukon, Canada. In: Proceedings of the 10th International Conference on Permafrost, Salekhard, Russia, pp. 261

M-Lepage, J. (2015). Experimentation of mitigation techniques to reduce the effects of permafrost degradation on transportation infrastructures at Beaver Creek experimental road site (Alaska Highway, Yukon). Mater's thesis, Laval University, Canada.

McAdams, W. H. (1954). Heat Transmission. McGraw-Hill, New York.

McGregor, R., Hayley, D., Wilkins, G., Hoeve, E., Grozic, E., Roujanski, V., Jansen, A., Dore, G. (2010). Guidelines for development and management of transportation infrastructure in permafrost regions. Transportation Association of Canada, Ottawa, Ontario.

Molmann, T., Bergheim, B., Valeriote, M. (1998). Svalbard airport geptechnical study: engineering methodology and results. In: Proceedings of the 7th International Permafrost Conference, Collection Nordicana, Whitehorse, Canada, pp. 745–755.

Mukhetdinov, N. (1971). Effect of nonlinear air filtration on thermal regime of rock-fill dam. Cold regions research and engineering lab, Hanover.

Nelson, F. E., Anisimov, O. A., Shiklomanov, N. I. (2001). Subsidence risk from thawing permafrost. Nature, 410(6831), 889.

Nidowicz, B., Shur, Y. (1998). Pavement thermal impact on discontinuous permafrost. Cold Regions Impact on Civil Works. ASCE, pp. 34–35.

Nield, D. A., Bejan, A. (2006). Convection in porous media. Springer-Verlag, New York.

Périer L., Lemieux C., Lamontagne, V., Nolet, A.-G., M-Lepage, J., Doré, G., Allard, M. (2016). Suivi du comportement thermique et mécanique de la route d'accès de Salluit et expérimentation d'une méthode de détection de la dégradation du pergélisol le long des structures linéaires. Rapport final. Ministère des Transports, de la Mobilité durable et de l'Électrification des transports du Québec, Université Laval, Québec, pp. 129

Pham, H. N. (2013). Heat transfer in waste-rock piles constructed in a continuous permafrost region. Ph.D. thesis. University of Alberta, Canada.

Popov, A., Vaaz, S., Usachev, A. (2010). Review of the current conditions for the application of heat pipes (thermosyphons) to stabilize the temperature of soil bases under facilities in the far North. Heat Pipe Science and Technology, 1(1).

Qin, Y., Zhang, J. (2013). A review on the cooling effect of duct-ventilated embankments in China. Cold Regions Science and Technology, 95, 1-10.

Esch, D., Rhode, J. (1976). Kotzebue airport runway insulation over permafrost. In: Proceedings of the 2nd International Symposium on Cold Regions Engineering. ASCE, pp. 44–61.

Richard, C. (2018). Stabilisation thermique des infrastructures routières construites sur pergélisol sensible au dégel à l'aide de surface à albédo élevé. Mater's thesis, Laval University, Canada.

Saboundjian, S., Goering, D. (2003). Air convection embankment for roadways: Field experimental study in Alaska. Transportation Research Record. Journal of the Transportation Research Board (1821), 20-28.

Shimizu, H. (1970). Air permeability of deposited snow. Institute of Low Temperature Science, 22, 1-32.

Smith, S. L. (2011). Trends in permafrost conditions and ecology in northern Canada. Technical Report No. 9 Canadian Councils of Resource Ministers, pp. 22.

Sun, B., Xu, X., Lai, Y., Fang, M. (2005). Evaluation of fractured rock layer heights in ballast railway embankment based on cooling effect of natural convection in cold regions. Cold Regions Science and Technology, 42(2), 120-144.

Straus, J. M. (1974). Large amplitude convection in porous media. Journal of Fluid Mechanics, 64(1), 51-63.

Vinson, T. S., Rooney, J. W., Haas, W. H. (1996). Roads and airfields in cold regions. Practical report, Technical Council on Cold Regions Engineering of ASCE.

Wakao, N., Kato, K. (1969). Effective thermal conductivity of packed beds. Journal of Chemical Engineering of Japan, 2(1), 24-33.

Wagner, A.M., 2014. Review of Thermosyphon Applications. The US Army Engineer Research and Development Center, Hanover, NH.

Warren, F.J., Barrow, B., Schwartz, R., Andrey, J., Mills, B., Riedel, D. (2004). Climate change impacts and adaptation: A Canadian perspective, Climate Change Impacts and Adaptation Directorate, Natural Resources Canada, Ottawa, Ontario, pp. 175.

Wendler, G., Shulski, M. (2009). A century of climate change for Fairbanks, Alaska. Arctic, 295-300.

Wu, J., Ma, W., Sun, Z., Wen, Z. (2010). In-situ study on cooling effect of the two-phase closed thermosyphon and insulation combinational embankment of the Qinghai–Tibet Railway. Cold Regions Science and Technology, 60(3), 234-244.

Wu, Q., Andreopoulos, Y., Xanthos, S., Weinbaum, S. (2005). Dynamic compression of highly compressible porous media with application to snow compaction. Journal of Fluid Mechanics, 542, 281-304.

Wu, Q., Li, M., Liu, Y. (2010). Thermal interaction between permafrost and the Qinghai-Tibet Railway. Journal of cold regions engineering, 24(4), 112-125.

Zarling, J. P., Connor, B., Goering, D. J. (1984). Air duct systems for roadway stabilization over permafrost areas. Technical report. U.S. Department of Transportation Federal Highway Administration.

Zarling, J. P., Braley, W. A., Esch, D. (1988). Thaw stabilization of roadway embankments. In: Proceedings of the 5th International Permafrost Conference, Trondheim, Norway, vol. 2, pp.1352–1357.

Zermatten, E., Schneebeli, M., Arakawa, H., Steinfeld, A. (2014). Tomography-based determination of porosity, specific area and permeability of snow and comparison with measurements. Cold Regions Science and Technology, 97, 33-40.

Zhang, M., Lai, Y., Yu, W., Huang, Z. (2007). Experimental study on influence of particle size on cooling effect of crushed-rock layer under closed and open tops. Cold Regions Science and Technology, 48(3), 232-238.

Appendix A

The Beaver Creek experimental site is located at 62° 20' N, 140° 50' W, about 8 km south of the community of Beaver Creek and about 30 km south of the Canada-United States border (Figure A.1). Eleven 50 m-length with mitigation techniques and one 50 m-length control section were constructed at Beaver Creek, Yukon, providing valuable data to test the specific thermal effectiveness (Figure A.2). These sections focus on activation of heat extraction during winter, or reduction of heat intake during summer. The layout of these techniques and the position of installed boreholes are shown in Figure A. 3. The brief description of all the techniques tested is summarized in Table A.1.

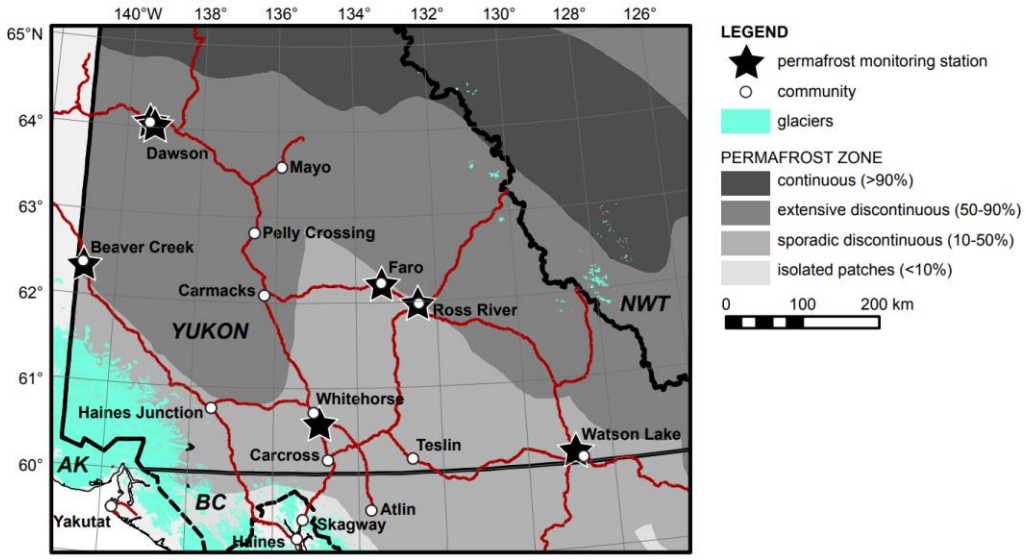

Figure A. 1: The location of the Beaver Creek experimental site, along the Alaska Highway, Yukon, Canada (Lipovsky, 2015).

Figure A. 2: The experimental test site at Beaver Creek, Yukon.

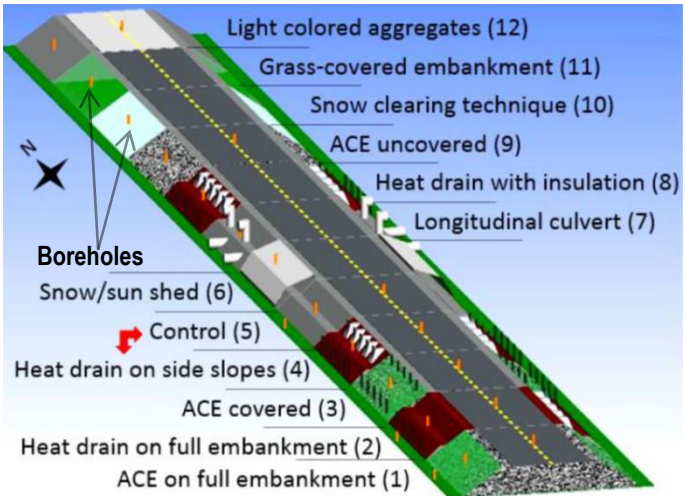

Figure A. 3: Schematic of Beaver Creek experimental site – Section 4 and 5 were interchanged (see red arrow) during the construction. Yellow point: borehole positions (modified from M-Lepage, 2015).

Table A. 1: Description of tested mitigation techniques at Beaver Creek site (modified from M-Lepage, 2015).

Mitigation techniques		Section number	Design description
Air convection embankment (ACE)	Full ACE (side slopes covered by organic soils)	S1	Based on heat extraction during winter; Crushed rock size of 150 -300 mm was used to generate convection cells.
	ACE on side slopes uncovered	S9	
	ACE on side slopes covered by organic soils	S3	
Heat drain (HD)	HD across the whole embankment	S2	Based on heat extraction during winter; 25 mm thick geocomposite was used to facilitate airflow in the system.
	Heat drain in the side slope	S4	
	HD in side slopes with insulation	S8	
Longitudinal culvert		S7	Based on heat extraction during winter; 750 mm-diameter culvert was buried under the embankment slope and parallel to the road.
Snow/sun shed		S6	Based on reduction of heat intake; Wooded sheds were employed above the side slope.
Snow cleaning technique		S10	Based on reduction of heat intake; Snow was cleared on the pavements surface and side slopes in winter.
Grass-covered embankment on the side slope		S11	Based on reduction of heat intake; Organic soils were spread on the side slope and the native seed mixture was planted in the organic soils.
High albedo surface		S12	Based on reduction of heat intake; Bituminous surface treatment was employed on the pavement surface.

Note: S is the abbreviation of "section" (e.g., . S1 = Section 1 in Figure A.3).

Information about the detailed designs, soil units in boreholes, thermistor sensor depths, thermal effectiveness in the first three years (2009-2011) after the construction for each tested section, were summarized in the master's thesis of M-Lepage (2015). Information about the descriptions of soil units in installed boreholes at Beaver Creek, is summarized in the master's thesis of Stephani (2013). The following figures (A.4 to A.15) are also from Stephani's master's thesis (2013).

Figure A. 4: Full air convection embankment (S1) a) during construction; b) after construction.

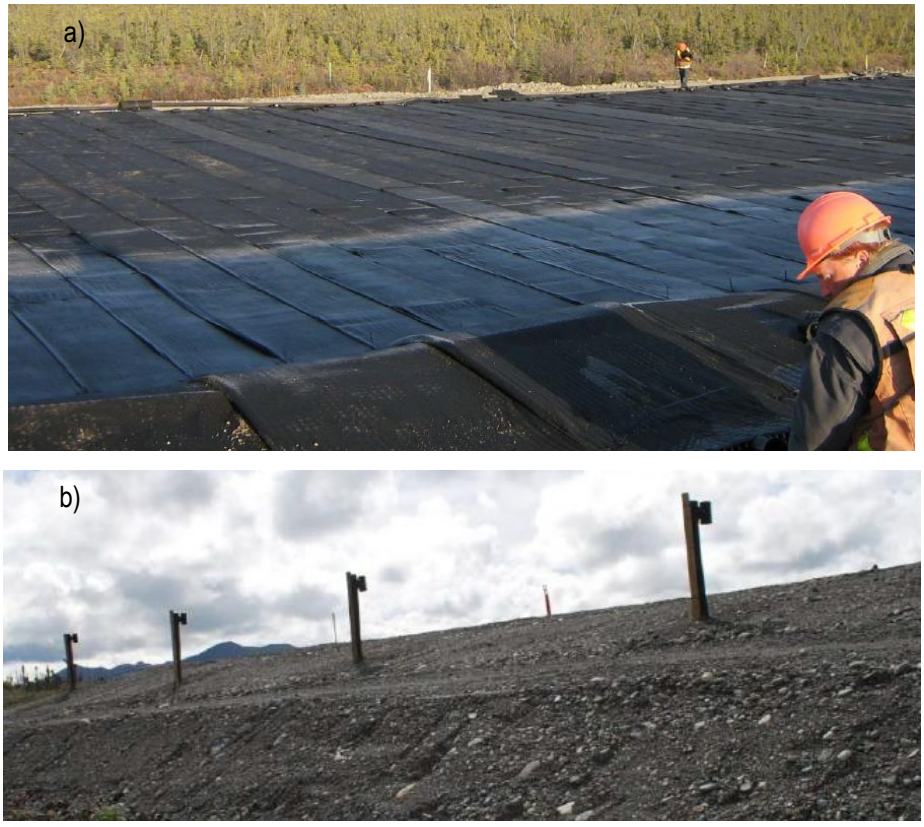

Figure A. 5: Heat drain across the whole embankment (S2) a) during construction; b) after construction.

Figure A. 6: ACE on side slopes covered (S3) a) during construction; b) after construction.

Figure A. 7: Heat drain in the side slope (S4) a) during the construction; b) after the construction.

Figure A. 8: Control section (S5).

Figure A. 9: Snow/sun shed (S6) after construction.

Figure A. 10: Longitudinal culvert (S7) a) during construction; b) after construction.

Figure A. 11: Heat drain in side slopes with insulation (S8) a) during construction; b) after construction.

Figure A. 12: Air convection embankment on side slopes uncovered (S9) after construction.

Figure A. 13: Snow cleaning technique (S10) after construction.

Figure A. 14: Grass-covered embankment on the side slope (S11) after construction.

Figure A. 15: High albedo surface (S12) after construction.

Appendix B

The village of Tasiujaq is located in the southwestern part of Ungava Bay at 58°71'N and 69°82' W (Figure B.1). At Tasiujaq test site, three techniques, including air convection embankment, heat drain and gentle slope, were constructed in 2007. The information about the detailed designs, soil units in boreholes, thermistor sensor depths, process of construction and thermal effectiveness for tested techniques, were summarized in the previous research (Lemelin et al., 2008; Jørgensen, 2008; Allard et al., 2009; Ficheur and Doré 2010; Doré et al., 2012; L'Hérault et al., 2012).

Figure B. 1: The location of the Tasiujaq Airstrip test site, Northern Quebec (Doré et al., 2007).

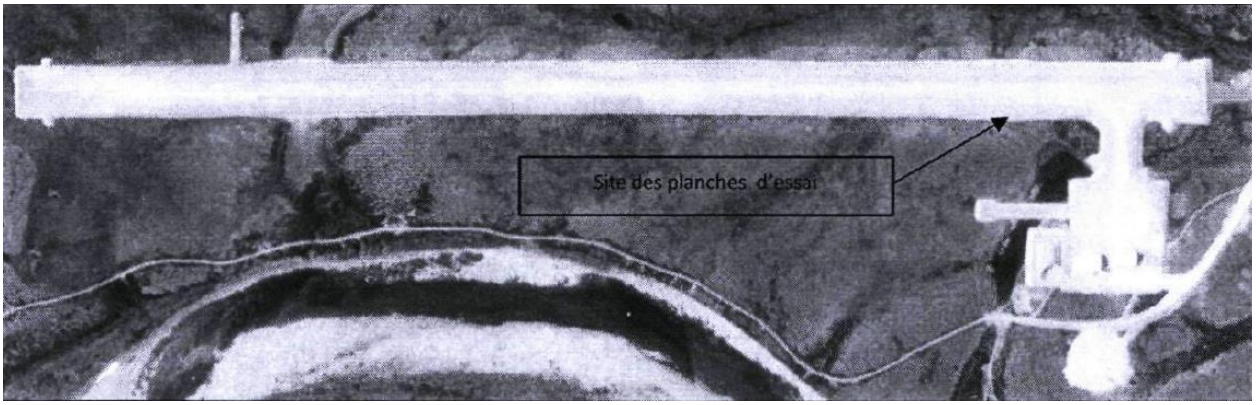

Figure B. 2: The location of the experimental techniques along Tasiujaq Airstrip (Ficheur and Doré 2010).

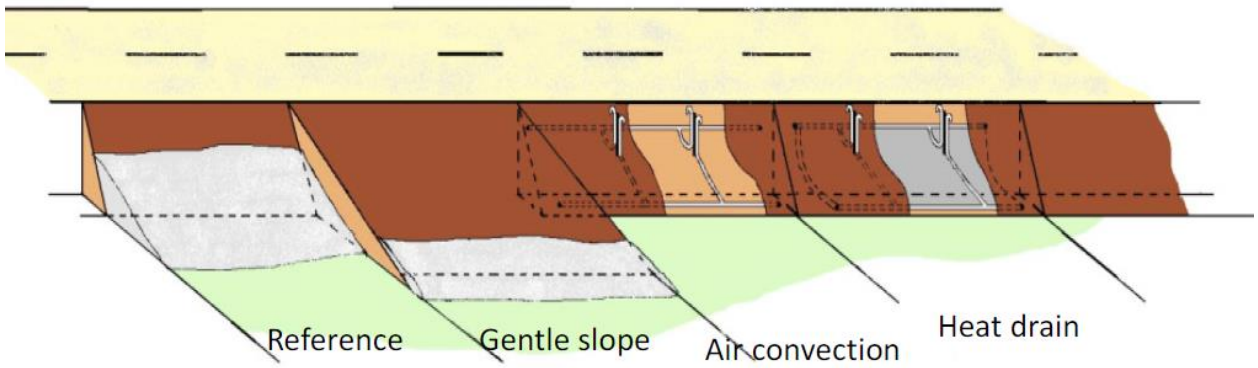

Figure B. 3: Schematic illustration of the Tasiujaq Airstrip test site, Northern Quebec (Doré et al., 2012).

Figure B. 4: Construction of the gentle slope (8H:1V) (Doré et al., 2007).

Figure B. 5: Construction of the air convection embankment (Doré et al., 2012).

Figure B. 6: Installation of the heat drain (Doré et al., 2012).

Appendix C

The heat balance charts for conventional embankments and heat extraction capacity charts for full ACE, shoulder ACE and heat drain, were proposed based on the specific site conditions. This appendix is proposing equations to simplify the calculation of the heat balance for conventional embankments and heat extraction capacity for full ACE, shoulder ACE and heat drain, for different types of foundation soils. The results of the quantification of heat balance through the embankment-soil interface at the centerline of the embankment, at the side slope for different embankment thicknesses and air temperatures are shown in Figure C.1 and Figure C.2. The equations to calculate the heat balance at the centerline and at the mid-side slope are summarized in Table C.1.

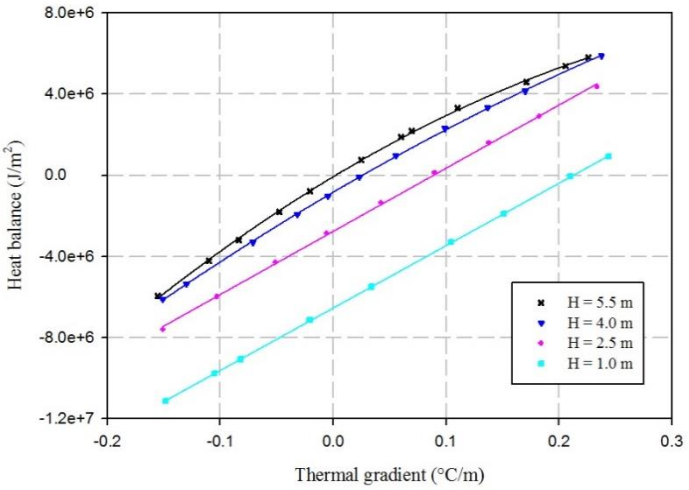

Figure C. 1: Heat balance through the embankment-soil interface at the centerline of the embankment as a function of embankment thickness (H) and thermal gradient.

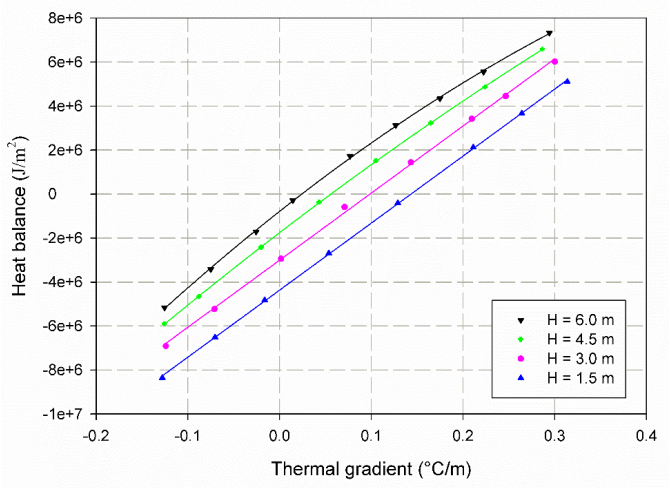

Figure C. 2: Heat balance through the embankment-soil interface at the side slope of the embankment as a function of the embankment thickness (H) and thermal gradient.

Table C. 1: Regression equations between heat balance at the embankment-soil interface, embankment thickness and thermal gradient.

Location	Regression equation	Coefficient of determination (R^2)
Centerline	$HB \times \frac{k}{k_{ref}} = -5.51 \times 10^6 + 3.96 \times 10^6 \times Grad + 6.82 \times 10^6 \times \log H$	0.994
Mid-side slope	$HB \times \frac{k}{k_{ref}} = -5.42 \times 10^6 + 3.03 \times 10^7 \times Grad + 5.51 \times 10^6 \times \log H$	0.998

HB is the heat balance (J/m^2) through the interface. $Grad$ is the thermal gradient (°C/m) between the average annual temperature at interface and permafrost temperature; k is the frozen thermal conductivity of foundation soil at the field site and k_{ref} equals to 1.21 W/m-K measured at Beaver Creek, Yukon. H is the embankment thickness (m).

In Table C. 1, the equation has been developed using the following data range:

- Thermal gradients ranging from -0.14 °C/m to +0.24 °C/m (centerline case); -0.13 °C/m to +0.31 °C/m (side slope case)
- Embankment thickness ranging from 1.0 m to 5.5 m (centerline case); 1.5 m to 6.0 m (side slope case)

Extrapolation beyond these values can induce errors in the estimation of the heat balance.

The relationship between heat extraction capacity and thickness and temperature difference (ΔT) between mean annual winter air temperature (MAWAT) and permafrost temperature is shown in Figure C. 3 for full ACE, and Figure C. 4 for the shoulder application of ACE. The equations to calculate the heat extraction capacity for different types of foundation soils are summarized in Table C.2.

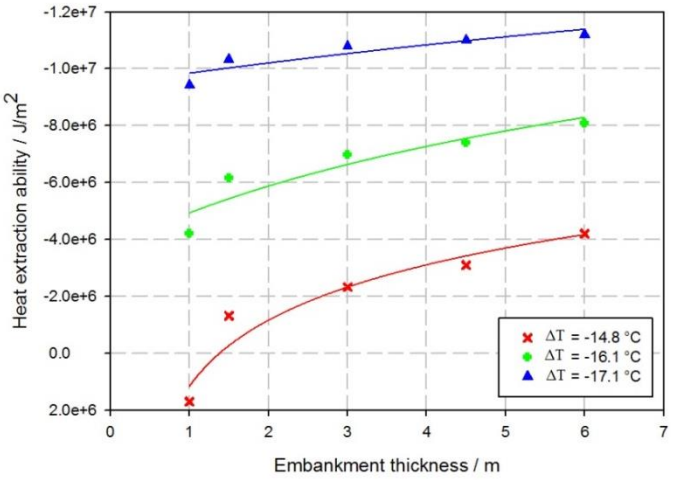

Figure C. 3: Heat extraction capacity of the full ACE at the embankment-soil interface as a function of embankment thickness and temperature difference (ΔT) between MAWAT and permafrost temperature.

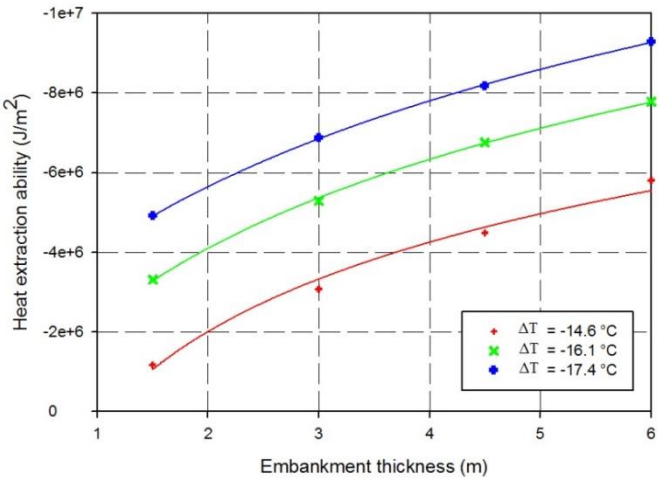

Figure C. 4: Heat extraction capacity of the shoulder ACE through the embankment-soil interface as a function of embankment thickness and temperature difference (ΔT) between MAWAT and permafrost temperature.

Table C. 2: Relationships between heat extraction capacity at the embankment-soil interface, embankment thickness and temperature difference (ΔT) between MAWAT and permafrost temperature.

ACE type	Regression equation	Coefficient of determination (R^2)
Full ACE	$HEC \times \frac{k}{k_{ref}} = 5.59 \times 10^7 - 3.77 \times 10^6 \times \Delta T - 4.34 \times \log H$	0.983
Shoulder ACE	$HEC \times \frac{k}{k_{ref}} = 1.94 \times 10^7 - 31.32 \times 10^6 \times \Delta T - 7.38 \times \log H$	0.990

HEC is the heat extraction capacity (J/m^2) at the embankment-soil interface; H is embankment thickness (m); ΔT is the temperature difference between mean annual winter air temperature and permafrost temperature (°C). k is the frozen thermal conductivity of foundation soil at the field site and k_{ref} equals to 1.34 W/m-K measured at Beaver Creek, Yukon.

In Table C. 2, the equation has been developed using the following data range:

- ΔT ranging from -14.8 °C to -17.1 °C (full ACE); -14.6 °C to -17.4 °C (shoulder ACE)
- Embankment thickness ranging from 1.0 m to 6.0 m (full ACE); 1.5 m to 6.0 m (shoulder ACE)

Extrapolation beyond these values can induce errors in the estimation of the heat extraction capacity. The quantification of heat extraction capacity through the interface in the mid-heat drain length for different embankment thicknesses and site conditions is shown in Figure C.5.

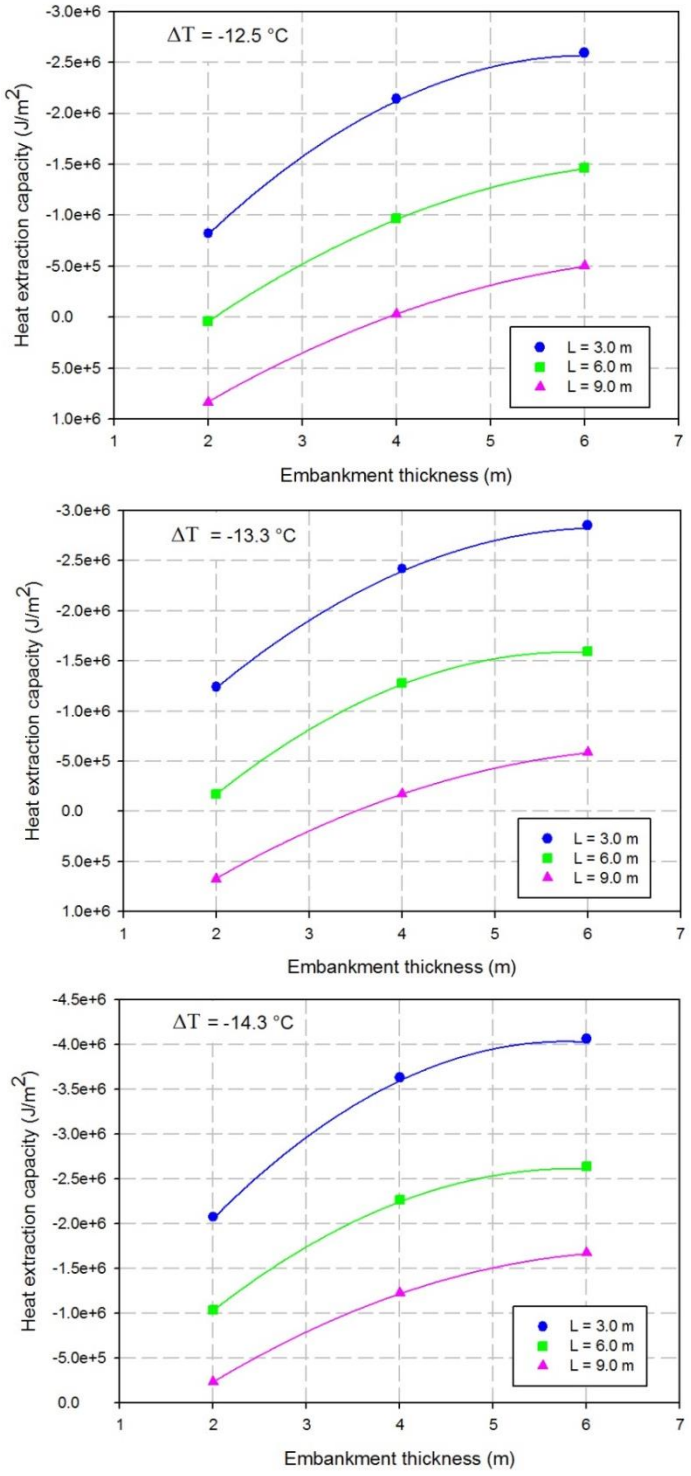

Figure C. 5: Heat extraction capacity of heat drain at the embankment-soil interface as a function of the embankment thickness, heat drain length (L) and temperature difference (ΔT) between MAWAT and permafrost temperature.

The equation to calculate the heat extraction capacity of heat drain for different foundation soils, expressed as:

$$HEC \times \frac{k}{k_{ref}} = 7.82 \times 10^6 + 7.01 \times 10^5 \times \Delta T + 3.50 \times 10^5 \times L - 3.29 \times 10^6 \times \log H \quad \text{(C. 1)}$$

where HEC is the heat extraction capacity (J/m^2); k is the thermal conductivity of foundation soil (W/m-K); k_{ref} is the reference frozen thermal conductivity (=1.19 W/m-K) at Tasiuajq airstrip, Northern Quebec; L is the heat drain length (m) (ranging from 3.0 m to 9.0 m) and H is the embankment thickness (m) (ranging from 2.0 m to 6.0 m). ΔT is the temperature difference between mean annual winter air temperature and permafrost temperature (°C) (ranging from -12.5 °C to -14.3 °C). The coefficient of determination (R^2) is 0.985. Extrapolation beyond these values can induce errors in the estimation of the heat extraction capacity.